INDUCED FLOCCULATION OF ANIMAL CELLS IN SUSPENSION CULTURE

by

JOHN GRANT AUNINS

B.S. Chem. Eng., University of Kansas, 1983

Submitted to the Department of Chemical Engineering
in Partial Fulfillment of the Requirements for the degree of

DOCTOR OF PHILOSOPHY IN CHEMICAL ENGINEERING

at the

MASSACHUSETTS INSTITUTE OF TECHNOLOGY

June, 1989

Author's Signature ____

Department of Chemical Engineering
April 21, 1989

Certified by _____

Daniel I.C. Wang
Chevron Professor of Chemical Engineering
Professor of Biochemical Engineering
Thesis Supervisor

Accepted by _____

William Deen
Professor of Chemical Engineering
Chairman, Committee for Graduate Students

To my grandmother,
Neola May Akin

"TUUM EST"

Motto of the University of British Columbia, Vancouver, Canada

INDUCED FLOCCULATION OF ANIMAL CELLS IN SUSPENSION CULTURE

by

John Grant Aunins

Submitted to the Department of Chemical Engineering
Massachusetts Institute of Technology
in Partial Fulfillment of the Requirements of Doctor of Philosophy
in Chemical Engineering

ABSTRACT

Recycle of suspension cell cultures is hindered by the small size of individual cells. To improve particle sedimentation and filtration properties, flocculation or aggregation is desirable. However, many animal cell lines of industrial interest do not form aggregates in suspension culture, and it is necessary to induce flocculation. In this thesis, a method for non-toxic aggregation of cells was developed for cell recycle use. In addition, the unknown parameters involved in the aggregation rate kernel were investigated experimentally and theoretically. These are the collision efficiency of particles, and the structure, or porosity of the resulting aggregates. These results are applicable to optimization of the flocculation process.

A flocculant search was conducted, and it was found that commercial flocculants were severely toxic to the cells, or were ineffective at flocculating cultures. A weakly cationic, poorly soluble polypeptide, poly-L-histidine (PLH), was capable of flocculating cultures of CHO, HeLa, U-937 and CRL 1606 hybridoma cells with no toxicity to the majority of cells. Culture experiments showed four-fold increases in viable cell levels over traditional batch culture using flocculation and sedimentation recycle. Flocculation was found to be mediated by micron-sized precipitates of the polymer.

The collision efficiency of CRL 1606 hybridomas flocculated with PLH was determined in Couette shear flow over a range of experimental conditions applicable to animal cell culture. At high surface coverage of the cells with PLH, the collision efficiency correlates with the particle zeta potential to the -2.4 power. This is consistent with literature empirical results and theoretical arguments on interparticle electrostatic forces. Over the entire range of PLH dose, the collision efficiency showed a sigmoidal trend, with a threshold level of polymer necessary to induce aggregation. This result is viewed as a minimum adhesion strength requirement for stable aggregation. The sigmoidal behavior has not been previously reported in the experimental literature; the apparently weak bonding between cells may also be partly responsible for the non-toxic nature of PLH flocculation relative to strongly cationic polymers. At high particle surface coverage, collision efficiency is weakly dependent on hydrodynamic conditions, and follows a power law dependency on the shear rate to the -0.32 power. This is consistent with fluid mechanical theory on ionic coagulation. At low surface coverage the collision efficiency is dependent on shear rate to the -1.2 power. This result corroborates the weak interparticle bonding found at low doses. Collision kinetics in the presence of high molecular weight dextrans showed steric hindrance to collision.

Complementing the experimental investigation, theory was developed to describe the collision of polyelectrolyte flocculated particles. Particle collision efficiency theories in the literature do not address both the modification of the particle surface by polyelectrolyte adsorption and the influence of hydrodynamic forces on the collision process for macrocolloids. Theory was developed for polymer flocculation of colloids which relates results from fluid mechanical simulations for ionic coagulation to existing probabilistic theories for polymer flocculation. Using dimensional analysis from fluid mechanical

arguments, and a constitutive relation for particle surface potential versus surface coverage, a form for the collision efficiency versus particle surface coverage is obtained. This form mimics literature probabilistic theory, but rather than viewing polymer adsorption as modifying the local particle "stickiness", it views the polymer as affecting the net electrostatic force between particles. While retaining a simple form that addresses polymer adsorption, hydrodynamic forces are also incorporated in the theory. The simple correlation form may be modified to account for local heterogeneity of polymer adsorption to the particle surface. The modified formulation describes several features of polymer flocculation not captured by previous theory. The current theory predicts that collisions will be more effective for large molecular weight polymers, and will be effective over a wider range of surface coverage, an experimentally observed fact which is counter to previous probabilistic theory. In addition, it predicts a distinct concave-upward trend of collision efficiency at low surface coverage. This behavior was demonstrated in experimental collision efficiencies for CRL 1606 flocculated with PLH.

The floc size versus the number of cells in the floc also enters into the aggregation rate kernel. The structure of flocs, specifically, the porosity versus size relation of flocs has been a subject of intense interest over the years. This thesis discusses floc structure theoretically and experimentally in terms of fractal geometry. The structure of CRL 1606/PLH flocs was investigated and found to follow the power law correlation required of fractal theory. The fractal dimensions found were in general agreement with theoretical and experimental literature data. The flocs show increasing fractal dimension with decreasing polymer dose and increasing shear, indicating that floc rearrangement or "survival of the densest" governs fractal structure in these systems.

In addition to the experimental study of floc structure, theory was developed to describe the frictional properties of a fractal cluster in the intermediate floc size range between very small clusters and very large, non-draining clusters. The theory states that the friction coefficient will follow a power law dependency on the floc size; the power law exponent will take on values dependent on the fractal dimension of the floc. The relation between the exponent and the fractal dimension is a universal one, and this relation is approximated in the form of a polynomial series expansion. The friction theory was applied to correct assessment of floc properties, specifically the floc sedimentary velocity versus size. Examination of literature porosity versus sedimentation velocity data indicates that the literature correlations change significantly when the increased frictional properties of a fractal cluster are accounted for. Recalculated fractal dimensions of both microbial and inorganic flocs from the experimental literature more closely follow those expected from theoretical literature.

The results of the experimental and theoretical suspension dynamics characterization form the basis for an analysis of flocculation optimization for animal cells. The results were employed in an aggregative population balance solution for a monodisperse suspension. The optimal conditions of polymer dosage and hydrodynamic environment for flocculation can be specified for a given set of constraints on the cell viability and sedimentary velocity enhancement.

Thesis Supervisor: Prof. Daniel I.C. Wang
Chevron Professor of Chemical Engineering
Professor of Biochemical Engineering

TABLE OF CONTENTS

ACKNOWLEDGEMENTS

☞ AthesiswithoutanacknowledgementsectionislikeafishstickwithoutCheezWhiz®.

I would like to thank all of the people who have aided me in this thesis, and made my life at M.I.T. an enjoyable experience. Here we go.....

My thesis advisor, Daniel I.C. Wang, has been a source of guidance and inspiration throughout my stay at M.I.T. I will benefit from his advice for years to come. I also thank Dr. Kenneth J. Himmelstein, who first introduced me to research as an undergraduate Jayhawk, and who encouraged my development and entrance to graduate school.

My thesis committee, Professors C.K. Colton, C.L. Cooney, R.F. Probstein, and A.J. Sinskey, have helped shape this thesis into a work I am proud of. I would especially like to thank Dr. Probstein for being a source of insight and information in the field of physicochemical hydrodynamics. I have profited greatly from his teaching and suggestions on the course of this research. The work presented in chapter 7 of this document is to me a serendipitous bonus which is largely due to his encouragement.

I thank the many people who have helped me directly with thesis work. First of all, Professor Manuel J.T. Carrondo for his help on the last stages of this thesis. He has been a superb source of encouragement and debate. I hope to maintain a friendship with him, his son André the giant, and his wife, Professor Maria Arménia Abreu Fonseca de Carvalho Teixeira Carrondo (say that five times fast!) across an ocean. Next, the UROP and REU students who have worked on this thesis and related projects: Jean Lee, Mike O'Brien, Maria Kang, Tim Hale and Sandra Terauds. I also acknowledge a debt to Dr. Pedro Bolsaitis for the use of his electrophoresis equipment, and to Professor Regina M. Murphy, for her assistance with quasielastic light scattering measurements.

The graduate chemical engineering class of '83 at M.I.T., my lab and office mates, and fellow BPECers as a whole (and assorted companions) have been a right rowdy crew,

there when you need 'em, and there when you don't. I have made many friendships among you I will keep for a lifetime. These thanks are for jolly, rollicking, madcap antics in the lab and in the office, at the Muddy, at TG's and parties, on the intramural fields, pools, and ice, at the beach, on the ski slopes, on road trips, in Atlantic City, at conferences, in the bathtub... I have also been fortunate to have and keep many other good friends, in some cases a continent away: Al, Bryan, Carolyn, Chris, Herb, John, Jono, Julio, Kip, Olga, Sandy and Sharon.

I thank my family for their support over the years. Thanks to my parents, who have instilled their values in me. Thanks to my siblings, who have been a pleasure to whack on, and a greater pleasure not to whack. To my grandparents, who have taught me the virtue and pleasure of hard work, and good humor.

My - my - fiancée, Anne Michele Hammons, has been a source of joy and friendship for the last three years, and I trust will continue to be so for many years to come. That's no lady, that's my duck!

Lastly, I thank the institutions which have provided support and facilities throughout this research. The National Science Foundation, for a graduate fellowship and creation of the Biotechnology Process Engineering Center. Biogen Research Corporation, for providing facilities and a pleasurable research experience early in my stay at M.I.T. Mediatech Inc., for providing culture supplies.

"So this guy walks into Merck with a beaver on his head, and..."

GLOSSARY

Aggregate	An assembly of single particles forming a cohesive single structure.
Aggregation	The process of aggregate formation by collision of single particles with aggregates, or by collision of aggregates with other aggregates.
Cluster	see Aggregate.
Coagulant	A substance promoting aggregation, usually a soluble, simple ion. Some hydroxide complex-forming ions are also classed as coagulants. see Flocculant.
Coagulation	Aggregation induced by the action of simple ions.
Floc	see Aggregate.
Flocculant	A substance promoting aggregation, usually polymeric. see coagulant.
Flocculation	Aggregation induced by the action of polymeric flocculants.
Fractal	An aggregate produced by random particle addition that exhibits a structure which is invariant on a change of length scale.
Orthokinesis	Bulk fluid motion induced particle transport. Orthokinetic flocculation describes fluid motion induced aggregation.
Perikinesis	Thermally induced particle transport. Perikinetic flocculation describes Brownian motion induced aggregation.
Primary particle	The smallest unit comprising an aggregate. In the case of cellular aggregation, single cells.

NOMENCLATURE

Roman Symbols

a, a_i	particle or cluster radius
a_g	limiting cluster radius in equation (3-34)
a_{pol}	characteristic polymer (flocculant) radius
a_{32}	Sauter mean particle radius
b	characteristic particle spacing in equation (3-46)
c	constant in equation (3-49)
c	radial particle (segment) concentration within a cluster
c_i	coefficient in equation (7-6)
c_o	particle (segment) concentration at the cluster center
d	particle or cluster diameter
e	electron charge
g	gravitational acceleration
i	number of particles per cluster
i_{max}	maximum number of particles per cluster
k	structural constant in equations (3-30), (8-6)
k''	structural constant in equation (3-33)
k_b	Boltzmann's constant
k_f	friction constant in equation (7-3)
$k(\lambda)$	constant in equation (3-13)
m	number of interacting sites in adhesive mode
n	number of interacting sites
n_i	number of interacting sites in the Hogg collision model
r	radial distance
$\bar{r}$	average collision size ratio
t	time
w	exponent in equation (6-2)
x	exponent in equation (6-2)
y	empirical constant in equation (3-39)
z	exponent in equation (6-2)
z_p	excess surface charge due to polymer adsorption
A	London-Hamaker constant
A	constant in equation (3-10)
A	ammonia concentration in equation (5-1)
A_s	particle surface area in equation (3-3)
B	constant in equation (3-10)
C	constant in equation (3-39)
C, C_b	particle concentration, bulk particle concentration
C_A	dimensionless parameter describing London-Van der Waals force magnitude relative to viscous fluid force magnitude
C_D	particle drag coefficient
C_{RA}	dimensionless parameter describing electrostatic force magnitude relative to London-Van der Waals force magnitude
C_S	dimensionless parameter describing steric force magnitude relative to viscous fluid force magnitude
C_w	wall particle concentration in equation (1-3)
D	polymer dose in equation (6-14)

D	fractal dimension (Hausdorff dimension)
D_f	friction exponent
D_W	particle trajectory dimension
G	glutamine concentration in equation (5-1)
H_{min}	minimum normal distance between particle surfaces
I	medium ionic strength
J	particle, fluid flux per unit surface area
K	medium dielectric constant
$K_{S,o}, K_A, K_G, K_L$	Monod constants for serum, ammonia, glutamine and lactic acid in equation (5-1)
L	channel length in equation (1-3)
L	lactic acid concentration in equation (5-1)
L	diffusion path length in equation (6-18)
N	particle number concentration
N_A	Avogadro's number
N_i	number concentration of i-sized particles
N_{ij}	number of interacting sites in the Deason collision model
N_o	Initial particle number concentration
N_{tot}	Total primary particle concentration
P	polymer concentration
P_o	initial polymer concentration
Pr_i	probability of event i occurring
Pe	particle Peclet number
Q	scattering parameter
Re	particle Reynolds number
S	serum concentration
T	absolute temperature
T_{steric}	dimensionless ratio of time constants in equation (6-19)
Ta	Taylor number
U, U_{term}	terminal particle/cluster velocity
U_o	primary particle terminal velocity
V_{10}	number mean particle volume
V_r, V_θ, V_ϕ	spherical coordinate system velocity components
Y	parameter in equation (3-43)

Greek Symbols

$\alpha_{i,j}$	collision efficiency of i and j-sized particles
$\beta_{i,j}$	collision frequency of i and j-sized particles
χ	exponent in equation (3-13)
ε_i	intrafloc porosity
ε_o	free-space dielectric permittivity
ϕ	fraction of active adsorption sites in equation (3-26)
ϕ_i	intrafloc particle volume fraction
$\dot{\gamma}$	fluid shear rate
η	fluid dynamic viscosity
φ	constant in equation (5-1)
κ	reciprocal Debye layer thickness in equation (3-27), (3-28)
κ_i	permeability of an i-sized cluster
λ	characteristic retardation wavelength in equation (3-13)

λ	correlation exponent for floc porosity in equation (3-30)
λ_o	cluster draining parameter in equation (3-46)
μ	cell growth rate
μ_{max}	maximum cell growth rate
ν	fluid kinematic viscosity
θ	fractional surface coverage of particle with flocculant
ρ_{liq}, ρ_l	fluid density
ρ_{cell}	cell density
σ	particle surface charge density
σ	structure dependent friction constant in equation (3-49)
σ_o	particle surface charge in the absence of flocculant
τ_{diff}	characteristic diffusion time
τ_{max}	maximum collision lifetime
τ, τ_3	characteristic flocculation time
ϖ	angular velocity
ω	dimensionless parameter in equation (3-42)
ξ	inverse relative cluster permeability
ψ_o^o	particle surface potential in the absence of flocculant
ψ_o	particle surface potential
ζ	single particle friction coefficient
Φ	particle/cluster volume fraction in suspension
Θ	dimensionless time

Script Symbols

$f(i)$	friction coefficient of a cluster with i particles
$\mathcal{D}$	particle, molecular diffusivity

Odd Symbols

$\mathbb{Z}_{steric}$	dimensionless ratio of time constants in equation (6-19)

1. - INTRODUCTION

1.1. - Motivation for Study

Animal cell cultures have been found to be a necessary technology in recent years, as complex proteins have been discovered which are difficult to produce in a functional form in bacteria or lower eukaryotes. Although animal cell cultures are currently more expensive and difficult to operate than bacterial cultures, they are gaining popularity for production of a range of protein products, mainly for therapeutic use in medicine. In order for many of these proteins to be useful, they must possess the correct three-dimensional conformation, and often need to be glycosylated to elude the immune system's defenses and maintain a useful serum half-life. Bacteria often produce denatured proteins, which must be refolded to be functional. Lower eukaryotes, plant and insect cells can properly process and fold mammalian proteins, but these cells glycosylate the protein incorrectly. It remains to be seen how important glycosylation will be to the majority of therapeutic proteins.

The motivation for the work in this thesis is a desire to improve the productivity of animal cell cultures. Although bacteria and lower eukaryote cultures do not give high yields of correctly produced protein, overall culture productivity is high, and technologies are being developed to refold and modify proteins *in vitro*. Thus, even with low yields of active protein, bacterial cultures may be competitive with animal cell cultures. In order to produce complex proteins more economically, one can either pursue modification of the protein after its manufacture, or one can improve the productivity of cultures which produce the correct form.

Although there are many advanced methods of animal cell production under study, a common industrial method for animal cell cultivation is the stirred tank in batch suspension culture. The major problem of these cultures is the low volumetric productivity, due to the low amount of cell mass, or "catalyst", attained in a batch culture.

Where bacterial cultures operate at one to one hundred grams of dry cell mass per liter of culture volume, batch suspension cultures of animal cells operate at about 100 milligrams of dry cell mass per liter, with correspondingly lower productivity. The low cell mass is in turn due to the low yield of cells per volume of medium. In order to increase productivity of the protein of interest, it is desirable to recycle the cells in order to increase biomass loadings in the reactor. Increasing cell loadings in animal cell reactors has several beneficial effects. First, the productivity per reactor volume increases, so capital equipment costs may be decreased. This is important not only from an economical standpoint, but also from the view of culture sterility, which can be problematic in large scale animal cell cultures. Second, it has been observed that as cell concentrations increase to near physiological densities, the need for expensive medium supplements, *i.e.* - serum and defined hormonal constituents, decreases since the small amounts of growth factors produced by cells are no longer diluted by vast amounts of culture liquid per cell. Third, cultures at higher concentrations tend to exhibit lower growth rates, which are associated with product formation in some cases, especially antibody production by hybridomas (Boraston, 1987).

1.2. - Criteria for Cell Retention and Examples

There are several criteria which an animal cell retention scheme must meet in order to be technically feasible. The retention scheme must be an aseptic operation, it should be simple, economical, and it should be non-toxic to the cells. Animal cell cultures grow at a much slower rate than bacterial cultures, and are thus extremely vulnerable to contaminations. A principle goal of animal cell culturing is to be as simple as possible, in order to ensure asepsis. The retention scheme should be inexpensive, both in operation and capital costs, since the goal of the retention is ultimately to make the process more profitable. Last, the retention scheme should be nontoxic to the culture. Animal, insect,

and plant protoplast cells are notoriously fragile in culture due to their lack of a cell wall and intolerance of physiochemical conditions outside the realm of physiological. The process should not cause loss of a large fraction of cells, since the purpose of a retention scheme is to keep viable cells. Several examples of cell retention schemes, their advantages and drawbacks are given below.

1.2.1. - Centrifugation

Centrifugation of animal cells has been used for cell recycle in several studies (Schönherr *et al.*, (1979)), and is perhaps most widely used in the separation of blood components. Centrifuges allow rapid cell-medium separation and have low residence times, keeping the cells away from culture conditions for the minimum time possible. Early attempts at suspension cell centrifugation, however, showed that high speed centrifuges cause large amounts of cell lysis, due either to fluid heating or to high shear zones generated in the centrifuge (Zoletto, (1985), Pay *et al.* (1985)). This has been improved to some extent by the use of low speed centrifuges. In addition to being lethal in some cases, centrifuges also possess rotating seals, which can be difficult to maintain aseptic over long periods. This difficulty discourages continuous medium exchange using centrifugation.

1.2.2. - Filtration

Microfiltration is an alternative to centrifugation for rapid cell-medium separation, and has gained popularity in recent years (Brown and Abdul Salam (1984), Kroner and Nissinen (1988)). Ultrafiltration has also been utilized since it may allow retention not only of cells, but also of large molecular weight growth factors essential for cell growth, reducing the requirement for these factors. However, filtrate flux is severely affected by cell and macromolecule buildup at the membrane face, known as concentration polarization.

This becomes especially problematic when cell concentration is increased to high levels in the reactor. Filtration devices used for cell recycle rely on hydrodynamic phenomena to reduce cell and protein buildup at the membrane surface. Tangential flow filters use a high speed flow parallel to the membrane to reduce cell buildup. Spin filters are cylindrical membranes which are rotated to produce Taylor vortices at the membrane face, reducing cell buildup. These filters must be carefully designed, however, to strike a balance between the amount of wall shear necessary to keep the membrane clean, and the amount which causes cell lysis.

1.2.3. - Immobilization

Although many immobilization schemes may be classed as entirely novel approaches to cell culture, or as methods for providing anchorage dependent cells a growth surface, others may be viewed as simple methods of retaining cells in a stirred tank reactor.

The classic example of cell immobilization is microcarrier culture. Van Wezel (1967) immobilized cells on Sephadex G50™ anion exchange resin, enabling anchorage dependent cells to grow in suspended culture. Although the cell growth requires a surface, the microcarrier beads also serve as large particles (200 μm diameter) with high sedimentary velocities, enabling them to be retained in culture by simple gravity sedimentation or slow speed spin filters (Feder and Tolbert, 1983).

Entrapment and encapsulation of animal cells have extended the concept of microcarriers to create particles which have cells growing internally, as opposed to externally, on the carrier (Lim and Moss, (1981), Nilsson *et al.*, (1983), Karkare *et al.* (1985)). This has two benefits. First, higher per particle cell loadings are possible than in microcarrier culture. Second, the cells are protected from fluid forces which cause cell lysis (Croughan (1988)). These processes are somewhat limited by the inconvenience of

initial generation of the particles, and the fact that diffusion limitations into the particle may play a role when the cells grow to fill the particle.

1.2.4. - Gravity Sedimentation

Gravity sedimentation is employed with larger cell immobilization particles, and has also been employed with large-scale suspension cell cultures to effect cell recycle (Radlett *et al.* (1985), Zoletto (1985)). Gravity sedimentation is attractive due to its simplicity. In essence, a sedimenter is a unit filled with closely spaced plates to minimize the distance through which the cells must fall to be separated from the medium. The capital equipment cost is low, with no seals, or immobilization procedures to follow. The drawback to sedimentary processes is the speed of the separation. Animal cells are very small, almost neutrally buoyant particles, and settle with a velocity on the order of centimeters per hour. It is thus necessary for large cultures to sediment the cells for a considerable length of time. This in turn necessitates the supression of cellular metabolism to minimize cell death in the quiescent environment which is oxygen and nutrient deficient (Radlett *et al.* (1985)). The alternative is to use sedimentation only on those cultures which naturally form aggregates in culture (Feder and Tolbert, 1980) and thus possess rapid sedimentary velocities and short sedimenter residence times.

1.3. - Aggregation of Cells and Cell Retention

The efficiencies of sedimentary and filtration processes for cell-medium separation are dependent on the nature of the particles being separated, particularly the particle size. The primary particle size is fixed as the size of a single cell; however, the effective particle size is changed when the cells form aggregates, or flocs. Aggregation beneficially affects the separation processes outlined above which have been used in animal cell recycle. The following sections outline the positive effects that cell aggregation has upon separation.

1.3.1. - Sedimentation and Centrifugation

For sedimentary or centrifugal separation processes, the ease with which the cells may be separated is dependent on their sedimentary velocity. For a spherical cell, terminal velocity is given by the Stokes-Einstein equation:

$$U_{term} = \frac{2a^2(\rho_{cell} - \rho_{liquid})\, g}{9\eta} \qquad (1\text{-}1)$$

where the particle Reynolds number is low:

$$Re = \frac{U_{term}\, a\rho_{liq}}{\eta} << 1 \qquad (1\text{-}2)$$

In these equations, U_{term} is the terminal particle velocity, a is the particle radius, ρ_{cell} and ρ_{liquid} are the cell and medium density, g is gravitational acceleration, and η is the fluid dynamic viscosity. The sedimentation velocity is dependent on the particle size squared, so moderate increases in the hydrodynamic radius of the particle result in large increases in the settling velocity. In practice, flocculated particles will not follow the Stokes-Einstein law. This is because the aggregates formed in flocculation are porous structures which have neither the buoyant density nor the friction coefficient of a sphere. Nevertheless, increases in particle size will still lead to greater sedimentary velocities.

1.3.2. - Filtration of Particles

Until recently, filtration of particulate suspensions has largely been an empirical science. Zydney and Colton (1986) found from dead end filtration studies on red cell suspensions that the flow resistance from a cell monolayer is sufficient to reduce fluid flux in tangential flow microfiltration of blood. These researchers viewed the problem as being much like a concentration polarization phenomenon in ultrafiltration. In this case, transmembrane pressure drives the cells toward the face of the microfilter. In concentration polarization of macromolecules, Brownian diffusion balances the flow of molecules toward

the membrane. In the polarization of particulates, a shear induced motion of the particles akin to a Brownian random walk causes the cell layer to equilibrate. The equation developed to describe the liquid flux was:

$$J = .078\left(\frac{a^4}{L}\right)^{1/3}\dot{\gamma}\ln\left(\frac{C_W}{C_B}\right) \qquad (1\text{-}3)$$

Here, J is the length averaged fluid flux per unit membrane area, L is the channel length, $\dot{\gamma}$ is the wall shear rate, and C_W and C_B are the wall and bulk particle concentrations. It is seen that the transmembrane fluid flux is proportional to the particle radius to the 4/3 power. For an aggregated suspension, where the particles are not able to pack efficiently at the membrane face, the flux will be enhanced further than this relation would predict (Henry (1972)). Hence, like the sedimentary velocity, filtration properties of a cell suspension will be strongly dependent on the particle aggregation state.

1.4. - Scope of Thesis

From the discussion in section 1.3, it is evident that cell aggregation is a useful concept in cell recycle. However, many types of animal cells do not normally form aggregates in suspension culture, and there are currently no methods available to induce cellular aggregation. The purpose of this thesis then is to induce and examine the aggregation of animal cells in suspension culture.

The thesis is conveniently divided into two parts. The first goal of the thesis is to invent a flocculation system which allows cell aggregation and cell-medium separation while retaining cell viability and productivity after the flocculation process. Previous investigations into cellular flocculation are reviewed in Chapter 2. The specific goals of this portion of the thesis are also formulated in this Chapter.

The second goal of the thesis is to characterize the kinetics of flocculation and the structures produced by flocculating animal cells. As mentioned in section 1.3.1,

aggregates of cells do not possess the same transport characteristics as smooth spheres of equal size. In addition to this difference, in order to characterize suspension properties, the knowledge of aggregate properties versus the degree of aggregation must be known, as well as the degree of aggregation versus flocculation conditions and time. Previous work on flocculation kinetics and floc properties is reviewed in Chapter 3. The specific goals of flocculation kinetics and structure characterization are also formulated in this Chapter.

2. - REVIEW OF NON-SPECIFIC FLOCCULATION OF CELLS

2.1. - Colloidal Stability

There has been considerable theoretical attention to the stability of colloidal systems over the years, giving rise to fundamental explanations of many aspects of suspension behavior. These theories are straightforward developments of the physical concepts of intermolecular attraction and repulsion as applied to colloidal particles. The mathematics underlying the theory will be omitted here; these developments are available in standard texts on colloidal science (Hiemenz (1986), Israelachvili (1985)). In essence, intermolecular attractions serve to bring colloidal particles together. Intermolecular repulsions serve to keep particles apart. The net free energy change caused by bringing the particles together determines the thermodynamic stability of the suspension under given conditions.

There are two attractive forces between colloidal particles; London-Van der Waals forces and hydrogen bonds. London-Van der Waals forces arise from the induced dipoles which occur between molecules in the opposed bodies. One can calculate the strength of the induced dipoles and integrate over all the molecular pairs in each body to obtain the net attractive force between the particles. Although intermolecular attractions are normally thought of as short range forces from the Lennard-Jones six-twelve potential, integration between macroscopic bodies results in a force which decays as the square of the distance between surfaces (for opposed spherical surfaces; for opposed plates, the decay is inversely proportional to the separation distance). The typical length scale for the interactions with water as the dielectric medium is 100 nm. Hydrogen bonds between surfaces are much shorter range; these require dipole groups to be brought within a range of 0.2 to 0.5 nm, and require alignment of the chemical bond axis to establish attraction. Once established, however, hydrogen bonding is responsible for very strong attraction between surfaces.

Repulsion between particle surfaces is caused by two separate effects, electrostatic charge, and steric hindrance. Electrostatic repulsion is caused by fixed charge groups at the surface of the particles. In a dielectric medium, these charges set up a counter-ion gradient in the medium known as the diffuse double layer (why it's called a double layer is obscure; the diffuse part is only one of two ionic layers). This gradient decays exponentially with distance from the surface of the particle, on a scale known as the Debye layer thickness. This thickness depends on the concentration, diffusivity and valency of the counter-ions to the surface charge; in cell culture medium, the Debye layer thickness is on the order of 0.8 nm. Steric hindrance is caused by the presence of macromolecules on the particle surface; it arises when the distance between particles is small enough such that the macromolecular chains on opposing surfaces tangle with one another. This limits the possible configurations of the macromolecular chains, thereby decreasing their entropy. In the absence of an attractive energy between the chains great enough to overcome the entropic effect, the net free energy of the process is negative and the suspension is stable. The range of steric effects is limited to the distance the macromolecules protrude from the surface of the particle, around 100 nm.

In addition to steric repulsion between surfaces, there may also be steric attraction between surfaces. The first kind of steric attraction is due to bound surface macromolecules. When the solvent for the macromolecules is poor, the enthalpy change for association of macromolecules with themselves may be large enough to overcome the entropic decrease from configurational restriction, and produces a net free energy decrease upon surface association. The second kind of steric attraction comes from suspended macromolecules. When particles surfaces are closer than the characteristic dimension of the macromolecules, it becomes favorable for the molecules to escape the entropic confinement of the gap. This induces an "unmixed" region in the gap, and it is then energetically

favorable for the two surfaces to come together and remix this fluid with the fluid outside the gap.

Flocculants act to modify either the surface of the particle, or the surrounding medium such that the net force is an attractive one. Attractive forces can be altered by changing the dielectric constant of the surrounding medium, or adding molecular species which enhance surface attraction. Macromolecules which have multiple hydrogen bonding moieties can be added which provide long range hydrogen bonds between surfaces. Ions can be added which screen the charge of the surface and reduce the electrostatic repulsion between surfaces. These ions may adsorb specifically to the surface. Medium conditions can be adjusted such that the surface charges are neutralized. Macromolecular ions, or polyelectrolytes, can be added which adsorb strongly to the surface and render the net charge of the particle neutral. Lastly, the surface can be treated or the medium properties changed to promote cleavage or desorption of macromolecules providing steric hindrance.

It will be noted that the net force will be a function of the distance between particles; where the force may be attractive at large distances, it can be repulsive at shorter distances before becoming attractive again at extremely short ranges where the London-Van der Waals and hydrogen bonding forces are strong. This distance dependency gives rise to minima and maxima in the energy between particles, depending upon the magnitude of the different forces. In situations where macromolecules are present, configurational and mixing entropies and enthalpies will also be functions of the separation distance. The goal of a flocculation process is to drive the particles into an energy minimum where they will experience a positive force strong enough to establish stable aggregation. To complicate the prediction of colloidal stability, the force between static particles is not sufficient to describe the kinetic stability of the suspension, which will be a function of particle and medium motion. Kinetic aspects of colloidal stability will be discussed in Chapter 3.

2.2. - Cell Surface Properties

Although some cell lines exist as aggregates in culture (Tolbert *et al.*, (1980)), many do not. Natural cellular adhesion is a subject of intense interest for the study of differentiation, development, and cancer, however it will not be discussed here. This review will address induced flocculation in those cell types which do not normally form large aggregates.

It is well known that animal cell surfaces are negatively charged. This is mainly due to sialic acid residues present on cell surface glycoproteins, although membrane phospholipids and glycolipids may also contribute to cell surface charge (Alberts *et al.*, (1983)). It is also known that many transformed cells, in particular virally transformed cells, possess more negative surface potentials than their untransformed counterparts due to increased sialylation of surface proteins (Forrester (1965), Warren *et al.*, (1972)). Cells in suspension culture are almost invariably transformed naturally, virally, or by recombinant DNA introduction. These cells exhibit anomalous adhesion compared to their normal counterparts. They often adhere less strongly to themselves (homotypic adhesion), and more or less strongly to other cells (heterotypic adhesion) and culture surfaces (Elvin and Evans (1984)) than their non-transformed analogues. Decreased homotypic and heterotypic adhesion are due to modification or absence of adhesive receptors, or adhesion protein expression (Darnell *et al.*, (1986)). They are probably also influenced by cytoskeletal changes and anchorage of structural proteins at the membrane. In addition, the increased surface charge and steric modifications to surface proteins may also play a role. There is evidence that surface glycoproteins or proteoglycans may cause steric effects between cells, and thus prohibit close approach to one another (Grieg and Jones (1976)). Despite a lack of specific adhesive mechanisms, modified cells may still adhere by non-specific mechanisms; in particular, the absence or minimization of surface charge is generally observed to destabilize cell suspensions.

2.3. - Flocculant Screening Approach

Over the past several decades a battle has been waged over competing mechanistic theories of microbial and animal cell adhesion and aggregation to form structures and tissues. The biophysical argument has held that cells are essentially identical to nonliving lyophobic colloids, and that the physical laws pertaining to aggregation and dissociation of colloids should also be applicable to cells. The contact hypothesis, or biochemical argument is that since cells possess the means to select their association with their surroundings there must exist highly specific biological (macro)molecules which perform these duties. Experiments and theoretical developments have been performed to prove both ends of the argument. Under a given set of circumstances, either side may be correct. The following provides an outline of the arguments and the likely situations existing in nature. This will hopefully lead the reader to the search rationale chosen for the flocculation inducing agent for animal cells.

2.3.1. - Biophysical Theory of Cell Adhesion

The adhesion of cells (microbial or animal) is not a well understood process from a physical standpoint. Through the 1960's and 1970's, civil engineers and biophysicists attempted to explain the natural and induced adhesion of cells based on the theories of lyophobic colloids. Many studies were devoted to explaining the adhesive properties of cells based on concepts of colloidal stability (Mill (1964), Curtis (1967), Parseghian and Gingell (1972), Calleja (1974), Bongrand and Bell (1984)). Experimental observations of induced aggregation of cells showed many of the same trends expected for inactive colloids. Flocculation of microorganisms was observed to be maximal when cell electrophoretic mobility approached zero. Coagulation by soluble ions was shown to follow the Shulze-Hardy rule in several instances. Theoretical calculations of electrostatic repulsion, Van der Waals attraction and steric repulsive forces predicted experimentally observed separation

distances between cells. The mass of *in vitro* results suggested that aggregation behavior could be described in terms of colloidal theory. However, it was difficult for colloidal theory to progress past the approach of geometrically well-defined surfaces, or to take into account local inhomogeneities in surface composition. Both issues definitely arise with living cells in natural adhesion and aggregation. Nevertheless, physical principles are still useful to predict non-specific destabilization of biological suspensions, such as flocculation of microorganisms in water and wastewater treatment processes (Tenney and Stumm (1965), Harris and Mitchell (1973)), and adherence of microorganisms to surfaces (Marshall (1985)).

2.3.2. - Biochemical Theory of Cell Adhesion

Beginning with investigations on sponge cell aggregation in the 1950's, add-back experiments to suspensions of cells suggested that there were specific, although unidentified molecules responsible for cellular aggregation. These observations gave rise to the "contact hypothesis", whereby lock-and-key receptors and ligands were responsible for cellular aggregation. Although the biophysicists' arguments initially appeared to be correct, more elegant experiments by biochemists, advanced knowledge of cell structure and identification of adhesion molecules has made the contact hypothesis a virtual certainty for naturally occurring adhesion. Recent findings make clear that natural cell adhesion is usually mediated by specific adhesion molecules both in bacterial and animal cell systems (Calleja (1984), Duband and Thiery (1984), Roos (1984)). Adhesive molecules such as fibronectin and laminin have been characterized down to the level of their amino acid sequence and tertiary structure. The identification of domains that are the recognition elements has also been achieved (Pierschbacher and Ruoslahti (1984a,b)).

2.3.3. - Generalities of Cell Adhesion

The adhesion of a cell to a surface or another cell is actually a complex series of events dependent on the cell state, and physical and chemical conditions. In order for a cell to adhere to a surface, it must first approach the surface to a distance within which it can initiate contact. Long range colloidal forces and the force with which the cells are brought together will govern whether the approach takes place, and how close it will be. Even if the distance is large, biological events may cause adhesion. If the cell is of microbial origin, contact may be initiated by a pilus, fimbria or other organelle which protrudes from the surface. If the cell is of animal origin, pseudopodia can protrude from the surface to establish local contact in the face of total forces unfavorable for adhesion. Once the initial contact is established, lock and key bonding of receptors and adhesion molecules may take place on the surface, strengthening the attachment and pulling the rest of the cell surface into intimate contact. Additionally, random fluid or Brownian motion can move the cells close enough to establish contact. Depending on the experimental design, all or some of the events above may occur, giving results confirming biochemical or biophysical theory. The contact hypothesis is almost certainly correct in natural adhesion phenomena, but is not necessarily operative in many of the experiments with cultured cells or systems which do not normally exhibit adherence. Animal cells which do not adhere to themselves or substrate may have lost the ability to form pseudopods, or may have altered or missing adhesive molecules or receptors. The culture medium or cell surface properties may weaken or eliminate the possibility of some adhesion mechanisms.

2.3.4. - Flocculant Selection

In order to make sedimentation processes attractive, and to enhance centrifugation and filtration for recycle of non-aggregating cells, a flocculant must be employed to increase particle size. Assuming an absence or modification of natural adhesion

mechanisms, steric hindrance from cell surface polymers and a large electrostatic repulsion between membranes are mostly responsible for nonadherence of suspension cell lines. Manipulating the attractive and repulsive forces between the cells should destabilize the suspension. It might be possible to find biologically specific receptor molecules which are missing in non-adherent cells, and add them to the suspension. However, cells interact with extracellular adhesion molecules assembled in a spatially regulated architecture known as the extracellular matrix. This matrix structure is not present in suspension cultured cells. Due to the absence of an extracellular matrix, the diversity of mutations in non-adherent cells and a poor understanding of the dysfunctions of adhesion mechanisms, obtaining a natural flocculation system capable of aggregating a wide variety of cell types is a daunting task.

Several of the options for suspension destabilization discussed in section 2.1. are not feasible, for physiological reasons. For example, lowering pH to the isoelectric point of the cell surface (pH≈3.5; Grieg, Jones & Ayad (1976)) can eliminate electrostatic repulsion and promote aggregation of cells, but would also cause cell death. Changing the solvent, or the ionic strength (beyond a small range) is also prohibited. Utilizing enzymes or chemicals to cleave the charge groups from the cell surface may also render the cells nonviable, or undesirably modify the product protein. There are, however, several types of flocculants commonly used to modify or exploit particle surface properties on a non-specific basis. These may be broadly classed as ionic coagulants (*e.g.*, aluminum nitrate, calcium phosphate), polymeric flocculants (*e.g.*, polyethylenimine, polystyrene sulfonate), and colloidal particulate flocculants (*e.g.*, bentonite clay, polysilicates). These compounds are potential flocculants of animal cells and are discussed below as they have been investigated for microbial and animal cell aggregation.

2.4. - Ionic Coagulants

2.4.1. - Ionic Coagulation of Microbes

There is a large amount of literature dealing with ionic coagulation of microorganisms with respect to process operating conditions. In wastewater treatment systems coagulation by ions is due to the increase in medium ionic strength and subsequent compression of the electrical double layer between cells. It is usually observed that coagulation follows the predictions of DLVO theory. Rubin and Hanna (1968) described completely the stability diagram for *Escherichia coli* aggregated by aluminum nitrate. In acid solutions, soluble aluminum destabilized the suspensions, where at high concentrations and pH, aluminum precipitates caused flocculation. At the conditions where soluble ions mediated flocculation, the critical concentrations of sodium, barium and aluminum were found to follow the Shulze-Hardy rule. Northrop and DeKruif (1922) found that *Bacillus typhosus* was aggregated by cuprous, lanthanum, aluminum, mercuric, and thorium ions. These authors' data also support the idea that the critical ion concentration required for coagulation follows the Shulze-Hardy rule for ion valency when no specific adsorption of ions is present.

In animal cell culture medium, the ionic strength (approximately 0.15 M) is sufficiently high that compression of the electrical double layer between cell surfaces from additional ions is insignificant. Hence, destabilization will chiefly depend on whether the cells will selectively adsorb multivalent ions, thereby neutralizing the surface charge. There is ample evidence that microbial cell surfaces adsorb multivalent ions quite strongly and selectively. Many studies in microbial systems have focussed on the abilities of various organisms to adsorb heavy metal ions, with a view towards reducing cost of mining operations (Tsezos and Volesky (1981), Strandberg, Shumate and Parrott (1981), Horikoshi, Nakajima and Sakaguchi (1981)). Van Haecht, Bolipombo and Rouxhet (1985) immobilized yeast cells onto glass slides by adsorbing Al^{+++} ions to the cells at pH

4. The cells remained immobilized after washing, indicating specific binding. Optimal immobilization was obtained by treating the cells with aluminum until the electrophoretic mobility was reduced to zero. The adsorption and immobilization treatments had no effect on the specific uptake and production rates of glucose and ethanol, respectively.

It will be noted here that much of the literature concerning flocculation of microorganisms by ionic compounds is muddled by the fact that in the presence (or absence) of certain nutrient ions, microbial cells will acquire biologically driven flocculation capabilities. A classical example is the aggregation of *Dictyostelium discoideum* into a slug and fruiting body in response to starvation. Calleja (1984) has conducted an excellent review of nutritional factors influencing natural microbial aggregation. In animal cell systems, spontaneous biological flocculation is not usually ionically triggered, but is usually due to the presence or absence of hormones or organic nutrients which affect cAMP levels in the cells (Ballard and Tomkins (1970), Grinnell, Milam and Srere (1973)).

2.4.2. - Ionic Coagulation of Animal Cells

Cells of higher organisms have long been known to possess adhesion mechanisms which are dependent to some extent on the presence of multivalent ions, most notably calcium and magnesium. Calcium has been shown to be necessary for the aggregation of sponge cells into a coherent organism by cross-linking the "aggregation factor", a high molecular weight proteoglycan (Humphreys, Humphreys and Sano (1977)). In animal cell tissues *in vivo*, tight junctions and gap junctions between cells are controlled by the concentration of calcium (Staehelin and Hull (1978)). Apart from *in vivo* experiments, calcium, magnesium, and other ions have been shown to play a role in the adhesion of cultured cells to themselves and to culture surfaces. Manganese, magnesium, and calcium have all been shown to have effects on the adhesion of cultured cells to culture surfaces (Takeichi and Okada (1972), Okada *et al.* (1974), Maroudas (1975)). It is for this reason

that ionic chelating agents such as EDTA are able to assist in the detachment of cells from these surfaces.

In the study of Grieg, Jones and Ayad (1976), it was shown that both calcium and lanthanum ions lowered the electrophoretic mobility of CHO cells and P338 (mouse lymphoma) cells in an isotonic sucrose and sodium chloride mixture with an ionic strength of .0172 M. Although the calcium added decreased the double layer thickness, there was no evidence of specific adsorption and the calcium ions did not promote cell aggregation. Lanthanum ions were shown to adsorb specifically to the surface and to promote aggregation of the cells in suspension at concentrations above 10 μM. However, the conditions used were not representative of animal cell culture since the ionic strength was an order of magnitude too low and the pH was 5.5. Urushihara *et al.* (1976) investigated calcium and magnesium induced aggregation of BHK and polyoma virus transformed BHK (pyBHK) following dissociation with trypsin or EDTA. For trypsin dissociated BHK, aggregation occurred presence of 1 mM calcium, but not in the presence of 1 mM magnesium. For trypsin dissociated pyBHK, either 1 mM calcium or magnesium would cause aggregation. For EDTA dissociation, both cell types aggregated in medium free from either ion. Although the trypsin dissociated results suggest the presence of ion-dependent adhesion, the EDTA dissociated results are inexplicable in terms of lyophobic colloid theory. The authors suggest that the trypsin results may be explained by a metabolic requirement for divalent ions to replace digested proteins. No explanation was offered for the aggregation of EDTA treated cells in the absence of ions.

The results of the above experiments suggest that the addition of ions to cell suspensions may bring about the aggregation of cells. However, cell culture medium contains calcium and magnesium in millimolar amounts. It is not obvious whether suspension cells which do not aggregate under normal culture conditions will be affected by further addition of soluble multivalent ions. Investigation is needed to this end.

2.5. - Colloidal Particulate Flocculants

2.5.1. - Colloidal Aggregation of Microbes

Colloidal particles may be used to aggregate suspensions of other colloids in many cases. At its simplest, adding an oppositely charged colloid to the suspension results in an electrostatic attraction between flocculant and particle and aggregation takes place. In many cases where ionic coagulants are added to suspensions, the suspension milieu is such that the added ion converts to an insoluble hydroxide form, and precipitates out of solution. The precipitate, or "inorganic polymer" as it is sometimes called, retains a surface charge due to ion vacancies on the hydroxide complex. This surface charge is responsible for adherence to the particles of interest. In other cases, such as the addition of colloidal clays, the forces attracting the flocculant and particle are less well known although evidence suggests primarily ionic interactions. The particle sizes are usually as large or larger than the characteristic length of the Debye layer, and are thus able to "bridge" between double layers to effect flocculation.

Alum and ferric ions have long been used as coagulants in wastewater treatment. Under conditions of neutral pH, the aluminum and ferric ions form hydroxide precipitates. These directly flocculate the cells in the suspension. Rubin and Hanna (1968) found that aluminum nitrate coagulated *Escherichia coli* in regions where an insoluble hydroxide forms, in some cases entrapping the cells. McGarry (1970) reported flocculation of pond algae with aluminum sulfate at pH 5.5, where aluminum precipitates were obtained. Several authors (Tenney and Stumm (1965), Wu (1978)) have pointed out the importance of ferric or aluminum phosphate complex formation and precipitation in the flocculation and removal of both phosphorus and microorganisms from wastewater streams. Gasner (1971) showed that treating suspensions of *Candida intermedia* with bentonite, hectorite, sodium silicate, and ferric hydroxide hydrocolloids effected flocculation over a dose range from 0.006 to 0.2 gm/gm dry cell mass. This flocculation was achieved in fermentation

broths with an ionic strength of 0.12 M and pH 4. In the study of Van Haecht, Bolipombo, and Rouxhet (1985), it was found that $Al(NO_3)_3$ solutions which had been autoclaved formed precipitated $Al(OH)_x$ complexes which flocculated *Saccharomyces cerevisiae* cultures at pH 4. In these experiments ionic strength was not controlled. Weeks, Munroe and Spedding (1983) found that calcium carbonate, iron sand, iron oxide powder, and nickel powder (all 2 - 7 μm diameter) were able to flocculate *Saccharomyces cerevisiae* in distilled water, however, were unable to flocculate the cells in medium with high ionic strength and pH 4.5. Cycling the pH of the fermentation to 8.0 achieved the desired flocculation with the particles; Gasner and Wang (1970) also noted flocculation using only a pH change to 9.0. In the studies of Weeks, Munroe and Spedding, the flocculated cells were left viable for further fermentation usage. Gasner made no mention of cell viability.

2.5.2. - Colloidal Aggregation of Animal Cells

To date there have been no literature reports of colloidal particulate flocculation of animal cells. Avgerinos (1988) found that hybridoma cultures could be aggregated with bentonite clay. The flocculation was toxic to the cells, however, and the research was not pursued further. It is not known what conditions were used for the aggregation.

2.6. - Polymer Flocculants

2.6.1. - Mechanisms of Action

Polymeric flocculants are more effective than soluble ions at flocculating particles when they are able to adsorb to the particle surface directly and modify surface properties. These compounds have multiple opportunities to interact with the particle surface due to the many functional groups present on a single molecule. Although individual group association with the surface is in dynamic equilibrium, at any given time a fraction of the

functional groups will be adsorbed, and hence the whole molecule is adsorbed irreversibly (kinetically) on the particle surface. Polymer flocculants have been postulated to operate on three different bases: blanket charge neutralization, charge patch neutralization, and bridging. In blanket charge neutralization, an electrostatic polymer (polyelectrolyte) associates with charge groups on the particle surface, rendering the particle net neutral. In the absence of the repulsive electrostatic force, the suspension is destabilized. In patch neutralization, the polyelectrolyte does not associate one-to-one with the surface charge, but adsorbs with loops and tails protruding from the surface. The effect is to create a region of opposite charge where the polymer is adsorbed. This region is then attracted to uncovered, oppositely charged regions on other particles, causing flocculation. In bridging flocculation, the polymer (not necessarily an electrolyte) adsorbs to the particle weakly, again leaving unadsorbed loops and tails. These are assumed to protrude from the particle beyond the range of the repulsive forces. These unadsorbed segments are free to associate with other particles they may encounter, forming a bridge across electrical double layers or steric layers. Depending on the polymer and particle characteristics, all three of these mechanisms may be operative.

2.6.2. - Polymer Flocculation of Microbes

Polymeric compounds have been in use for flocculation of microorganisms in wastewater treatment for the past four decades. The application is so established that recent articles describing flocculant applications are scarce. There are comprehensive studies on flocculant polymer candidates by Hodge and Metcalf (1958), Tenney *et al.* (1969), McGarry (1970), Gasner (1971), Harris and Mitchell (1973), and Gutcho (1977) in the not too distant past. In general, any cationic polyelectrolyte will aggregate cells if the proper conditions are found, dependent on the charge density of the polymer, and the other ions present. This is a direct result of the negative charge of the cell surface. Nonionic and

anionic polymers have also been shown to aggregate cells. In general, co-flocculants, *i.e.*, multivalent soluble ions, are required to mediate aggregation when the flocculant and cell are both negative (Teot and Daniels (1969), McGarry (1970), Brossmer and Pfliederer (1966)). Although there is an immense literature dealing with the aggregation of microbes by polyelectrolytes, this will only be reviewed where it pertains to cell recycle or cell physiology.

Water and wastewater treatment applications of polymer flocculants are usually for the purpose of debulking excess microbial sludge for disposal. These treatments usually consider the flocculated cell mass to be waste material; for this reason, most studies are not concerned with the physiological effects on the cells. There are several instances, however, where microbial physiological response has been studied. Katchalski, Bichowski-Slomnitzki and Volcani (1953) investigated the effects of water soluble poly-α-amino acids on bacteria as a model for the antibacterial peptides of some fungi and higher animals. The authors found that poly-L-alanine, poly-L-glutamate, and poly-L-aspartate caused no agglutination of *E. coli* or *Staphylococcus aureus* up to 500 mg/L. They also were not toxic to the cells. Poly-L-lysine, poly-DL-lysine, poly-DL-ornithine, and poly-DL-arginine all caused growth inhibition from 5 to 75 mg/L, and cell death above 75 mg/L. The cells were aggregated in the presence of poly-L-lysine at concentrations from 10 to 40 mg/L for *E. coli*, and 10 to 50 mg/L for *S. aureus*. Above these concentrations the suspensions were restabilized and the electrophoretic mobility of the cells became positive. The bacteriostatic action of the basic polymers was reversible upon addition of an acid polymer in 1:1 ratio. D' Souza *et al.* (1986) immobilized *S. cerevisiae* by treating the cells with polyethylenimine for two hours before allowing them to adsorb onto glass slides. In this case, the authors noted no loss of viability of the cells. Jensen, Debusk and Debusk (1984) isolated a cationic polymer of D-galactosamine (pI ≈ 8.4) from *Neurospora crassa* which aggregated these cells. The polymer also caused leakage of low molecular weight

components from the cells and reduced cell viability up to 50% in two minutes. Inclusion of 1.2 M KCl reduced the lethality of the polymer; this was attributed to the fact that high ion concentrations screen the attraction of the negative cell surface to the positive polymer, weakening the association between the two. KCl addition also reduced the efflux of metabolites. Knorr and Teutonico (1986) found that immobilization of *Amaranthus tricolor* plant cells in chitosan (a polymer of N-acetylglucosamine and glucosamine) resulted in increased permeability of the cells to oxalate ion. The authors reported that viability of the cells during exposure was not a problem.

In addition to studies of microbial flocculation by polyelectrolytes, it has been shown that under selected conditions, anionic, nonionic, and cationic polymers can all aggregate animal cells. In contrast to the literature on water treatment, much of the literature deals not only with aggregative mechanisms but also cell physiological response.

2.6.3. - Polyanion Flocculation of Animal Cells

Although anionic polymers would not ordinarily be expected to associate with negative cell surfaces, there have been varying reports of the efficacy of polyanions at associating with and aggregating cells. Brossmer and Pfleiderer (1966) found that dextran sulfate and polyvinylsulfate aggregated erythrocytes in blood in the presence of calcium, but not with the addition of 0.1% EDTA. It was proposed that the calcium specifically adsorbed to the cells, and coordinated a bridge between the polymer and cell membrane. This mechanism for anionic flocculation of negative colloids has been proposed extensively in the literature (Teot and Daniels (1969)). No mention is made of cell physiology.

In recent patents, Kenney (1985, 1986) found that polygalacturonic acid ($pK_a = 3$) aggregated hybridoma cells in DMEM/5% serum at low pH with doses from 40 to 1000 mg/L. The patent claims a pH of 5 to 6 is optimal for aggregation, which occurs over the range from 4 to 7. The process of aggregation took 2 hours under the conditions used. It

was proposed that the cells become partially positively charged at the low pH region, and that the local domains of positive charge were complemented by the structure of the polymer. No aggregation was observed with dextran sulfate, polyvinylsulfate, poly-L-glutamic acid, alginic acid, or carrageenan. No mention is made of the treatment's toxicity to the cells. In contrast to Kenney's findings with hybridoma cells, Sirica and Woodman (1971) reported that no aggregation of mouse L1210 leukemia cells occurred upon treatment with polygalacturonic acid at 78 mg/L and pH 7.0.

2.6.4. - Neutral Polymer Flocculation of Animal Cells

Nonionic polymers might likewise be expected to be inefficient at aggregation of animal cells. However, neutral polymers are not subject to electrostatic effects as are anionic polymers. They may adsorb to surfaces via London-Van der Waals forces or hydrogen bonds, and bridge across the double layer to adhere to other particles. A key factor is the size of the polymer; since it does not neutralize or exploit the surface electrostatics, it must be large enough that it spans the effective repulsive distance between cells. The aggregation and disaggregation of erythrocytes by nonionic polymers has been a subject of interest in biomedical technology due to its implications for blood rheology in the use of dextran and other polymers as plasma substitute components. Knox *et al.* (1977) used viscometry to show that lower molecular weights of dextran promote disaggregation of red cell rouleaux, while high molecular weights enhance aggregation. Both Knox *et al.* and Jan, Usami and Chien (1982) report promotion of aggregation for dextrans with molecular weights greater than 40,000. The aggregation is not dramatic, however, and the bonding is fairly weak since it disappears at moderate shear rates. High molecular weight dextrans are inert and are not internalized by the cells. Since dextran does not apparently affect cell physiology at the doses required, the aggregation/disaggregation effect was proposed to be a colloidal phenomenon resulting from London-Van der Waals attraction or

hydrogen bonding of the polymer to the cell surface. Knox *et al.* speculated that the smaller molecular weights enhance the exclusion of shielding ions in the medium from between the double layers due to increases in the cell zeta potential in the presence of dextrans. Unlike the large molecular weight polymers, they do not extend from the cell surface sufficiently far to bridge across the double layer. Brossmer and Pfleiderer (1966) also investigated the effect of dextran, 2000 MW, and found no aggregation of erythrocytes in its presence.

2.6.5. - Polycation Flocculation of Animal Cells

Of all the polyelectrolytes, cationic polymers are most effective at flocculating cells, directly neutralizing the cell surface charge and/or bridging between cells. Polycations are the most widely used polymers in wastewater treatment and other flocculation applications, as most colloidal particles possess a net negative surface charge. There has been a fair amount of research on polycation mediated flocculation or immobilization of cells and the physiological effects of polycations on animal cells. As with the microbial literature, this review will confine itself to the studies where physiology or colloidal phenomena were studied.

In the 1950's and 1960's there was interest in the use of polycations as potential cancer therapy agents, due to the apparent selectivity of adsorption to more negative tumor cell membranes. In addition, there was interest in polycations as antibacterial therapeutics (see the review of microbial aggregation above). To this end, research was directed at polymer toxicity to tumor cells and the erythrocytes which would necessarily be exposed to the polymer. A. Katchalsky and co-workers, and E. Katchalski and co-workers published a series of articles in the late 1950's and early 1960's on polyelectrolyte properties and association with cells (DeVries *et al.* (1954), Nevo, DeVries and Katchalsky (1955), Katchalski and Sela (1958), Katchalsky *et al.* (1959)). The results of the findings are well

summarized in a review by A. Katchalsky (1964). These authors primarily worked with polylysine-erythrocyte systems, although polyvinylpiperidine, polyvinylamine and protamine sulfate were also used. It was found that polylysine adsorption to red blood cells could be fitted to a Freundlich isotherm, and that adsorption reversed the electrophoretic mobility of erythrocytes at high doses. Absolute levels of adsorption and the non-saturability of the isotherm suggested a weaker adsorption to cells than that observed for solid glass surfaces. Low molecular weight polylysine, MW 4,800, could be desorbed from the erythrocytes by addition of equivalent amounts of acid polyelectrolytes in the same molecular weight range. Agglutination of the cells occurred at "critical" surface potentials less than zero. The critical potentials observed were in the -7 to -11.4 mV, decreasing with increasing polymer molecular weight. Lower concentrations of polymer were also required as molecular weight increased, with thresholds from 1.7 to 0.3 mg/L. Electron micrographs of aggregated cells showed intermembrane distances on the order of 60 to 80 nm, equal to the length scale of the polylysine molecules. These results are consistent with the idea that agglutination occurs from patch neutralization/bridging phenomena.

The idea that electrostatic forces are responsible for nonadherence of cells was bolstered by the above studies, as well as the work of Deman and Bruyneel (1974). These authors found that addition of low molecular weight polylysine was unable to aggregate cells at low concentrations. It was hypothesized that the lower molecular weights were not able to bridge the double layers between cells until sufficient polymer had adsorbed to reduce the double layer. When the sialic acid residues on the cell surface had been removed by neuraminidase, reducing electrostatic repulsion, the low molecular weight polymers were able to produce aggregation at the lowest concentrations.

Ryser (1967) investigated the uptake enhancement of ^{131}I labelled albumin by S-180 sarcoma cells in the presence of polybases. He found that polymers of ornithine,

arginine, histidine and lysine, and DEAE dextran all promoted uptake of macromolecules at 3 mg/L, in direct proportion to their molecular weight. Extrapolation of an uptake enhancement versus molecular weight plot to zero enhancement suggested that the minimum necessary polymer size was an octapeptide unit. This is consistent with the idea that polymer adsorption to the cell surface is more efficient than small ion adsorption. Cytotoxicity was observed above 30 mg/L polymer concentration.

Sirica and Woodman (1971) showed that chitosan at pH 7.0 to 7.2 aggregated mouse L1210 leukemia cells at concentrations from 1.1 to 9.1 mg/L, but did not aggregate erythrocytes, bone marrow cells, Sarcoma 37 or Ehrlich ascites cells. Beyond 36 mg/L, chitosan induced aggregation of erythrocytes. At aggregative conditions for all cell types, the authors noted increased trypan blue permeability of the cells. The authors also tested polylysine and polyethylenimine in concentrations from 0.8 to 426 and 0.25 to 134 mg/L, respectively. Again, these polymers were found to cause cytolysis at conditions where aggregation was significant. The authors observed that in the presence of the polyanions heparin or polygalacturonic acid, threshold concentrations necessary to induce aggregation were increased approximately thirty-fold. In the presence of 33% serum, aggregation and cytolysis were blocked completely.

Larsen and Olsen (1968) incubated 10^6 cells of the leukemic tumor line NJA with 100 μg polyornithine or 1000 μg DEAE dextran from 5 to 60 minutes before injecting the cell suspensions into C3H/A mice, and monitored the fraction of mice surviving the tumor injection. The fraction of surviving mice increased greatly with incubation time, indicating that the cells had been either killed or immobilized and rendered unable to metastasize. Incubation of the cells for 60 minutes followed with heparin addition for 5 minutes resulted in death of all the injected mice. It was noted that 2 mg/L polyornithine was capable of inducing aggregate formation; addition of high molecular weight heparin did not disperse

the aggregates. Even though the aggregates were not dispersed, the heparin evidently enabled some cells to survive.

Whiteley and Galivan (1982) studied the enhanced cytotoxicity of methotrexate to rat hepatocytes and hepatomas when linked to polylysine polymers. Cytopathic studies on the carrier polymers alone showed greater than 60% viability up to 10 mg/L polymer for either poly-L-lysine or poly-D-lysine with either hepatocytes or hepatomas. The unique finding of the study was that above 10 mg/L, poly-D-lysine was extremely toxic to hepatocytes, where toxicity for poly-L-lysine or hepatomas was not nearly as great. This suggests that not only polymer and cell charge, but also polymer conformation can be important in non-specific aggregation systems.

Recently, Biesinger and Stokes (1986) investigated the effects of polyelectrolytes on several higher aquatic organisms: daphnids, fathead minnows, gammarids, and midges. The authors found that polyanions were nontoxic to the organisms tested, as well as nonionic polymers. Polycations showed LD_{50}'s from 0.13 to greater than 100 mg/L. The polymer species used were hidden in this study.

2.7. - Flocculant Identification and Characterization Goals

Flocculation of animal cells for recycle is a non-trivial problem. The cells must not only be aggregated, but they must also remain alive and in a functioning state to be of use in further production of the desired product. The literature is very confusing, and often appears contradictory. It has been found that typical commercial flocculants which are applicable to wastewater treatment are sometimes highly toxic to cells, while biological compounds known to promote cell aggregation sometimes affect only certain cell lines.

Considering the state of the literature, it is necessary to screen for suitable flocculants which will aggregate cells without regard to their origin or physiological state, yet leave the cells in a viable, growing state for recycle to a fermentation process. The goal

of the initial screening is to find a compound which will flocculate a variety of cell types, and which lacks acute toxicity, or immediate cell death. The search for a flocculant will employ the general surface properties of the cells rather than specific surface receptor molecules. Although the latter are more elegant, they may not lead to a flocculation system which may be employed on all cell types. In addition, many of the biospecific compounds known to flocculate cells are unavailable commercially, or are prohibitively expensive.

In a non-specific approach, a generic property of the membrane, such as its charge or hydrophobicity is used as the driving force for flocculant association and hence cell aggregation. The drawback to a generic approach is the effect of arbitrarily interacting with the cell membrane, which has important ramifications for cell physiology. Thus, an investigation of the effects of flocculation on cell health is important. The second goal of the screening and characterization is to define whether, in addition to a lack of acute toxicity, flocculation has undesirable chronic effects on cell growth.

There are no easy conclusions to be drawn from the survey of flocculation of biological colloids, as much of the information seems contradictory. The findings of the above studies may be summarized, however, and observations drawn which are relevant to the problem at hand, the viable flocculation of animal cells.

Studies of microbial and animal cells under ideal conditions show that ions may coagulate cells. In many instances this is due to ion precipitation or the increase in ionic strength of the medium. The former will be discussed below. Exploiting the latter is not a possibility for animal cells since medium composition is fixed at high ionic strength initially, and since animal cells are sensitive to changes in osmotic pressure. Specific adsorption of ions for flocculation is still a possibility, since this mechanism has been shown to aggregate cells. This possibility is remote, though, as culture medium already contains several of the cations shown to induce aggregation.

The flocculation of animal cells by colloidal particles has not been investigated in the literature, although these are frequently used to aggregate microbes. Anecdotal information from Avgerinos (1988) suggests that the method is effective for animal cell cultures, but his experiments showed poor viability after aggregation. This area deserves further research.

From the literature above, it is hard to predict the success of polymer flocculation of animal cells. Studies with anionic polyelectrolytes show that aggregation is induced only with specific systems. This will require screening polymers and co-ion combinations to find a system that operates for animal cells. The success of a system will largely depend on whether the cells will adsorb cations from the medium in order to link the anionic polymer and cell surface. There is a possibility that specific recognition of cell surface components by the polymer may occur, as suggested by the patents of Kenney (1985, 1986). Nonionic polymer flocculation may be possible, as shown by studies on erythrocytes; however, the aggregation induced by the polymer is weak, and requires large amounts of polymer. The practical drawback to this is that large polymer concentrations increase the viscosity of the suspension, decreasing the sedimentation velocity and filterability of the suspension. The weak aggregation may not manifest itself at the shear conditions necessary to flocculate the suspension expediently.

Polycation aggregation of cells will certainly be successful. The question with cationic flocculants is whether the aggregation will be toxic to the cells. The literature is conflicting on this point. Experiments with yeast and microbes suggest that either no growth inhibition occurs, or that the inhibition is reversible by addition of compounds which weaken cell-polymer interactions. Experiments with erythrocytes and animal cells claim that aggregation and polymer adsorption is reversible, however, they make no mention of the level of acute or chronic toxicity due to the polymer. It is not known what doses affect the cells, how fast the kinetics of toxicity are, or whether there is chronic

toxicity after neutralization of the aggregation. In addition, the polymers investigated are strong cations which bind tenaciously to the cells. Milder cationic species have not been investigated. In view of the simplicity and universality of the flocculation of cells by polycations, it is worthwhile to investigate these compounds as potential flocculants.

3. - REVIEW OF SUSPENSION DYNAMICS LITERATURE

3.1. - Mathematical Description of Aggregation

The second portion of the thesis is devoted to the examination of dynamics of aggregating animal cell suspensions, and the structures produced by aggregation. The ultimate goal of theoretical description of a flocculation process is to be able to predict the suspension properties of interest, *i.e.* the sedimentary velocity distribution, versus the process physical and chemical conditions and time. Flocculation is a dynamic process involving the formation and breakage of aggregates of particles in a suspension. It involves several steps which occur simultaneously or in sequence. The surface conditions preventing aggregation must first be destabilized so that the particles will adhere upon contact. This often involves adsorption of a flocculant, which may be fast or slow. The speed of adsorption will depend on the interaction of particle and adsorbant, size of particle and adsorbant, the system temperature and mixing state. Next, the particles must be brought into contact with each other. The speed of this process will vary depending on the size of the particles, and the temperature and mixing of the system. Once particles are brought together under destabilizing conditions, aggregates of particles will be formed, and these will in turn collide with each other to form larger aggregates. Collisions continue until the aggregates are large enough to be affected by bulk fluid or thermal motion which breaks them apart. The speed of breakage will depend on the strength of the adhesion between particles, the size of the aggregates, and the forces tending to rupture them. The distribution of aggregate sizes in the suspension for a given time and conditions will depend upon the relative velocities of all these processes.

In addition to the flocculation and breakage velocity, the structure of the aggregates produced by flocculation is also of interest. It is generally observed that flocs are not space-filling. Due to the random addition of particles, and due to particle immobility upon deposition, the aggregates are not solid spheres, but are porous structures. The amount of

space filled by the particles is important for two reasons. The first is that the porosity will directly affect the sedimentation and filtration characteristics of a floc, so that it must be known to predict properties for a given aggregate size. The second is that the porosity will determine the number of cells in a floc of given size. This will affect the aggregation velocity calculations, as the number of cells in the flocculating suspension is conserved, but the hydrodynamic volume occupied by the cells is not.

As stated above, the general end goal of mathematical characterization of flocculation is to be able to elucidate the state of aggregation and the associated properties of the flocs, given the conditions of aggregation. The general procedure for this is to construct a population balance equation (PBE) to describe the distribution of floc sizes over time given a knowledge of the flocculation conditions. The PBE solution is combined with the properties of the individual particle classes in the distributed system to give the overall suspension property distribution (SPD). Generation of the PBE and SPD involves several related sets of knowledge; the kinetic parameters of aggregation and suspension destabilization, the structure of the aggregates formed by aggregation as a function of the aggregation conditions, and constitutive relations describing the properties of the aggregates based on their structure.

The ultimate objective of system characterization, a complete description of the sedimentary property distribution of the aggregated suspension, is beyond the scope of this work. The constituent pieces which are needed to complete this description are amenable to fairly straightforward experimentation and theoretical analyses, however. Fundamental characterization of the individual issues in flocculation of animal cell cultures will not only lay a framework for the thorough description of the SPD, but may also uncover interesting behavior not previously found in the literature. Since induced flocculation of animal cells has not been previously investigated in the literature from a physical perspective, it will be of interest to investigate the parameters affecting flocculation kinetics and suspension

properties versus the flocculation conditions. The major issues this thesis will be concerned with are the rate constant of aggregation, the quantification of floc structure, and the description of floc properties versus floc structure. The following sections discuss animal cell characteristics, outline the current state of knowledge of flocculation kinetics and floc structure, and more narrowly define the goals of the thesis.

3.2. - Colloidal Properties of Animal Cells

There are several aspects of animal cell flocculation which are unique from a colloidal science viewpoint. These are due to the physical characteristics of the animal cell.

To begin with, the animal cell is large for a colloidal particle, ranging from 8 to 20 microns in diameter. Typical colloids studied in the literature range from macromolecules, tens or hundreds of nanometers in diameter, to particulate sols, submicron to several microns in diameter. Bacteria and yeast are 0.5 to 4 microns in diameter, also smaller than an animal cell. The size of an animal cell borders on the range which delineates colloidal particles from macroscopic. This will affect the nature of the phenomena which drive the flocculation process; unlike most colloidal aggregation, which is driven by Brownian diffusion (and fluid motion), animal cell aggregation is solely due to bulk fluid motion. It is reasonable to expect flocculation behavior to be different from that encountered previously in the literature.

The animal cell surface is poorly characterized compared to most particulates investigated in the literature. Although much is known about the physiochemical properties of the cell (Curtis, 1967), and about the chemical functionalities present on the surface (Roseman, 1984), a complete picture correlating surface macroscopic properties with the state and the ultrastructure of the cell membrane is not available. The animal cell surface is not in general smooth, nor is it a regular lattice structure, whereas inorganic latex and mineral colloids are apt to be. Rather, it possesses invaginations and protrusions, and is

more like a two-dimensional fluid than a solid surface. Its properties may change with the state of the cell, either with respect to the culture conditions, or the position of the cell in the growth cycle. These properties make the animal cell unique for study.

Another way in which animal cells differ from particles encountered in previous studies is the cell rigidity. Unlike solid latex, minerals, bacteria, yeast, and red blood cells, the structure which gives a cell rigidity, *i.e.*, the cytoskeleton, of the animal cell in suspension culture is poorly characterized. While interactions between individual cells to form flocs may occur as if the cells are rigid spheres, the structure and strength of a large floc may depend on the mechanical properties of the cells and the bonds joining them. The combination of animal cell size, surface and internal properties may lead to behavior different than previously investigated particle suspensions.

It is evident that suspension culture animal cells are greatly different from non-biological colloids and the microorganisms which have been characterized in the literature to date. From the above differences in the nature of the particle, it is reasonable to expect flocculation behavior different from previously investigated suspensions. This expectancy, and a lack of quantitative experimental knowledge of polymer flocculation of large colloids is the driving force for investigation of animal cell aggregation kinetics.

3.3. - Flocculation Kinetics Modelling

Aggregation may be modelled from two viewpoints, deterministic and stochastic. Each approach has advantages and drawbacks, however, the most popular of the techniques has traditionally been the deterministic approach. This approach will be followed in this thesis for description of flocculation kinetics. The stochastic approach has analogues in the study of floc structure, however, and for completeness, it will be included in the discussion below as well.

3.3.1. - Stochastic (Monte Carlo) Aggregation Modelling

Stochastic methods for aggregation kinetic modelling are Monte Carlo methods for randomly generating flocs from individual particles. The utility of this technique lies in the fact that floc formation is in reality a random process of particle collision, and may not be well described by deterministic methods. It can be shown that under certain conditions, the size of the particle ensemble necessary for a deterministic (averaged) description is so large that the volume encompassing the ensemble will not be well mixed. That is, the particles will be spatially distributed such that aggregation rates between size classes will not be in equilibrium and cannot be described accurately by a homogeneous model (Ramkrishna (1981), Sampson and Ramkrishna (1985)). When the particle ensemble is well mixed, however, the deterministic and stochastic methods differ only in the averaging procedure for the floc aggregation rates. In the deterministic procedure, the rates are pre-averaged, where in the stochastic method, rate $_i$ are averaged over the ensemble of collisions. An advantage of stochastic simulation is that it is also possible to obtain aggregate structure information from the same simulations. This will be discussed in section 3.6.1.

In stochastic methods, one starts with a list, or ensemble of aggregates, and proceeds to select the aggregates randomly (or by a weighted frequency) from the list and bring them together along an appropriate path. For perikinetic aggregation, the path may be a random walk, where for orthokinetic aggregation, the path may be a ballistic trajectory. The relative positions of the particles within each floc are monitored, and upon contact, the two flocs are combined to make a larger floc and this is returned to the list of aggregates. The time is incremented by an appropriate scale, and the process is repeated with two new aggregates. The stochastic approach to flocculation is advantageous because it not only provides information about the aggregation state, but also determines the structure of the individual flocs at each time point in the aggregation. There are drawbacks to the stochastic method, however. The first is that it requires large ensembles of flocs (>10^6 initial, or

primary particles) and large amounts of computer time to achieve realistic simulations. The second is that it is difficult to incorporate interparticle forces and hydrodynamic interactions into the calculations. This in turn affects the method of floc selection from the list, which strongly influences the results of the simulation. Realistic methods of floc selection should be dependent on the floc size, structure, and the degree of particle destabilization. Due to these limitations in describing particle aggregation physics in a viscous medium, the deterministic approach to describing particle aggregation will be used.

3.3.2. - Deterministic Aggregation Modelling

In deterministic methods, the particle population is divided into size classes, and a differential equation describing the rate of disappearance and appearance of particles in each class is written. The resulting set of integral-differential equations (the population balance equation, or PBE) is then solved with appropriate initial and boundary conditions to give the concentration of particles in each class as a function of time. The population balance is usually posed in a discretized form rather than a continuum for particulate aggregation, since the aggregate size spectrum can be represented according to the number of individual, or primary particles contained in each class. The PBE in discrete form is formulated as below:

$$\frac{dN_1}{dt} = - N_1 \sum_{j=1}^{i_{max}} \beta_{1,j} N_j + (\text{BREAKAGE TERMS}) \qquad (3\text{-}1a)$$

$$\frac{dN_i}{dt} = \frac{1}{2} \sum_{j=1}^{i-1} \beta_{j,i-j} N_j N_{i-j} - N_i \sum_{j=1}^{i_{max}} \beta_{i,j} N_j + (\text{BREAKAGE TERMS}) \qquad (3\text{-}1b)$$

$$i = 2,3,....,i_{max}$$

This is subject to the conservation of particle mass:

$$N_{tot} = \sum_{i=1}^{i_{max}} i\, N_i = N_{tot}(0) \tag{3-2}$$

Here, N_i is the number concentration of i-size particles, N_{tot} is the total particle concentration, t is time, and $\beta_{i,j}$ is the rate constant of aggregation between particles of size i and j. Equations (3-1) are combined with the mass conservation equation (3-2) (the boundary condition), and the initial spectrum of particle sizes (initial condition), and are integrated over time to give the particle size distribution. In these equations, only the aggregative terms have been shown, although other terms may be included to account for floc degradation over time. In equation 3-1b, the first term on the right hand side represents the collision of all flocs smaller than i to form i-size flocs, and the second term represents collision of i-size flocs with all other flocs to form larger flocs.

Each term in the PBE is a function of concentration of one or two particle classes, multiplied by the rate constants $\beta_{i,j}$, known as kernel functions. There are kernel functions for both aggregation of flocs and breakage of flocs. The latter will not be addressed in this thesis. The aggregation kernel function is not well described for aggregation of colloids as large as animal cells from either a theoretical or experimental standpoint, and it is this function which is necessary to characterize animal cell aggregation. Classical, idealized kernels are reviewed in section 3.4. The goal of this thesis is to elucidate on a fundamental level the parameters necessary for a description of the aggregation kernel function for flocculation of animal cells. To complete the description of the kernel $\beta_{i,j}$, two functionalities must be known. The first is the relationship between the collision rate and process conditions. This will be reviewed in section 3.5. The second is the relationship between floc size and the number of particles the floc contains versus process conditions. This will reviewed in section 3.6. In addition to the effects the floc size relation has on cell aggregation kinetics, the effects of floc size on floc properties will also be reviewed in section 3.6.

3.4. - Particle Aggregation Kernels

The aggregation kernel function is a rate constant describing the frequency of effective collisions between particles as a function of the particle size, nature, and the motion driving the particles together. There are many theories on the form of the aggregation kernel (von Smoluchowski (1917), Camp and Stein (1943), Saffman and Turner (1956), Levich (1962), Rietema (1964), Kuboi, Komasawa and Otake (1972a,b), Delichatsios and Probstein (1976), Coulaloglou and Tavlarides (1977)). Most variants are those for the differing cases of turbulent coagulation. These diverge depending on the scale of the turbulence relative to the particle size, the correlation of turbulent fluid velocity components, and the existence of the inertial subrange of turbulence. In animal cell cultures agitation is usually mildly turbulent, and the turbulence microscale (Kolmogorov microscale) is large, usually above 200 microns. The particle size of interest in an animal cell flocculation scheme ranges from single cells, 10 to 20 microns in diameter, to flocs which settle with velocities on the order of 1 cm/min, about 100 to 500 microns. Thus, collisions between individual cells and small flocs will be mainly due to laminar shear rather than extensional turbulent flow. Consequently, the kernels of interest are those which apply for aggregation of particles by a viscous flow.

In a classical work which established the field, von Smoluchowski (1917) calculated the kernel functions for aggregation due to diffusion (perikinetic aggregation) and to shear flow (orthokinetic aggregation). Since both of these relations will be of use in characterizing animal cell destabilization and aggregation, they are presented below.

For the Brownian motion case, von Smoluchowski solved Fick's law for spherical particle flux towards an identical collector sphere, with boundary conditions of zero particle concentration at the collection surface ($C = 0 @ r = 2a$), and bulk concentration far from the surface ($C = C_b @ r = \infty$). The flux of particles towards the collector sphere per unit time is:

$$\frac{dN}{dt} = JA_s = -8\pi a\mathcal{D}N \tag{3-3}$$

where $\mathcal{D}$ is the diffusion coefficient of the spherical particles, N is the particle number concentration, and a is the particle radius. Taking into account that the collector particle is itself diffusing, the diffusion coefficient is multiplied by two. Multiplying by the total collectors in the suspension, N, the rate of collision in the suspension is then:

$$\frac{dN}{dt} = -16\pi a\mathcal{D}N^2 \tag{3-4}$$

Lumping the leading terms on the right-hand side gives the perikinetic aggregation rate kernel. This may be combined with the Stokes-Einstein equation for sphere diffusivity to give a fundamental rate kernel:

$$\beta_{1,1} = 16\pi a\mathcal{D} = \frac{8k_bT}{3\eta} \tag{3-5}$$

When the particles are of unequal size, the diffusivities are not additive; this case leads to a general perikinetic kernel function:

$$\beta_{i,j} = \frac{2k_bT}{3\eta}\frac{(a_i + a_j)^2}{a_ia_j} \tag{3-6}$$

For shear induced aggregation, Von Smoluchowski solved for the collision rate of spheres in a simple shear flow. Particles on different streamlines will possess velocities relative to each other due to the shearing motion. A collision area for a target particle can be defined as a circle of radius $(a_i + a_j)$ normal to the flow direction. Any particle on a streamline that lies within the target cross-section will collide with the target particle. The fluid flow velocity relative to the target particle is then integrated over the target area to define the convective fluid flux for collision. Multiplying this flux by the particle concentration gives the particle flux to the target particle. Another multiplication by the target particle concentration gives the total rate of collision. In the case of different sized spheres this is:

$$\frac{dN_i}{dt} = \frac{dN_j}{dt} = -\frac{4}{3}\dot{\gamma}(a_i + a_j)^3 N_i N_j \qquad (3\text{-}7)$$

The rate kernel for orthokinetic aggregation is then:

$$\beta_{i,j} = \frac{4}{3}\dot{\gamma}(a_i + a_j)^3 \qquad (3\text{-}8)$$

This development assumes there is no interaction between the two approaching spheres, *i.e.*, the particles follow rectilinear trajectories. It ignores the effects of interparticle forces, and also the modification of particle trajectories by hydrodynamic interaction. Despite these limitations, the von Smoluchowski kernel has been found accurate in some cases for aerosol and hydrosol aggregation. In many cases, however, it is not accurate; here the aggregation kernel must be modified to include the effects of destabilization and hydrodynamic interaction. In addition, not all collisions may result in adhesion. These non-idealities are corrected for by introducing a collision efficiency factor into the rate kernel:

$$\beta_{i,j} = \frac{4}{3}\alpha_{i,j}\dot{\gamma}(a_i + a_j)^3 \qquad (3\text{-}9)$$

The factor $\alpha_{i,j}$ is defined as the ratio of actual collisions resulting in adhesion to the number of collisions calculated by the von Smoluchowski kernel.

The collision efficiency factor incorporates all of the suspension non-idealities; as mentioned above, non-idealities result from hydrodynamic interactions, and the colloidal forces discussed in section 2.1. Since the colloidal forces operative in animal cell flocculation are not known, the form of the collision efficiency is not easily predicted. In addition to the uncertainty in the colloidal forces which determine collision mechanisms, the nature of animal cells as primary particles is also ill-defined, as discussed in Section 3.2. To predict the aggregation of animal cell suspensions, it is essential to possess a knowledge of the collision efficiency factor as a function of the process conditions. Although a purely empirical approach may be taken to animal cell aggregation, it is desirable to explain

experimental results on a physical basis. For this purpose, it is useful to review past theoretical and experimental literature on collision efficiencies of non-biological colloids.

3.5. - Particle Collision Efficiency

3.5.1. - Collision Efficiency Theory

Like aggregation kinetics, collision efficiency factors may be approached by either a stochastic or deterministic method. The first method consists of defining the probability of adhesion between colliding spheres based on assumptions about particle motion and interactions between opposing surfaces. It has been the preferred method when an adsorbing polymer is the flocculant. The deterministic methods are rigorous calculations of particle collision. For these methods, the physics of particle approach in a viscous medium are taken into account, and the actual trajectories of the particles determined to find whether they will collide. This approach has been preferred for ionic coagulation of particles, where the colloidal force interactions are well-described. Each method has advantages and drawbacks; these will be discussed below.

3.5.1.1. - Deterministic Collision Efficiency

In deterministic formulation of the collision efficiency, the equations of motion are solved for the approach of two spheres in creeping flow. In addition to the viscous and pressure force terms in the momentum equations, the colloidal body forces on the spheres are incorporated. These calculations have a long history in the fluid mechanics literature; review of the early work and the general method of solution may be found in Adler (1981b).

The fluid mechanical approach to calculating collision efficiency was originally undertaken by Curtis and Hocking (1970) for equal-sized spheres influenced by Van der Waals and electrostatic forces. Many variations have been performed since. Van de Ven

and Mason (1976, 1977), Zeichner and Schowalter (1977), and Higashitani *et al.* (1982) solved the same problem as Curtis and Hocking, adding refinements to the forms of the interparticle forces versus particle separation, and correcting for an improper definition of the collision efficiency. Adler (1981a,b,c,d) solved the equations of motion for unequal-sized (conducting and insulated) spheres influenced by electrostatic and Van der Waals forces in shear and planar extensional flows, and under the influence of electric fields. Feke and Schowalter (1983, 1985) included the influence of Brownian motion on the collision efficiency of equal spheres in shear and planar extensional flows. Melik and Fogler (1984) dealt with coagulation of different size particles due to a gravitational field. Mifflin and Schowalter (1988) investigated the effects of medium viscoelasticity on collision efficiency.

The equations for the approaching sphere velocities are posed as follows for the case of same-sized spheres in a spherical coordinate system:

$$\frac{dr}{dt} = V_r = \dot{\gamma} r (1 - A) \sin^2\theta \cdot \sin\phi \cdot \cos\phi + F_r \qquad (3\text{-}10a)$$

$$r\frac{d\theta}{dt} = V_\theta = \dot{\gamma} r (1 - B) \sin\theta \cdot \cos\theta \cdot \sin\phi \cdot \cos\phi \qquad (3\text{-}10b)$$

$$r \sin\theta \frac{d\phi}{dt} = V_\phi = \dot{\gamma} r (\cos^2\phi - (B/2) \cos 2\phi) \sin\theta \qquad (3\text{-}10c)$$

The terms A and B are dimensionless functions of the radial separation between the spheres. Interparticle forces enter as the radial force term, F_R, in equation (3-10a). For Van der Waals attraction and electrostatic repulsion as the dominant interparticle forces, F_r is a nonlinear function of particle separation distance, and necessitates numerical solution of the equations. Expansions of F_r, A and B can be found in Van de Ven & Mason (1977).

To determine collision efficiency, the set of fluid streamlines which defines the collision cross-section must be determined, and the particle flux along these streamlines is integrated to determine the collision rate. The result of the integration is divided by the von

Smoluchowski collision rate to determine the collision efficiency. There are two techniques for deriving the collision producing streamlines. The first method is to pick streamlines far from the collector sphere, and integrate the trajectory until the sphere either contacts or passes the collector. By trial and error, a perimeter may be defined within which all streamlines produce collisions. Alternately, the equations may be integrated backwards from the surface of the collector to a point at which the trajectory is suitably rectilinear.

The studies are laudable in their advancement of the field; however, the utility of the results is not what it might be. In order to study animal cell aggregation, for instance, one must explore a parameter space of particle size, shear rate and force magnitudes which was not addressed by the above studies. The studies also have not considered colloidal forces other than the Van der Waals attractive and electrostatic repulsive forces, as the results were intended to describe ionic coagulation of rigid spheres. Other forces may be important for biological particle collision, especially forces resulting from steric interactions between macromolecules. In addition, the simulations require parameters for input which are not readily obtainable experimentally, notably the London-Hamaker constant, and the characteristic retardation wavelength for the London-Van der Waals forces. In several instances, the solutions have been used to back-calculate London-Hamaker constants and retardation wavelengths for particle-fluid systems from experimental collision efficiency data.

Although the studies have not produced cases for all conditions of aggregation, they have yielded generalizations about the collision behavior of spheres. In equation (3-10a), the magnitude of the London-Van der Waals attractive force is normalized to the magnitude of the viscous fluid terms by the group:

$$C_A = \frac{A}{6\pi\eta\dot{\gamma}a^3} \qquad (3\text{-}11)$$

Here, A is the London-Hamaker constant, η is the medium dynamic viscosity, $\dot{\gamma}$ is the fluid shear rate, and a is the particle radius. The electrostatic repulsive forces may be normalized through C_A and a dimensionless group relating the electrostatic force magnitude to the London-Van der Waals attraction:

$$C_{RA} = \frac{4\pi\varepsilon_o K\psi_o^2 a}{A} \tag{3-12}$$

Here, ε_o is free space permittivity, K is the medium dielectric constant, and Ψ_o is the surface potential. In many regimes, collision efficiency can be described by semi-empirical correlations of these dimensionless quantities.

Van de Ven and Mason (1976) found that when $C_{RA} < 25$ and $10^{-5} < C_A < 10^{-1}$, electrostatic repulsion is rendered negligible, and the collision efficiency is dominated by the viscous fluid interaction. The collision efficiency could be described by the semi-empirical relation:

$$\alpha = k(\lambda)C_A^{\chi} \tag{3-13}$$

Here, $k(\lambda)$ is a constant dependent on the characteristic retardation wavelength, λ, of the London-Van der Waals forces. This equation was found to give an error of less than 1% compared to the rigorous solution within the given constraints on C_A and C_{RA}. For the simulation of Van de Ven and Mason, χ was found to be 0.18.

The results of Feke and Schowalter (1985) including the effects of Brownian diffusion showed that the collision efficiency could be described by equation (3-13). The exponent χ was found to be 0.23 in the high Peclet number limit:

$$Pe = \frac{\dot{\gamma} a^2}{\mathcal{D}} = \frac{6\pi\eta\dot{\gamma} a^3}{k_b T} >> 1 \tag{3-14}$$

Here, $\mathcal{D}$ is the particle diffusivity. This is posed as the Stokes-Einstein hard sphere value in the far right hand side of (3-14), where k_b is Boltzmann's constant and T is absolute temperature.

Melik and Fogler (1984) solved the equations of motion for particles of different size approaching each other under the influence of gravity. For particle size ratios close to unity ($a_i/a_j > 0.2$), and when electrostatic forces were negligible, the collision efficiency was proportional to the dimensionless equivalent of C_A to the 0.20 power.

O'Brien (1977) found that for Pe going to infinity and $C_A < 10^{-8}$, the collision efficiency dependency on C_A increases to $\chi = 1$. Since the collision frequency is directly dependent on the shear rate, this result means that the net rate of aggregation does not change with shear rate in this region of interparticle forces.

Adler (1981a) calculated collision efficiency between unequal spheres undergoing ionic coagulation. This work has application for the collision of animal cells for the reason that a suspension of animal cells is not monodisperse. Since the cells are in different growth phases, their volumes will be different. Thus, even if the suspension is initially all single cells (no aggregates), there will be a distribution of particle sizes. Adler's work showed that for two particles whose size ratio is around 0.5, the collision efficiency is lower than for two equal size spheres. The collision efficiency is also more sensitive to C_A, and under conditions where (3-13) would apply, the value of χ would be expected to be larger. Adler's plots also show that when C_A is much less than 10^{-5}, the collision efficiency is more strongly dependent on C_A. Melik and Fogler (1984) found that when the size ratio approaches zero ($a_i/a_j < 0.2$), the collision efficiency is a power law function of C_A to the 0.33 power.

Although the value or dependency of the collision efficiency in these correlations can not be calculated without knowledge of the Hamaker constant and $k(\lambda)$, the theories provide a basis for collision efficiency expectations, and may be useful in correlations of experimental data. From the above studies, we expect that when electrostatic repulsive forces are negligible, and when steric and other forces are inoperative, the collision efficiency should be a power law function of C_A, with a dependency from 0.18 to 0.33.

When C_{RA} is significantly greater than 25, calculations show the collision efficiency to be a complex function of C_A for ionic coagulation. This is due to the presence of primary and secondary minima in the interparticle attraction energy versus particle separation distance. At low C_A (high viscous force relative to attraction), collision efficiency increases with C_A as particles aggregate only in the primary energy minimum. As C_A is increased further, collision efficiency levels off until a "critical" C_A, when the attractive forces bringing the particles together are strong enough to pull more trajectories into the secondary energy minimum. This aggregation takes the form of stable orbiting pairs. When this C_A is surpassed, collision efficiency once again increases.

Unfortunately, there has been no theoretical work which describes collision efficiency under the conditions relevant to animal cell collision. For animal cells at 37 C and a equal to 8 μm, the collisions are shear-dominated (Peclet > 60) for $\dot{\gamma} > 0.06\ s^{-1}$. This is well below typical shear rates in animal cell culture. A generous estimate of the London-Hamaker constant for animal cell membranes is on the order of 10^{-14} erg (Israelachvili (1985)). For the above shear rate, C_A is 1.7×10^{-3}. For shear rates from 6 to 60 s^{-1}, the value of C_A ranges between 1.7×10^{-5} and 1.7×10^{-6}. This is on the border of the applicable range for the Van de Ven and Mason results, but well above the range of O'Brien's results. For higher values of the shear rate or lower values of the London-Hamaker constant, the C_A values are even more into the no-man's land between the two theoretical results. In addition to the uncertainty of applicability under these low C_A values, the absolute cell surface potential must be less than 2 mV to have C_{RA} less than 25. This requirement is in contrast to typical values of -25 mV for animal cells under culture conditions (Forrester (1965)) and illustrates that cell surface charge may play a role in stabilizing animal cell suspensions. Other factors may also combine to render these correlations less useful. One example which may be pertinent is the possible presence of steric interactions between surface macromolecules on animal cells. Another example would be the presence of a non-

smooth surface on the scale of the electrostatic and Van der Waals force interaction distances.

3.5.1.2. - Probabilistic Collision Efficiency

The alternative to rigorous numerical calculations of the collision efficiency is an estimation based on statistical considerations (Smellie and LaMer (1958), Hogg (1984), Deason (1987), Moudgil, Shah and Soto (1987)). These models are usually employed for the scenario where a charged polymer is adsorbing onto a particle with opposite charge. When the polyelectrolyte does not lie flat upon the surface on adsorption, the total adsorbed charge does not correspond in a 1:1 fashion with the charge it is neutralizing. This results in a charge reversal for the covered region, so that the region becomes attractive to uncovered regions on other particles. When a covered region on one particle encounters an uncovered region on another particle, adhesion results. Probabilistic calculations of collision efficiency have idealized polymer adsorption as occurring onto discrete sites on the particle. Pairs of these sites on different particle surfaces interact with each other upon particle collision, and if one or several of the site interactions is net attractive (the sites are oppositely charged), adhesion results. This picture of particle collision is shown in Figure 3-1 for five site pairs interacting with each other. For the situation shown in the figure, adhesion may result since there is one site pair in an attractive mode. The number of possible site pair configurations resulting in adhesive interaction may be calculated by making various assumptions about particle behavior. This may be divided by the total number of possible configurations to calculate a collision efficiency. The convenience of such a calculation is that the minimum information required is the adsorption isotherm of the polymer to cells, in order to calculate the fraction of sites covered by the polymer.

Probabilistic collision efficiency calculations were first introduced by Smellie and LaMer (1958). The latter author has published a series of articles modelling flocculating

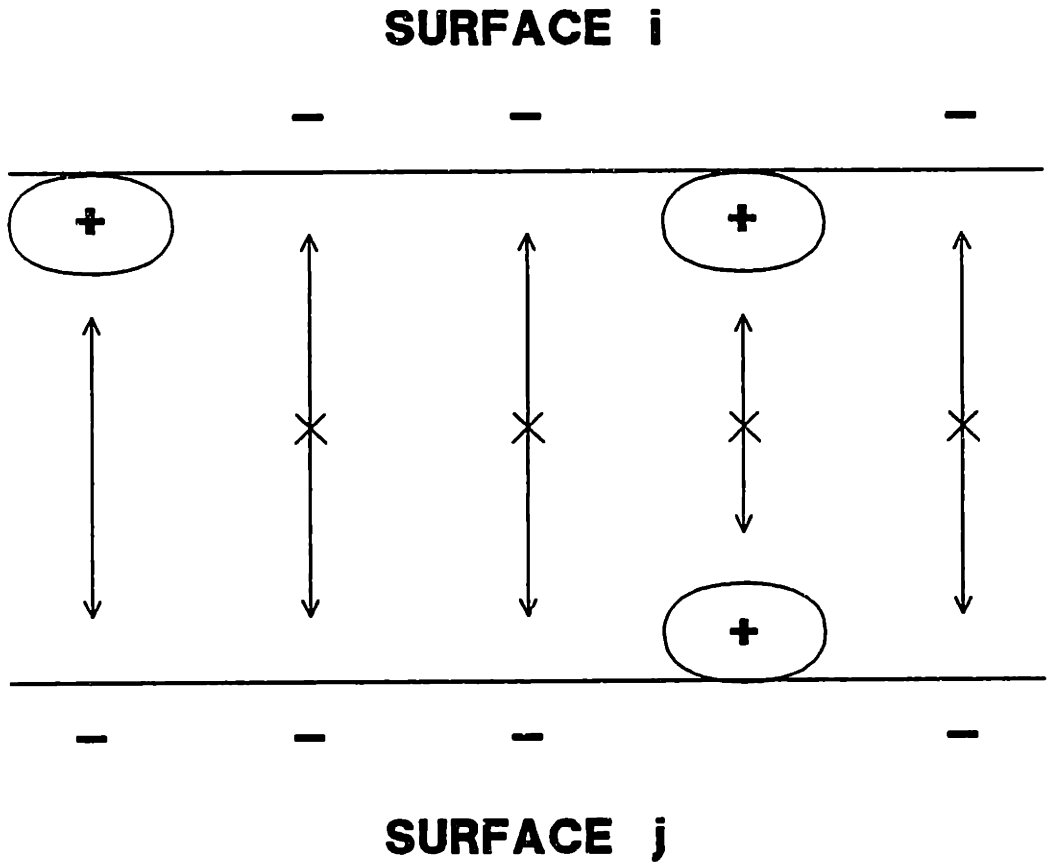

Figure 3-1. Schematic of colliding particle surfaces partially covered from polymer adsorption.

suspension behavior, and the Smellie and LaMer work will be referred to as the LaMer model throughout this thesis. These researchers calculated the collision efficiency for two particles with one site pair interaction. For a particle with one adsorption site, the probability of the site being covered with polymer is the fractional surface coverage, θ. The probability of the site being uncovered is $(1 - \theta)$. Attraction (adhesion) occurs for pair configurations where the sites on the colliding particles have opposite charges (coverage states). The probability of finding the configuration pairs which result in adhesion are:

$$P_i(0, 1)P_j(1, 1) = (1 - \theta_i)\theta_j \tag{3-15a}$$

$$P_i(1, 1)P_j(0, 1) = \theta_i(1 - \theta_j) \tag{3-15b}$$

The other two possible configurations, $P_i(0,1)P_j(0,1)$, and $P_i(1,1)P_j(1,1)$, produce electrostatic repulsion and do not adhere on collision. Summing the above probabilities and assuming the particles are equally covered with polymer ($\theta_i = \theta_j$) gives the joint probability of adhesion, or collision efficiency:

$$\alpha_{i,j} = 2\theta(1 - \theta) \tag{3-16}$$

In this model, $\alpha_{i,j}$ goes through a maximum of 0.5 at half-coverage of the particles ($\theta = 0.5$). The existence of an optimum dose is a general feature of polyelectrolyte flocculation. Although equation (3-16) describes the general features of flocculation efficiency in polyelectrolyte flocculation, it may under- or overestimate the collision efficiency. Experimentally, collision efficiencies can be greater than or less than 0.5 (this will obviously depend on hydrodynamic influences), and are often optimal over a wide range of polymer dose. Several implicit assumptions in the derivation of the LaMer collision efficiency may account for these discrepancies. In particular, only one site is allowed to interact, and the distribution of polymer on adsorption is ignored. Correcting for these and other factors may lead to better agreement with experimental observations,

and they have been addressed in more sophisticated models by Hogg (1984), Deason (1987), and Moudgil *et al.* (1987).

Hogg (1984) generalized the LaMer model to multiple site interaction. He assumed that small particles were infinitely free to rotate ($\mathcal{D}_{rot} = \infty$) in response to interparticle forces, and would expose themselves to adhesion whenever possible. He also assumed as above that one attractive site interaction is sufficient to establish permanent adhesion. The probability of adhesion is then one minus the probability of completely bare particles encountering each other and completely covered particles encountering each other. In order to have such a situation without unit collision efficiency at all surface coverages, adsorption cannot be equal on all particles. If adsorption of polymer occurs onto n_i discrete sites on a particle i, the probability that any given site is covered is still θ. The probability that m of the n_i sites are covered at an average coverage θ is expressed by the binomial distribution:

$$P(m,n_i) = \frac{n_i!}{m!(n_i - m)!}\theta^m (1 - \theta)^{n_i - m} \tag{3-17}$$

The probability that a particle will be completely covered is:

$$P(n_i, n_i) = \theta^{n_i} \tag{3-18}$$

The probability that it is completely bare is:

$$P(0, n_i) = (1 - \theta)^{n_i} \tag{3-19}$$

Summing the probabilities that these situations occur for two particles i and j, the collision efficiency is:

$$\alpha_{i,j} = 1 - \theta^{n_i + n_j} - (1 - \theta)^{n_i + n_j} \tag{3-20}$$

Here, n_i and n_j represent the number of polymer adsorption sites on the i and j particles. In the limit of $n_i = n_j = 1$ site per particle, the Hogg model reduces to equation (3-16), the LaMer model.

The number of sites per particle must be known in order to calculate the collision efficiency. For this purpose, Hogg defined the number of sites per particle as equal to the particle surface area divided by the area projection of the polymer radius of gyration:

$$n_i = \frac{4\pi a_i^2}{4\pi a_{pol}^2} \tag{3-21}$$

Since polymer molecules are usually much smaller than the particle to which they adsorb, $n_i >> 1$, and it can be calculated from equations (3-18) and (3-19) that only a very few particles are completely bare or completely covered. This leads to very few collisions being discounted as ineffective, and the Hogg model predicts much larger collision efficiencies than the LaMer model for $n_i > 1$. This is seen in Figure 3-2, which shows the Hogg model predictions for different values of $(n_i + n_j)$. The curve for $(n_i + n_j) = 2$ corresponds to the LaMer model of collision efficiency. For large $(n_i + n_j)$, the curves rapidly attain unity, and remain there over a large range of surface coverage.

For animal cell flocculation, the Hogg model is not likely to account for collision efficiency well. This is for two reasons. The first is that the large size of animal cells compared to most flocculants means that n_i calculated by (3-21) will take on large values, and collision efficiency would be predicted to be unity at virtually all values of θ. The second reason is that the assumption of infinite particle rotational diffusivity is unrealistic for particles as large as animal cells. It is apparent that Hogg originally intended the development to apply to small particles undergoing diffusive flocculation, where the above limitations would not be apparent. The original concept may be ignored, however, and the development may be viewed as applicable to only a small region on the particle surface rather than the whole particle. For example, for the situation of Figure 3-1, if we are allowed to rearrange the configurations to promote adhesive interactions whenever possible, equation (3-20) will express correctly the fraction of encounters resulting in adhesion.

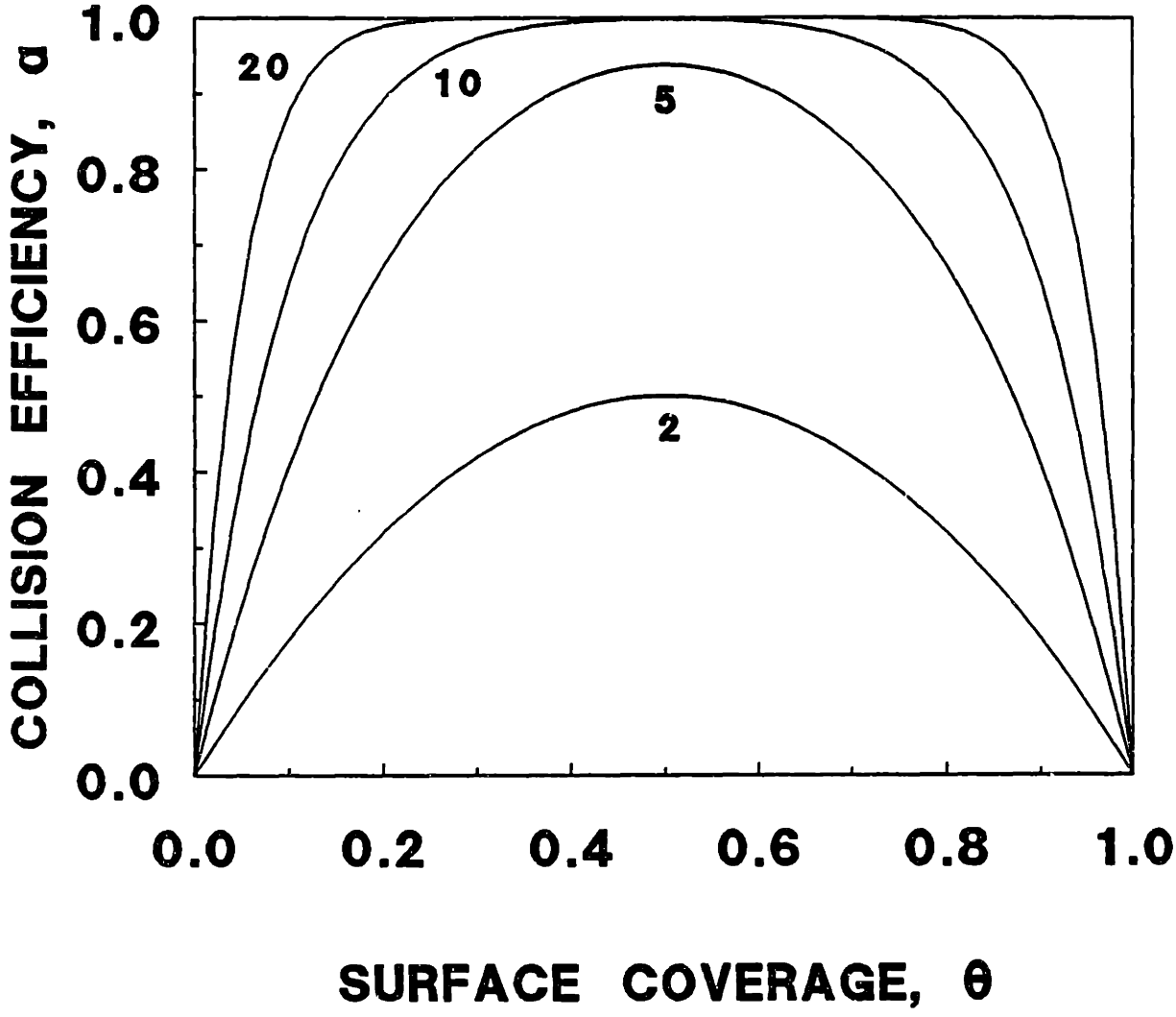

Figure 3-2. Collision efficiency versus fractional surface coverage for the Hogg literature model. Numbers indicate the value of $(n_i + n_j)$.

Deason (1987) combined the Hogg concept of multiple adsorption/interaction sites with the idea that the polymer extends itself into solution. This follows from the concept of non-monolayer adsorption. Due to this polymer extension, more than one apposed site pair can interact to produce adhesion. For a given site pair, there are four possibilities for interaction, as outlined in equations (3-15). These result in the average attractive interaction probability $2\theta(1 - \theta)$ per site. For N_{ij} potentially interacting site pairs, the probability that m of these will be in the attractive mode is again given by the binomial distribution:

$$P(m, N_{ij}) = \frac{N_{ij}!}{m!\,(N_{ij} - m)!} [2\theta(1 - \theta)]^{m} [1 - 2\theta(1 - \theta)]^{N_{ij} - m} \qquad (3\text{-}22)$$

Assuming that one polymer bridge is sufficient to establish adhesion, the probability that adhesion will occur is one minus $P(0,N_{ij})$:

$$\alpha_{i,j} = 1 - [1 - 2\theta(1 - \theta)]^{N_{i,j}} \qquad (3\text{-}23)$$

Figure 3-3 shows the Deason model predictions for various N_{ij}. Again, in the case of $N_{ij} = 1$, the model reduces to the LaMer development. Comparison with Figure 3-2 shows that for $(n_i + n_j) = N_{ij}$, the values of collision efficiency predicted by the Deason model are smaller than the Hogg model, but larger than the LaMer predictions.

As in the Hogg model,the value of N_{ij} must be calculated in order to use the development. Deason calculated the number of potentially interacting site pairs by geometric arguments regarding the adsorption site size, the extension of the polymer into solution, and the closeness of approach of the particles. It was again assumed that the polymer covers an area proportional to its gyrational radius as in equation (3-21). Polymer extension from the surface was assumed equal to an adsorbed layer thickness defined as $2a_{pol}$. In addition to these polymer related variables, the minimum approach distance of the

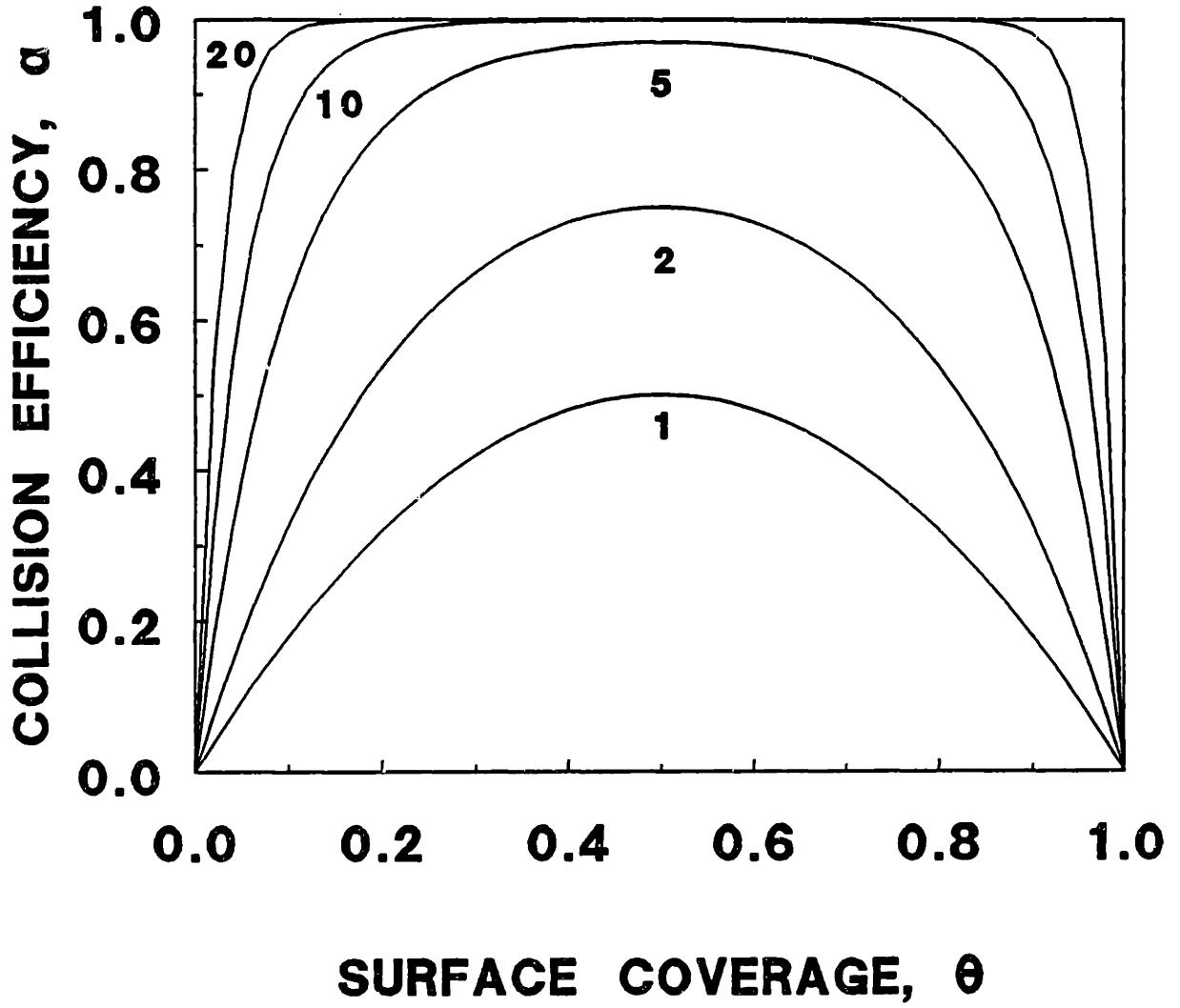

Figure 3-3. Collision efficiency versus fractional surface coverage predicted by the Deason literature model. Numbers indicate the value of N_{ij}.

particles, H_{min}, must be included to calculate N_{ij}. For equal sized spheres, Deason derived N_{ii} to be:

$$N_{ii} = \frac{a_i(2a_{pol} - H_{min})}{4a_{pol}^2} \tag{3-24}$$

For unequal sized spheres, N_{ij} was derived as:

$$N_{ij} = \frac{a_j^2}{2a_{pol}^2} \cdot \frac{2a_i(2a_{pol} - H_{min}) - (2a_{pol} - H_{min})^2}{2(a_i + a_j - (2a_{pol} - H_{min}))} \tag{3-25}$$

where the j particle is the smaller of the two. Although a_{pol} can be calculated through the polymer radius of gyration, N_{ij} is still governed by the minimum approach distance, H_{min} between the spheres. This distance is unknown. Deason suggests that H_{min} may be approximated by static force calculations of the separation distance at the energy minimum between surfaces.

The Deason model may apply to animal cell aggregation more readily than the the Hogg model. This is because the model examines only a region of the particle surface rather than the entire particle. As pointed out in section 2.1., the Debye layer thickness, or range of electrostatic interactions in animal cell culture medium will be on the order of 1 to 10 nm, or 0.001 particle radii. This means that only local interactions will be relevant in determining the interaction between particle surfaces. Again, due to the usually small polymer size and the large size of the animal cell, the N_{ij} calculated by equations (3-24) and (3-25) will be unrealistically large unless H_{min} is also large. Experimental values of N_{ij} might indicate whether the model is realistic. When N_{ij} is large, it implies that H_{min} approaches zero and the particles easily contact each other. When N_{ij} is small, H_{min} approaches $2a_{pol}$, and it may be inferred that hydrodynamic and interparticle forces are keeping the particles separated, consistent with the expectations of the deterministic theory discussed in section 3.5.1.1. Knowledge of N_{ij}, and polymer and cell size would allow calculation of an experimental H_{min} value to test the theory.

Moudgil, Shah and Soto (1987) introduced the concept of "active" and "inactive" polymer adsorption sites on the particle surface. This model was developed to describe selective flocculation when more than one particle specie is present. Under their development, only a fraction of the surface may be active towards adsorbing polymer and produce adhesive patches. This is incorporated into the calculations of (3-15) by introducing the active site fraction, ϕ_i, into the probability statements. For the LaMer analogous case, this results in:

$$\alpha_{ij} = \phi_i(1 - \theta_i)\phi_j\theta_j + \phi_i\theta_i\phi_j(1 - \theta_j) = 2\phi^2\theta(1 - \theta) \qquad (3\text{-}26)$$

The development seems to be a half-hearted attempt to rationalize flocculation differences between systems which have different physiochemical conditions. It does not produce a different functionality than the LaMer, Hogg, or Deason models, but merely adjusts the absolute magnitude of the collision efficiency by the arbitrary constant, ϕ^2. Although animal cell surfaces may not be homogeneous towards polymer adsorption, this formulation is not likely to yield an accurate picture of flocculation.

3.5.2. - Experimental Collision Efficiencies

3.5.2.1. - Direct Determinations of Collision Efficiency

Despite the considerable speculation on the form of the collision efficiency and its functionality, there have been relatively few direct determinations of collision efficiency. These are reviewed below for shear aggregation of model latex systems and common colloids.

In one of the more widely referenced papers in the literature, Swift and Friedlander (1964) investigated the ionic coagulation of 0.87 μm polystyrene latex in a Couette shear field. Coagulation was initiated by 1 M sodium chloride. Aggregation rates were assessed by electronic particle counting over time. These authors investigated aggregation for shear rates from 1 to 80 s^{-1}, corresponding to particle Peclet numbers calculated from equation (3-

14) between 0.28 and 23. Under these low Peclet conditions Brownian motion collisions were significant, so the authors assumed that the shear and Brownian coagulation rates were additive in processing data. A constant collision efficiency of 0.364 was reported for all of the shear rates investigated. This is counter to the idea that hydrodynamic shear will play a role in collision efficiencies of particles. The results illustrate that Brownian motion effects on both diffusive and flow induced collisions may have been the dominant factor in these experiments, leading to the observed constancy of the collision efficiency versus shear rate. Whereas the shear rate governs collision frequency, shear independent Brownian motion could have controlled the particles' ability to surmount the energy barrier opposing stable adhesion. It has since been demonstrated by Feke and Schowalter (1983) that Brownian and shear induced rates of collision are not strictly additive, and this may have also played a role in the results.

Hahn and Stumm (1968) studied the ionic coagulation of 1.1 μm silica by alum in a turbulent stirred tank. Aggregation rates were determined by microscopic particle counting over time. The kernel of Levich (1962) was used to calculate theoretical rates of collision. The authors reported collision efficiencies versus alum concentration at a mean shear rate of 110 s^{-1}. The resulting particle Peclet number was 84. In addition to determining collision efficiencies, the authors determined alum adsorption to the silica, and fitted the data to the Langmuir isotherm. From this data, fractional surface coverages could be obtained. Although the authors do not present the collision efficiency versus the fractional surface coverage, this plot may be generated using the data available. The collision efficiency versus the calculated fractional surface coverage is shown in Figure 3-4. Although the collision efficiency goes through a maximum, it is asymmetric with respect to a fractional surface coverage of one half. This is counter to the probabilistic theories reviewed in section 3.5.1.2., and reflects the magnitude of physical forces between the particles which

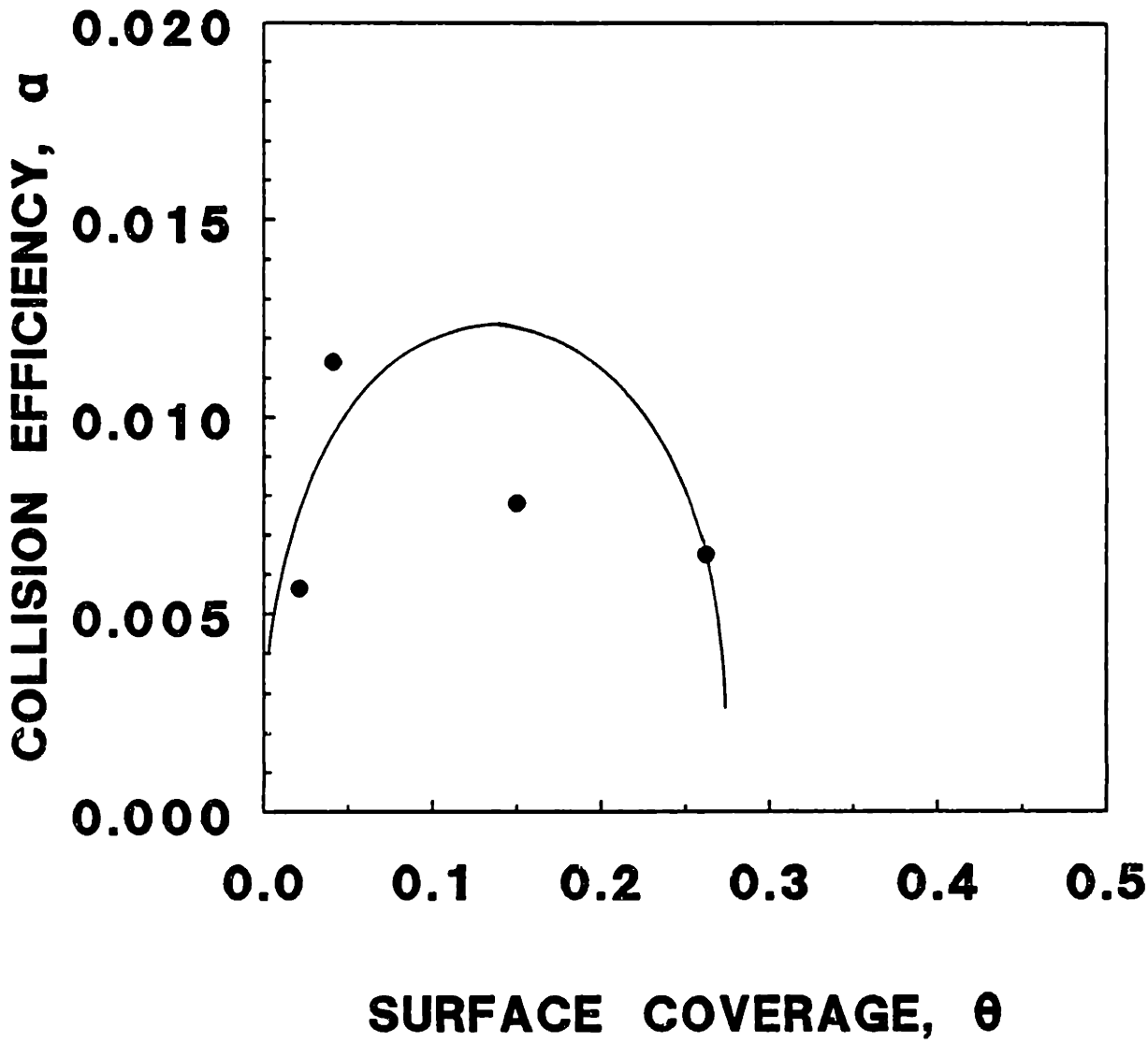

Figure 3-4. Collision efficiency of alum flocculated silica versus calculated fractional surface coverage from the data of Hahn and Stumm (1968).

the probabilistic collision efficiency does not account for. As noted in section 3.5.1.2., the change in surface charge induced by flocculant adsorption is not necessarily one-for-one. That is, adsorption of alum to a bare site with -1 charge does not necessarily result in a covered site with +1 charge, so we should not necessarily expect symmetry in collision efficiency about a surface coverage of 0.5. Hahn and Stumm state that zeta potential measurements show particle charge reversal over the alum concentrations used, but do not present data to determine the magnitude of the reversal.

It can be seen in Figure 3-4 that the collision efficiency does not approach unity. This may reflect the difficulty in calculating a theoretical collision rate in a poorly characterized, turbulent tank. The Levich kernel used here predicts a coagulation rate 7.5 times faster than the Saffman and Turner kernel (Delichatsios and Probstein (1975)) which has been used extensively throughout the literature, and may be responsible for the low reported collision efficiencies.

Birkner and Morgan (1968) reported the flocculation of 1.3 μm latex with 35,000 molecular weight polyethylenimine and by 1 M sodium chloride coagulation. This study employed a turbulent stirred tank for the mixing vessel, and the authors used the isotropic turbulent aggregation kernel of Saffman and Turner (1956) to calculate the theoretical rate of aggregation. Samples were withdrawn and counted for total particles versus time using a Coulter counter (see section 4.2.1. for description). The authors presented data versus shear rate for several particle concentrations. Shear rates varied between 11 and 120 s^{-1}, giving particle Peclet numbers between 14 and 150. Although values were obtained versus polymer dose, the dependency of the collision efficiency on the polymer dose was not tabulated. The shear rate data is presented in Figure 3-5. It is seen that the collision efficiency decreases with increasing shear rate for both flocculation and coagulation, as predicted by fluid mechanical theory. For polymer flocculation, regression of the log-log plot shows that the dependency on shear rate is -0.92±0.07. For ionic coagulation, the

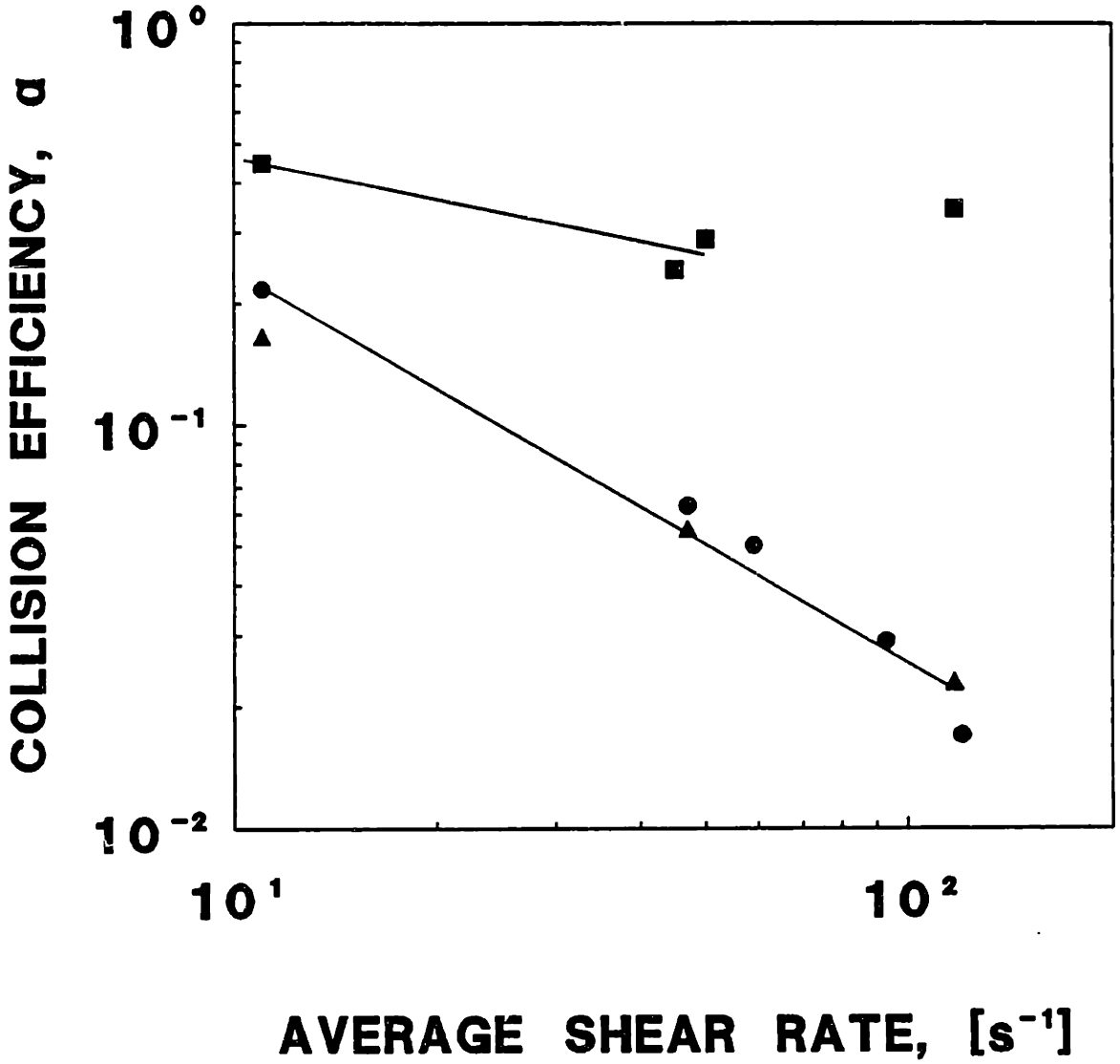

Figure 3-5. Collision efficiency of polyethylenimine flocculated latex versus fluid shear rate from the data of Birkner and Morgan (1968). ■ - ionic coagulation, ●,▲ - polyethylenimine flocculation.

calculated dependency is -0.31±0.19. It will be noted that the ionic coagulation dependency is close to the theory developed a decade later. This is surprising given the low Peclet numbers used. The reason for the strong shear dependency for polymer flocculation is unknown. Ionic coagulation is seen to have higher collision efficiencies overall than polymer flocculation. The reason for this is not apparent, since polymer extension and bridging would be expected to increase the effective particle collision cross-section and thus the calculated collision efficiency. This behavior is somewhat surprising in light of the claims of Hogg (1986) and Deason (1987) that polymer flocculation collision efficiencies are near unity.

In an accompaniment to their theoretical development, Curtis and Hocking (1970) reported the ionic coagulation of 2 μm polystyrene latex in a Couette viscometer at shear rates between 0.5 and 120 s^{-1}. The particle Peclet numbers ranged from 2 to 380. Sodium chloride was added to render the particle surface potential less than 2 mV. A Coulter counter was used to assess particle concentration over time. A log-log plot of collision efficiency versus shear rate shows that the collision efficiency roughly follows a power law dependency. This is shown in Figure 3-6. A linear regression of the data provides a dependency on the shear rate of -0.097±0.001. This is in contrast to the -0.18 power dependency predicted by Van de Ven and Mason (1976) per equation (3-13). Since the particle Peclet numbers were near unity for the lowest shear rates, Brownian motion collisions were significant, and should have contributed to the calculated collision efficiencies. Like the Swift and Friedlander experiments, the results may reflect Brownian motion effects on shear induced collision efficiencies. The anomalous results may also stem from the fact that the particles were initially stabilized with sodium dodecyl sulfate; incomplete cleaning of the suspension may have left a surfactant coating on the particles which would obscure the results.

Delichatsios and Probstein (1975) investigated the coagulation of 0.6 μm

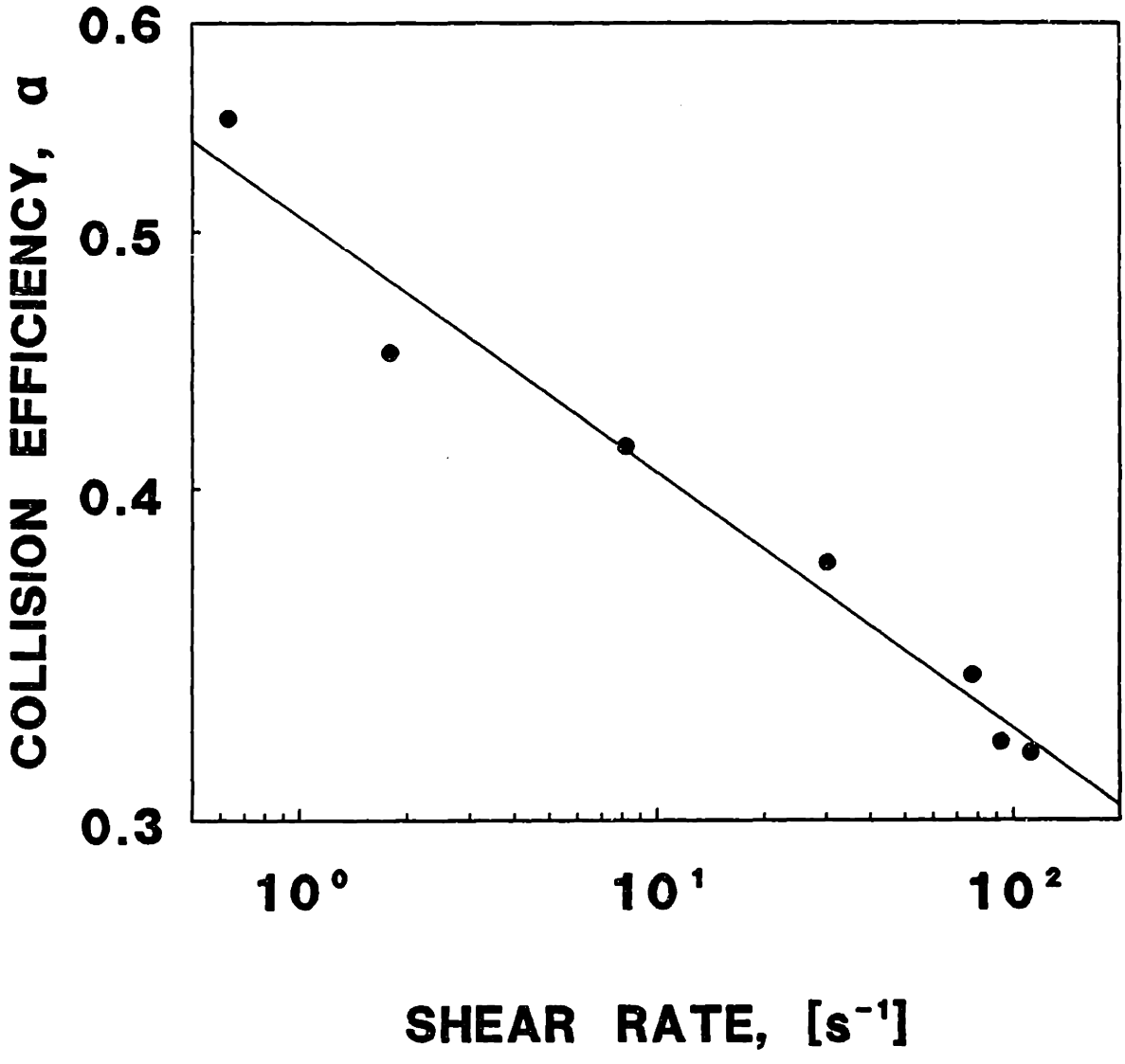

Figure 3-6. Collision efficiency of salt coagulated latex versus fluid shear rate from the data of Curtis and Hocking (1970).

polystyrene latex by Brownian motion and in a locally isotropic turbulent pipe flow. Coagulation was induced by a mixture of 1 M HCl and 5.6 M calcium chloride, which simultaneously screened electrostatic repulsions and protonated the acidic polystyrene surface to effect destabilization. In addition to the experimental data, the authors presented a theoretical development on the form of the turbulent collision rate kernel. This theory predicts that for particles smaller than the Kolmogorov microscale, the collision rate will be 0.63 times as fast as the Saffman and Turner kernel. The difference arises from assuming the x,y, and z fluid velocity components will be positively correlated rather than statistically independent, as Saffman and Turner assumed. It was found that for both Brownian motion and shear aggregation, five volume percent of the destabilizing mixture was necessary to induce maximum destabilization. The shear aggregation data showed that at maximum destabilization, particle aggregation rates were slightly higher than the proposed theory, but were lower than predicted by the Saffman and Turner kernel by a factor of 0.70 (= α). Since this value is between the two theoretical kernels, it indicates that there are two effects in operation. First, hydrodynamic interactions between particles may be lowering the collision efficiency. Second, the turbulent fluid velocity components may show an intermediate degree of correlation, placing the actual collision frequency somewhere between the two theories.

Below five percent coagulant, the stability ratio (= $1/\alpha$) followed a power law dependency on the coagulant volume fraction, with a slope of -1.7. We may relate this result to the particle surface potential by the Debye-Hückel approximation for particle surface potential:

$$\psi_o = \frac{4\pi\sigma}{\varepsilon_o K\kappa} \tag{3-27}$$

The parameters ε_o, K, and ψ_o in this equation are the same as in equation (3-12); σ is the

surface charge density, and κ is the reciprocal Debye layer thickness. This last parameter is given by the relation:

$$\kappa = \left(\frac{8\pi e^2 N_A I}{1000 \epsilon_o k_b T} \right)^{1/2} \tag{3-28}$$

In this equation, e is the electron charge, N_A is Avogadro's number, and I is the medium ionic strength. Equation (3-28) shows that κ is dependent on the square root of the medium ionic strength, which is directly proportional to the molarity, or volume fraction of coagulant added. It is easily seen that the coagulant concentration should affect the repulsive electrostatic forces through the surface potential. Inserting equation (3-28) into (3-27) and using the slope of the experimental data, the dependency of the collision efficiency on the particle surface potential follows a power law functionality with an exponent of -3.4. This suggests that collision efficiency may be correlated to C_{RA} as well as C_A for intermediate degrees of destabilization. This conclusion is encouraged by the results of Melik and Fogler (1985), who investigated the Brownian coagulation of 0.166 and 0.255 μm latex by magnesium sulfate. These authors show that the stability ratio follows a power law functionality on the coagulant concentration. Again applying the Debye-Hückel solution, it can be shown that collision efficiency in the Brownian motion case is dependent on the particle surface potential to the -6.4 and -3.8 power for the small and large particles, respectively. The observation that collision efficiency in Brownian coagulation follows a power law functionality on the coagulant concentration is a common one (Hiemenz (1977), Reerink and Overbeek (1954)). However, this has not been suggested previously for orthokinetic aggregation of large colloids.

Zeichner and Schowalter (1979) investigated ionic coagulation of 0.5 μm, surfactant-free polystyrene latex by both Brownian motion and fluid shear. A Couette flow chamber was used in the fluid shear experiments, with shear rates between 100 and 1800

s^{-1}. This gave particle Peclet numbers between 7 and 130. Sodium chloride was added to 0.6 M to "completely" destabilize the suspension. Particle aggregation was assessed by light scattering measurements over time. This method is potentially less destructive than microscopic or electronic counting methods. The experimental results were compared with the authors' theoretical calculations, which parallel those of Van de Ven and Mason. Good agreement with the theory was obtained for shear rates greater than 400 s^{-1}, where Brownian motion was negligible. Below this, the particle Peclet numbers were less than 30, giving significant Brownian coagulation. The collision efficiency under these conditions was shear independent, which may explain the results of Swift and Friedlander, and Curtis and Hocking. In light of this conclusion, it is odd that the Birkner and Morgan results do not also show a shear independence for the low Peclet number range.

Gregory (1981, 1982) investigated the ionic coagulation and polymer flocculation of 1.7 μm latex in a Poiseuille flow tube. By assaying the entrance and exit particle concentrations, it was possible to back-calculate values of α. Although data was obtained versus the average shear rate, the dependency was not reported. Gregory reported a single α value of 0.19 at 170 s^{-1} shear rate for coagulation by calcium nitrate, and values of 0.48 and 0.55 for flocculation by 5,000 and 150,000 molecular weight cationic polymers. The latter values are higher than the ionic coagulation case, and may result from either polymer bridging effects or differing colloidal force interaction. For bridging, the polymer could have increased the effective hydrodynamic radius of the latex. However, in conducting the experiments, Gregory dosed half the particles to produce a positively charged suspension which was then mixed with a suspension of untreated, negatively charged spheres. Thus, although polymer bridging may have contributed to the increase in collision efficiency, the presence of an electrostatic attraction between particles changed the nature of the collision process from the ionic coagulation case, where electrostatic repulsive forces are simply neutralized.

Higashitani *et al.* (1983) investigated the ionic coagulation of 0.85 μm polystyrene and 2.17 μm polyvinyltoluene latices in a turbulent stirred tank. 0.75 M potassium chloride was used as the coagulant. Power inputs were measured directly and translated to fluid shear rates assuming isotropic turbulence. The theoretical rate of coagulation was calculated by the kernel of Saffman and Turner (1956). Shear rates used were between 4.2 and 280 s^{-1}, corresponding to particle Peclet numbers from 1.5 to 100 for the small particles, and 24 to 1600 for the large particles. Assuming that electrostatic repulsion was negligible, the experiments were conducted in the region of applicability for equation (3-13). Although the absolute values of the collision efficiency deviated slightly from theory using accepted London-Hamaker constants, the dependency of the collision efficiency on C_A coincided with the predictions of Van de Ven and Mason. The authors recognized that the deviance in absolute values from the laminar shear flow theory probably results from poor estimation of the power input and hence the effective collision rate. The results of the small particle collision efficiency experiments are surprising, since the Peclet number is small enough to be in the region where Brownian coagulation should be significant. The large particle Peclet numbers were in the diffusion independent region.

Van Diemen and Stein (1983) investigated the ionic coagulation of quartz particles with hydrodynamic diameters of 1.5, 3.0, and 5.0 μm in Couette flow. These particles are irregular needles with an aspect ratio of 4:1. Shear rates between 11.2 and 350 s^{-1} were employed. At the higher shear rates the conditions of aggregation were such that Taylor vortices, and eventually turbulent eddies were present in the shear apparatus. The Taylor vortex contribution to the mean shear rate was accounted for by the equations of Stuart (1958). These shear rates gave particle Peclet numbers between 22 and 700, 180 and 5400, and 800 and 25,000 for the small, medium, and large particles respectively. The degree of aggregation was assessed by monitoring suspension turbidity over time. At low shear rates, the collision efficiency decreased with increasing shear rate, although the

authors did not calculate the dependency. In the region of shear rate close to the onset of vortices, the collision efficiency of the quartz was seen to increase, counter to theory. This was attributed to inaccuracy in calculating the true shear rate. At large shear rates where turbulence was present, the collision efficiency dropped to 0.005 for 1.5 μm particles. Counter to the ionic coagulation theory predictions, collision efficiencies were greater for larger particles. The authors proposed that since the quartz was denser than the suspending medium ($\rho = 2.65$ gm/cm^3), centrifugal forces in the Couette shear field created a radial particle velocity component which led to underestimation of the collision frequency, and hence overestimation of the collision efficiency. This was most important for the 5 μm particles, hence the higher reported collision efficiencies. In addition to this factor, the sedimentary velocity of the quartz due to gravity would also increase the effective collision frequency, especially for larger particles. Aside from these collision frequency enhancing effects, the shape of the particles probably affected the collision process. On the one hand, a needle shape would be able to penetrate electrical double layer repulsion more easily than a sphere, and might produce higher collision efficiency. On the other hand, less surface area would be in contact, making the attraction between particles easier to break. The balance of these two effects is unknown for the particles investigated.

Logtenberg and Stein (1985) investigated the ionic coagulation of submicron zinc oxide in a turbulent stirred cylindrical cuvette. The particles were in the form of hexagonal prisms, with an aspect ratio of 4:1. The equivalent spherical diameter of the particles was 0.48 μm, but a mean hydrodynamic diameter of 0.66 μm was found by sedimentary velocity analysis. Mean shear rates in the cuvette were estimated by laser Doppler anemometry measurements of average velocity. Shear rates between 200 and 400 s^{-1} were found, giving particle Peclet numbers (based on the hydrodynamic radius) between 33 and 66. Aggregation rates were determined by monitoring the decrease in suspension turbidity with time. Collision efficiencies were calculated by comparing the aggregation rate to an

experimental "maximum" rate at high salt concentration and the same shear rate. Due to the ill-defined hydrodynamic conditions and the normalization of collision rates, direct comparison across hydrodynamic conditions is not possible. Comparisons between different chemical conditions may still be made, however. The collision efficiency was given as a function of the particle zeta potential for several shear rates. The reported data are reproduced in Figure 3-7. It should be stressed that with the collision efficiency normalized to an experimental maximum value, it is not possible to interpret trends at constant zeta potential and different shear rates. It can even be seen that for one datum at 400 s^{-1} and $\zeta = 0$, the reported collision efficiency is greater than unity! Figure 3-7 shows that for aggregation at high shear rates, the collision efficiency is strongly dependent on the particle surface potential. As the shear rate is decreased, the zeta potential is less influential on the collision efficiency. At the lowest shear rate, 200 s^{-1}, there appears to be no effect of the particle surface potential. The lack of surface potential dependency at low shear rates is disturbing, and contradicts the observations of Delichatsios and Probstein and others discussed above. It will be noted that when the Peclet number is based on the equivalent spherical radius, the particle Peclet numbers in the experiments were from 13 to 26, within the limit of Brownian motion dependence defined by Feke and Schowalter (1983). In addition, the 4:1 aspect ratio of the particles and the high density (5.60 gm/cm^3) relative to the suspending medium probably produced effects similar to those found by Van Diemen and Stein above. Due to the anomalous behavior and the generally poor experimental methodology, the reported collision efficiencies of both of these papers are of dubious value.

In the only paper dealing with viscosity effects on the collision process, Mifflin and Schowalter (1988) investigated the rapid coagulation of 1.2 μm polystyrene latex by 1.2 M KCl in viscoelastic, semi-dilute hydroxyethylcellulose solutions. Although collision efficiencies are not readily calculated from these authors' results, the authors found that

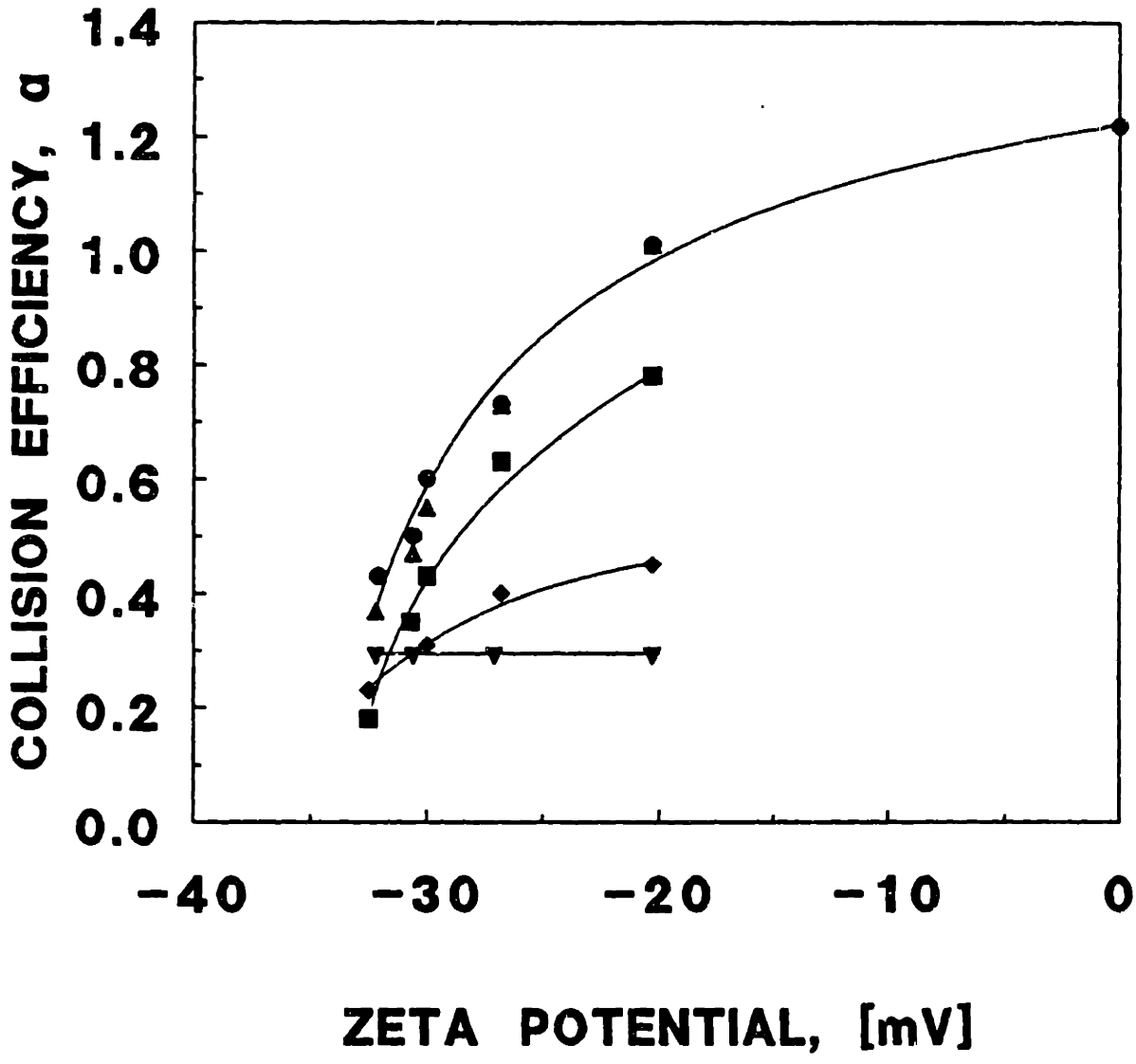

Figure 3-7. Collision efficiency of salt coagulated zinc oxide versus particle zeta potential. Reproduced from Logtenburg and Stein (1985). ● - 400 s^{-1}, ▲ - 350 s^{-1}, ■ - 300 s^{-1}, ◆ - 250 s^{-1}, ▼ - 200 s^{-1}.

collision efficiencies were an order of magnitude lower than Newtonian efficiencies at the same viscosity. The authors ascribed this result to the viscoelasticity of the solution.

In addition to these measurements of average, global collision efficiency, S.G. Mason, H.L. Goldsmith, and their coworkers have published a series of articles dating from the early 1950's which have microscopically visualized individual collisions (Manley and Mason (1952), Bartok and Mason (1957), Goldsmith and Mason (1975), Adler (1981d), Goldsmith *et al.* (1981), Takamura, Goldsmith and Mason (1981)). The general purpose of the visualization experiments is not to obtain collision efficiencies, but to obtain experimental collision trajectories, which can be compared to theoretical trajectories predicted by equations (3-10). This is because data analysis and reduction is a tedious operation and only a few collision observations can be readily processed. These experiments have corroborated the deterministic models of collision efficiency for ionic coagulation, and provided values of the Hamaker constant and retardation wavelength. Two papers are of particular interest, dealing with collision trajectories of colliding blood cells (Goldsmith *et al.* (1981)), and with collision trajectories of latex spheres destabilized with a cationic polymer (Takamura, Goldsmith, and Mason (1981)). The former paper will be discussed in section 3.5.2.3. The latter is discussed below.

The paper of Takamura, Goldsmith and Mason (1981) is interesting as it is the only literature dealing with polymer flocculation effects on the microscale of individual particle collisions. The authors studied the flocculation of 2.6 and 4.0 μm diameter polystyrene latex by poly-N,N-3,5-methylene pyridinium chloride ("Cat-floc", Calgon) of unknown molecular weight in 0.01 M ionic strength medium. Particle Peclet numbers were above 1000 for the conditions used. Particle zeta potential was -45 mV for the native latex. At 0.03 mg/L polymer, the particle zeta potential was increased to -41 mV. Trajectory calculations taking into account this change in surface potential adequately modelled the experimental collision paths, indicating that at this surface coverage, the effect of the

polymer is solely to change the electrostatic repulsion, and not to create bridging between particles. At a polymer dose of 1 mg/L, the particle surface potential was reversed to a value of +35 mV. At this surface coverage, incorporation of the surface potential into the coagulation theory accurately predicted collision trajectories except for one doublet which appeared to have bridging. At a polymer dose of 0.06 mg/L, particle surface potential was increased to +20 mV, an intermediate surface coverage. At this dose, aggregation of the suspension was pronounced, and presented experimental difficulties. For particles whose trajectories led to large minimum separation distances, the trajectories were predicted by the trajectory equations incorporating the particle surface potential. There were anomalous encounters at both large and small h_{min}, however, producing permanent doublets which suggested that polymer bridging had occurred. It is notable that these anomalous doublets were by no means rigid; the minimum distance of approach oscillated about a large mean value. This illustrates that polymer bridging in the classical sense, which implies multiple short range interactions that lock particles into relative position, did not occur. The authors attributed the results to polymer extension. In a theoretical modification, the authors were able to show that most of the anomalous trajectories could be accounted for by moving the electrostatic potential out from the surface a distance equal to the polymer adsorbed layer thickness. Thus, for polyelectrolyte flocculation of particles, it appears that incorporating the surface potential change into the equations of motion for ionic coagulation can accurately describe the collision process.

3.5.2.2. - Indirect Measurements of Collision Efficiency

In addition to direct measurements of collision efficiency, several authors have used particle size distribution data to fit parameters to population distribution models. When this procedure is performed, the form of the population balance may affect the results obtained. That is, by including terms for floc breakage, the values of the fitted collision efficiency

and its dependency on flocculation conditions may be altered. As such, these values should be considered speculative. However, they have produced some results corroborating collision efficiency theory and the direct experimental determinations.

Wigsten and Stratton (1984) investigated flocculation of 0.535 μm latex by ionic coagulation, and by polyvinylamine with molecular weights of 130,000 and 1,000,000. The flocculation was conducted in turbulent pipe flow at mean shear rates of 1800 and 8000 s^{-1}. This gave Peclet numbers of 160 and 700. Mixing of polymer with the latex occurred at a tee just before the flocculation tube. The authors posed a population balance with no breakage terms, but included polymer adsorption kinetics. The collision efficiency form used was a modified LaMer model, $\alpha_{ij} = \alpha_F[\theta_i(1- \theta_j) + (1-\theta_i)\theta_j]$. The fractional surface coverages for this expression were time dependent due to the nature of polymer addition to the suspension. These values were calculated using von Smoluchowski kinetics, and were inserted into the collision efficiency expression at each time step in the population balance solution. The parameters necessary to determine the flocculant adsorption kinetics were obtained by sampling the end suspension and determining the residual unadsorbed polymer. Particle size distributions were determined and fitted to the population balance equations to calculate values of α_F. It will be noted that the collision efficiency is independent of particle size.

Flocculation was conducted at low and high pH, and at low and high shear rate, where the polymers have different charge properties, configuration, and adsorption characteristics. The reported values are shown in Table 3-1. The results of the data fits are qualitatively consistent with theory. The collision efficiency decreases with increasing shear rate as expected. Assuming a power law dependence, for alum coagulation and the pH 10 experiments, the collision efficiency is dependent on the shear rate to the -0.34 power. Similar behavior for the two polymers and for the alum coagulation case is

expected because the polymers are only slightly charged (3% ionized) at pH 10, and do not have large gyrational radii. At pH 3, the polymers are highly charged, and are in an

Table 3-1
Collision Efficiencies Reported by Wigsten and Stratton (1984)

Flocculant	pH	$\dot{\gamma}$, [s^{-1}]	α_F
alum	3	1800	0.33
alum	3	8000	0.20
130,000 MW	3	1800	0.30
130,000 MW	3	8000	0.26
130,000 MW	10	1800	0.20
130,000 MW	10	8000	0.12
1,000,000 MW	3	1800	0.36
1,000,000 MW	3	8000	0.34
1,000,000 MW	10	1800	0.20
1,000,000 MW	10	8000	0.12

extended configuration. This is reflected in the higher collision efficiencies, and a changed dependence on the shear rate. For the low molecular weight polymer, the power law shear rate dependency is -0.10, where for the large molecular weight polymer, the dependency is -0.04. The reason for the different dependencies is not evident. It may be an artifact of the fitting, as the collision efficiency did not take into account the effects of particle size. This would give an average value which would be more dependent on the extent of destabilization than hydrodynamics. Alternately, the results may reflect flow induced extension of the polymer at higher shear rates. Polymer extension might be expected to be more important for the larger polymer, explaining the reduced dependency. In addition, since no floc breakage terms were included in the population balance, any breakage that may have occurred would be incorporated as a decrease in the collision efficiency. It is possible that flocs created with the large molecular weight polymer were stronger than those created by coagulation or small molecular weight polymer. This would lead to a less sensitive observed collision efficiency.

It will be noted that Wigsten and Stratton's fitted population equation results are in direct conflict with the comparable studies of Birkner and Morgan (1968). Birkner and

Morgan found lower collision efficiencies for polymer flocculation than for ionic coagulation, and a weaker dependency on the shear rate for ionic coagulation than for polymer flocculation. The difference between the Birkner and Morgan results and the Wigsten and Stratton values may point out the inherent limitations in fitting parameters to population balances rather than determining them under controlled conditions.

Lu and Spielman (1985) investigated the turbulent flocculation of 4.5 μm Kaolin clay by a high molecular weight polycation (Primafloc C-7, Rohm & Haas). The aggregation vessel was a turbulent stirred tank, and aggregation rates were calculated by the Saffman and Turner kernel. Aggregation was conducted at different shear rates and at "optimum" flocculant dosage, as assessed by residual turbidity measurements. Mean shear rates were between 84 and 200 s^{-1}, giving particle Peclet numbers between 4,400 and 10,400. The primary goal of the work was to assess floc breakage rates in shear flow; thus, particle size distributions were fitted to a population balance which included breakage terms. The fitted collision efficiency factors were found to vary between 0.35 and 0.32. Assuming a power law functionality, the dependence on shear rate was to the -0.10 power. The insensitivity of the collision efficiency to the hydrodynamic conditions probably reflects two factors. First, the range of shear rates investigated was small, and a weak dependency such as predicted by equation (3-13) is difficult to assess. The uncertainty associated with the fitted collision efficiencies is probably large. Second, the authors were interested in providing a functionality for the breakage rate of the aggregates versus hydrodynamic conditions, and the parameter optimizations may have incorporated lower collision efficiencies into larger floc breakage rates at high shear rate.

Koh, Andrews, and Uhlherr (1987) investigated the flocculation of 2.0 μm scheelite ($CaWO_4$) by a coagulating mixture of sodium oleate and sodium carbonate. The flocculation was conducted in a baffled, turbulent stirred tank at mean shear rates between 484 and 1370 s^{-1}. This gave particle Peclet numbers greater than 2200. Particle size

distributions were determined by a sedimentation-light extinction method. The authors used an aggregative population balance to fit the particle size distributions. Rather than incorporating breakage terms into the population balance, the authors posed the collision efficiency as a decreasing function of floc size, given by equation (3-35) in section 3.6.3.1. The fitted collision efficiency of single particles (α_{11} in equation (3-35)) followed a power law functionality on the shear rate, with a dependency to the -1.3 power. This is the result of three factors. The first is that the collision efficiency dependency is forced to account for both decrease in collision efficiency, and increase in floc breakage rate with increasing shear rate. This should result in a stronger dependency on the fluid forces. The second is that the suspension is destabilized by addition of a surfactant, which presents a different physical mechanism for flocculation than for traditional polymeric bridging or ionic coagulation. The effects of destabilization mechanism on the flocculation characteristics are unknown. The third factor is that the floc size distributions obtained by the sedimentary technique were probably erroneous, as will be discussed in section 3.6.2.2.

3.5.2.3. - Determination of Collision Efficiency for Cells

In addition to the experiments performed on non-biological colloids, there has been some work determining the adhesive properties of cells under more or less natural conditions. The purpose of most of this work is to explain differences in cellular adhesion with an eye towards providing a physical basis for tumor metastasis, cell agglutination (lectin or immune based), and embryonic development. The vast majority of the work has been done under such ill-defined hydrodynamic conditions that the data is not useful for prediction of absolute cell collision rates. There are several papers, however, which present useful information on the relative collision behavior of cells. These are reviewed below.

In one of the only reliable measurements of cell collision efficiency, Curtis (1969) investigated the aggregation of embryonic chick cells and tissue culture lines in Hanks's salts plus 199 Medium. Aggregation was conducted in a laminar flow Couette viscometer. Shear rates used were from 2.08 to 11.5 s^{-1}, which gave cell Peclet numbers between 850 and 4700. Cell aggregation was assessed by hemocytometry over time. The results of the experiments are shown in Table 3-2. Curtis reports only one series of experiments from which the collision efficiency dependency on fluid shear rate may be calculated. This is for 7-day neural retina cells; the data versus shear rate is presented as a log-log plot in Figure 3-8. A linear regression of the data shows a dependency on shear rate to the -0.24 power, which agrees well with ionic coagulation theory. This is despite the fact that the mechanism of adhesion is unknown for these cells, and probably involves specific biological macromolecules. Using the theoretical results from Curtis and Hocking (1970), London-Hamaker constants were calculated for the cells assuming a London-Van der Waals driving force for adhesion. These calculations ignored the cell surface potential. Values from 2×10^{-15} to 2.5×10^{-14} erg were found from this exercise, which is consistent

Table 3-2
Collision Efficiency Results from Curtis (1969)

Cell Type	Temperature, C	$\dot{\gamma}$, [s^{-1}]	Mean $\alpha \pm$ s.d.
5-day ventricle	37	3.60	0.038±.005
5-day liver	37	2.25	0.037±.006
5-day limb bud	2	2.60	0.026±.002
5-day limb bud	37	2.08	0.017±.004
7-day liver	37	11.46	0.098±.019
7-day neural retina	37	2.32	0.216±.029
7-day neural retina	37	4.23	0.171±.010
7-day neural retina	37	7.88	0.167±.016
7-day neural retina	37	12.96	0.147±.020
7-day neural retina	37	17.12	0.124±.017
BHK 21/C 13	37	5.18	0.145±.019
BHK 21/C 13	1	5.18	0.187±.050
L929	37	8.20	0.215±.070

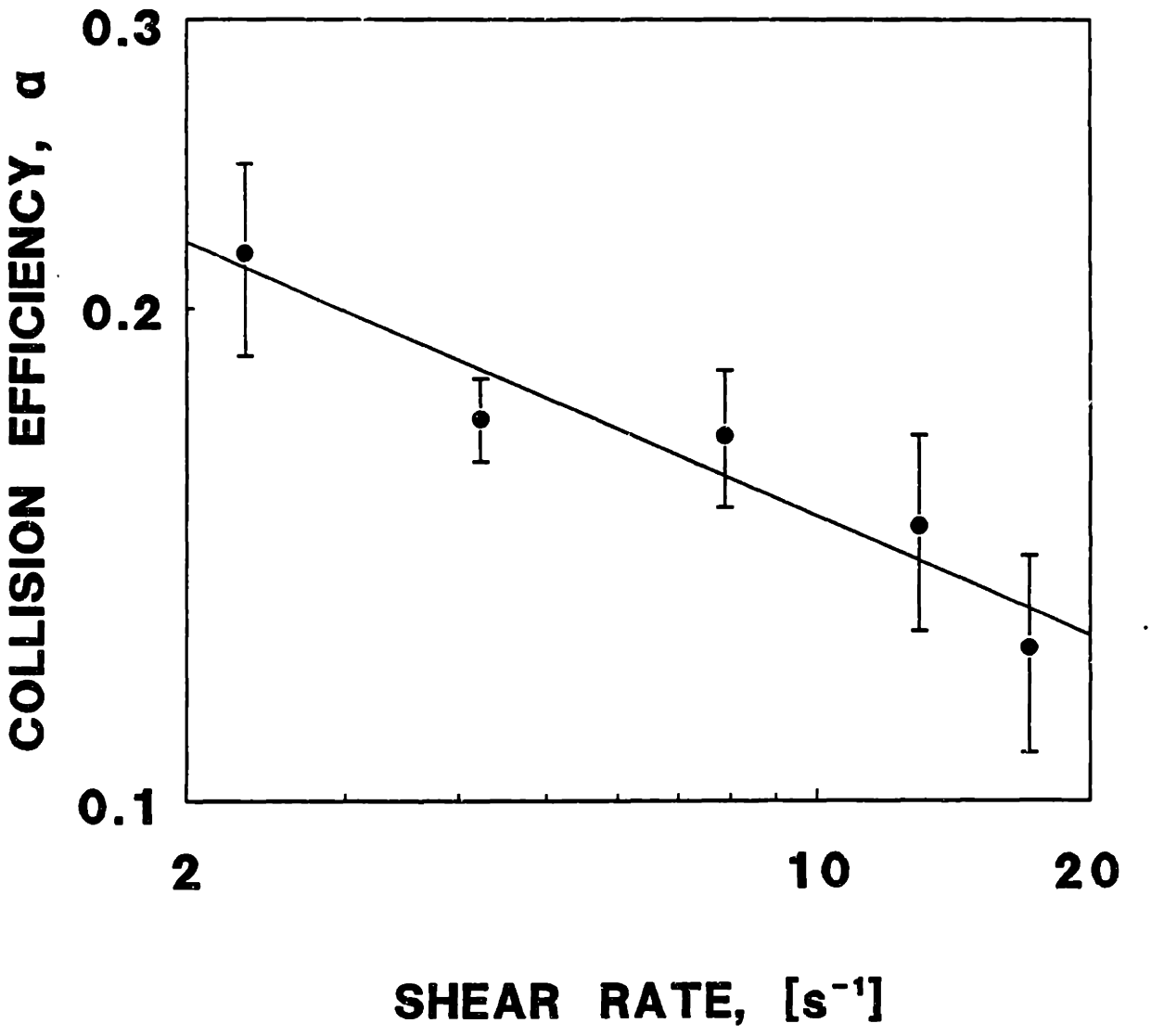

Figure 3-8. Collision efficiency of 7-day neural retina cells versus fluid shear rate from the data of Curtis (1969).

with other estimates of the London-Hamaker constant between biological membranes (Israelachvili (1985)). One of the notable observations of these experiments is the temperature dependency of the collision efficiency for embryonic limb buds and for BHK 21/C 13 cells. For the embryonic cells, collision efficiency decreases, suggesting that cell metabolism is necessary for specific adhesion mechanisms to operate. This has been shown in a variety of qualitative experiments on developmental cell adhesion. For the cultured BHK cells, the collision efficiency increased with decreasing temperature. This suggests a temperature-independent adhesion mechanism, and may reflect the loss of specific adhesion mechanisms for these cultured cells.

Linnemans *et al.* (1976a,b) investigated the agglutination of the soil amoeba *Acanthamoeba castellani* by concanavalin A (conA) in a stirred cuvette. The degree of aggregation was monitored by the decrease in suspension turbidity over time. The rate constant of aggregation was calculated at short times versus conA concentration, before appreciable aggregation had occurred. Unlike the work of Swift and Friedlander (1964), the authors found that initial aggregation rates were dependent on the square of the cell number concentration. The shear rate in the cuvette was not determined, although two agitation rates were used, 370 and 520 rpm.

This work is interesting, because it provides a concrete example of "bridge" formation by a flocculant. The lectin conA interacts on a very specific basis with α-D-mannopyranoside and α-D-glucopyranoside carbohydrates on cell surface glycoproteins. Since conA is present as dimers in solution, it is able to attack groups on the surfaces of opposed particles. The interaction is a very specific one, and relies on stereospecific bonds which are short range in character. Thus, aggregation is not mediated by gross physical property changes on the cell surface, but by a specific bridge formation. The likelihood of adhesion, or bridge formation, should be proportional to the relative abundance of vacant and occupied adsorption sites for the lectin. This should be well described by the

probabilistic collision efficiency theory discussed in section 3.5.1.2. In addition to calculating rates of aggregation, the authors modelled conA association by a Langmuir relationship, and derived the equilibrium constant and the number of sites for conA adsorption per cell. From this relation, it is possible to re-plot the authors' collision rate versus conA concentration data as collision rate versus fractional surface coverage. This is shown in Figure 3-9 for the stir speeds investigated. It is not possible to reduce the data to collision efficiencies since the authors do not provide cell size or shear rate data.

The data show two features which have previously been discussed in the theoretical review section. First, the collision efficiency is remarkably symmetric about half-coverage of the cells with conA, and exhibits the concave downward shape that is expected from the probabilistic collision efficiency models shown in Figures 3-2 and 3-3. From the shape of the data one can speculate on which probabilistic model describes the data best, but without accounting for hydrodynamic effects it is not possible to discriminate between models quantitatively. The second feature of the data is that the effective collision rate decreases with increasing agitation rate. The magnitude of this effect is surprising; since the absolute collision rate is less at the higher shear condition, this means that the collision efficiency is more sensitive to the fluid conditions than the collision frequency. It will also be noted that the collision rate is more sensitive to conA surface coverage at the higher shear rate. This may indicate that only under conditions where adhesion strength is maximal can the cell aggregates withstand fluid forces tending to separate the cells.

Jones and Perry (1978,1979,1980) investigated natural and conA induced aggregation of cultured Chinese Hamster cells in a turbulent, end-over-end rotating tube. Aggregation was monitored by Coulter counting and sizing the suspension over time. For natural aggregation, the authors fit an aggregative population balance to the size distributions obtained, and using the kernel of Saffman and Turner for the collision rate, fit values of the collision efficiency. Due to the ill-characterized nature of the flow field used,

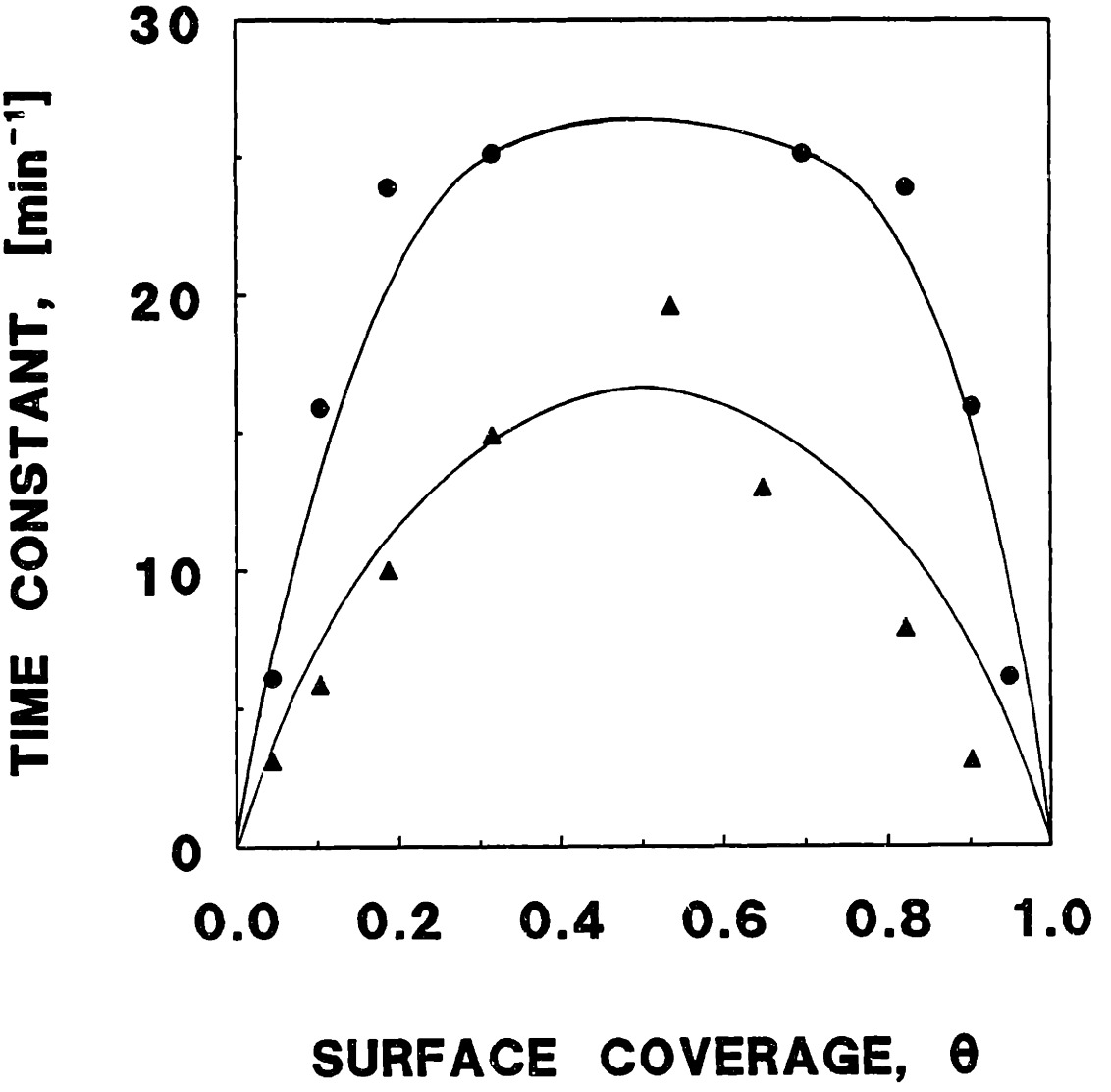

Figure 3-9. Collision rate constant for concanavalin A agglutinated *Acanthamoeba castellani* cells versus calculated fractional surface coverage from the data of Linnemans *et al.* (1976). ● - 370 rpm, ▲ - 520 rpm.

the authors' estimation of the average shear gradient in the suspension is questionable, and the collision efficiency values should be considered relative. These values are shown in Table 3-3. It is seen that for the CH23 cells, the collision efficiency decreases with temperature. This may indicate that the adhesion is an active biological mechanism that

Table 3-3
Collision Data of Jones and Perry (1979)

Cell Type	Temperature	$\dot{\gamma}$, [s^{-1}]	α
CH23	25	13.2	.000525
CH23	37	15.0	.00105
CHO	25	13.2	.0012
CHO	37	15.0	.000724

requires cellular metabolism. Alternately, it may signify a change in the cell surface properties, such as membrane rigidity. For CHO cells, the collision efficiency decreased with temperature. The reason for this is not evident, although it may also be related to changes in membrane properties.

For conA induced aggregation, Jones and Perry reported initial rates of aggregation versus conA concentration, like Linnemans *et al.* As with the above results, Jones and Perry found the collision rate to be proportional to the square of the cell concentration. The initial aggregation rate constant was reported versus the conA dose between one and 400 μg/mL. The collision time constants showed a maximum with conA dose, as expected. Unfortunately, these authors did not determine adsorption behavior of the conA on the cells. If the data of Linnemans *et al.* are correct, however, the equilibrium constant measured by these authors assays only an interaction between conA and the polysaccharides it recognizes. This equilibrium constant should be applicable to the Chinese Hamster cells as well. To make a rigorous calculation of surface coverage, the number of adsorption sites per cell needs to be known. However, assuming that the cells adsorbed a negligible amount of the total conA in solution, it is possible to use the Linnemans *et al.* equilibrium constant to calculate the fractional surface coverage. The current authors' collision rate data

is plotted in Figure 3-10 versus the calculated fractional surface coverage. Like the data of Linnemans *et al.*, the collision efficiency goes through a maximum in the vicinity of half-coverage of the surface. It is remarkable that the collision rate is this consistent due to the indirect calculation of the surface coverage.

The paper of Goldsmith *et al.* (1981) is interesting since it represents the only literature dealing with microscopic examination of animal cell collision behavior. The experiments conducted by these authors are similar to those conducted by Takamura, Goldsmith and Mason (1981) discussed in section 3.5.1.1. It is not obvious that the collision efficiency theory presented in section 3.5.1. developed for rigid spheres stabilized by electrostatic forces is applicable to animal cells. This is for the reasons outlined in section 3.2. The authors observed the collisions of sphered erythrocytes and granulocytes (leukocytes) in Poiseuille tube flow with maximum (wall) shear rates between 4 and 20 s^{-1}. For the 5.6 μm sphered red blood cells used, Peclet numbers were greater than 2000. Cell surface potentials were -25 mV, and experiments were conducted in 0.01 M ionic strength saline. It was not possible to fit the trajectories obtained to realistic values of the London-Hamaker constant given the known repulsive potential of the cell surface. However, scanning electron micrographs showed the presence of surface asperities from 50 to 300 nm projecting from the cells. These features were an artifact of the erythrocyte sphering procedure, and affected the range of the interparticle forces. When the presence of the surface projections was incorporated into the trajectory equations as a minimum approach distance, the trajectory equations were able to fit the observed trajectories with realistic Hamaker constants. The minimum membrane separation distances calculated indicated that the separation was too large for traditional colloidal colloidal attractive and repulsive forces to be operative. Nevertheless, some collisions produced adhering doublets, especially in the presence of antisera (antibodies) to the erythrocytes. Permanent doublet formation was also noted for granulocytes which had "ruffled" surfaces. These results indicate that in

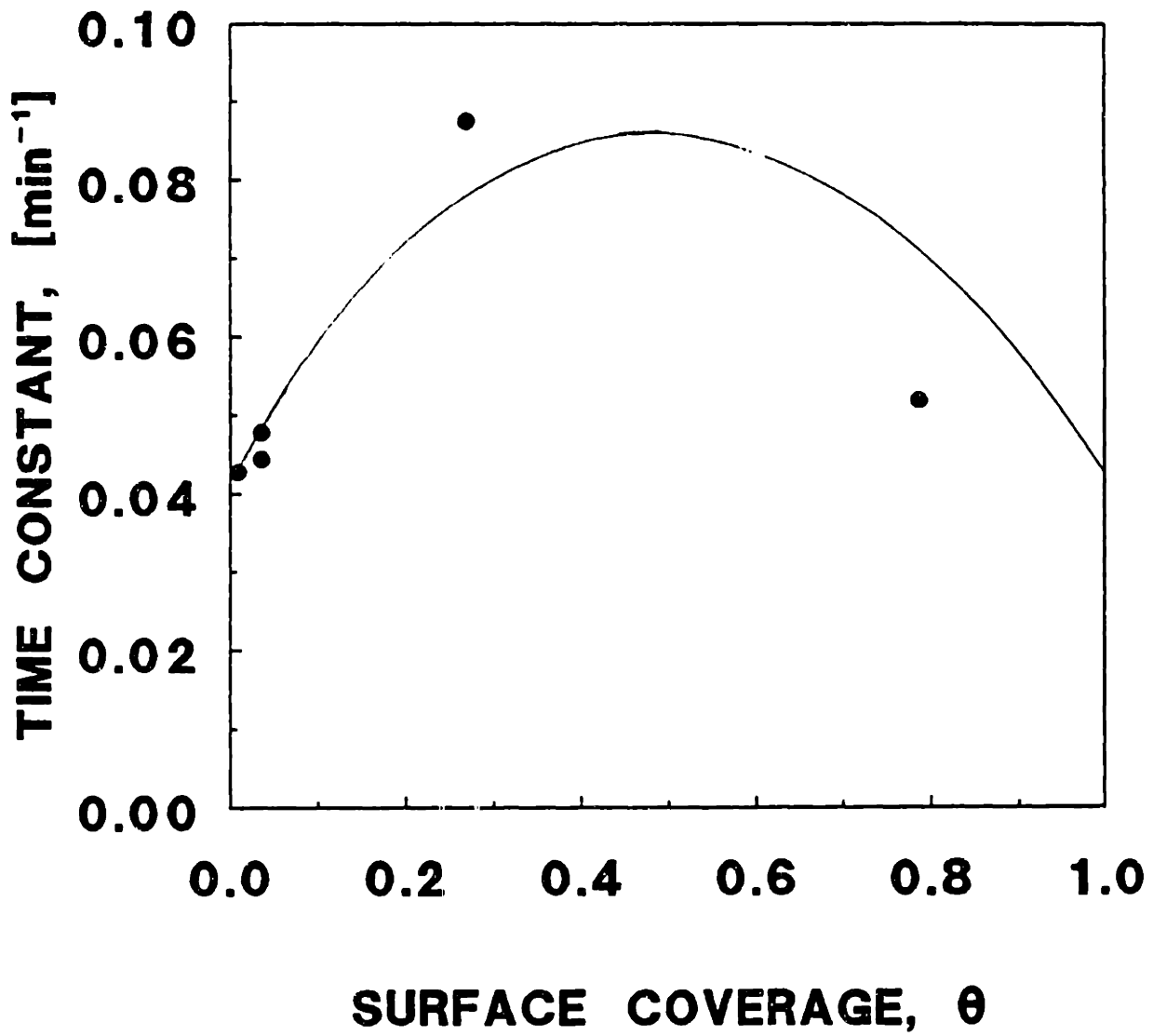

Figure 3-10. Collision rate constant for concanavalin A agglutinated Chinese Hamster Ovary cells versus calculated fractional surface coverage from the combined data of Jones and Perry (1978) and Linnemans *et al.* (1976).

order for animal cell adhesion to occur, the attractive forces must come from cell surface projections, or from compounds which can bridge the distance between membranes. This distance will be the length of any projections which are present.

3.5.3. - Collision Efficiency Review Summary and Thesis Goals

Two classes of collision efficiency theory were reviewed in section 3.5.1.; deterministic fluid mechanical calculations, and probabilistic calculations. Certain features of colloidal flocculation are ignored by both. The probabilistic calculations represent crude calculations of attractive interaction between microscopic domains, or "sites", on the particle surface. Their utility lies in the ability to relate the collision efficiency in a simple way to the heterogeneous particle surface properties caused by flocculant adsorption. Since these calculations are incomplete as a description of the absolute force magnitude existing between particles, they are not expected to be able to quantitatively predict collision efficiencies between particles. These formulations do, however, capture the essential features of particle flocculation. It is possible that they may even be used as correlaters of collision efficiency data, with the addition of factors to account for changing hydrodynamic conditions. Unfortunately, where there has been considerable reference to the theory in the literature, there has been virtually no experimental verification of their form or functionality for polymer flocculation. This is evident from the review in section 3.5.2.1., where only Hahn and Stumm (1968) have reported directly obtained collision efficiencies versus polymer dose. Even here, the authors failed to compare the results to a fractional surface coverage. It should be noted that there is a substantial body of literature which reports gross measurements of flocculation, such as zone settling velocities, or residual turbidity, as a function of flocculant dose. However, this data incorporates not only collision efficiency, but also floc breakage, floc structure, and a host of other variables. As such, it is not useful as a true measure of suspension destabilization. The results of Linnemans *et*

al. (1976) for lectin induced aggregation of animal cells show that for ideal situations of bridging flocculation, the functionality of the collision efficiency is described very well by probabilistic theory. This is additionally supported by the data of Jones and Perry (1979). With refinements, this branch of collision efficiency theory may prove to be a very utilitarian method of correlating experimental collision efficiency.

The fluid mechanical calculations are appealing for a complete physical description of aggregation including hydrodynamic interactions. From the review of the experimental literature in section 3.5.2., it is evident that much of the supporting experimental literature has been performed under poorly characterized conditions of absolute shear rate and aggregation regime such that the results regarding hydrodynamic dependency are inconclusive. However, the more carefully controlled experiments in the literature support this theory as incorporating all of the relevant physics of interaction for ionic coagulation. The results of Delichatsios and Probstein (1975) and Melik and Fogler (1985) versus coagulant concentration are especially encouraging; these indicate that not only may the collision efficiency be correlated versus the attractive parameter C_A, it may also be possible to obtain a collision efficiency correlation versus the electrostatic force term C_{RA} in the partially destabilized region. Thus, if the electrostatic, London-Van der Waals and hydrodynamic forces govern animal cell collision, it should be possible to pose a dimensional analysis of the problem and correlate collision efficiency versus the variables in C_A and C_{RA}.

It is questionable whether the ionic coagulation modelling is applicable to polymer flocculation, since it ignores the surface heterogeneity which is present with polymer adsorption. It also ignores the effects of polymer extension from the surfa. . Despite considerable speculation on interparticle bridging behavior by polymers, it seems that in certain cases polymer adsorption may be treated as simply modifying the particle surface potential, and exerting no other influence on particle collision (see review of Takamura,

Goldsmith and Mason (1981) above). This raises the prospect of applying the ionic coagulation theory to polymer flocculation in general. The major difficulty is to calculate the effects of flocculant destabilization on the particle properties which enter into equations (3-11) and (3-12).

It will be the major goal of the experimental portion of this thesis to examine the aggregation of animal cells using a flocculation system which leaves the cells viable for recycle. As discussed in section 3.2., there is ample reason to believe that cells may not behave as ideal colloids. However, the direct measurements of Curtis (1969) suggest that embryonic cells undergoing natural aggregation obey the ionic coagulation results versus shear. The results of Linnemans *et al.* (1976) suggest that bridging aggregation follows the expected dependencies from probabilistic theory versus the degree of destabilization. However, in this case the shear dependency of the collision efficiency is much stronger than that found by Curtis. This may be due to bond breakage in the high shear situation which is inadvertently incorporated into the collision efficiency. One difference between cellular and model colloid collisions is pointed out by the studies of Goldsmith *et al.* (1981). This is the idea that cell surfaces are not microscopically smooth on the scale of colloidal force action, and will not follow classical ionic coagulation trajectories. Compounds which are able to bridge across cells may be necessary to achieve flocculation. This and other factors may modify the absolute cell collision efficiency and its dependency on physical parameters.

It is evident that for a given flocculant and cell combination, it is impossible to predict *a priori* what the collision efficiency or its dependency on flocculation conditions will be. This points out the necessity of experimental determination of animal cell stability, and of revised theoretical relationships to account for deviations from the classical, idealized theoretical literature. The experiments and theory which have been conducted to this end are found in Chapter 6.

3.6. - Floc Structure

Floc structure is recognized as an important part of the process of flocculation and growth of many microorganisms. The packing arrangement and packing density of the constituents of the floc affect the physical properties of the floc as well as the physiological characteristics of the microorganisms that comprise the floc. In the physical realm, the structure affects the flocculation kinetics, floc strength, transport of substances into and out of the floc, and the sedimentary behavior of the floc. In the physiological realm, the transport of nutrients and the dynamics of floc formation and breakage, which are dependent on the floc structure, determines whether the microbes at the floc center are starved or not.

Flocs produced by aggregation of solids are not space-filling structures; unlike the aggregation of liquids, the particles colliding to produce a floc do not coalesce into a space equal to the sum of the constituent volumes. That is, the number of particles in a floc is not given by the Euclidean geometrical argument:

$$i = \frac{\frac{4}{3}\pi a_i^3}{\frac{4}{3}\pi a_1^3} \tag{3-29}$$

This is due to the random addition of particles to the floc and their immobility after deposition. When particles adhere, they tend to form extended, tenuous structures. It is the goal of this portion of the thesis work to describe the structures produced by aggregation of animal cells, and to describe their properties.

It has been observed in experimental and theoretical studies that the structure of particle clusters may be accurately described in many cases by fractal geometry. Fractal geometry is a branch of mathematics formalized by Mandelbrot (1982) to describe chaotic structures and their properties. When a geometric form is created by a random process, it often possesses a scale invariance, such that the appearance of the form is similar upon a change of length scale. When the form possesses such self-similarity, or scale invariance,

it is often described well by fractal geometric properties. Many naturally occurring bodies are fractal in nature. For example, island coastlines, cloud surfaces, and galactic clusters are chaotic fractal forms in one, two, and three Euclidean dimensions. For a thorough layman's description of fractal geometric concepts and natural examples, the reader is referred to Mandelbrot (1982).

The reason that flocs may possess fractal properties may be pictured as follows. A floc is created by random addition of particles to form small clusters, which randomly combine to form clusters of clusters, and so on. If one examines the packing of particles with a magnifying glass which views a length scale of clusters, the view will be very similar to the view of cluster packing using a magnifying glass with a length scale of clusters of clusters. Due to the random nature of addition and the self-similar construction of the floc versus scale, it is probable that the floc may be described by fractal geometry. This review will proceed with the premise that flocs can be described as self-similar fractal clusters in space.

3.6.1. - Fractal Cluster Theory

The evidence for fractal geometry in aggregate structure has been thoroughly reviewed recently by Meakin (1988a). The reader is directed there for descriptions of fractal clusters, and their generation via computer simulation. This section will give a brief overview of the issues in aggregate formation, and the dimensionalities of the structures that have been produced by theoretical simulations of floc formation. One of the results of the proposition that flocs are fractal bodies is that floc size dependence on the number of constituent particles in the floc should be representable as a power law functionality:

$$i = k a_i^{D} \tag{3-30}$$

Here, i is the number of cells present in the floc, k is an unknown empirical constant,

$k \approx \alpha(a_1^{-D})$, a_i is a characteristic radius of the i-sized floc, and D is the fractal dimensionality of the floc. The value of a_i can be any of several measures of the floc size; the hydrodynamic radius, the radius of gyration, or maximum radius, to name a few. This is compared to equation (3-29) for a coalescent system, which is equivalent to having D = 3. D represents among other things the "space-fillingness" of the floc. If D is three, floc porosity is constant versus particle size. When D is less than three, porosity increases with floc size.

Flocs, or clusters, are formed by addition of particles in somewhat random fashion to existing flocs. Actual mechanisms of particle addition are largely uninvestigated from an experimental, microscopic perspective. However, the mechanisms which have been proposed are amenable to idealized computer simulation. The basic approach to theoretical generation of clusters is the same as that described in section 3.3.1. for Monte Carlo simulations of aggregation kinetics. In this case, the aggregate size distribution is of ancillary interest, and the properties of the flocs are the main object of study. The variations of aggregate structure studies are distinguished by three major features. These are the method of floc creation, the type of particle approach trajectory, and the amount of floc restructuring allowed. A fourth variation which will be discussed is the degree of particle destabilization.

The first feature distinguishing simulations is the nature of floc construction. The original works in the field created clusters by addition of single particles to a central floc (Vold (1963), Sutherland (1966)). Later models combined flocs of the same size, and flocs of unequal size. For otherwise identical simulations, the method of particle combination affects the resulting structure. Clusters generated by addition of single particles are more compact than clusters generated by addition of unequal-sized flocs, which are slightly more compact than clusters created from equal-sized flocs. When the floc sizes differ, the selection frequency, or collision frequency of a cluster size class will

affect the fractal dimension as well as the cluster size distribution. For Brownian aggregation simulation, the selection frequency for flocs of different sizes should be constant, consistent with the von Smoluchowski diffusive rate kernel, equation (3-6). The selection frequency for a simulation representative of shear aggregation would be highly size dependent, consistent with equation (3-8). However, simulations representative of shear coagulation have not been performed to the knowledge of the author.

The second major difference between models is the nature of the particle trajectories. To date, the hydrodynamic equations have not been solved for the trajectories of irregular aggregates in a viscous medium incorporating interparticle forces. Therefore, the particle trajectories are idealized in computer simulations. In fact, the trajectory, or "walk", of the particles may be described by a fractal dimension, D_W. For Brownian diffusion, the walk is of dimension two since the actual distance travelled by a randomly walking particle going between two positions is proportional to the distance between initial and final positions squared. Straight-line, or ballistic trajectories have D_W equal to one. For reaction-limited aggregation the probability of adhesion rather than the trajectory governs whether the flocs or particles will combine. In this case, the walk may be said to be zero order. In addition to these fairly straightforward concepts, the walk may also be fractal, as in Lévy flight models which have non-integer values of D_W (Meakin (1984)). In general, for higher values of D_W, looser structures are produced.

The third difference between models is the amount of floc rearrangement that takes place upon contact. In the simplest models, no rearrangement is allowed, so that once the initial contact is made, the flocs are locked into their relative positions. In reality, it is likely that multiple contacts will result since flocs are not infinitely rigid. This is especially so for cases of shear aggregation, where hydrodynamic forces might be expected to modify floc structure. In computer simulations, rearrangement is accounted for by rotating the colliding flocs about their initial (and subsequent) contact point(s) until two or more contacts are

made to stabilize the new aggregate. The fractal dimension increases with each restructuring rotation stage. Up to three stages of restructuring have been investigated.

In addition to the above issues, the influence of particle destabilization may be roughly modelled by aggregating particles with different properties. Three types of simulations have been performed. In the first, the particles are given anisotropicity, making one hemisphere "positive" and the other hemisphere "negative" (Meakin *et al.* (1987)). The particles are brought together as in the other models, but adhesion results only if a positive particle face contacts a negative particle face. The second model brings together two different particle species, which are only adhesive with respect to the other (Meakin and Djordjevik (1986)). In these simulations, the amount of each particle specie can be varied. The results suggest that the presence of two species does not affect the fractal dimension on large scales, but slows down the aggregation kinetics much like a partially destabilized suspension. One interesting result of these simulations is that indefinitely large clusters can only be generated for a certain range of mixtures of the two species. When the mixture is close to containing all one particle type or the other, the sticking probability for large clusters becomes vanishingly small. The third type of simulation incorporates a dipole into the primary particles, which tends to create linear, end-to-end floc structures with lower fractal dimensions. This has been investigated for various dipole intensities by Jullien, Botet and Mors (1987), and Mors, Botet and Jullien (1987).

The simulations which have incorporated floc restructuring have also taken into account the other major factors in the aggregation models; the fractal dimensions resulting from these and other simulations are presented in Table 3-4. It should be stressed that the fractal dimensions produced by the simulations are degenerate; that is, a flocculation mechanism may not be deduced from an experimental measurement since there are several mechanisms which produce similar dimensions. It is possible to interpret trends in experimental data, however.

It is not difficult to select the simulations which would most closely approximate induced animal cell aggregation. Since particle collision frequency is proportional to a_i^3 for shear flocculation, models for single particle addition to flocs are unrealistic. Since this collision frequency dependency will also lead to a divergent population distribution, it is reasonable to expect that same-sized models would also not be accurate. Thus, disperse models would be expected to be the most appropriate. As noted above, there are no simulations using a selection frequency representative of shear driven aggregation.

Table 3-4
Floc Dimensionalities Produced from Different Computer Simulation Assumptions (Adapted from Meakin (1988a))

		# of Restructuring Steps			
Colliding Particles	Trajectory, Dim.	0	1	2	3
Floc-Particle	Reaction, 0	3	-	-	-
Floc-Particle	Ballistic, 1	3	-	-	-
Floc-Particle	Diffusion, 2	2.52	-	-	-
Similar Flocs	Ballistic, 1	1.89	2.08	2.13	2.13
Similar Flocs	Diffusion, 2	1.78	-	-	-
Disperse Flocs	Reaction, 0	2.09	2.18	2.24	2.25
Disperse Flocs	Ballistic, 1	1.95	2.13	2.18	2.19
Disperse Flocs	Diffusion, 2	1.80	2.09	2.17	2.18
Floc-Dipolar Particle	Reaction, 0	1.46-1.78			

For shear driven flocculation, the trajectories would be expected to be approximately ballistic, although it was pointed out in section 3.4. that this will not strictly be the case. For partially destabilized suspensions, reaction-limited simulations might be particularly appropriate. Although Brownian random walk trajectories might ordinarily be excluded, real aggregation processes are usually conducted under turbulent fluid flow. For flocs which are on or above the Kolmogorov microscale, flocs will travel with the fluid eddies in a random walk, so larger trajectory dimensions should not be excluded. It is also reasonable to expect restructuring to take place within the floc, dependent on the fluid shear in the aggregation step. Many authors (Gasner and Wang (1971)) have shown experimentally that intense agitation produces more compact floc compared to flocs produced at more moderate agitation levels. Although only three levels of restructuring

have been investigated theoretically, it is easy to imagine bending and buckling of flocs under fluid shear which would produce more than this amount of restructuring and commensurately higher fractal dimensions.

3.6.2. - Experimental Investigations of Floc Structure

Experimental descriptions of floc structure have traditionally used empirical data fits to describe floc porosity. These correlations usually follow power-law functionalities of the form:

$$(1 - \varepsilon_i) = k a_i^{-\lambda} \tag{3-31}$$

In this equation, ε_i is the floc porosity and k and λ are constants dependent on the flocculation conditions. It is only recently, with the recognition that cluster formation may produce fractal structures that researchers have investigated the fractal dimension of experimentally produced clusters directly. The relationship between the above correlation and the fractal dimension is readily seen by rearranging equation (3-29), incorporating the floc porosity, and inserting equation (3-30) for i:

$$(1 - \varepsilon_i) = \frac{\frac{4}{3}\pi a_1^3 i}{\frac{4}{3}\pi a_i^3} = (a_1^3 k) a_i^{D-3} \tag{3-32}$$

It can be seen from comparison of (3-32) with (3-31) that the value of $-\lambda$ correlated in the empirical studies is analogous to [D - 3]. This section will examine experimental correlations of both floc porosity and fractal dimension.

3.6.2.1. - Direct Measurements of Floc Structure

In one of the earlier measurements of floc structure, Lagvankar and Gemmel (1968) used a pycnometric technique to study the density of iron hydroxide flocs formed by precipitation of ferric chloride in alkaline solution. The authors immersed flocs in sucrose

solutions of known density, and by trial and error the proper solution density was found at which the floc did not sediment or float. The floc dimension was recorded and the process repeated. In this manner, the authors found a correlation like equation (3-31), with lambda values of 0.22 for flocs larger than 1 mm diameter, and 0.68 for flocs smaller than 1 mm diameter. These values translate to fractal dimensions of 2.78 and 2.32. This is high compared to the computer simulations of Table 3-4, and may indicate other factors present in the aggregation. In particular, the handling of the flocs for measurement may have caused floc compression.

Weitz and Oliviera (1984), and Weitz *et al.* (1985) investigated the Brownian coagulation of aqueous gold sols destabilized by adsorption of pyridine. The flocs were dried and subjected to transmission electron microscopy, giving a two-dimensional projection of the original floc. Using image analysis of the micrographs, the particle-particle density distributions as well as the floc dimensions were analyzed. These methods gave identical fractal dimensions. Under conditions where aggregation was rapid, the authors obtained a fractal dimension of 1.75±.05. Under conditions where the suspension was only partially destabilized, the fractal dimension obtained was 2.05±.05. These differences reflect the nature of aggregation. In the first case, floc formation was probably diffusion limited, and in the second case floc formation was probably reaction limited. From Table 3-4 it is apparent that the experimental results closely match the values predicted by the theoretical simulations for cluster-cluster aggregation.

Schaefer *et al.* (1984) investigated the diffusive ionic coagulation of silica sols by both x-ray and light scattering. Mie scattering theory predicts that a plot of the scattered energy intensity versus Q, where $Q = (4\pi\sin\theta)/\lambda$, will give the density correlation of the scattering centers. In this relation, θ is the scattering angle, and λ is the incident energy wavelength. For a fractal structure, the density correlation, or radial particle concentration, between particles (which are scattering centers) is given as:

$$c(r) = k'' r^{D-3} \qquad (3\text{-}33)$$

Thus, a log-log plot of scattered intensity versus Q should yield a straight line with slope equal to [D - 3]. Using this method, the authors found a fractal dimension of 2.12±0.05 for both x-ray and light scattering. The scattering spectra did not exhibit the expected straight line behavior until 32 hours into the experiment, suggesting slow aggregation. This is consistent with the above gold sol experiments.

Sonntag and Russel (1986a) investigated the aggregation of 0.14 μm polystyrene latex undergoing ionic coagulation. The fractal dimension of the flocs produced was measured by the same light scattering method as above. For Brownian diffusive aggregation of the latex spheres, the authors found fractal dimensions of 1.61 at 0.4 M and 1.65 at 1.0 M ionic strength. These values are close to those in Table 3-4 for diffusive aggregation with no rearrangement. When the flocs were allowed to cream at the top of the suspension over a week's time, the fractal dimension increased to 2.20, suggesting floc rearrangement with time. Shear flocculation at shear stresses up to 200 dyne/cm^2 gave fractal dimensions of 2.48. This high value probably reflects further floc rearrangement.

In the only direct measurement to date on biological particles, Davis and Hunt (1986) reported fractal dimensions for flocs produced by naturally aggregating yeast strains. These authors used a light microscopic technique to measure the fractal dimension. A floc was measured using a calibrated eyepiece, and then the slide was gently heated, dissociating the floc. The dissociation allowed the individual cells to be counted, and the fractal dimension could be calculated by measuring a range of floc sizes. The authors found dimensions between 1.75±0.15 and 2.25±0.15. The experimental conditions of aggregation were not described. It is somewhat surprising that higher fractal dimensions were not found for flocs produced in a high shear fermenter environment. Under these conditions of aggregation, floc rearrangement and compaction might be expected to take place.

Axelos, Tchoubar and Jullien (1986) used small angle x-ray scattering to measure the fractal dimensions produced by diffusively aggregating aluminum hydroxide complex, $Al(OH)_x$. For x = 2.5, a fractal dimensionality of 1.45 was found, and for x = 2.6, D was found to be 1.86. The authors rationalized the lower value in terms of the dipolar aggregation simulations of Jullien, Botet and Mors (1987), which produced a fractal dimensionality of 1.46. Their idea was that at the lower hydroxide value, lattice ion vacancies in the precipitate produce a particle dipole. This conclusion is dubious due to the small difference between the two x values used, although the reason for the low value at x = 2.5 is not evident. These results also stand in contrast to the results of Lagvankar and Gemmel for iron hydroxide floc. The lower dimension may reflect the differences in measurement techniques; where the current method is *in situ*, Lagvankar and Gemmels' measurements may have modified floc structure as discussed above.

Kim and Brock (1987) investigated the aggregation of ferromagnetic iron and cobalt particles using transmission electron microscopy. These authors found fractal dimensions of 1.54 and 1.72 for the two respectively. These results were also explained in terms of the theoretical simulations of Mors, Botet and Jullien (1987), for aggregation of dipolar particles. The theoretical simulations show that for particles with small dipoles D approaches 1.78, and for larger dipoles, D decreases continuously to 1.46. This is consistent with the large and small magnetic moments of iron and cobalt, respectively.

Hurd and Flower (1988) investigated the *in situ* growth of silica aggregate aerosols in a flame by light scattering. These authors found a low value of 1.49±0.15 for the aggregates produced. No explanation for the low dimension was given. It will be noted that this is the only study of aerosol clusters known. Absence of a highly viscous medium and low dielectric constant would increase the effects of colloidal interparticle forces on the aggregation, which may lead to different fractal dimensions.

Tang, Colflesh and Chu (1988) investigated the effects of temperature on the ionic coagulation of 15 nm silica hydrosols. These authors used both a light scattering technique and image processing of electron micrographs, and found good agreement between the two. As with the investigations of Weitz and Oliviera (1984), and Weitz *et al.* (1985), these authors found that under conditions where the suspension is partially destabilized, *i.e.* is reaction-limited rather than diffusion-limited, the fractal dimension increases. This was manifest as a fractal dimension of 2.03 at low temperatures. At high temperatures, fractal dimensions of 1.79 to 1.85 were reported, dependent on the measurement and calculation method. The reaction limitation can be attributed to a colloidal force energy barrier which governs sticking probability at low temperatures, but is negligible at higher temperatures.

Wong, Cabane, and Duplessix (1988) studied the structure of polymer flocculated 20 nm silica particles by small angle neutron scattering. This technique allowed detailed investigation of the particle density correlation in the floc. The effects of polymer charge density on the floc structure were investigated, with surprising results. For situations where the silica surface charge was not neutralized by low charge density polymers, the flocs showed short range ordering, possibly due to repulsive effects. This was not present for ionically coagulated particles or particles flocculated by strongly cationic polymers. In both cases, medium and long range correlations showed the flocs to be fractal. For the weak cation flocculation, the fractal dimension was 2.5, and for the strong cation flocculation, the fractal dimension was 1.9. The lower value for the strongly cationic polymer suggests immobility and inflexibility of the structure upon formation, where the weak cation result suggests ordering and rearrangement caused by residual forces and absence of rigid physical links caused by the macromolecules.

Ben Ohoud *et al.* (1988) attempted to investigate the porosity-size relation of several inorganic powders with sizes between 50 and 1500 μm. These powders might be expected to possess fractal structure since they are compacted masses of small particles. However,

the sizes of the powders commonly used is so large compared to the constituent particles that we might expect to be in the scale invariant region of the particle density correlation, where c(r) is constant ($r >> a_1$). Thus, porosity of these large powders versus size may show no dependence on scale, that is, D should equal three. These authors used simple mass and packed bed volume measurements to determine an apparent porosity versus particle size. It was concluded that the apparent porosity was unchanged versus particle size, giving fractal dimensions of three for all the powders investigated. What these authors were actually measuring, unfortunately, was the bed porosity rather than the particle porosity, so these results are invalid. One wonders whether the paper reviewer is not an invalid as well...

3.6.2.2. - Sedimentary Measurements of Floc Structure

Most of the above experiments were conducted with submicron sized suspensions undergoing Brownian motion coagulation. The results which will apply most directly to animal cell aggregation, however, is the shear flocculation of micron-sized colloids. Unfortunately, many of the techniques used above, especially light scattering, are inapplicable for large particles. A conventional method of obtaining floc porosity versus size for large aggregates is to measure the size and sedimentary velocity of individual flocs and relate the velocity to the effective density. Knowing the density of an individual particle, and assuming a particle friction coefficient, the absolute floc porosity can be calculated. If the primary particle density is unknown, an equation of the form of (3-31) can still be obtained, however, the absolute porosity value will be undetermined. This method has been used by many authors in the literature, not only for porosity versus size measurements (Tambo and Watanabe (1967, 1979a), Hermanowicz and Ganczarczyk (1983), Glasgow and Hsu (1984), Klimpel and Hogg (1986), Klimpel, Dirican and Hogg (1986), Ray and Hogg (1986), Li and Ganczarczyk (1987)), but also for measurements of

floc size distributions using the obtained porosity measurements (Magara (1967), Davis and Hunt (1986), Ray and Hogg (1986), Koh, Andrews and Uhlherr (1987)).

The difficulty in interpreting the literature which correlates porosity using sedimentary velocity measurements is that the frictional properties of the flocs are unknown versus the scale of the floc and the actual porosity. In all of the above articles, hard sphere friction coefficients have been used to calculate the porosity; this assumption is probably not correct for porous flocs. It is of interest to know the frictional properties of flocs versus their size and structure, and the literature concerning this issue will be discussed in section 3.6.3. In spite of this limitation, the findings of the literature will be reviewed here.

Tambo and Watanabe (1967) correlated the structure of several different types of flocs under shear aggregation by the form of equation (3-31). This original work was in Japanese, but was republished along with new data in a later paper (Tambo and Watanabe (1979a)). The authors used the relation $C_D = 45/Re$ to calculate the drag coefficients of the flocs. These researchers performed a thorough study of floc structure versus flocculation conditions. The conditions and results of their experiments are shown in Table 3-5, along with the nominal fractal dimension calculated from the correlations via equation (3-32). Table 3-5 shows effects of flocculant specie and dose on the floc structure. From the Kaolin:alum flocculation data, it is evident that increasing the flocculant dosage decreases the fractal dimensions of the floc. This may be interpreted in terms of floc strength; as lower alum to clay ratios are used, the flocs produced are weaker, and are more susceptible to rearrangement. The results using iron and magnesium hydroxides are not directly translatable to the alum data since the molar amounts used differ and the metal hydroxide stoichiometry will differ. Solution chemistry differences probably also account for the differences in color floc structure versus pH. In addition to investigating coagulant dose, the authors investigated aggregation of Kaolin with alum including cationic flocculant polymers as flocculation aid. There was no effect of flocculant aid on the floc structure

using 0.1 to 0.3 mg/L AccoFloc N100 at a flocculant:Kaolin ratio of 1:10. The effect of agitation speed was also investigated; power inputs were estimated from the flocculation vessel dimensions, the agitation conditions, and the correlations of Rushton *et al.* (1950) to

Table 3-5
Floc Porosities and Fractal Dimensions Versus Flocculation Conditions for the Data of Tambo and Watanabe (1979a)

Flocculated Substance	Coagulant	$-\lambda$	$D_{calc.}$	Coagulant Dose	Notes
Kaolin	$AlOH_x$	1.41	1.59	1:10	
Kaolin	$AlOH_x$	1.40	1.60	1:12	
Kaolin	$AlOH_x$	1.30	1.70	1:17-1:20	
Kaolin	$AlOH_x$	1.23	1.77	1:20-1:23	
Kaolin	$AlOH_x$	1.03	1.97	1:50	
Kaolin	$AlOH_x$	1.05	1.95	1:60	
Kaolin	$AlOH_x$	1.11	1.89	1:100	
Kaolin	$FeOH_x$	1.08	1.92	1:5	
Kaolin	$MgOH_x$	1.09	1.91	2:5	
Color	$AlOH_x$	1.33	1.67	7.7:10	pH 6.00
Color	$AlOH_x$	1.23	1.77	7.7:10	pH 4.92
Color	$FeOH_x$	1.42	1.58	7.7:10	pH 3.70
Color	$FeOH_x$	1.31	1.69	7.7:10	pH 4.95
Color	$MgOH_x$	1.52	1.48	7.7:20	pH 11.40
Activated Sludge	-----	1.70	1.30	-----	
Bulking Sludge	-----	2.00	1.00	-----	

range between 60 and 490 cm^2/s^3. This translates into average shear rates between 77 and 220 s^{-1}. The authors found no effect of agitation speed on the floc density correlation. This might be explained by the small range of average shear rates investigated.

Tambo and Watanabe also presented data for biologically active sludges; the lambda values derived from their Figure 14 are presented in Table 3-2. The fractal dimensions derived from these correlations, 1.45 to 1.0, are low compared to the values for inorganic floc. This may reflect the differences between artificially flocculated material and flocs which are produced by the growth of living microorganisms. At first glance, one might expect microbial flocs to possess a higher fractal dimension, since fission growth of non-motile microorganisms would imply that the short range correlation of cell density would

be large. The current results suggest two scenarios. The first is that the cells in the floc are not fission reproducers, but are budding, or mycelial, and effectively possess "dipoles" (from end-to-end growth) as in the theoretical models of Jullien, Botet and Mors (1987). The second is that metabolically active flocs limit their density by some mechanism to prevent nutrient starvation.

Glasgow and Hsu (1984) investigated the structure of Kaolin clay flocculated by a 10 million molecular weight anionic polyacrylamide in a stirred tank. Flocculation was conducted at 62 s^{-1} average shear rate, and the pH was varied to study its effects on floc structure. Although the authors introduce the idea that floc permeability will affect the frictional properties, there is no indication what friction coefficient was used to calculate the floc density versus size relationship. The authors reported the dependence of the apparent floc density on the floc diameter as a power law relation. From the relations presented, fractal dimensions may be calculated between 1.83 and 2.41.

Klimpel and Hogg (1986), Klimpel, Dirican and Hogg (1986), and Ray and Hogg (1986) investigated the structures of aggregates of 3 to 40 μm diameter quartz particles destabilized by nonionic polyacrylamide. These researchers used the hard sphere relations of Concha and Almendra (1979) for the floc drag coefficients. The floc porosity versus size relationship was correlated to a modified form of (3-29):

$$\log(1 - \varepsilon_i) = \frac{\log(1 - \varepsilon_\ell)}{1 + \left(\frac{a_i}{a_g}\right)^{-\lambda}} \qquad (3\text{-}34)$$

This empirical correlation form was proposed to account for the observation that floc porosities tend to unity below a certain size, a_g, and tend to attain a limiting value, ε_ℓ at large sizes. From the viewpoint of fractal cluster theory, the low floc size limit represents the inapplicability of fractal theory for very small aggregates. The limiting value at large floc sizes represents the fact that fractal theory describes the cluster structure only over a

certain range of floc size. On extremely large length scales, floc structure will again become uniform, corresponding to a gelation network. In addition, different flocculation mechanisms may become operative at large scales which give different fractal dimensions. Examination of the authors' raw data shows that for most of the conditions, the floc porosity versus size correlation could be equally represented by (3-31). The values of λ which may be calculated from the data using (3-31) are well represented by the authors' λ values calculated by (3-34). Table 3-6 shows the range of λ values reported versus the conditions of aggregation.

Agitation was varied between mean shear rates of 356 and 2917 s^{-1}. The effect of agitation intensity is to decrease the fractal dimension of the floc; this is in contrast to the findings of Tambo and Watanabe, who observed no effect of agitator speed. This result is counter to intuition, as increased stress would be expected to either destroy flocs or compact them. It is not obvious why the increased fluid forces would create looser, ostensibly weaker flocs. The effect of mixing time on the fractal dimension should also assay the aging, or rearrangement taking place upon flocculation. Table 3-6 shows that increased agitation times again leads to decreased fractal dimensions. Like the agitation intensity results, the reason for this trend is unknown.

The effect of polymer concentration is inconclusive, with no discernible trend in the data. This is in contrast to the data of Tambo and Watanabe, and may reflect the difference between the systems. The flocculant here is a 13 million molecular weight polymer, where the flocculant in the previous study was an ionic coagulant. The primary particle size does not have an effect on the floc structure either. This is not surprising, although the floc size and the turbulence scales might be expected to interact and produce differences. Likewise, the solids concentration in the flocculator has no effect on the floc structure.

Li and Ganczarczyk (1987) investigated the structure of activated sludge flocs under unspecified agitation conditions. Using the Stokes-Einstein relation, these researchers

correlated the floc settling velocity by $U_{term} = 1.47\ d^{0.55}$. From this equation, a fractal dimension of 1.45 may be derived. This compares favorably to the Tambo and Watanabe values for activated sludge and bulking sludge, and again suggests that active mechanisms, or the mode of cellular division may limit the packing of the microorganisms in naturally occurring flocs.

Table 3-6
Floc Porosities and Fractal Dimensions Versus Flocculation Conditions for the Data of Klimpel and Hogg (1986)

Flocculant Dose, [mg/L]	Mean Shear Rate, [s^{-1}]	Mixing Time, [s]	Solids [wt %]	Particle Size, [μm]	- λ	$D_{calc.}$
0.9	356	60	3	3.4	0.96±0.34	2.04
0.9	1031	60	3	3.4	1.34±0.24	1.66
0.9	1895	60	3	3.4	1.49±0.19	1.51
0.9	2917	60	3	3.4	1.53±0.25	1.47
0.9	1031	80	3	3.4	1.56±0.21	1.44
0.9	1031	100	3	3.4	1.50±0.16	1.50
0.9	1031	120	3	3.4	2.95±1.67	0.05
0.35	1031	60	3	3.4	1.23±0.15	1.77
1.17	1031	60	3	3.4	1.18±0.23	1.82
2.33	1031	60	3	3.4	1.24±0.24	1.76
5.82	1031	60	3	3.4	1.19±0.28	1.81
0.9	1031	60	5	3.4	0.88±0.20	2.12
0.9	1031	60	10	3.4	1.15±0.29	1.85
0.9	1031	60	3	19	1.09±0.61	1.91
0.9	1031	60	3	22	0.99±0.09	2.01
0.9	1031	60	3	30	1.26±0.15	1.74
0.9	1031	60	3	36	1.27±0.14	1.73
0.9	1031	60	3	39	1.06±0.14	1.94

3.6.3. - Floc Structure and Suspension Properties

The effects of non-space-filling flocs are widespread, as alluded to in section 3.6. This section will deal with those structural effects which bear directly on suspension dynamics and properties. These are the effects of the floc structure on aggregation kinetics, floc density, and floc friction coefficient.

3.6.3.1. - Floc Structure Effects on Aggregation Kinetics

When aggregation occurs to form clusters which are not space-filling, the hydrodynamic volume occupied by the suspension solids increases over time. If the initial volume fraction of particles in suspension is high enough, eventually the clusters will grow to form a single cluster which fills the volume of the container. This phenomenon is known as gelation, and occurs widely in macromolecular polymerization reaction systems. Although aggregation of cells is unlikely to produce a gelling system, the rate of aggregation will still be affected by the expansion of the volume fraction occupied by the suspended cells. This volume expansion effect has been incorporated into population balance solutions by Tambo and Watanabe (1979b) to model the aggregation of Kaolin by alum, and by Thomas (1987) to model latex coagulation.

Not only will the size of the floc enter into the aggregation kernel, the shape of the particle and its porous nature will enter into the collision efficiency calculation. Collision efficiency relations such as equation (3-13) pertain only to the case of solid spheres colliding in a shear flow. The issue of collision efficiencies for aggregates has been addressed by several authors (Tambo and Watanabe (1979b), Adler (1981e), Koh, Andrews, and Uhlherr (1987), Brakalov (1987)). All of these studies have addressed the collision efficiency of larger particles in terms of the results of the theoretical simulations of section 3.5.1.1. An observation of the ionic coagulation simulations is that the collision efficiency decreases as particle size increases (per equation (3-13)), and becomes zero at a limiting particle size. Since floc sizes do not in general increase to a gelation point, but tend to reach a steady value, either the flocs must be breaking, or the effective collision rate must be decreasing with floc size. Although the former is a more realistic view of what is occurring in flocculation, this latter conclusion is easily incorporated into the collision efficiency as a functionality on the floc size. This formulation is expedient for population balance solution since it eliminates breakage terms that are otherwise necessary to achieve a steady-state solution.

Tambo and Watanabe (1979b) proposed an empirical relation for collision efficiency versus cluster size in the form:

$$\alpha_{ij} = \alpha_{11}\left(1 - \frac{i+j}{2i_{max}+1}\right)^n \qquad (3\text{-}35)$$

This equation gives a decreasing value with size up to zero at the maximum floc size. However, this collision efficiency formulation is not satisfactory since for clusters with both i and j greater than $i_{max}/2$, equation (3-35) predicts a non-zero collision efficiency for a collision that produces a floc size greater than the maximum allowed. These authors fitted α_{11}, i_{max}, and n to their flocculation data, and found constant values of 0.3 for α_{11}, and 6 for n. In a similar formulation, Koh, Andrews and Uhlherr (1987) found no significant change in the predicted size distributions using n values from 3 to 9. They also determined non-constant α_{11} values versus the mean shear rate in the flocculator; these were reported above in section 3.5.2.2.

Adler (1981d) considered the collision cross-section presented by a uniformly porous sphere in simple shear flow by a streamline analysis. For flow around a body, there exists a separation surface between closed and open streamlines. When the body is porous, this separation surface can lie within the radius of the porous body. Adler reasoned that all fluid flow on open streamlines that pass within the floc radius will produce collision. His solutions showed that for open streamlines to exist within the particle radius, the reduced inverse permeability of the body, $\xi = a_i/\kappa^{1/2}$, must be less than 3.30. Here, κ is the particle permeability. For ξ less than this value, the collision efficiency is a complex function of ξ. Figure 3-11 shows Adler's calculated values of α for ξ values less than 3.30. An empirical fit to the values gives:

$$\alpha = \frac{2}{3}\exp\left(-\frac{\xi^{10/3}}{11.31}\right) \qquad \xi < 3.30 \qquad (3\text{-}36)$$

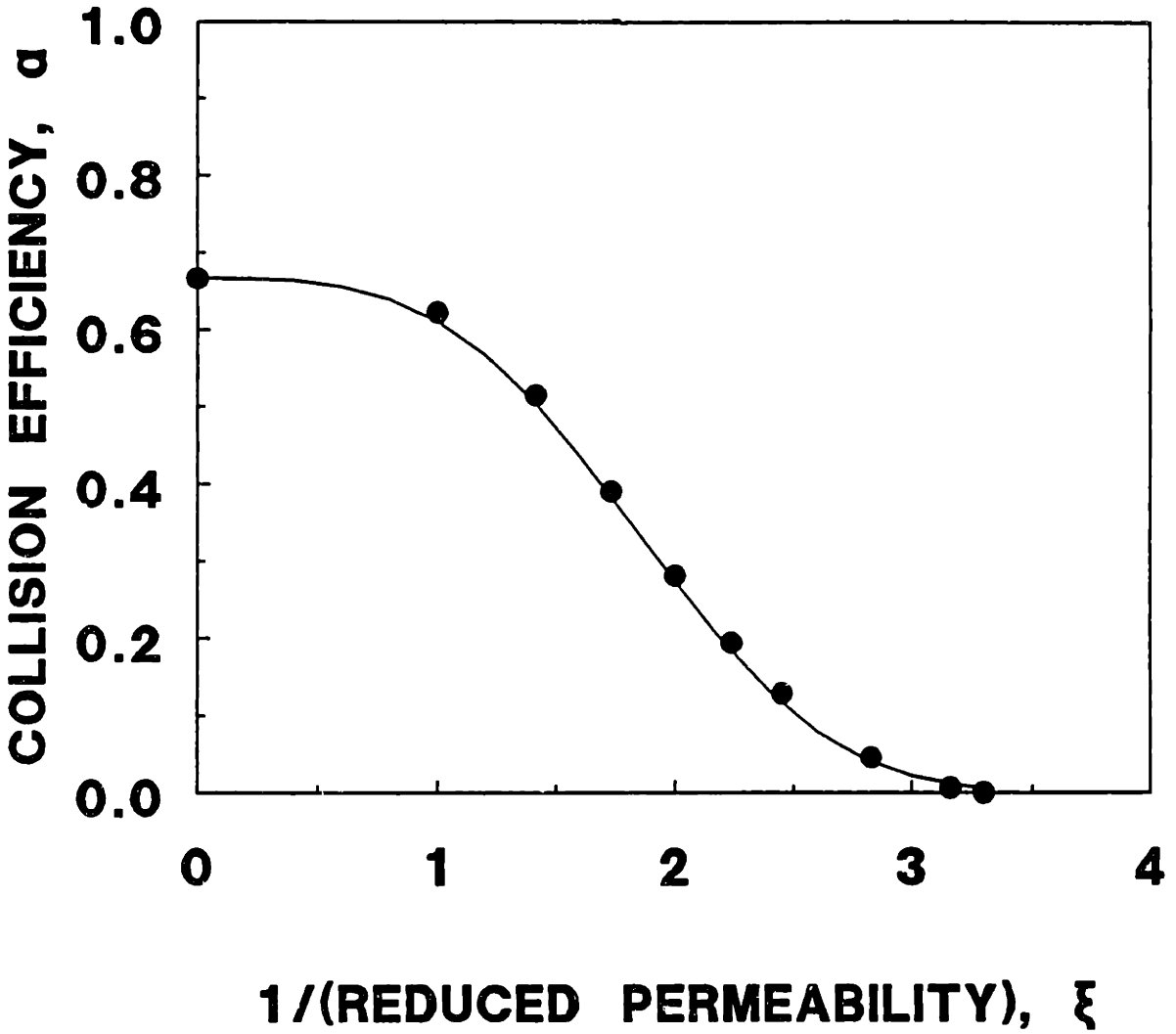

Figure 3-11. Collision efficiency versus the inverse of the normalized floc permeability, $\xi = a_i/\kappa^{1/2}$ from the calculations of Adler (1981d). The solid line is the prediction of equation (3-36).

This relation is shown as the solid line in Figure 3-11. In order to use the Adler results, the relation for the floc permeability versus size must be known, which limits the applicability of the relation. In addition to this limitation, the relation applies only to spheres of constant permeability, where a fractal floc will have a variable permeability which approaches infinity at the floc "edge".

Brakalov (1987) determined values of a_{max} for magnesium hydroxide aggregates versus aggregation conditions. These values were used to optimize the solution of equations (3-10) (applicable for impermeable spheres) and fit the London-Hamaker constant value which predicted a_{max} accurately. Brakalov's results were not presented in a form amenable to application to other cases. The London-Hamaker constants found were within accepted limits.

Although the observation that in ionic coagulation of solid, smooth spheres there exists a maximum particle size at which the collision efficiency equals zero, these solutions do not realistically translate to the aggregation of flocs. There will be two determinants of floc collision efficiency; the porosity and relative sizes of the colliding flocs. In reality, flocs with a fractal dimension less than three will be highly irregular, and may have branches extending well beyond the mean radius, or radius of gyration (Meakin (1988b)). These branches can touch and adhere to other passing flocs even though the center of gravity of a passing floc follows a trajectory that would not ordinarily result in contact. In addition, floc permeability and its distribution will reduce the magnitude of the hydrodynamic interactions as the flocs approach one another. The liquid film that would ordinarily have to be displaced tangentially to the surfaces can flow through openings in the flocs or channels at the floc surface. As the floc dimension approaches three, however, the assumptions of decreasing collision efficiency with increasing floc size may be valid. For single particles approaching flocs, one might expect that the normal hydrodynamic and interparticle forces posed in section 3.5.1.1. would influence collision since a single

particle may see the floc as a collection of individual spheres. This again will depend on the amount of floc permeability and the surface roughness. If the pores in the floc are on the scale of single particles or small flocs (at low D), it is possible that a small particle may pass through the pores without contacting the floc. It is unlikely that this situation would arise. Unfortunately, except for the empirical data fits mentioned above, there are no direct studies of collision efficiency for fractal clusters of particles, either theoretically or experimentally.

3.6.3.2. - Floc Structure Effects on Floc Sedimentation

The floc structure will have two effects on the floc sedimentary properties; it will change the floc buoyant density and the floc friction coefficient from solid sphere values. Using the fractal porosity relation (3-32), the dependency of the buoyancy difference on floc size is straightforward. This is the single particle density difference multiplied by the particle volume fraction in the floc:

$$\Delta\rho_i = (\rho_1 - \rho_f)(1 - \varepsilon_i) = \left[(\rho_1 - \rho_f)a_1^3 k\right]a_i^{D-3} \qquad (3\text{-}37)$$

Here, ρ_1 and ρ_f are the single particle and medium densities, respectively.

The dependency of the friction coefficient is not as straightforward as the density relation. The translational friction coefficient of porous bodies has been a subject of intense interest over the years, as it has ramifications throughout science for transport properties of materials. In general, the drag on a permeable body is less than the drag on an impermeable body of the same hydrodynamic radius. However, as pointed out above in section 3.6.3.1., the branches of a fractal structure will extend beyond the nominal hydrodynamic radius. Consequently, comparing theoretical solutions for geometrically well-defined, uniformly porous bodies with ill-defined, geometrically random flocs is not easy. Although absolute values for friction coefficients are ultimately desirable to describe

floc properties, the functionality of the drag is the immediate goal of theoretical description, and the major stumbling block to the prediction of suspension properties. The literature on hydrodynamic interactions of closely spaces spheres and swarms of spheres is itself immense; the following review will limit itself to developments readily applicable to clusters of particles. There are two basic methods to calculating transport properties of porous particles. The first approach is to calculate the porosity as a function of radial position, relate this to permeability, and solve Brinkman's equation (a modified Darcy's law) with appropriate boundary conditions at the sphere surface. The second approach is to model the individual particles in the floc as points of resistance to fluid flow, and calculate the hydrodynamic interactions between them to find the total drag on the cluster.

The first method was introduced by Brinkman (1947), and Debye and Bueche (1948). These initial solutions were provided for uniformly permeable spheres. For fractal flocs, these results will not be applicable due to the radial variation of the particle density. Brinkman's equation was solved for a Gaussian permeability distribution by Wiegel and Mijnlieff (1977,1978), and later by Davidson (1988). For both of these works, the segment density correlation from the center of the body was approximated as a Gaussian distribution:

$$c = c_o \exp\left(- \frac{3r^2}{2a_i^2} \right) \tag{3-38}$$

Here, c and c_o are the particle density at a radial position r and at the floc center. This relation will be compared to equation (3-33) which is applicable for fractal clusters. In the semi-dilute range of polymer concentration, permeability was related to segment concentration by the empirical relation:

$$\kappa = C c^{-y} \tag{3-39}$$

Here, C is a constant of proportionality, and y is a constant determined by the draining properties of the cluster. When y = 1, the cluster is freely draining, and there is no

hydrodynamic screening between segments (particles). This was assumed by Wiegel and Mijnlieff. Davidson assumed a higher factor of y = 2, which is more appropriate to a random-walk, freely-jointed chain where the segments will hydrodynamically interact with each other. Combining equation (3-39) with (3-38) gives rise to the cluster permeability distribution:

$$\kappa_i(r) = \frac{C}{c_o^y} \exp\left(\frac{3yr^2}{2a_i^2}\right) \tag{3-40}$$

Using this distribution, the authors showed that the friction coefficient of the body follows:

$$f(i) = 4\pi\left(\frac{2}{3y}\right)^{1/2} \eta a_i \, \omega Y(\omega) \tag{3-41}$$

Here, ω is a dimensionless quantity given by:

$$\omega = \frac{2c_o^y a_i^2}{3yC} \tag{3-42}$$

The function $Y(\omega)$ is calculated from the solution. This was calculated by Davidson (1988) for a value of y equal to two. Davidson found that $Y(\omega)$ could be approximated closely by the empirical expression:

$$Y(\omega) = \frac{2.22}{\omega + 5.77} \tag{3-43}$$

This expression was in agreement with numerical calculations to 1% for $10 \leq \omega \leq 60$. In addition, the solution matched the Wiegel and Mijnlieff values for y = 1 within 3% for $\omega \leq 17$. In addition, the value of c_o may be specified as:

$$c_o = \left(\frac{2}{3}\pi a_i^2\right)^{-3/2} \tag{3-44}$$

The combination of equations (3-41) to (3-44) can give a dependency of the floc friction coefficient on the cluster size. At large a_i, $f(i)$ is directly proportional to a_i. This means that in the infinite size limit, the cluster is non-draining. Unfortunately, the value of C can

only be determined experimentally, and it is necessary to know this value to ascertain whether the cluster is approaching the limiting behavior. This development may be valid for flocs with D near two; however, for other floc structures the model is inapplicable. In order to obtain values for other structures, the Brinkman equation would have to be solved at other values of y, C and c(r) appropriate for the fractal dimension at hand.

One result of fractal theory is that for a fractal body, the particle density correlation from the center of the floc should not follow the Gaussian decay of equation (3-38), but should follow equation (3-33). For floc structures anticipated from the literature, with fractal dimensions from about 1.5 to 2.5, the density of particles versus radial position decreases more rapidly for the fractal relation than for the Gaussian exponential decay. This implies that the flocs will have relatively impermeable cores with dangling, free-draining branches compared to the random-walk polymers simulated above. This will change the functionality of the friction coefficient, and may mean that a non-draining limit is only reached for extremely large clusters.

The second method for calculating the floc friction properties was originally performed by Kirkwood and Riseman (1948). In this method, the particles in the cluster are modelled as point resistances which perturb the fluid flow at other resisting points. The equations of motion are solved for an average cluster configuration. This was originally done for linear polymers, where the average conformation is well known for a freely-jointed chain. Kirkwood and Riseman modelled a random-walk, freely-jointed chain like the authors above, which corresponds roughly to a cluster with D = 2. The end result of the Kirkwood-Riseman development is:

$$f(i) = \frac{\zeta i}{1 + \frac{8}{3}\lambda_o i^{1/2}} \qquad (3\text{-}45)$$

Here, ζ is the average friction coefficient of a single particle within the cluster, and λ_o is a draining parameter given by:

$$\lambda_o = \frac{\zeta}{(6\pi^3)^{1/2}\eta b} \qquad (3\text{-}46)$$

Here, η is the solvent viscosity, and b is a characteristic bond length, or particle spacing. For small i, equation (3-45) predicts that $f(i)$ is proportional to i, that is, the cluster is free-draining and each particle experiences free stream drag. As i approaches infinity, $f(i)$ is dependent on $i^{1/2}$. This is equivalent to a non-draining, impermeable sphere. Like equations (3-41) to (3-44), equation (3-45) is difficult to apply without knowledge of the fundamental parameters ζ and b. This is to say that we don't know what value of i constitutes infinity. If ζ and b are approximated by $6\pi\eta a_1$ and $2a_1$, respectively, the equation predicts the friction coefficient in aqueous solution at room temperature should approach non-draining conditions for i greater than 6! In addition to this limitation, like the Brinkman equation developments, the equations need to be solved for the particle distribution appropriate to a fractal structure.

The Kirkwood and Riseman solution employs averaging of the polymer segment or particle density over all configurations of the cluster, and was performed only for a structure roughly equivalent to D equals two. In the only directly applicable simulation for fractal structures, Chen, Meakin and Deutch (1984) calculated the translational friction coefficient of individual fractal clusters with D = 2.52 using the Kirkwood-Riseman procedure. These authors sought the relationship between the cluster size and the friction coefficient, and reasoned as follows. In the free draining limit, each particle in the floc experiences the free stream fluid flow and hence possesses its single cell friction coefficient. The aggregate friction coefficient, $f(i)$, is then the sum of the individual coefficients, given for the creeping flow regime as:

$$f(i) = i\zeta = 6\pi\eta a_1 i \qquad (3\text{-}47)$$

It is readily seen that the free-draining limit dependency on i is unity. This approximation should only be valid as the floc is very small, or very loosely structured, that is, D

approaches one. If the floc is non-draining, the friction coefficient should be the same as for a hard sphere, $f(i) = 6\pi\eta a_i$. Substituting equation (3-30) for a_i gives the equation:

$$f(i) = 6\pi\eta\left(\frac{i}{k}\right)^{1/D} \tag{3-48}$$

In a non-draining floc, then, the dependency on i is the inverse of the fractal dimension. This should be a valid approximation only as D approaches three, or as the cluster size approaches infinity. The actual dependency for a finite size, non-space filling floc should be between the non-draining and free-draining cases, and it is this relationship that was sought. A general relation was proposed to describe cluster behavior:

$$\ln\left[\frac{f(i)}{\zeta}\right] = \ln c + \sigma \ln i \tag{3-49}$$

For a non-draining floc, comparison with equation (3-48) shows that $c = (a_1 k^{1/D})^{-1}$, and $\sigma = 1/D$. For a free-draining floc, $c = \sigma = 1$. Substituting the fractal dimension of the clusters examined shows that for the non-draining case, the expected dependency is $\sigma = 1/2.52 = 0.40$. The Kirkwood and Riseman procedure was employed on individual clusters with $10 < i < 600$ and the friction coefficients averaged. A log-log plot of $f(i)$ versus i showed a linear relation with $\sigma = 0.479 \pm .01$. This coefficient is 20% greater than the non-draining case, and indicates that even for these "tight" clusters at high D, friction coefficients will be substantially higher than for non-draining clusters. This result is significant since the largest clusters examined should be in or near the non-draining size limit of the literature presented above. The authors unfortunately did not extend the calculations to larger clusters to determine whether a non-draining limit is reached, and where it occurs. In the above case, the authors maintain that increase in friction does not arise from classical floc permeability, that is, flow through the floc. The increased friction comes from the considerable surface irregularity and dangling branches of the floc. For the computer generated fractals studied, the radius of gyration was significantly greater than the

nominal hydrodynamic radius (Meakin (1988b)). It is notable that this was observed regarding a tight floc structure with D = 2.52. For fractal flocs with lower dimensionality, the effects of a fractal particle distribution will influence the friction behavior more profoundly and at larger cluster sizes.

3.6.4. - Floc Structure Review Summary and Thesis Goals

The above sections have reviewed the state of the literature with regard to the structure of fractal flocs and the ramifications for aggregation and separation operations. It has been amply demonstrated in the review of section 3.6.2.1. that submicron colloids undergoing diffusive aggregation form fractal structures. These structures more or less correspond to theoretical simulations of floc structure. There have been only two direct measurements demonstrating a fractal dimension for shear aggregated colloids, those of Davis and Hunt (1986) on yeast aggregates, and of Sonntag and Russel (1986) on latex aggregates. However, there is a substantial body of experimental literature on the porosity of large colloids which suggests that orthokinetically aggregated flocs are fractal in nature. The measurements of Klimpel and Hogg suggest that over large ranges of size, the floc structure is not truly fractal. However, these and the other floc porosity measurements are indirect, and incorporate solid sphere friction coefficients for calculation. As discussed in section 3.6.3.3., this is a poor assumption for porous bodies, and may have led to error in the floc porosity determinations. The fractal dimensions of the flocs calculated from the porosity measurements may also be in error. It is therefore of interest to determine by a friction independent method whether animal cell flocs form fractal structures. It is anticipated from the theoretical and experimental literature reviews that the degree of destabilization and the fluid mechanical conditions will affect floc structure. To complement studies on the destabilization (collision efficiency) of the suspensions, the

structure of the flocs should be determined over the same range of flocculant and hydrodynamic conditions. This work may be found in Chapter 7.

Although there is a considerable amount of literature dealing with uniformly permeable bodies, and for bodies with a Gaussian permeability (particle) distribution, there is limited information on fractal clusters. The results of Kirkwood and Riseman (1948), Wiegel and Mijnlieff (1977,1978), and Davidson (1988) for bodies with variable permeability suggest that over the entire spectrum of cluster sizes, the cluster friction coefficient goes from a free-draining functionality to a non-draining limit. There is only one theoretical study of frictional properties of fractal flocs, that of Chen, Deutch and Meakin (1984). The work of these authors is laudable in that it is a direct calculation of friction coefficients for fractal bodies by the Kirkwood-Riseman method. Their results suggest that the non-draining limit lies substantially above the region of cluster size investigated. Although the friction coefficient must reach a non-draining dependency eventually, these authors' results suggest there will be a region of cluster sizes over which the cluster friction coefficient is intermediate between free- and non-draining, and may be related to the fractal dimension of the structure. Unfortunately, this work was neither extended to large clusters, or to more than one fractal dimension, and thus we are left with a void for predicting the friction coefficient versus the floc size and the fractal dimension for the general case. An additional goal of studying floc structure is then to develop a general relationship for the floc friction coefficient versus the floc size and fractal dimension. A simple theory is proposed in Chapter 7 to describe the friction coefficient of a generic fractal structure. This development may allow us to better interpret past floc structure data without the limitations of hard sphere friction coefficient assumptions.

The relation will be useful to predict the properties of the animal cell flocs generated. With the specification of the floc density, it will be possible to predict floc sedimentary properties based on the size and structure of the floc. This can be directly interfaced with a

population balance solution using experimental collision efficiencies and fractal dimensions to predict the sedimentary enhancement of a suspension versus process conditions and time. Solution of the population balance for a partially destabilized, fractal, distributed system is beyond the scope of the thesis. However, a simple theoretical development of sedimentary enhancement for a non-distributed dispersion combining the experimental knowledge is presented in Chapter 8.

4. - MATERIALS AND METHODS

4.1. - Cultured Lines and Growth Conditions

Experiments were mainly performed with suspension cultures of ATCC CRL 1606 (American Type Culture Collection, Rockville, MD), a murine-murine hybridoma producing anti(human fibronectin). Experiments were also performed with a Chinese Hamster Ovary cell line expressing tissue plasminogen activator (tPA-CHO), the human lymphoma line U-937 (ATCC 1593) and HeLa cells. The tPA-CHO line was obtained from Biogen Research Corp. (Cambridge, MA). U-937 is the ATCC line designated CRL 1593. HeLa cells were obtained from Donald Giard, M.I.T. Cell Culture Center (Cambridge, MA).

All these cell types are present largely as single cells in suspension culture. However, CRL 1606 is present exclusively as single cells in agitated suspension culture, and was thus chosen for the majority of the flocculation investigations. This cell line was grown in Iscove's Modified Dulbecco's Medium (IMDM, donated by Mediatech, Inc., Herndon, VA) supplemented with 0.5% v/v fetal bovine serum (Sigma Chemical Co., St. Louis, MO), 5 mg/L transferrin (Sigma), 5 mg/L insulin (Sigma), 0.2 μM/L ethanolamine (Sigma), 6.25 μL/L α-thioglycerol (Calbiochem, San Diego, CA), 10 U/mL Penicillin (Mediatech) and 10 μg/mL Streptomycin (Mediatech). For serum-free culture experiments, the same formulation less the serum was used. The HeLa, U-937 and CHO cells were grown in IMDM supplemented with 5% fetal bovine serum and antibiotics as above. Cells were propagated for experimentation in 125, 500, and 1000 mL spinner culture vessels (Corning Glass, Corning, NY). Cells used for flocculation studies were assayed to be greater than 95% viable by Trypan Blue (Sigma) staining, and were in exponential growth phase.

4.2. - Cell and Floc Enumeration and Sizing

Viable cell counting was performed by hemocytometry using an improved Neubauer hemacytometer (American Scientific, McGaw Pk., IL) and 100x magnification with a phase contrast objective. Cells were placed in Trypan Blue solution, 1.0% in phosphate buffered saline (no magnesium or calcium (Freshney (1983)) for five minutes before counting to determine viability. Total cell counts were also obtained using a Coulter Z_F electronic particle counter (Coulter Electronics, Hialeah, FL). The Coulter Counter had a 100 μm diameter orifice, and settings were adjusted to correspond to the microscopic cell counts. The normal settings used for the majority of the experiments were AMP = 4, APC = 4, and T = 5, although these were adjusted when necessary.

Cell sizes were obtained by using the Coulter counter in conjunction with a Coulter C1000 particle size discriminator. It was found that calibration of the C1000 with latex size standards did not produce cell sizes corresponding to the microscope values. The C1000 was thus calibrated by microscopically sizing 60 cells at 400x using an eyepiece graticule, and calculating the number mean volume of the cells:

$$V_{10} = \frac{\sum N_i V_i}{\sum N_i} \tag{4-1}$$

This number mean was then used to calibrate the C1000 channel values to give the same V_{10}. This converts the channels to true volume. For collision efficiency and adsorption calculations, the number mean size was not used. Rather, the mean cell size was based on the Sauter mean radius, a_{32}, of the cells:

$$a_{32} = \frac{\sum N_i a_i^3}{\sum N_i a_i^2} \tag{4-2}$$

It will be appreciated that for a distributed system, the mean radius calculated from the number mean volume ($a_{10} = (3V_{10}/4\pi)^{1/3}$) is not the same as the Sauter mean radius. The latter is the parameter of interest for adsorption since it gives an accurate value of the

surface area of the suspension. It is the parameter of interest for collision calculations since it also accurately assesses the mean cross-sectional area of the cell suspension. The number mean radius is of interest for other studies, for example, calculating rates of metabolic activity based on average cell volume.

Photography of flocculated cells for floc sizing was performed with an inverted microscope using a phase contrast objective and total magnification of 40x. Where necessary, latex size standards were included in the cell suspension to allow floc sizing.

4.3. - Flocculant Screening and Characterization

4.3.1. - Flocculant Screening

Five categories of flocculant were screened; anionic, nonionic, and cationic polymers, and colloidal solids and simple cations. Anionic polymers tested were guar gum, xanthan gum, locust bean gum, pectin, amylopectin, carboxymethylcellulose, dextran sulfate, poly-L-glutamic acid (all obtained from Sigma), polystyrene sulfonate (Aldrich Chemicals, St. Louis, MO), and Primafloc A10 (Rohm & Haas, Philadelphia, PA). Nonionic polymers tested were 78,000 and 500,000 MW dextran, and 400,000 MW ficoll (polysucrose) (Pharmacia Fine Chemicals, Piscataway, NJ). Cationic polymers tested were polyethylenimine (Aldrich), BETZ 1155, BETZ 1158, BETZ 1160, BETZ 1190, BETZ 1192, BETZ 1195 (all Betz, Trevose, PA), Primafloc C3 (Rohm & Haas), DEAE dextran (Pharmacia), poly-L-lysine, poly-L-arginine, poly-L-ornithine, and poly-L-histidine (all obtained from Sigma). Colloidal solids tested were kaolinite, bentonite, and montmorillonite clays, and silica sol (all obtained from Aldrich), and multivalent cations tested were aluminum, ferric, calcium and magnesium chlorides (all Sigma). For most screening, the flocculant was simply dissolved or suspended as an aqueous saline solution, and tested "as received".

To test for toxicity due to adventitious contaminants, samples of poly-L-lysine were dissolved and dialyzed against a 20x volume of PBS overnight. These were tested along with the "as received" solutions. For this same purpose, colloidal flocculant suspensions were prepared, centrifuged, the supernatant decanted and the pellet resuspended in fresh PBS. The suspensions were then tested along with the "as received" samples.

Since aluminum and ferric chlorides are strong oxidants, dissolution of these compounds results in an extremely acidic solution. These solutions were neutralized with sodium hydroxide, which resulted in the formation of a hydroxide precipitate of aluminum or iron. The precipitate suspensions were homogenized to disperse the precipitate, and tested for flocculation promotion and toxicity.

Flocculant screening was conducted by placing 4 mL of cell suspension at 10^6 cells/mL in 12x75 mm glass centrifuge tubes along with flocculant spanning several decades of concentration. Each tube was then covered and inverted several times to mix the contents and allow flocculation to occur. Visibly effective flocculants were then retested to determine the minimum concentration required for flocculation. The cells were withdrawn after 15 minutes of exposure and stained with Trypan Blue in PBS to determine cell viability.

The kinetics of flocculant toxicity for poly-L-lysine and poly-L-histidine were further studied by exposing cells to flocculation inducing doses for various times and recording the fraction viable at that time via hemocytometry using trypan blue staining.

Flocculation of particles with a polymeric flocculant is an adsorptive phenomenon, with polymers usually exhibiting strong, kinetically irreversible adsorption to the surface. For this reason, the amount of polymer per particle surface area is usually more pertinent than the polymer concentration when cell concentrations vary. Although cell concentrations were maintained constant for experiments where possible, results have been reported based on the dose of the polymer per unit cell surface area.

4.3.2. - Characterization of Poly-L-Histidine (PLH) Effects on Cell Growth

To determine the effects of PLH on cell viability and growth after a flocculation process, a 1,000 mL seed spinner flask (Corning Glass, Corning, NY) was grown to $1.5x10^6$ cells/mL and split into duplicate 125 mL spinner flasks (Corning) (100 mL liquid volume). PLH was added as a sterile 200-2000 mg/L stock solution in water to concentrations from 4 to 64 mg/L, and the cultures were allowed to aggregate for 10 minutes at 40 RPM. The agitation was discontinued, and the flocs were allowed to sediment for 15 minutes. The supernatant, 90% of the total culture volume, was removed and replaced with fresh medium, and agitation was resumed. The cultures were sampled 15 minutes after re-feeding, at which time the flocs had dispersed to single cells. Viability was assayed by Trypan Blue for these samples. Growth of the cells was monitored per above.

The effect of cell inoculum concentration on cell growth was determined by growing CRL 1606 in a 1,000 mL spinner to $1.5x10^6$ cells/mL. The cells were centrifuged and resuspended in fresh medium at concentrations from $3.3x10^5$ to $1.1x10^6$ cells/mL. The cells were then cultured in 125 mL spinner vessels and growth monitored over the first 48 hours after centrifugation. Comparison of the effects of flocculation and centrifugation on cell growth was conducted in a similar manner. A 1000 mL spinner was split into two 500 mL spinners, and medium was changed in both. In the flocculated spinner, flocculation was conducted per above. In the centrifuged spinner, the cell suspension was remove to 250 mL centrifuge tubes, and centrifuged for 10 minutes. Ninety percent of the medium was removed and the cells resuspended and replaced in the spinner vessel. This procedure was repeated several times for both spinners to determine the potential for repeated polymer flocculation treatments of the cells.

4.4. - Cell Zeta Potential Measurements

Measurements of cell surface zeta potential were conducted by treating a cell suspension at 10^6 cells/mL with poly-L-histidine stock solution. All samples were at pH 6.9. The treated suspension was gently mixed and allowed to stand for at least five minutes to allow adsorption of polymer to the cells. The suspension was then injected into the sample cell of a free-zone particle electrophoresis device (Model 501, Pen Kem, Bedford Hills, NY) and the zeta potential of 10 to 20 cells was observed. The electrophoresis device used was equipped with a laser illumination system and closed circuit video camera to allow visualization of the particle suspension against a dark field. However, it was found that operation using the microscope white light source and the eyepieces allowed for more accurate determination of particle zeta potential.

4.5. - Poly-L-Histidine Physical Characterization

4.5.1. - Potentiometric Titration

Potentiometric titration of poly-L-histidine, d.p. 151, was conducted at 23° C in 0.15 M NaCl with a polymer concentration of 3.0 gm/L and total volume of 1,000 mL. The titration was performed by starting under acidic conditions and adding 0.30 M NaOH. A standard pH electrode and meter were used to record the pH over the range of the titration. Due to the high ionic strength of the medium and the large solution volume relative to the added titrant, no correction for the sodium ions added with the titrant was necessary.

4.5.2. - Solubility Determination

Solubility of PLH in saline versus pH was determined by mixing a 5 gm/L solution of PLH in water with concentrated phosphate buffered saline at varying pH to make final concentrations of 1 gm PLH/L and physiological ionic strength PBS. The resulting

precipitate was centrifuged in a microcentrifuge for 30 minutes at 13,000 RPM and the supernate absorbance was read on a spectrophotometer at 190 nm. Absorbance was found to be linear with polyhistidine concentration at this wavelength and invariant with pH. Chloride ion absorbance was corrected for by subtracting the signal from known concentrations of sodium chloride, and the concentration of the PLH was calculated from the absorbance of known concentrations of histidine•HCl.

4.5.3. - Precipitate Size Determination

The size of polyhistidine precipitates were determined by dynamic light scattering measurements using a Coulter N4 submicron particle analyzer light scattering machine (Coulter Electronics, Hialeah, FL). The scattering signal was gathered at 90° to the source beam. The light scattering device measures the autocorrelation function of the scattered light intensity, and relates the time constant for the correlation decay to the diffusivity of the scattering particles. From this diffusivity, an equivalent Stokes-Einstein radius is calculated for the particles.

Samples of polyhistidine stock solution were placed in the bottom of 0.5 x 5.0 cm test tubes; PBS was added and the tube placed into the light path of the scattering device. Data acquisition was commenced, typically for 20 seconds every two to three minutes. Precipitate size over time was thus obtained. Samples tested were between 1 and 33 mg/L; beyond the lower limit, the light scattering signal to noise ratio was too weak to extract precipitate sizes. Beyond 33 mg/L, the precipitate size rapidly exceeded the size limit of the device. Fortunately, these concentrations encompass the range of most experiments conducted in this thesis.

4.6. - Collision Efficiency Determination

4.6.1. - Apparatus and Procedure

Collision efficiency experiments were conducted in a Brookfield Model LVT1 Couette viscometer (Brookfield Instruments, Brookfield, MA). The bob radius was 1.25 cm, and the cup radius was 1.375 cm, giving a gap width of 0.125 cm. The viscometer rotational speed was between 6 and 60 rpm. The viscometer shear rate is given by:

$$\dot{\gamma} = \frac{2\varpi r_i^2}{r_o^2 - r_i^2} \tag{4-3}$$

With the given viscometer dimensions, the shear rate in s^{-1} is equal to the rotational speed, ϖ, in rpm. The suspension was sheared at rates between 6 and 60 s^{-1}; typical average shear rates in cell culture vessels are on the order of 100 s^{-1} or less. This range is considered to be representative of an animal cell flocculation process. For a typical animal cell radius of 8 μm, the range of particle Peclet numbers is between 14,000 and 140,000. This is well into the range of orthokinetic aggregation, precludes Brownian motion effects on the aggregation process.

When the inner cylinder of a Couette flow device is rotated, the flow becomes unstable and has a rotational component in addition to the pure shear component above a threshold Reynolds number. The Taylor number, Ta, characteristic of hydrodynamic instability in Couette flow where the inner cylinder is rotated is given by Stuart (1958) as:

$$Ta = \frac{\varpi^2 r_i (r_o - r_i)^3}{\nu} \tag{4-4}$$

Here, ν is the fluid kinematic viscosity. When Ta is greater than 50, hydrodynamic instability occurs and vortices form in the flow field. For the viscometer speeds used, Taylor numbers ranged from 0.153 to 1.53. It is thus concluded that rotational flow is not a problem with the viscometer, and that a pure shear flow was present.

Collision efficiency experiments were conducted by placing a cell suspension into the viscometer along with PLH as a 200-2000 mg/L stock solution in water to the appropriate concentration. The suspension was then sheared and samples were collected over time by stopping the apparatus and sampling using pipettes with wide mouth tips. The samples were diluted 1:150 in phosphate buffered saline, and counted for total particle number using the Coulter particle counter. These counts were verified for selected runs by hemacytometer counting the particle number.

4.6.2. - Collision Efficiency Calculations

Calculations of collision efficiency were performed assuming that in the first stages of aggregation, the particle collision cross-section and the collision efficiency are constant. The initial rate of change of total particle concentration,

$$\frac{dN_{tot}}{dt} = - \alpha_{1,1}\beta_{1,1}N_{tot}^2 \qquad (4\text{-}5)$$

is integrated to:

$$\frac{N_{tot,o}}{N} = 1 + \alpha_{1,1}\beta_{1,1}N_{tot,o}\, t \qquad (4\text{-}6)$$

under these assumptions. Here, $\beta_{1,1}$ is the von Smoluchowski ideal rate constant for collision of single cells with each other. The collision efficiency, $\alpha_{1,1}$, is defined as the rate of collisions producing adhesion relative to the von Smoluchowski rate. The von Smoluchowski rate constant for identical particles is given by:

$$\beta_{1,1} = \frac{32}{3}\dot{\gamma}\, a^3 \qquad (4\text{-}7)$$

If the assumptions of constant particle cross-section and collision efficiency hold, a plot of $N_{tot,o}/N$ versus time should be linear with a unit intercept. Figure 4-1 shows the results of a typical collision efficiency run, demonstrating the linearity of such a plot. Knowing the cell size, shear rate and initial particle concentration, the collision efficiency is back

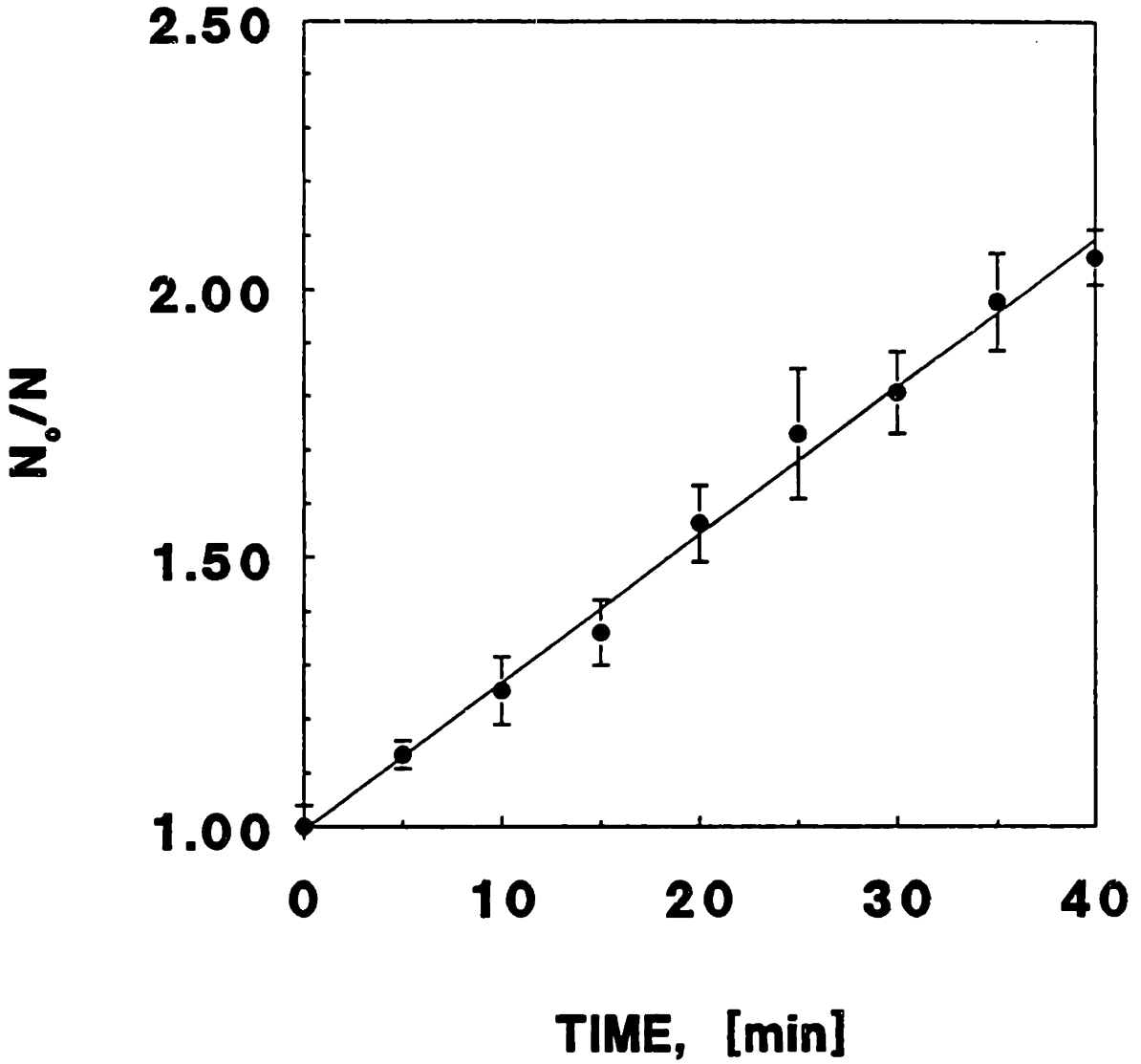

Figure 4-1. Inverse normal particle concentration, N_o/N, versus time for a typical collision efficiency experiment. N_o = 50,100 cells/mL, a = 7.8 μm, 26 mg PLH/m^2, shear rate = 12 s^{-1}.

calculated from the slope of the plot using equation (4-7) to calculate $\beta_{1,1}$. Cell concentrations were adjusted over the range of flocculation conditions so that $N_o/N < 2$ for all experimental conditions and times. Linear regressions of N_o/N versus time with correlation coefficients $r^2 \leq 0.97$ were not used. This method of calculation is a departure from the Swift and Friedlander (1964) approximation of orthokinetic aggregation as a first order process in the particle concentration. This departure is not without precedent; similar calculations have been used by Linnemans *et al.* (1976), and Jones and Perry (1978,1979) for lectin agglutination and natural aggregation of animal cell suspensions. A regression of $\ln(N/N_o)$ versus time, appropriate to the Swift and Friedlander calculations gives a worse correlation coefficient ($r = 0.91$ versus $r = 0.996$) and does not have an intercept of one.

A potential issue in the determination of collision efficiencies for a non-ideal animal cell suspension is the polydispersity of the cell suspension and its ramifications for particle collision. In a typical animal cell suspension, the cell size is not a single value since the cells are in various stages of the cell cycle, and are in the process of doubling their mass. Since the cells are not all the same size, the average collision will not take place between two cells of the same size, but between cells of slightly different size. It is desirable therefore to know what the average size ratio of a typical collision is, in order to relate it to theory discussed in section 3.5.1.1.

As a convenient approximation, the cell size may be assumed to be distributed normally about a mean value. When this is the case, the probability of finding a cell with radius a is given by:

$$Pr(a) = \frac{\exp\left(-\frac{1}{2}\frac{(a-\bar{a})^2}{\sigma^2}\right)}{\sqrt{2\pi\sigma}} \qquad (4\text{-}8)$$

Here, $\bar{a}$ is the mean radius, and σ is the standard deviation about the mean. The probability of finding a cell with radius $b = a/r$ is given by the equation (4-8) as well, substituting br

for a in the equation. The probability of collision between two cells with radius a and b is equal to the joint probability of finding a and b. Thus, the probability of finding a collision size ratio r = a/b is equal to the integral of the joint probability statement over all values of a and b = a/r:

$$Pr(r) = \int_{-\infty}^{\infty} Pr(a)Pr(a/r))da \tag{4-9}$$

The Gaussian probability statements (4-8) may be inserted into equation (4-9), and the equation integrated to give the result:

$$Pr(r) = \frac{\exp\left(-\frac{\bar{a}^2}{2\sigma^2}\left[\frac{(1 - 1/r)^2}{(1 + 1/r^2)}\right]\right)}{\sqrt{2\pi(1 + 1/r^2)}} \tag{4-10}$$

The average size ratio for collision is given by the integral average of equation (4-10) weighted by r and then divided by the integral of the unweighted probability over values of r from zero to unity:

$$\bar{r} = \frac{\int_0^1 rPr(r)dr}{\int_0^1 Pr(r)dr} \tag{4-11}$$

These integrals of equation (4-10) may be performed numerically for various values of the reduced dispersity, $\sigma/\bar{a}$, of the cell suspension. The resulting values of the average collision size ratio for $\sigma/\bar{a}$ values between 0.0 and 0.5 are shown in Figure 4-2. For the values typical of cell suspensions, from 0.15 to 0.20, the average collision size ratio ranges from 0.874 to 0.840. The results of Melik and Fogler (1985) show that for particles with this size ratio, the collision efficiency is not altered substantially. Only when $\bar{r}$ drops to near or below 0.5 are the particles sufficiently polydisperse to affect the collision efficiency dependency on hydrodynamic conditions.

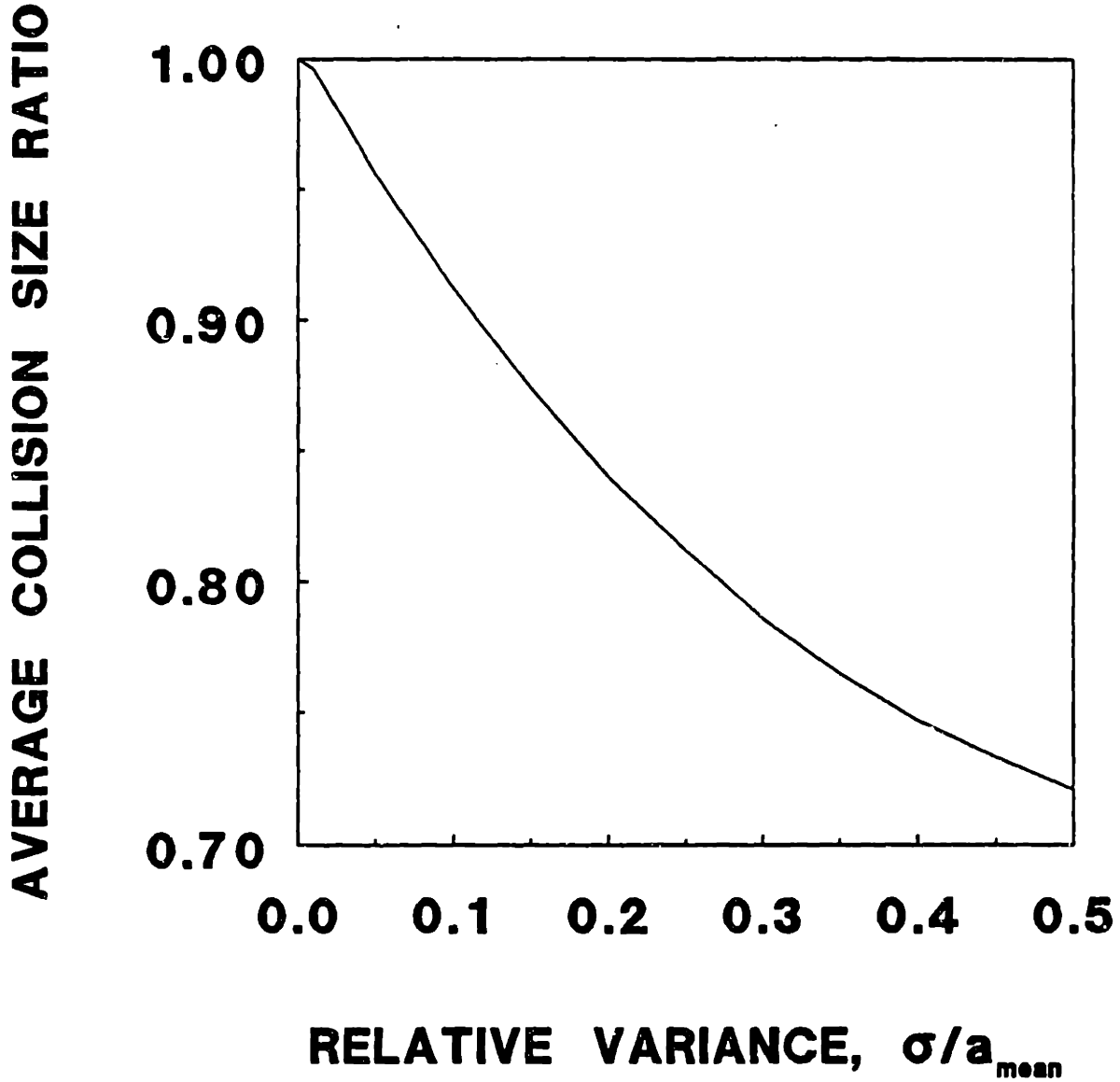

Figure 4-2. Average collision size ratio versus the relative standard deviation about the mean of a normally distributed suspension.

4.7. - Floc Structure Determination

Animal cell flocs were produced by treating CRL 1606 with a 23,000 MW polypeptide of histidine to induce flocculation. The cells were suspended in Iscove's Modified Dulbecco's Medium. The destabilized cell suspension was then placed in one of two agitated vessels. The first was the viscometer described in section 4.6., and the second was a 125 mL cell culture spinner vessel (Corning Glass, Corning, NY). Average shear rates in the culture vessel were calculated from the correlations of Nagata (1975) for the power input to the vessel versus the agitation speed. Aunins *et al.* (1990) have shown these correlations to be good approximations to the actual power input in the 125 mL vessel. Samples were removed from the agitation vessel and were pipetted carefully using a wide mouth pipette onto a Spiers-Levy Eosinophil counter (Thomas Scientific, Swedesboro, NJ). The cover slip was spaced out from the stage surface by additional coverslips under the one covering the floc liquor, to a distance of 800 μm from the hemacytometer stage. The flocs were then viewed using a Hoffman modulation objective (Modulation Optics, Greenvale, NY) and total magnification of 200x. An eyepiece graticule was used to size the flocs along the maximum dimension. A second measurement was taken perpendicular to this axis at the bisecting point, and the floc characteristic dimension was taken to be the geometric mean of the two. The Hoffman objective allowed viewing through several cell layers; by travelling up and down through the focal planes containing the floc, it was possible to count the number of cells in the floc. Minimum floc sizes counted were greater than 10 cells per floc, to avoid the range of floc size where fractal correlations such as equation (3-30) are inapplicable. Maximum floc sizes measured and counted always comprised greater than 100 cells, and were usually from 200 to 300 cells. Beyond about 400 cells, accurate counts were difficult due to the great number of cells to be counted as well as the increasing floc depth. Flocs with large numbers of cells were counted several times and the mean cell count recorded.

5. - FLOCCULANT SCREENING AND CHARACTERIZATION RESULTS

Flocculation of animal cells for recycle is not a straightforward task. The cells must be aggregated, and remain alive and functioning to be of use in further production of cell mass and the desired product. There has been only limited literature in the past dealing with aggregation of animal cells, mainly in the cancer and developmental biology, and blood rheology literatures. This was reviewed in Chapter 2. Various compounds, both biological and non-biological, have been found to aggregate cells, under widely varying conditions. Due to the incompleteness of the literature on animal cell aggregation and its physiological effects, it was necessary to screen for suitable flocculants, and to characterize their effects on the cells.

There were two goals of this portion of the thesis. The first was to screen flocculants to find a compound which could flocculate a variety of cell types, and which do not exhibit acute toxicity to the cells. The screening results are presented in section 5.1. The second goal was to define whether, in addition to a lack of acute toxicity, flocculation had undesirable long-term effects on cell growth and culture productivity. The characterization of one flocculant which was found to be effective and non-toxic, poly-L-histidine, is presented in section 5.2.

5.1. - Flocculant Screening Results

Three classes of flocculants were screened: multivalent ions, colloidal particulates, and polyelectrolytes. The compounds tested are listed in Table 5-1. It was unknown whether multivalent ions would be able to flocculate animal cells, as these compounds are already present in cell culture medium. Colloidal particulates have not been tested as flocculants of animal cells, although these are usually metal hydroxides which have analogues in the ceramic matrices used for immobilized cell culture (Lydersen *et al.* (1985)). It is known that polyelectrolytes are capable of aggregating both animal cells and

microorganisms; they are widely used in water and wastewater treatment processes for flocculation. Cationic polymers are especially effective at aggregating cells, however, they are also toxic or growth inhibitory in many cases (Katchalsky (1964)). The doses which

Table 5-1
Compounds Screened in Flocculant Search

Multivalent Ions
Mg, Al, Ca, Fe

Particulate Flocculants
γ-alumina, silica, Kaolinite, Bentonite, Montmorillonite

Anionic Polyelectrolytes
dextran sulfate, polygalacturonic acid, hyaluronic acid, locust bean gum, guar gum, xanthan gum, pectin, amylopectin, carboxymethylcellulose, polystyrene sulfonate, poly-L-glutamic acid, Primafloc A10, gelatin, alginic acid, κ-carrageenan

Neutral Polymers
dextran 40, dextran 78, dextran 500, Ficoll 400

Cationic Polymers
polyethylenimine, Primafloc C3, BETZ 1155, BETZ 1158, BETZ 1160, BETZ 1190, BETZ 1192, BETZ 1195, DEAE dextran, poly-L-lysine, poly-L-arginine, poly-L-ornithine, poly-L-histidine, chitosan

induce flocculation and cell death are not well described in the literature; for this reason, negative, neutral and positive polyelectrolytes were screened for their capacity to aggregate cells viably. The screening results from each class of compounds are reviewed in the order of Table 5-1 in the following sections.

5.1.1. - Multivalent Cationic Coagulants

Four multivalent cations were tested as flocculants of CRL 1606 cells in Iscove's Modified Dulbecco's 's Medium (IMDM). These were calcium, magnesium, iron, and aluminum chlorides. The first two ions are present in IMDM in quantities of 1.5 mM, and 0.8 mM, respectively. Calcium and magnesium were added from 0 to 12 mM, beyond the solubility limit in culture medium. Neither ion promoted aggregation of the CRL 1606

suspension. In addition, neither ion was acutely toxic to the cells over the range tested. Iron and aluminum chlorides are very strong oxidants which create strongly acidic solutions when exposed to water; it was necessary to first create solutions of the chloride form and then reduce the solution to neutral pH by base addition. The neutralization results in the formation of insoluble ferric and aluminum hydroxide complexes due to the low solubility product at pH 7. The suspensions of precipitated metal hydroxide were then added to the cell suspension at concentrations ranging from 1 to 300 mg/L (6 μM to 1.85 mM for Fe, 7.5 μM to 2.25 mM for Al). The addition of iron hydroxide resulted in moderate aggregation at doses between 30 and 300 mg/L. However, for both iron and aluminum hydroxide complex, the treatment was found to be toxic, rendering all cells nonviable by Trypan Blue staining within a few minutes.

The results of these experiments are not surprising. Whereas calcium and magnesium are necessary for some biological aggregation mechanisms, they are already present in culture medium at concentrations which promote these mechanisms. In addition, the addition of these ions to their solubility limits does not significantly change the medium ionic strength. The addition of more calcium or magnesium should only aggregate the cells if it changes adsorption onto the cell surface. The fact that aggregation does not occur indicates that these ions are not preferentially adsorbed to the cell surface. The addition of ferric and aluminum coagulants is expected to promote aggregation of animal cells, since these compounds are widely used as coagulants of bacteria in wastewater treatment. Where the aluminum hydroxide did not promote aggregation, the iron hydroxide complex was effective at aggregating the cells. This probably reflects differences in the precipitate hydroxide stoichiometry at pH 7, leading to different charge properties of the precipitates. Regardless, both the aluminum and iron were toxic to the cells, and were not further investigated.

5.1.2. - Colloidal Particulate Flocculants

In addition to the aluminum and ferric hydroxide complexes, which might be classed as particulate flocculants, several colloidal minerals were investigated as flocculants. These are listed in Table 5-1. Although these compounds are usually net negative and might not be expected to associate with an anionic cell surface, the minerals are crystalline in nature, and some crystal edges or planes may possess anion vacancies. These vacancies will produce a positively charged region on the colloid which can associate with the cell. In the case of γ-alumina the particles are net positively charged in aqueous suspension at neutral pH.

With the exception of Bentonite clay, these compounds did not aggregate suspensions of CRL 1606 over the range of concentrations tested, from 25 to 2000 mg/L. Bentonite was shown to aggregate the cells above 85 mg/L. To preclude toxicity due to soluble adventitious contaminants, the colloids were washed with PBS, centrifuged, and resuspended in fresh PBS prior to use. However, Bentonite was toxic to the cells at flocculation inducing doses. Silica and γ-alumina were toxic as well. The Bentonite results are consistent with the findings of Avgerinos (1988). Overall, the lack of flocculation promoting activity may be attributed to the net negative charge for most of these colloids. This does not account for the lack of activity for γ-alumina, however. It is not clear why this substance does not adsorb to the cells; due to its toxicity, this is a moot point. It is also not clear why Bentonite, a negatively charged colloid, is active at flocculating the cells. This may be due to anion vacancies as proposed above, or may be due to hydrophobic interactions with the cell surface.

5.1.3. - Anionic Polymer Flocculants

Although anionic polymers would not ordinarily be expected to associate with negative cell membranes, dextran sulfate has been found to aggregate thrombocytes in the

presence of multivalent cations which may adsorb to the cell surface (Brossmer and Pfliederer (1966)). Polygalacturonic acid has been found to aggregate murine hybridomas at low pH where the cells may become partially positively charged (Kenney (1985,1986)). As a class, the anionic polymers listed in Table 5-1 did not aggregate CRL 1606 at IMDM levels of calcium and physiological pH. Neither high molecular weight dextran sulfate, nor pectin aggregated CRL 1606 under the conditions investigated. The pectin used was 7.7% methoxylated polygalacturonic acid. Screening with dextran sulfate at calcium concentrations up to 12 mM also showed no flocculation. This indicates that the multivalent calcium ions in the medium do not adsorb to the cell surface in quantity, and hence do not allow anionic polymer association with the cell surface. This will be shown in section 6.2.1. by the negative zeta potential of cells with no added flocculants. Addition of other multivalent ions and changing pH to promote anionic polymer flocculation was not investigated. Anionic polymers were observed to be non-toxic in general, having no effect on cell viability at the concentrations investigated.

5.1.4. - Nonionic Polymer Flocculants

High molecular weight dextrans have been shown to enhance aggregation of erythrocytes, ostensibly by adhering to cells via Van der Waals attraction and bridging across the electrostatic double layer between cells (Knox *et al.* (1977)). Lower molecular weights promote disaggregation of red cell rouleaux since they are too small to effect bridging. These dextrans also enhance the exclusion of shielding ions in the medium from between the double layers, and can provide steric hindrance to the close approach of the membranes. The aggregation effect is seen for dextrans with molecular weights as low as 70,000 (Jan, Usami and Chen (1982)). In this investigation, dextrans of 78,000 and 400,000 molecular weight did not promote aggregation at doses from 1 mg/L to 40 gm/L. The 400,000 MW dextran had no effect on cell growth up to 10 gm/L. Ficoll, a cross-

linked polymer of sucrose, 400,000 MW also had no effect on cell aggregation or growth from 1 mg/L to 1 gm/L.

The results of the nonionic polymer screening reflects the generally weak interactions of these polymers with the cell surface. In the blood rheology studies which show dextrans to promote aggregation, the aggregation only occurs significantly at low shear rates, below about 1 s^{-1}. This means that a flocculation process using nonionic polymers will be slow. It is interesting that Knox *et al.* (1977) found aggregation for erythrocytes at an optimum concentration of 30 gm/L, which was encompassed by the range of dextran concentration in this study. The fact that CRL 1606 hybridomas do not aggregate under the same conditions may point out fundamental differences between the cell surface chemistry and physical conformation of these two cell types. One of the problems of employing nonionic polymers in large amounts is that significant viscosity increase occurs with the addition of high concentrations, and this will slow sedimentation. Due to the negative dextran results and the apparent unsuitability of nonionic polymers for a rapid flocculation and sedimentation scheme, no further candidates were investigated.

5.1.5. - Cationic Polymer Flocculants

Cationic polymers aggregate cells of many types by charge neutralization and/or bridging between cell surfaces. Due to the many segments on a single molecule which can interact with negative groups, these materials show much stronger adsorption characteristics than simple cations (Gad (1983)). These polymers are commonly employed as adsorbed layers on cell culture surfaces in order to promote adhesion and growth of adherent cell types (McKeehan and Ham (1976)). In addition, polycations are known to flocculate erythrocytes and other cell lines (Katchalsky (1964)). Several researchers have shown polycations to be toxic to animal cells, or to cause erythrocytes to lyse (see Katchalsky (1964)); however, the doses of polymer which result in flocculation and/or

lysis have not been well described. It was thus desired to test whether polycations could induce flocculation without causing extensive cell death.

As a class, polycations were very effective at flocculating CRL 1606, tPA-CHO, U-937 and HeLa cells at doses from 5 to 200 milligrams of polymer per square meter of cell surface area (≈ 5 to 200 mg/L). However, these polymers were also very toxic in solution, and killed the majority of cells in the culture at flocculating doses. This result confirms the previous literature studies of strong polycation association with cultured animal cells. Kinetics of cell death for CRL 1606 treated with 40 mg/m^2 of 25,000 MW poly-L-lysine•HCl are shown in Figure 5-1. Death is rapid, and after 90 minutes less than 10% of the cells remain viable. The dose response of the cells to poly-L-lysine at 15 minutes incubation time is shown in Figure 5-2. At flocculation inducing doses, above 5 mg/m^2, the majority of the cells were nonviable after 15 minutes exposure. Viability decreased at longer times at these doses. This was typical behavior for the strongly cationic polymers studied; death was rapid and essentially complete at flocculation inducing concentrations. To preclude the possibility of toxic polymerization side products or catalyst presence causing cell death, solutions of poly-L-lysine were dialyzed for 24 hours against 20 volumes of PBS. The samples were retested, and were found to cause flocculation and cell death as before.

It had previously been shown by Nevo, DeVries and Katchalsky (1955) that polylysine association with erythrocyte surfaces could be abolished by the addition of low molecular weight poly(glutamic acid); for the 25,000 MW poly-L-lysine tested, addition of 8,000 MW poly-L-glutamic acid in equal or excess amounts did not cause dissociation of the cells or reduce toxicity. Rather, it aggregated the cells further, and caused more rapid cell death.

The behavior of the strong polycations such as poly-L-lysine towards the cells is consistent with the findings of the literature discussed in section 2.6.5., and clarifies the

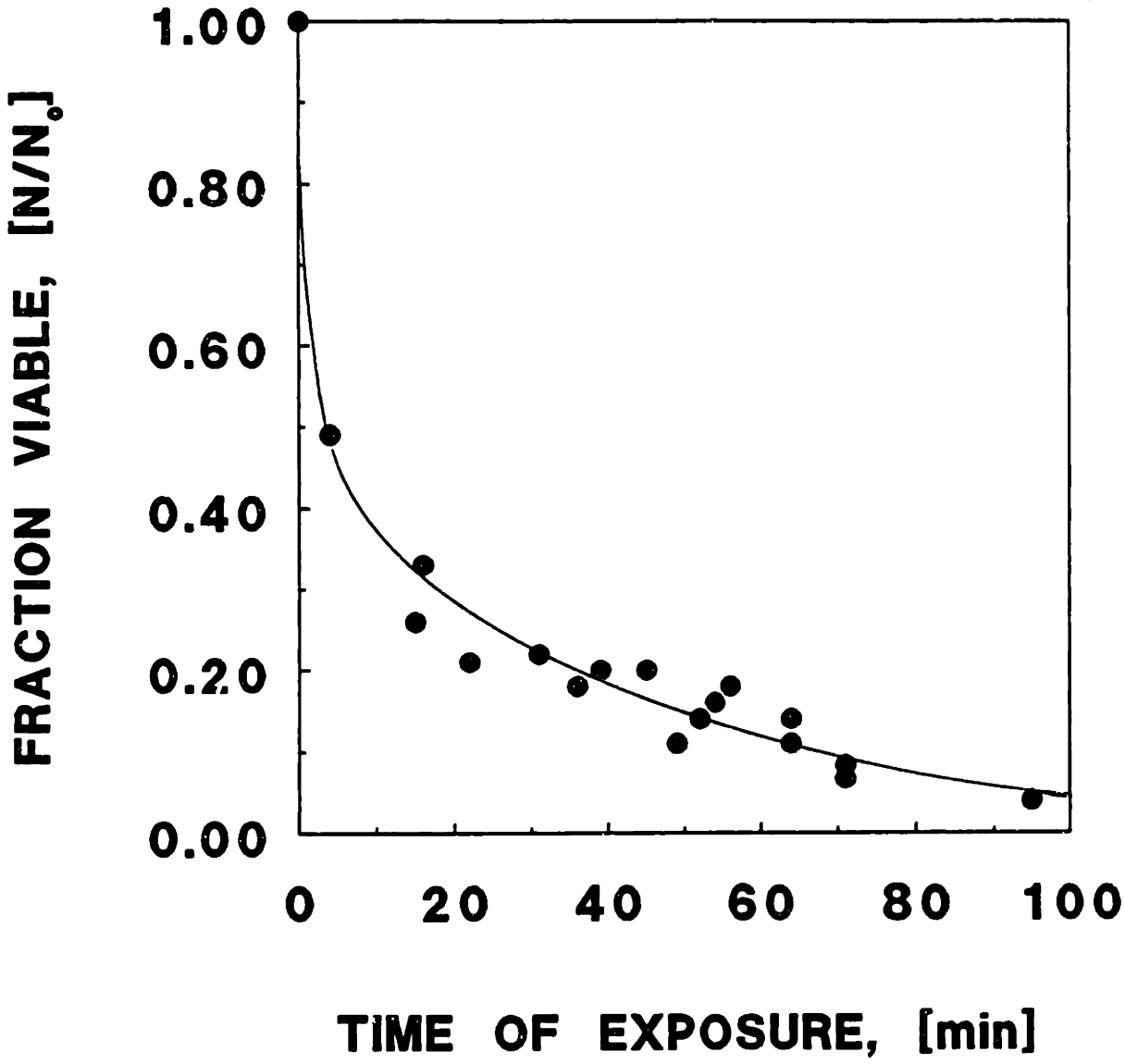

Figure 5-1. Fractional viability for CRL 1606 cells versus time of exposure to 40 mg/m^2 poly-L-lysine, 25,000 MW.

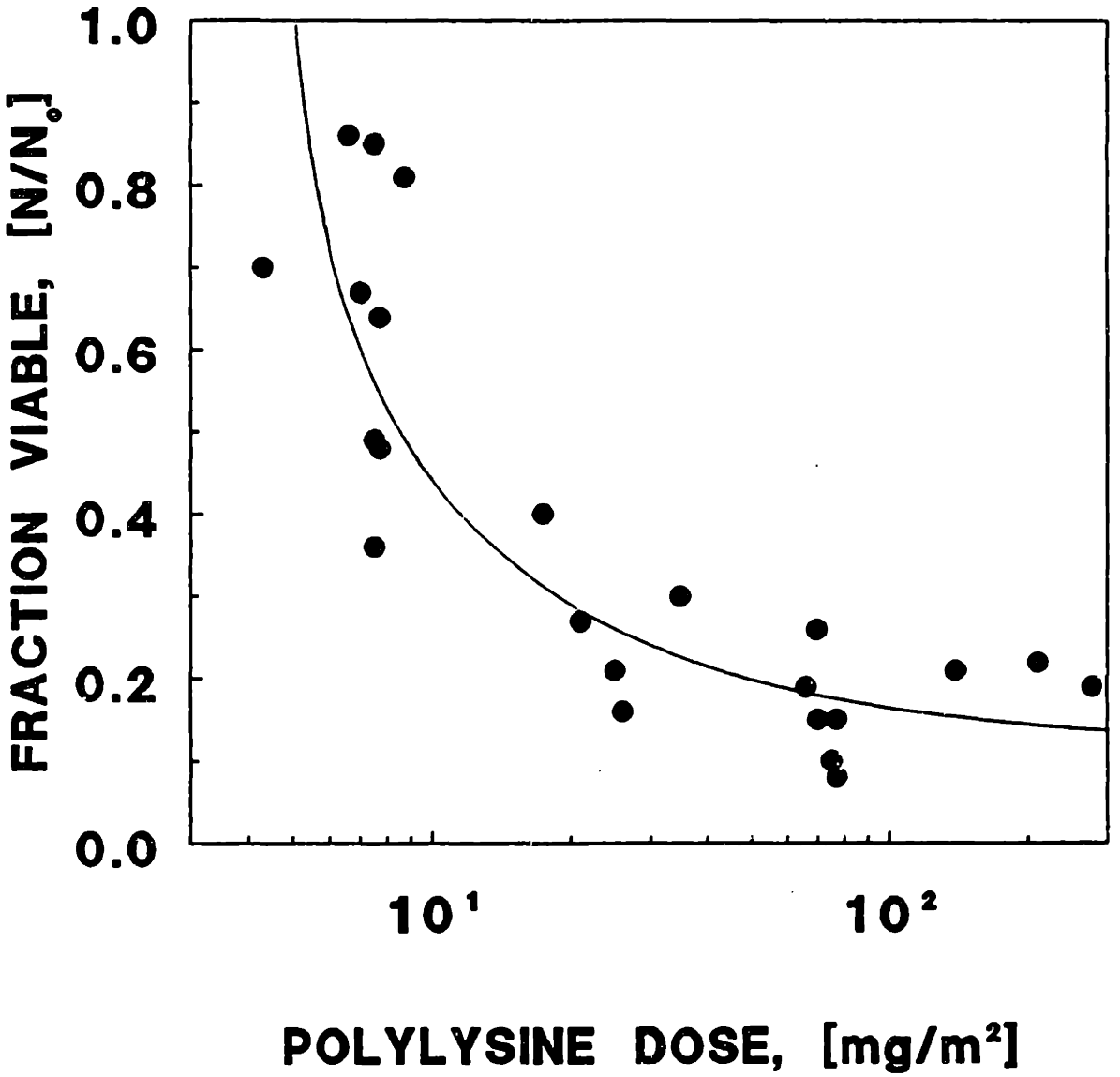

Figure 5-2. Fractional viability of CRL 1606 cells versus 25,000 MW poly-L-lysine dose after 15 minutes exposure time.

notion that strong polycation adsorption onto the cell membrane in amounts which induce flocculation are also toxic. It will be noted that poly-L-lysine is used widely in an adsorbed form to promote adherent cell attachment to tissue culture plastics (McKeehan and Ham (1976)). Under these conditions of usage, the polymer is nontoxic. The toxicity of the polymer in free solution suggests that when the polymer is able to conform closely to the cell membrane, it is able to disrupt the function of the membrane, and also cause cell leakage (Mamelak and Wissig (1969)). When the polymer is in an adsorbed, confined configuration, it is not able to closely associate with the membrane and disrupt function. NMR studies of polylysine association with phosphatidic acid liposomes indicate that the polymer association with the membrane induces polymer conformational change from a random coil to an ordered α-helical configuration, and lipid conformational change from a liquid to a crystalline state (Hartmann and Galla (1978)). Although a model liposome system cannot imitate the true complexity of a cell surface, these results are indicative of the strong association of highly charged polymers with negatively charged membranes. Similar to polylysine use for adherent cell culture, cross-linked DEAE dextran is the substance of which several brands of microcarriers are made. Again, the results of the current experiments suggest that when cationic dextran is in free solution and can associate with the membrane closely, toxicity results. However, cross-linked DEAE dextran microcarriers are also known to be toxic to adherent cells when the charge density of the dextran is too high (Levine, Wang and Thilly (1979)). This suggests that in addition to being in an immobilized state, having a low charge density polymer will lead to less harmful association with the cell surface.

5.2. - Poly-L-Histidine Characterization

The flocculant screening studies above indicated that the charge on the flocculant was responsible for its effectiveness, and also for its toxicity. Cationic flocculants (*e.g.*

DEAE dextran) were effective flocculants and were toxic, where nonionic and anionic analogues (*e.g.* - dextran, dextran sulfate) were ineffective but non-toxic to the cells. In keeping with the microcarrier results of Levine, Wang and Thilly (1979), the flocculant search was directed at finding a weakly cationic polymer which could mediate non-toxic aggregation. The underlying hypothesis was that a slightly cationic polymer may be able to aggregate cells without the severe toxicity shown by the industrial flocculants and highly cationic polymers. Copolymer peptides with varying ratios of tyrosine and lysine were initially selected to test this hypothesis, however, these polymers were difficult to solvate in aqueous solution. Dextran polymers were derivatized with diethylaminoethyl groups to varying degrees, but the degree of derivatization was difficult to assess for low charge density polymers. Thus, an alternate agent, poly-L-histidine (PLH), was selected. This is a synthetic polypeptide with a pendant imidazole ring. The pK_a of the imidazole amine in free histidine is about 6.05. Thus, polymer charge should vary considerably with pH in the range of 5 to 7 pH units. The amount of polymer charge is also easily assessed by titration.

5.2.1. - Poly-L-histidine Charge and Solubility

The ionization behavior of a polymer depends on its conformation in solution, which is determined by the polymer charge and structure, and the ionic milieu. Although it was initially synthesized in the late 1950's (Patchornik, Berger and Katchalski (1957)), the conformation of PLH is a subject of debate. X-ray diffraction studies show that it forms left-handed helices in the crystalline state (Oshima and Kumanotani (1986)). Circular dichroism experiments suggest that it assumes a left-handed helix or β-sheet structure in aqueous solution above pH 5, although an absolute conformation has not been confirmed. Below pH 5, the polymer is a random coil. Since the conformation of PLH is unknown for our conditions, it is not possible to predict the charge of the polymer (Patchornik,

Berger and Katchalski (1957)). For this purpose, a potentiometric titration was performed at 0.15 M NaCl to elucidate the fractional ionization of the polymer over the range of pH 4 to 9. The titration was complicated by the onset of polymer precipitation above pH 6.4, which necessitated vigorous agitation and long times between base additions to allow equilibration to the true solution pH. The experimental charge curve and the theoretical ionization for a free histidine monomer are shown in Figure 5-3. PLH charge goes from a maximum of 7.5 mEq/gm at low pH to a negligible charge above pH 8. Polylysine possesses a constant charge density of 8.7 mEq/gm over the pH range shown. As can be seen from Figure 5-3, the ionization of the polymer does not follow that of free histidine. In addition to having a broader ionization curve, the apparent pK_a of the imidazole amine is depressed from 6.05 to 5.5. The diffuse nature of the curve results from the difference in microenvironments of individual histidine residues in the polymer, caused by segment interactions and precipitation. The change in the observed pK occurs because a majority of residues experience different physical conditions than they would if in free solution as monomer. The polymeric state favors uncharged histidine residues at a given bulk liquid hydrogen ion concentration. Altered equilibrium behavior such as this is well documented for polyelectrolytes (Tanford (1962)). In addition, precipitation of the polymer above the pK_a will place many residues in the interior of a particle where interactions between segments will be enhanced. The fact that the polymer forms a precipitate is an indication that electrostatic repulsion between segments is small enough that hydrophobic forces can drive polymer self-association and precipitation. Regardless of the cause of the polymer behavior, Figure 5-3 shows that the charge is low, and varies considerably over the range of pH 6 to 7.

The solubility of poly-L-histidine versus pH in PBS is shown in Figure 5-4. Solubility is large at pH values where the polymer is significantly charged. As the polymer charge decreases with pH increase, the solubility decreases. Above pH 6.6, the solubility

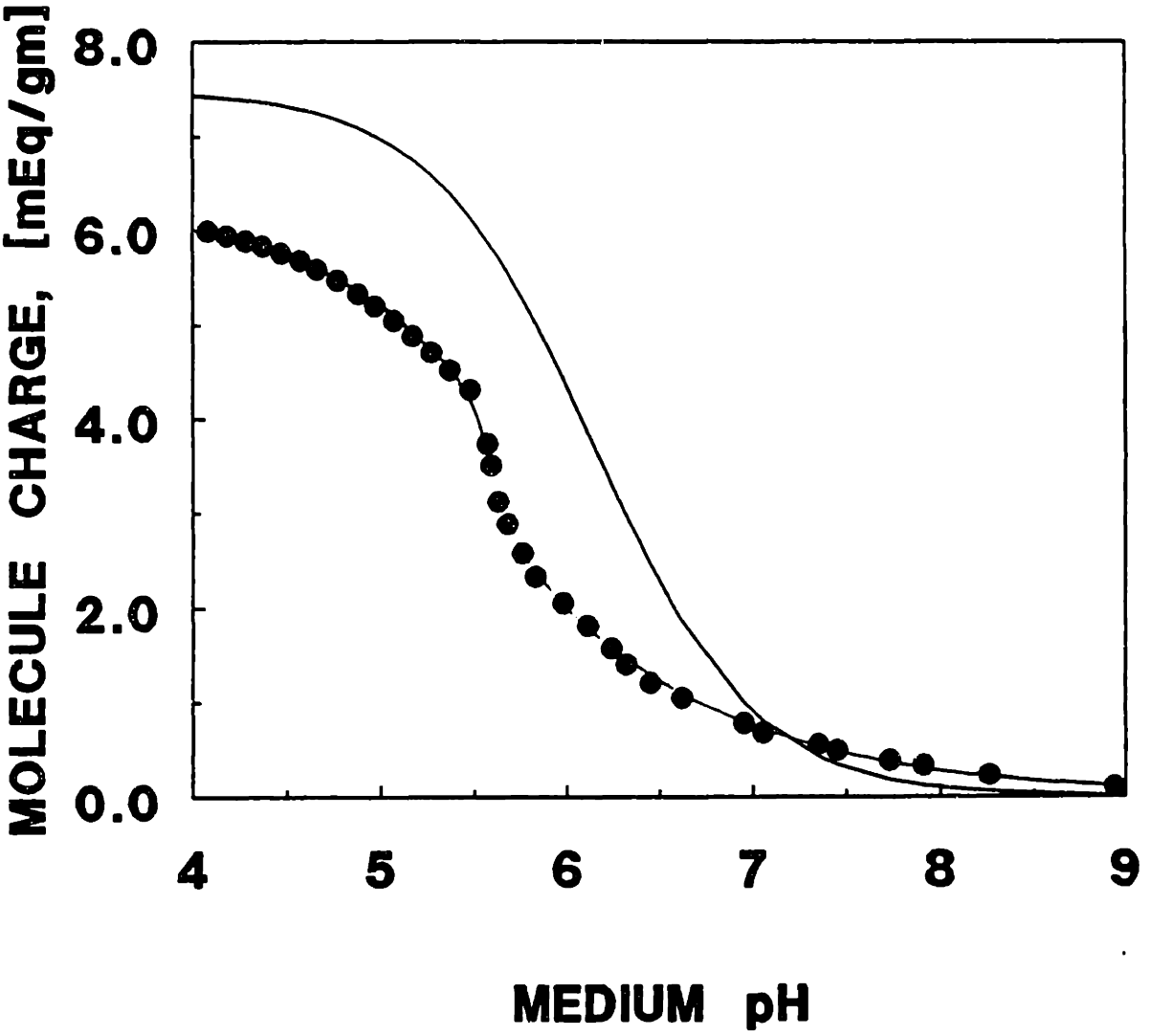

Figure 5-3. Charge density of poly-L-histidine, 23,000 MW, at 3.0 gm/L in 0.15 M NaCl. The solid curve is the theoretical ionization for monomeric histidine, $pK_a = 6.05$.

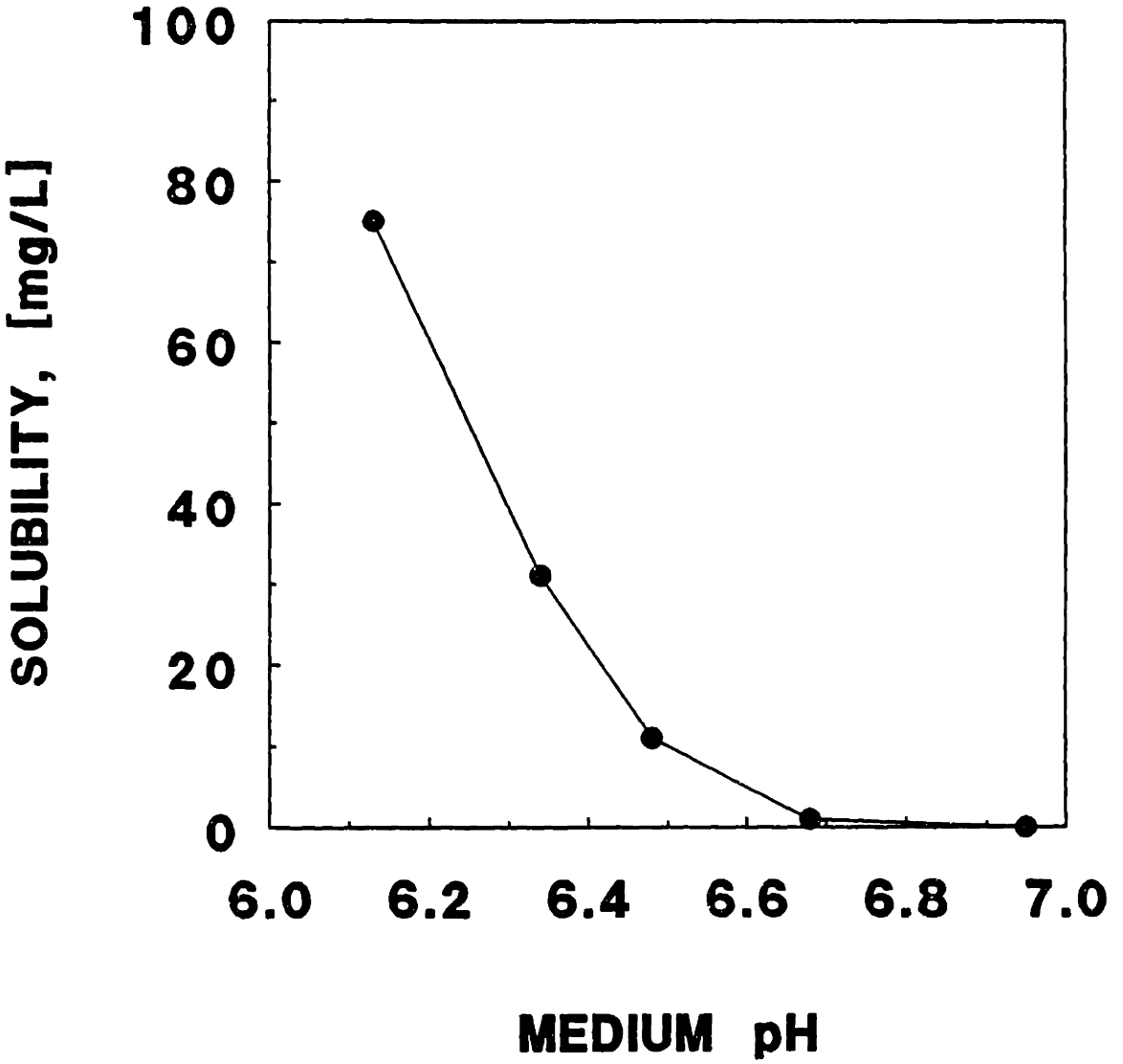

Figure 5-4. Solubility of poly-L-histidine, 23,000 MW, in 0.15 M NaCl versus pH.

decreases to below 1 mg/L, the limit of detection by the assay method. This is considered negligible for cell flocculation purposes. As noted above in section 5.1.5., flocculation inducing doses of polycations were typically above 5 mg/L. At pH 7, the polyhistidine is completely insoluble.

In keeping with the experimental results on strong polycations, it was expected that poly-L-histidine would show variable behavior toward cells with changing medium pH. Below neutral pH, the polymer is substantially charged, and is soluble. Both of these qualities should make it physically analogous to poly-L-lysine and soluble DEAE dextran, and thus toxic. At neutral pH, however, poly-L-histidine is slightly charged, and is an insoluble precipitate. This should reduce the toxicity of the polymer by reducing the strength of interaction, and by effectively immobilizing the polymer in a solid-like state. As mentioned above, Gad (1983) demonstrated the ability of polycations to disrupt membranes by liposome fusion using polylysine. Similar experiments by Wang and Huang (1984) with PLH show that liposome fusion only occurs at acid pH. This raised the prospect that polyhistidine may be able to mediate flocculation at neutral pH without the severe membrane disruption of strong polycations. It was thus desired to know whether the polymer would mediate aggregation under the two extremes, and whether toxicity would change with the polymer characteristics.

5.2.2. - Initial PLH Toxicity Screening

As with the other flocculants, poly-L-histidine effectiveness and toxicity was tested using CRL 1606 murine-murine hybridoma cells. At pH 6 and 7, CRL 1606 cells are present only singly and as pairs in normal suspension culture. This is shown in Figure 5-5a and 5-5b for pH 6 and 7 respectively. Magnification is 40x. Figure 5-6a shows CRL 1606 cells aggregated in a Couette viscometer at a shear rate of 12 s^{-1} for 10 minutes at 40 mg/m^2 PLH and pH 6. Magnification is again 40x. In this photograph, very large flocs

are visible; it can additionally be seen that there are very few individual cells in the photograph. Figure 5-6b shows CRL 1606 cells aggregated under identical conditions of agitation, time, and polymer dose, but at pH 7.2. The dark circular objects in the photograph are 87 micron diameter latex size standards. In this photograph, it is evident that aggregation is not as strong as at pH 6. The flocs produced are smaller, and there are more small flocs and single cells. Nevertheless, the polyhistidine is still able to mediate aggregation to an appreciable extent, producing flocs with diameters in excess of 100 microns. It remained to be seen whether the polymer exhibited differences in toxicity versus pH as well.

Figure 5-7 shows the kinetics of cell death from exposure to 40 mg PLH/m^2 between pH 5.8 and 7.1. For this experiment, the cells were placed into a test tube along with a sample of PLH and Trypan Blue, mixed gently and allowed to rest. Cell counts were conducted over time. At pH 5.8 and 6.3, where PLH has significant solubility, cell death is rapid, as was shown for poly-L-lysine treatment at the same dose in Figure 5-1. This cell death is not simply an effect of pH, since the control experiment without PLH at pH 5.8 did not exhibit rapid cell death. At pH 7.1, where PLH is an insoluble precipitate, cell death is slow and negligible. This result was encouragement for continuing investigation of PLH as a flocculant of animal cells.

Subsequent assay showed that PLH was effective at flocculating other cell types. Figures 5-8, 5-9, and 5-10 show U-937, HeLa, and tPA-CHO cells in normal culture. Figures 5-11, 5-12, and 5-13 show these same cell types flocculated for 10 minutes at 12 s^{-1} shear rate, pH 7, and 40 mg PLH/m^2. Cell viability was also high under these conditions. It was concluded that the first goal of the flocculant system identification had been achieved, that of finding a flocculant for recycle of animal cell suspension cultures.

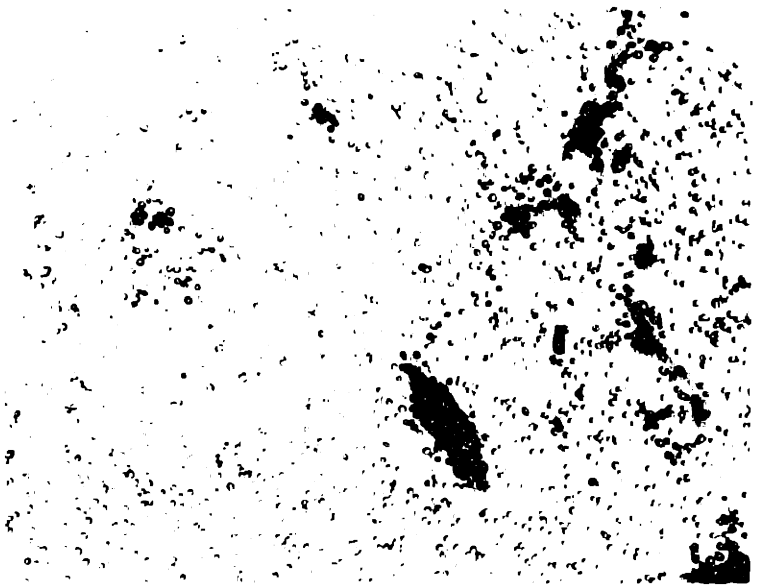

A

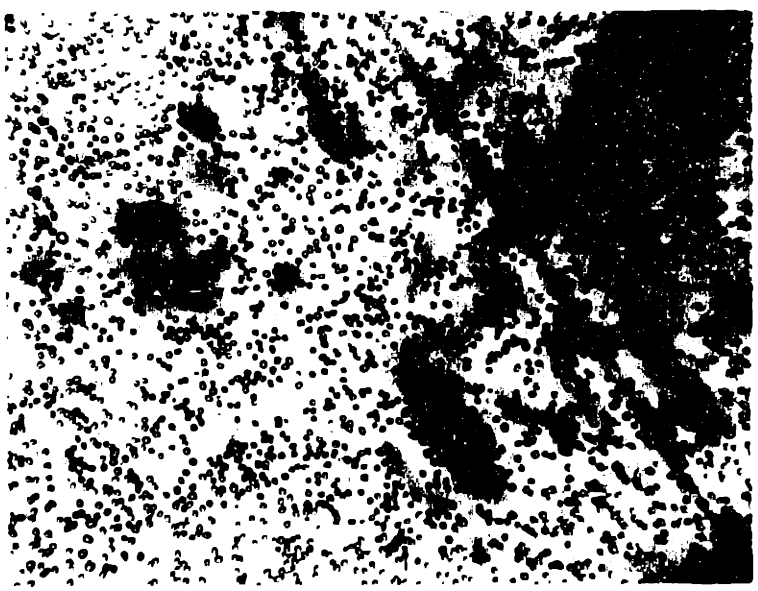

B

Figure 5-5. CRL 1606 cells in normal suspension culture. a) pH 6. b) pH 7.2.

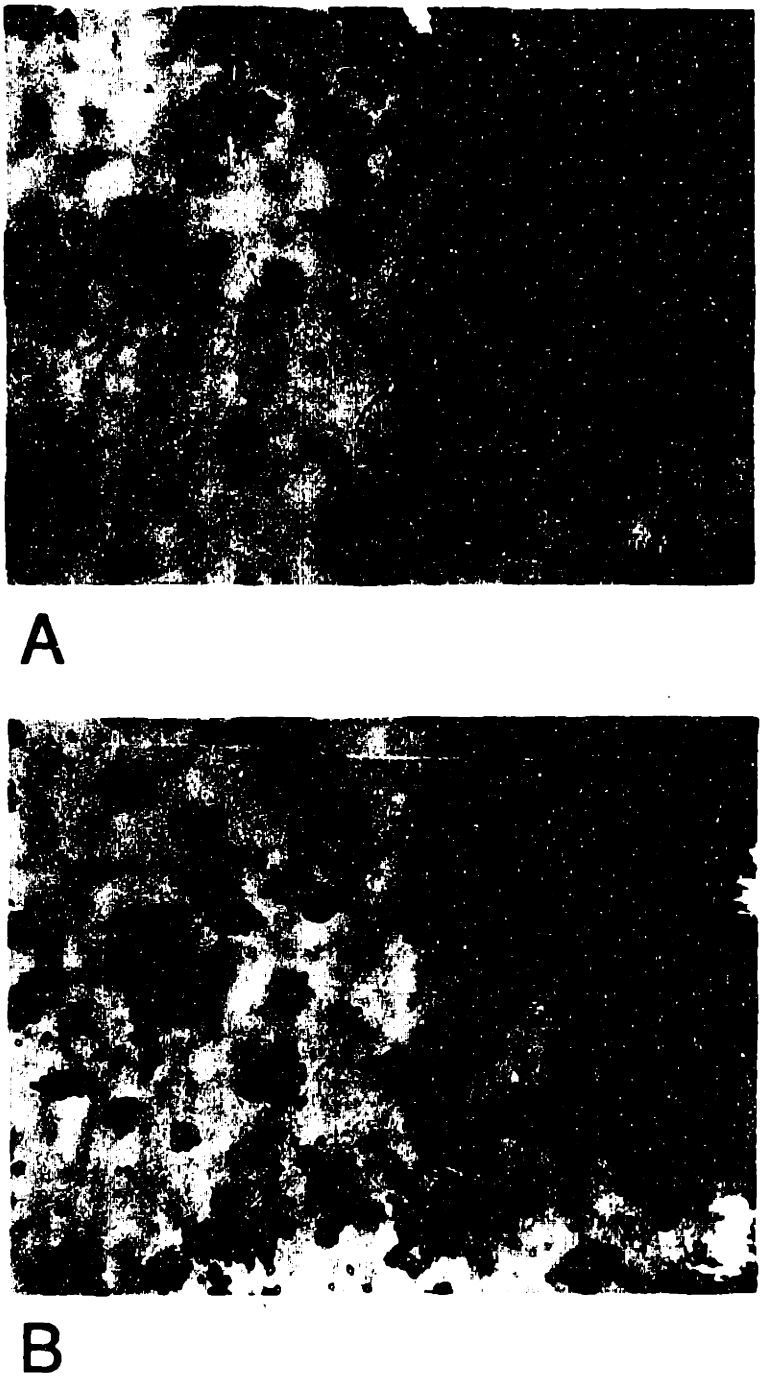

Figure 5-6. CRL 1606 cells aggregated in Couette flow using 40 mg/m^2 poly-L-histidine, 23,000 MW. Aggregated at 12 s^{-1} shear rate for 10 minutes. N = 10^6/mL, serum = 0.5% v/v. Black circular objects are 87 μm latex size standards. a) pH 6. b) pH 7.2.

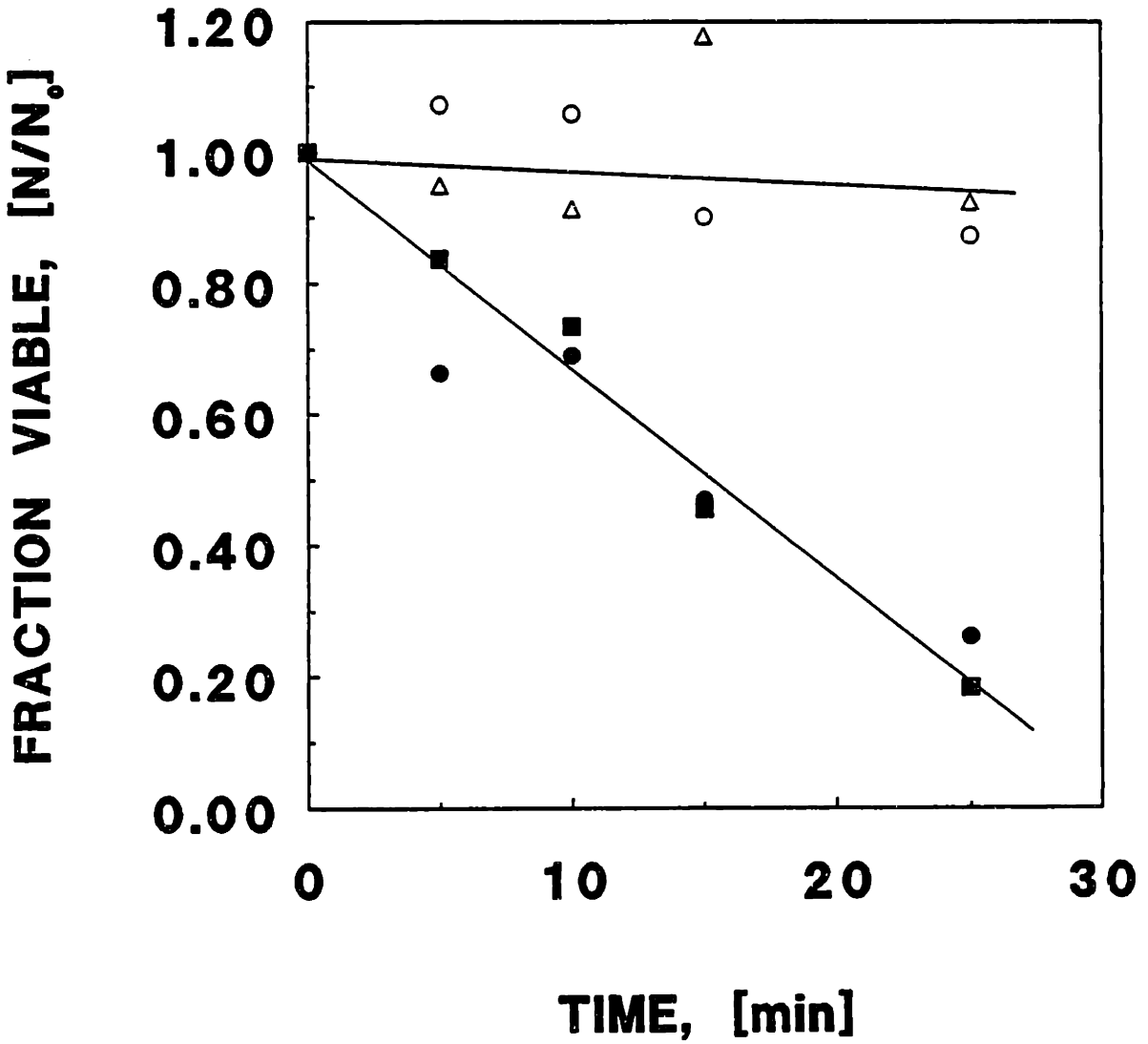

Figure 5-7. CRL 1606 cell viability versus time of exposure to poly-L-histidine, 23,000 MW, versus pH at 50 mg PLH/m^2. ○ - no PLH, pH 5.8, ● - pH 5.8, ■ - pH 6.3, Δ - pH 7.1.

Figure 5-8
U-937 cells under normal culture conditions. 40x mag.

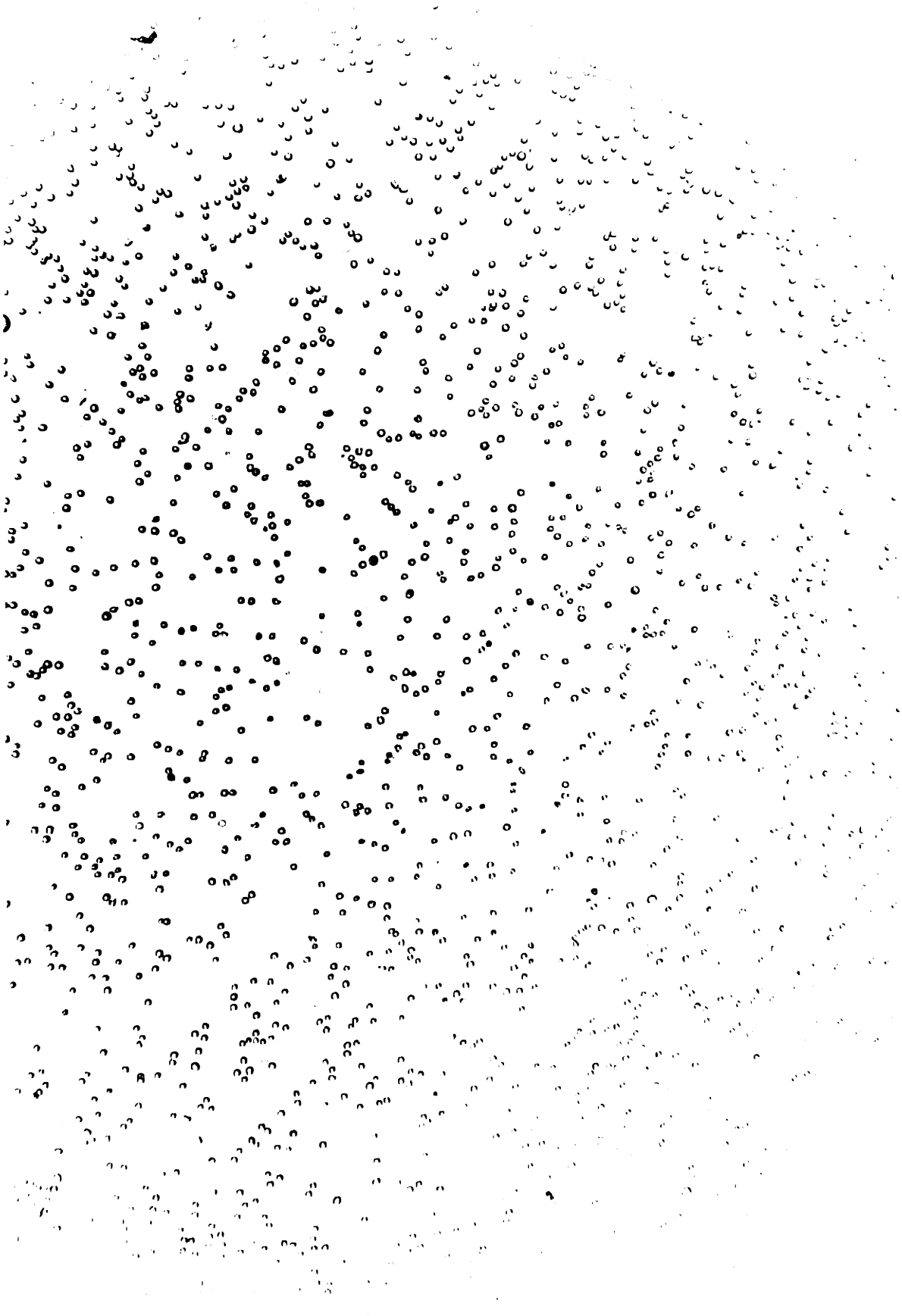

Figure 5-9
HeLa cells under normal culture conditions. 40x mag.

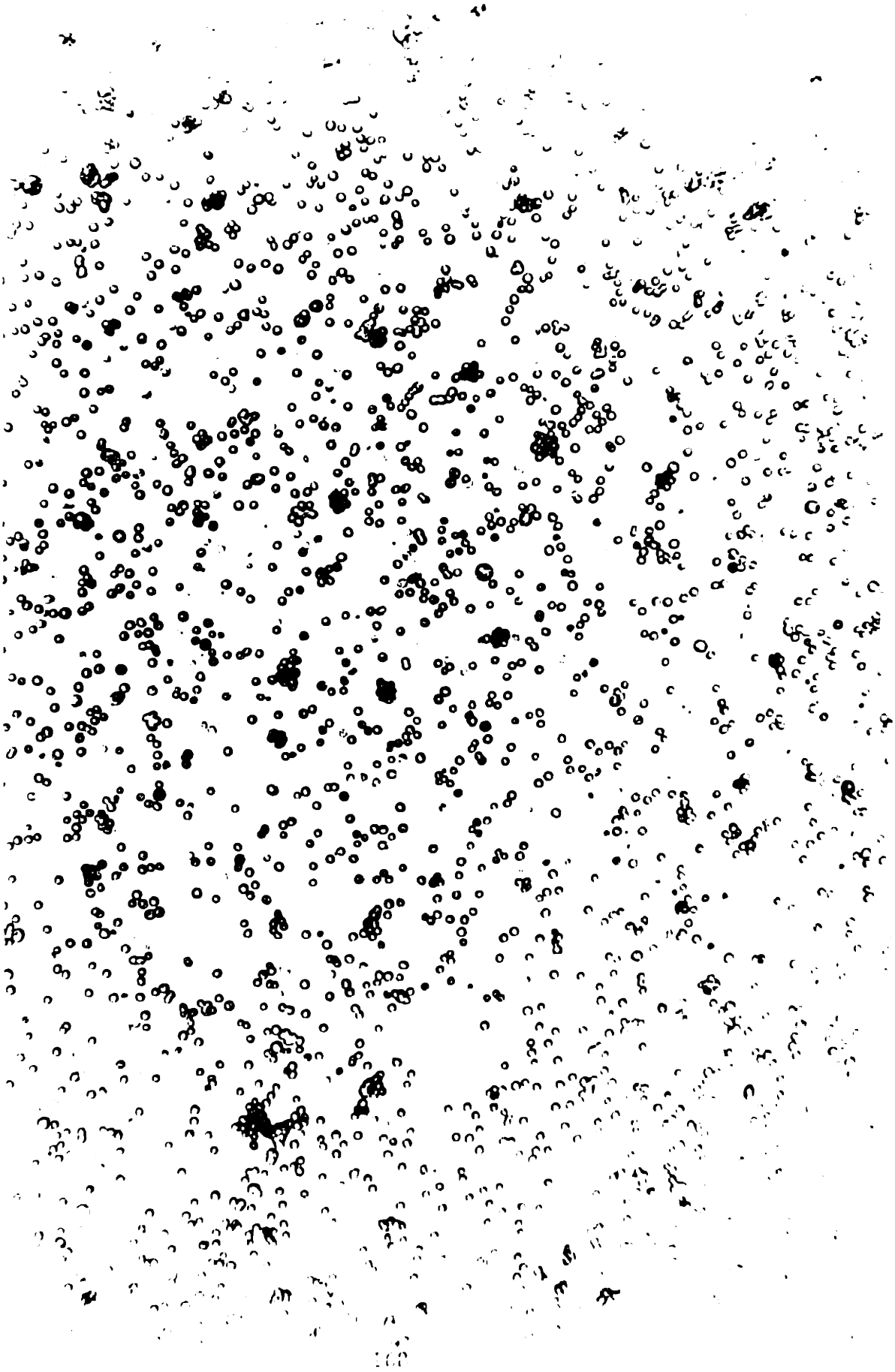

Figure 5-10
tPA-CHO cells under normal culture conditions. 40x mag.

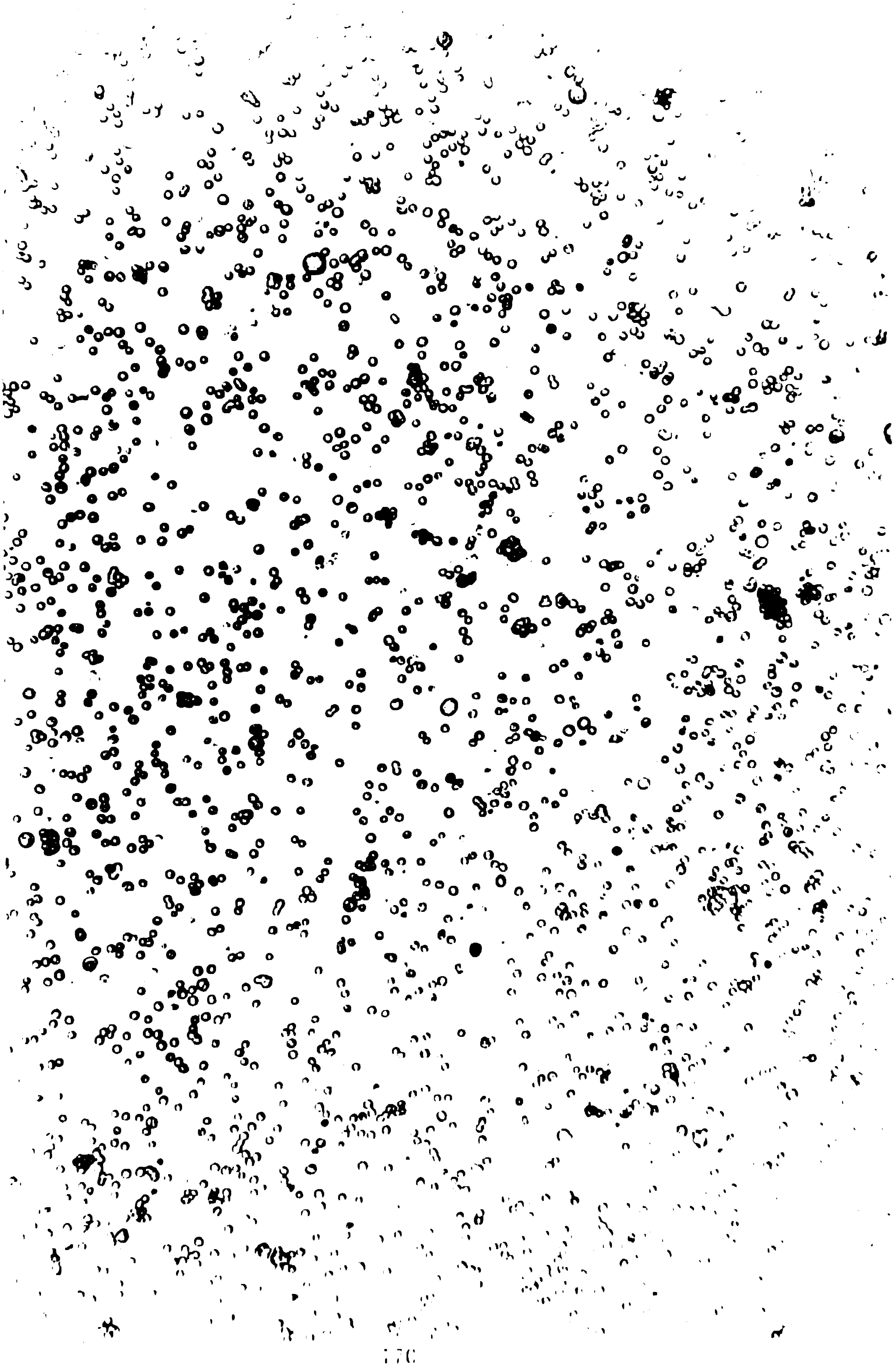

Figure 5-11
U-937 cells flocculated by PLH. 40x mag.

Figure 5-12
HeLa cells flocculated by PLH. 40x mag.

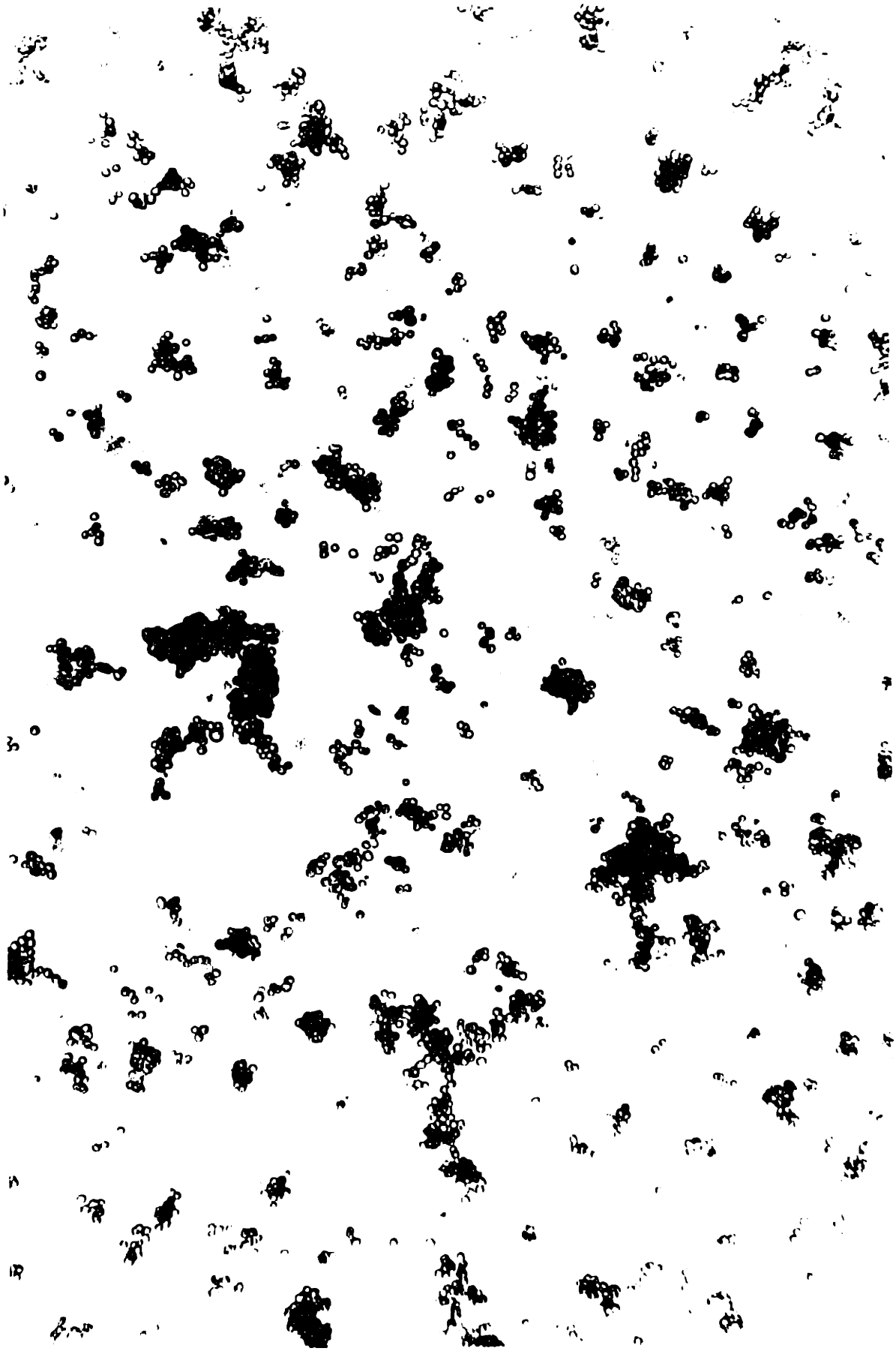

Figure 5-13
tPA-CHO cells flocculated by PLH. 40x mag.

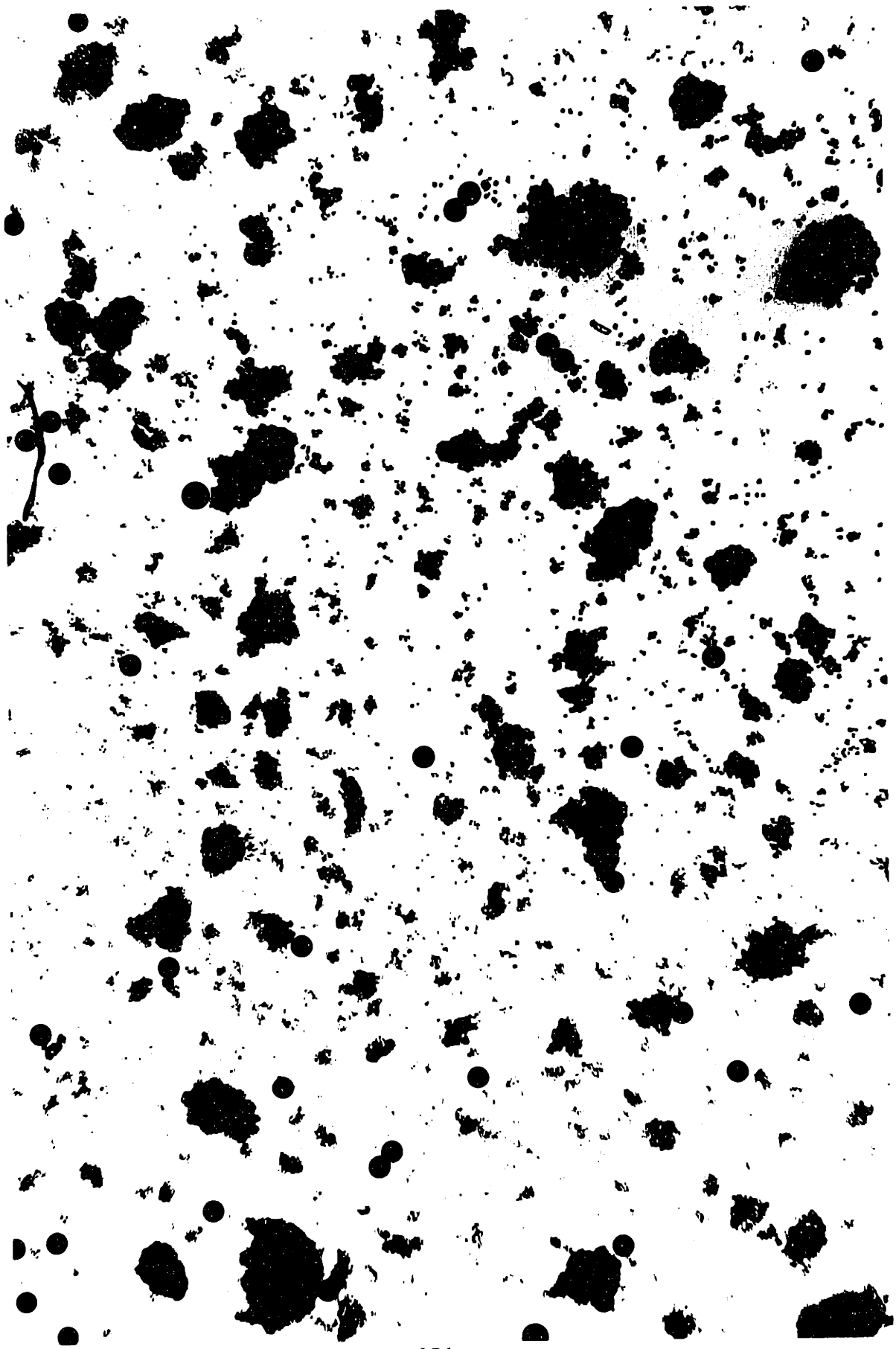

5.2.3. - Flocculation Harvest Performance

Although the above assay did not show significant cell death, it is not representative of a cell harvesting process using flocculation, with cell binding into large flocs and subsequent floc dissociation. It was desired to quantify the amount of cell death due to a flocculation harvest process (acute toxicity), and to ascertain whether the polymer affected subsequent cell growth (chronic toxicity).

The flocculation process used for harvesting toxicity studies at pH 7 is outlined in section 4.3.2.; briefly, the cells were flocculated under agitation for 10 minutes, allowed to settle for 15 minutes, and 90% of the supernatant was replaced with fresh medium. The cultures were then redispersed under agitation for 15 minutes before counting. The data thus collected represent the endpoint toxic effect of the polymer. Figure 5-14 is a plot of the viable cell fraction remaining after dispersion for several experiments on PLH flocculation of CRL 1606 at pH 7. Significant flocculation, as judged by visible floc appearance, is first seen for polymer doses greater than 20 mg/m^2. At this level of polymer, over 80±10% of the cells remain viable. Greater than 50% of the cells are viable at 200 mg/m^2. It might be expected that at higher dosages the fraction of viable cells would decrease until all the cells became nonviable. However, as seen in Figure 5-14, as PLH dosage is increased, the fraction of cells remaining viable plateaus to a constant value beyond about 100 mg PLH/m^2. It will be noted that the doses of polymer necessary to cause flocculation and maximal cell death are quite high. Typical polymer and protein monolayers are on the order of 1 mg/m^2 (Donaldson, Boonstra and Hammond (1980)). The large doses are due to polyhistidine precipitation which buries a large portion of the polymer in the center of an aggregate.

It was of interest to know whether the cells remaining after flocculation were damaged or in a viable, growing state. Figure 5-15 shows growth curves of cultures which have been flocculated by PLH treatment, settled out and fed by replacing 90% of the

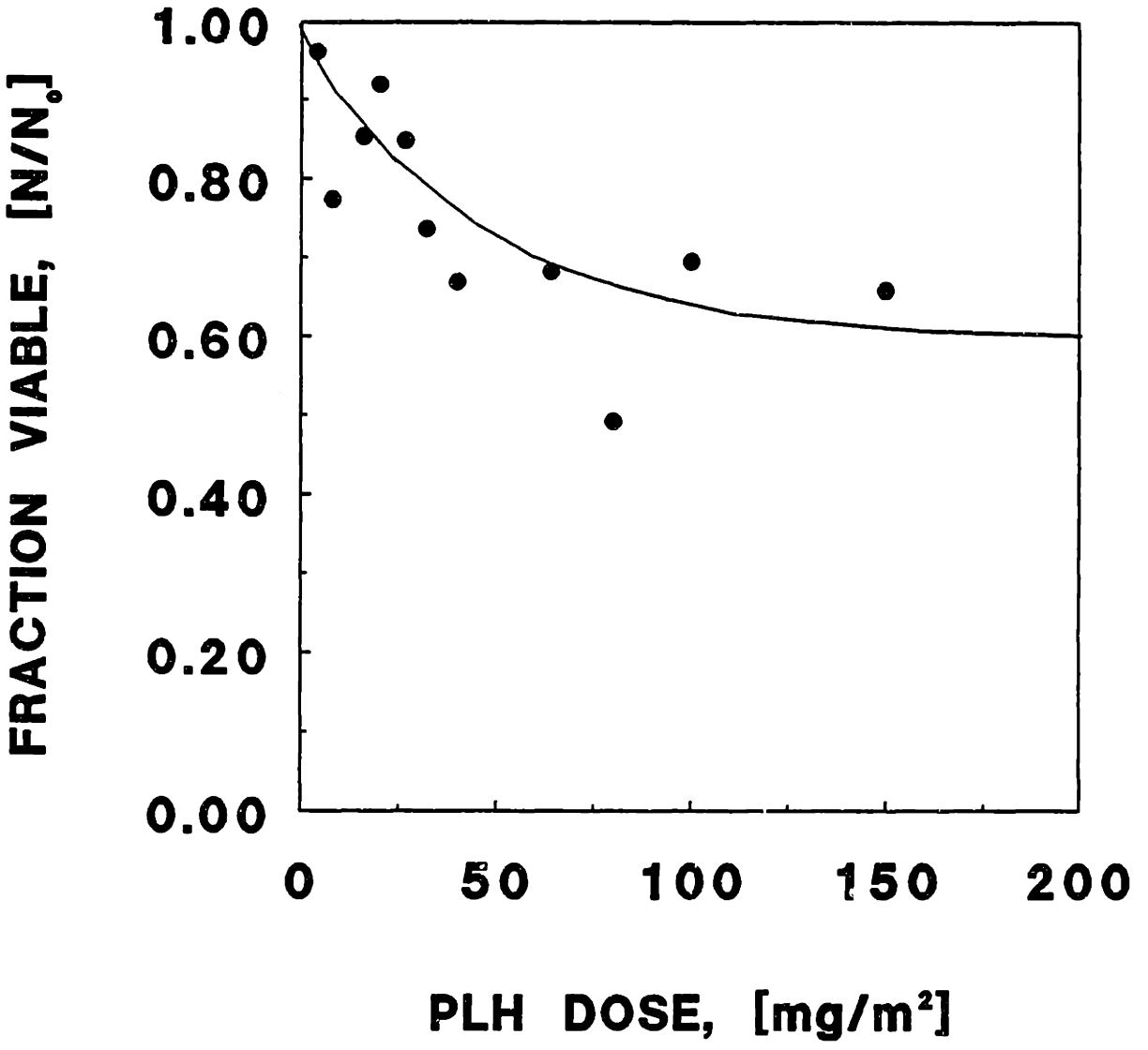

Figure 5-14. CRL 1606 cell viability versus poly-L-histidine dose, 23,000 MW, at pH 7.

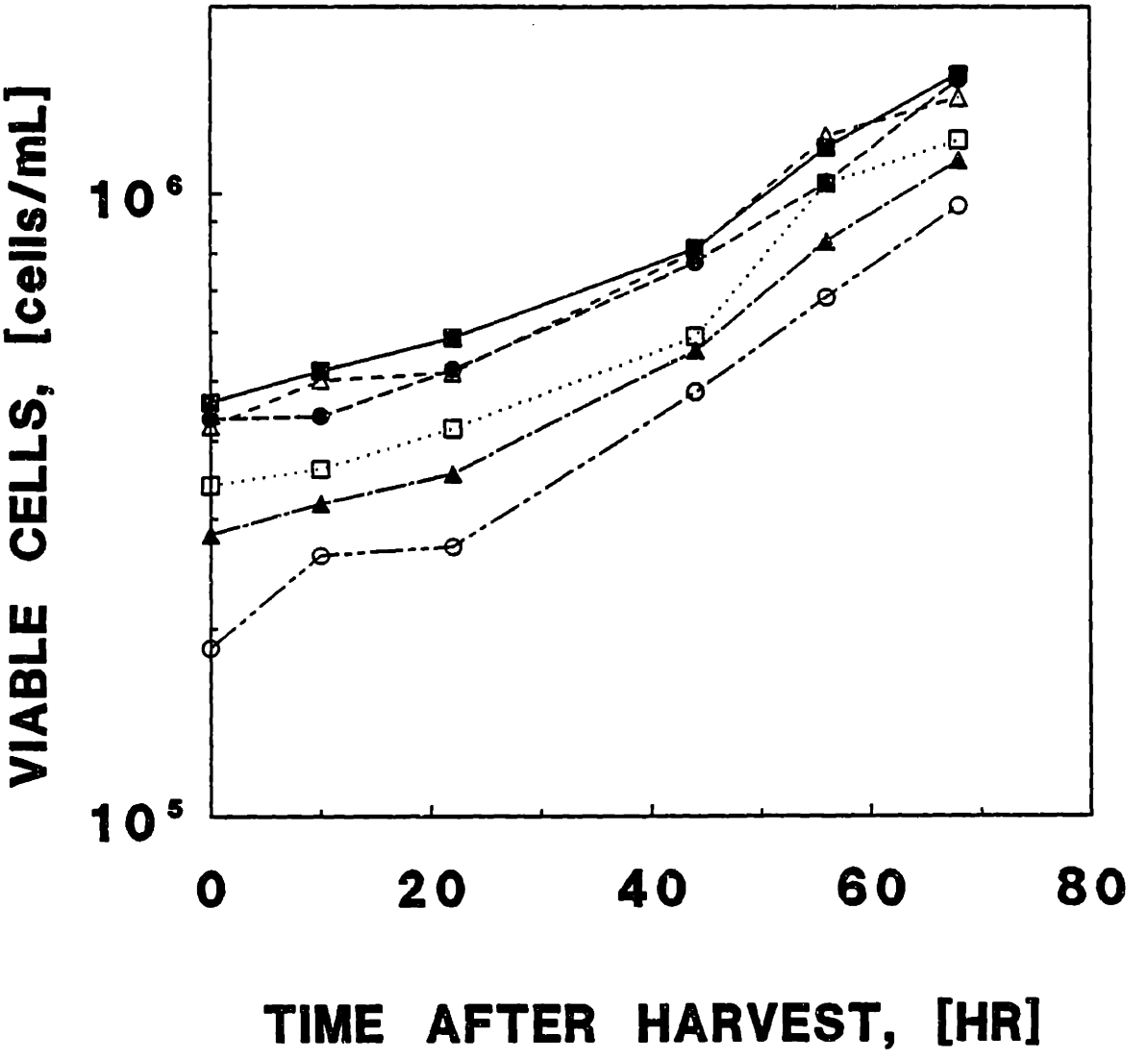

Figure 5-15. CRL 1606 cell growth after exposure to poly-L-histidine, 23,000 MW, at pH 7. ■ - 0 mg/m^2, Δ - 4 mg/m^2, ● - 8 mg/m^2, □ - 16 mg/m^2, ▲ - 32 mg/m^2, ○ - 64 mg/m^2.

medium. The cells were allowed to regrow in the spinner vessel, and were counted by hemacytometer for viable cells. The results show that for the PLH doses investigated, up to 70 mg/m^2, no appreciable lag phase is induced by the polymer harvesting treatment. Flocculation cell harvesting does not apparently affect the cell growth rate, either. Figure 5-16 is a plot of the cell growth rate for the first 48 hours after harvest versus PLH concentration. The results show that the growth rate after harvest increases with the PLH dose! However, it is not likely that a flocculation treatment which is toxic to a fraction of the cells stimulates the growth of the rest of the cells. This figure may be interpreted as demonstrating that there is no decrease in growth rate with increasing polymer dosage. That is, harvesting by polymer flocculation produces only an acute toxicity and neither a lag phase nor suppression of growth is subsequently encountered.

The results of Figures 5-16 may be explained as an effect of the cell concentration in the spinner. From Figure 5-15 it is apparent that not all cultures begin at the same cell density. This is due to the varying dosage of polymer (and associated toxicity) used in the experiments. If the initial growth rate after harvest is plotted versus the initial cell concentration, a decreasing linear correlation of growth rate results. Figure 5-17 is a plot of growth rate versus cell inoculum concentration for several PLH harvest experiments. This graph shows that the initial cell growth rate decreases with increasing initial cell density in a batch process at high cell inocula. The ordinate intercept of the linear best fit line through the points is 0.028 hr^{-1}, at infinite dilution of cells. This value corresponds well to that reported for CRL 1606 at 0.5% serum and low cell concentrations (Glacken (1987)). The abcissal intercept, at which growth rate is zero, is 3.3x10^6 cells/mL. Several possible causes of the growth behavior come to mind; nutrients or oxygen may be limiting, waste product accumulation may be suppressing cell growth, or the cells themselves may be secreting or carrying over a substance which is inhibiting growth.

Since the data represent initial growth rates, there should be no nutrient limitations

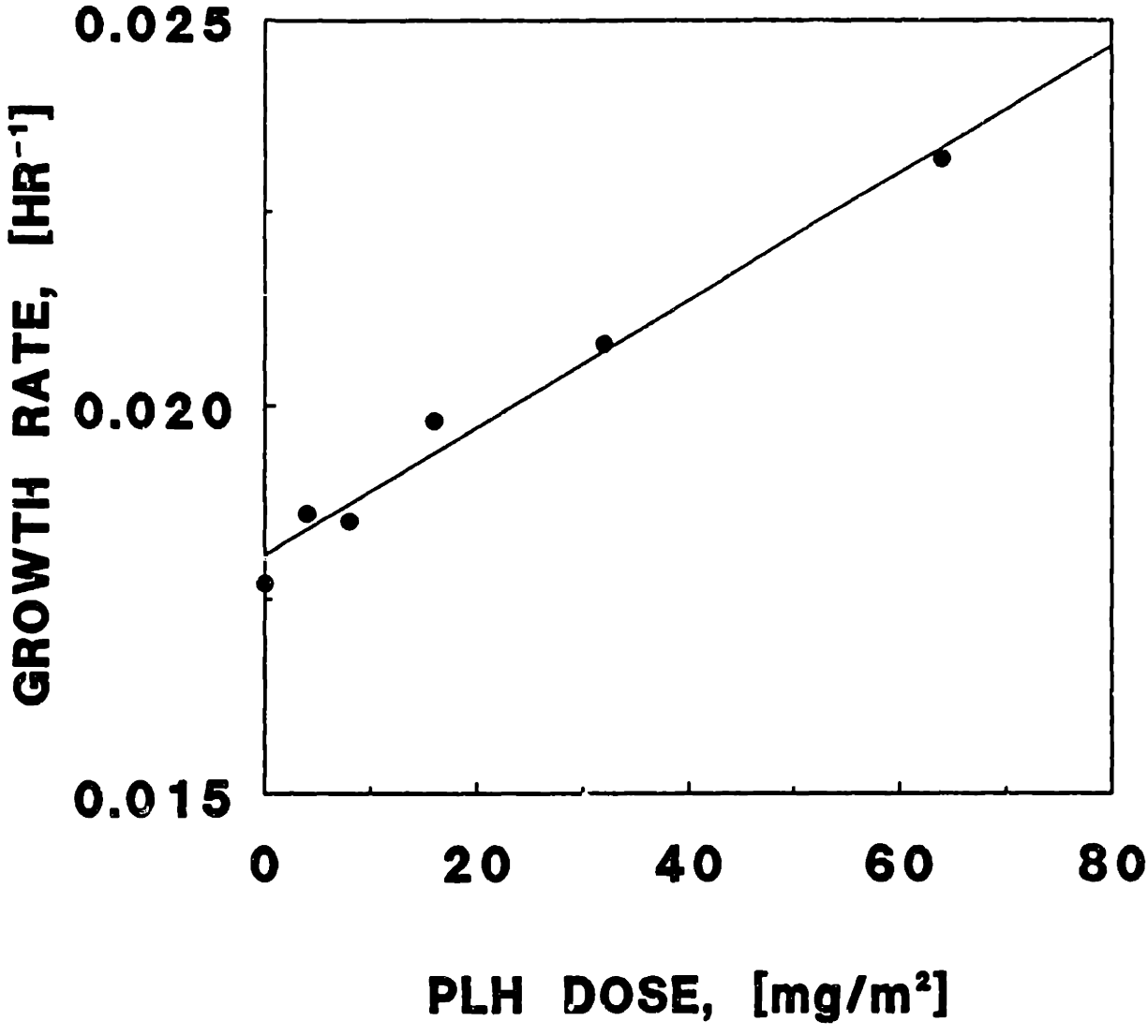

Figure 5-16. CRL 1606 cell growth rate versus poly-L-histidine dose for the data of Figure 5-15.

or waste accumulations in the cultures; 90% of the medium is changed in the re-feeding procedure. The results of the metabolic studies of Glacken (1987) may be used to compare the culture usage of nutrients and secretion of growth inhibiting metabolites. Glacken correlated the growth rate of CRL 1606 cells by the following Monod-type equation:

$$\mu = \frac{\mu_{max} S G}{\left[S + K_{S,o} C^{-\varphi}\right]\left[1 + \frac{A^2}{K_A}\right]\left[1 + \frac{L^2}{K_L}\right]\left[G + K_G\right]} \qquad (5\text{-}1)$$

In this equation, μ and μ_{max} are the growth rate and maximum growth rate, S is the serum concentration, G is the glutamine concentration, A is the ammonia concentration, L is the lactate concentration, and C is the cell concentration. $K_{S,o}$, K_A, K_L, and K_G are Monod constants, found equal to 6.5±2.9 volume percent, 45±8 mM, 12,000 mM, and 0.15 mM, respectively for CRL 1606. The constant φ is equal to 0.21±.002. This constant describes the dependency of the serum promotion of growth rate on the cell concentration. It will be noted that under conditions of low serum (<< 6.5 %), as used here, the form of the equation predicts that an increase in the cell concentration should lead to an increase in the growth rate of the cells. This is opposite to the observation of the above experiments, and may reflect the fact that Glacken's equation was derived from extremely low cell concentration data, from 8,500 to 85,000 cells/mL. Using this equation, the cell concentration data from Figure 5-15, and Glacken's data on the consumption rates of nutrients and production of lactate and ammonia, it can be shown that the growth rate of the cells is not affected by the glutamine, lactate and ammonia concentrations experienced.

Surface mass transfer experiments in the spinner vessels (Aunins *et al.* (1990)) showed that the maximum oxygen transfer rate at the impeller speed used is equal to 1.3×10^{-2} mmole/L/s. The oxygen uptake rate of the cells at the 10^6 cells/mL is 3.3×10^{-5} mmole/L/s. It is evident that the cells are not oxygen limited in the spinner vessels. The decrease in cell growth rate with increasing cell concentration was then attributed to a factor

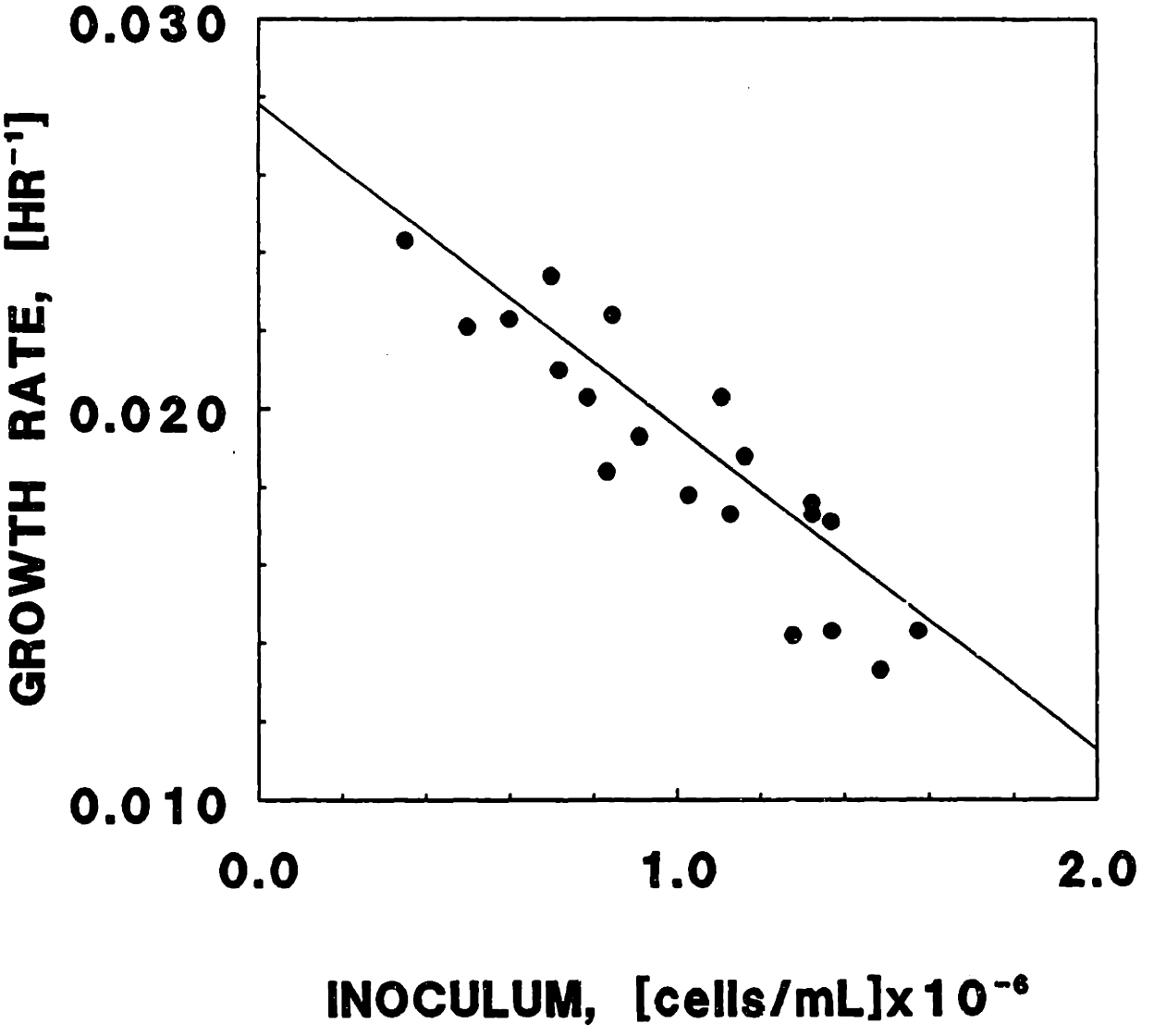

Figure 5-17. Growth rate of CRL 1606 cells versus initial cell concentration for cultures harvested and fed using PLH flocculation.

independent of nutrient limitations. Since the decrease in initial growth rates was apparently unrelated to polymer dose, nutrient limitation, or waste accumulations, it was postulated that the effect of cell inoculum on growth rate was not the result of the flocculation procedure, but was due to cell concentration itself.

To test the above hypothesis, cells were centrifuged and resuspended at different concentrations in fresh medium supplemented with 0.5 and 2.0% serum. The growth rates versus initial cell density are shown in Figure 5-18. The trend of decreasing growth rate with increasing inoculum concentration is also seen with the centrifugally harvested cultures. These cells have never been flocculated, thus the effect cannot be related to the polymer treatment. These results reinforce the conclusion that the growth rate is dependent on the inoculum concentration. Again, depletion of nutrients and accumulation of waste metabolites was not present in these cultures, nor was there oxygen starvation. It is unclear what is responsible for the behavior, however.

It is plausible that a growth inhibitor or promoter is involved in growth suppression. It is possible that CRL 1606 growth is inhibited by the secretion or carryover of such compounds in a batch harvest scheme. Since the medium was completely replaced in the centrifugation experiment, the carryover of growth inhibitors from spent culture fluid is prohibited. However, if a growth inhibitor is carried over via adsorption to a cell surface receptor, its concentration should vary directly with cell inoculum concentration. Alternately, carryover of lysed or nonviable cells may have inhibited culture growth. The flocculated cultures at the highest polymer doses had the highest nonviable cell concentrations, but showed the highest growth rates, however, so this theory is not satisfactory. The inhibition of growth with cell density (or a related variable) is not apparently a general phenomenon but is specific to this cell line and procedure. This is because it has been amply demonstrated that high density cultures of other cell types are possible. In addition, the effect is only apparent when the cells are cultured in batch

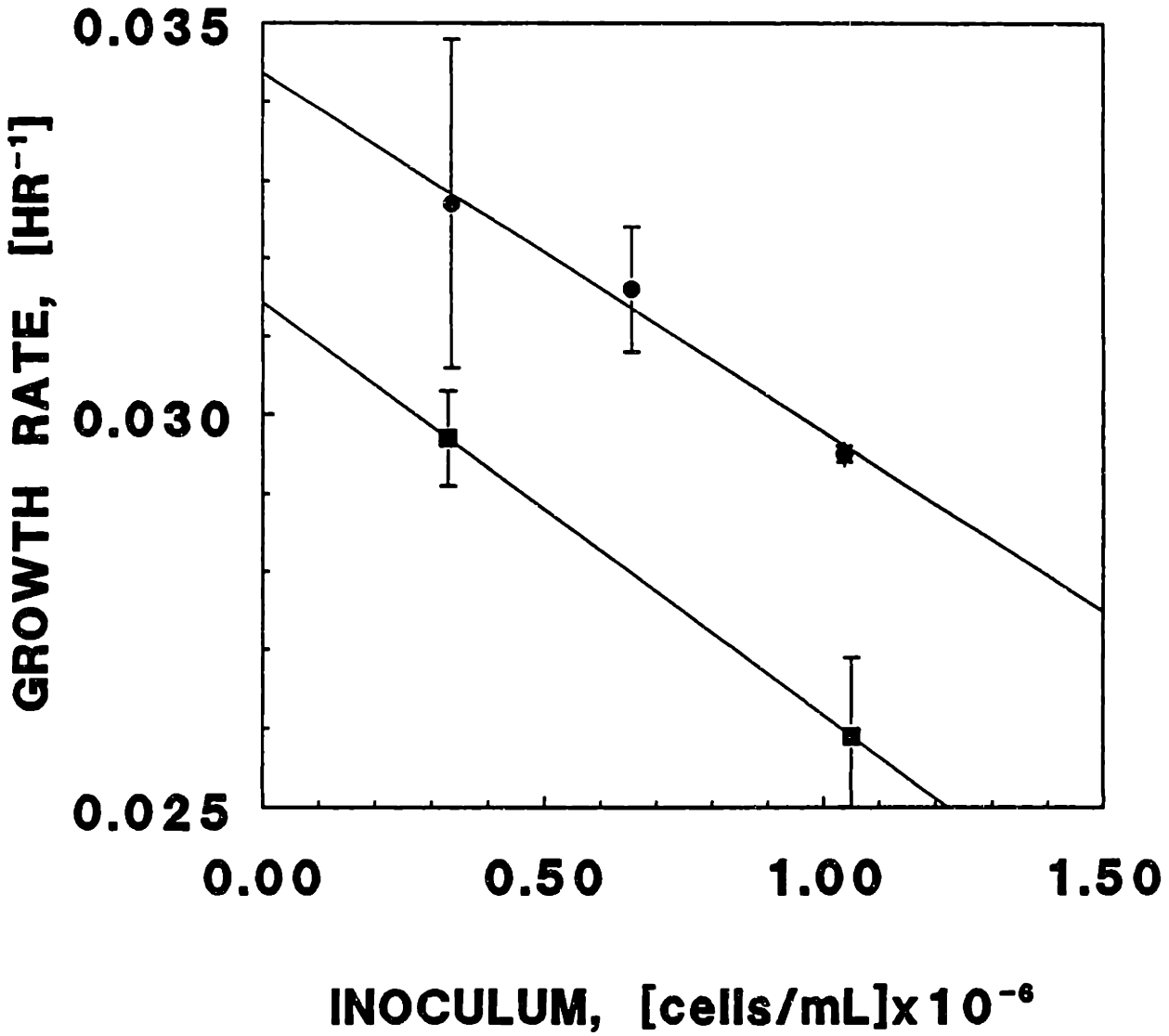

Figure 5-18. Growth rates of CRL 1606 versus initial cell concentration for cultures harvested and fed by centrifugation and complete medium exchange. ● - 2.0% serum, ■ - 0.5% serum.

fashion, since this cell line has been successfully cultured to high concentrations in immobilized systems (Piret and Cooney (1988)) without apparent deterioration in growth rate from cell concentration. An immobilized system undergoing perfusion may allow an inhibitor to wash out, and thus permit further growth of the cells. Although additional experimentation may elucidate the nature of the growth inhibition, it is not considered to be a phenomenon linked to the flocculation system, and no further investigation was carried out.

It remained to be seen whether polyhistidine flocculation and sedimentation harvesting presented a viable method to increase cell concentration in a reactor. The ability to repeatedly harvest the cells by flocculation was demonstrated by splitting a 1000 mL spinner flask into two 500 mL spinners, and growing the cells in these vessels after harvesting and feeding. One of the two spinners was harvested by centrifugation, and the other was harvested by flocculating the cells and allowing them to sediment per above. The cells were allowed to grow, and were counted for viable cell number. This process was repeated several times, and the resulting viable cell counts are shown in Figure 5-19. These cultures were conducted using a serum-free medium formulation described in section 4.1., unlike the single harvest experiments above, which were conducted in 0.5% serum containing medium. Under serum-free conditions, cells are notoriously susceptible to chemical toxicity, and cell viability can be problematic. Unfortunately, some of the basal IMDM which was used for flask feeding in this experiment was flawed; this resulted in the death of the centrifuged spinner after the second feeding, and the death of the flocculated spinner after five feedings. Regardless of this complication, it is possible to observe that after the first feeding, both spinner vessels grew comparably, indicating that the flocculation scheme was the equal of the centrifugation harvesting procedure. The flocculation harvested vessel attained a maximum viable cell concentration of 3.5×10^6 cells/mL, which is roughly four times the maximum viable cell density achieved in batch

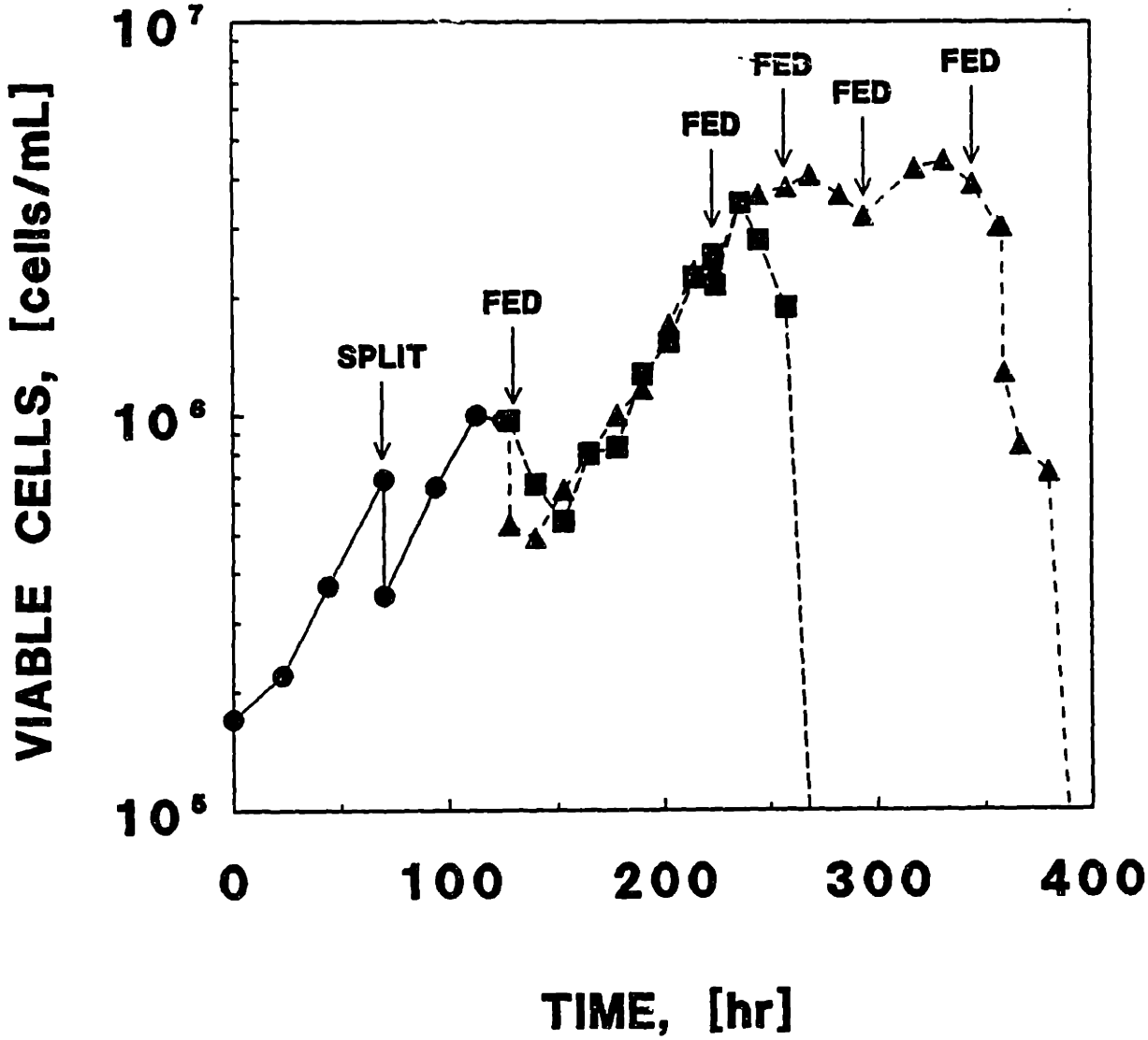

Figure 5-19. Concentration of viable CRL 1606 cells versus time for cultures harvested by centrifugation and by PLH flocculation and sedimentation. ● - seed spinner, ■ - centrifuged spinner, ▲ - flocculated spinner.

culture with this medium formulation (Adema (1987)). It will be noted that the abcissal intercept (cell concentration at zero growth rate) projected by the data in Figure 5-17 is $3.3x10^6$ cells/mL. It is possible that cell density did not increase further in the multiple feeding experiment due to the growth inhibition discussed above. From the above experiments it was concluded that although system optimization has not been performed, flocculation cell harvesting with poly-L-histidine is a working alternative to other cell-medium separation techniques.

6. - COLLISION EFFICIENCY RESULTS

There were two objectives to the current study of collision kinetics of animal cells. The first was to quantify experimentally the extent of destabilization of the suspension versus the major independent variables of flocculation: the flocculant dose, and the fluid shear rate. The second goal was to be able to model the experimental results, and to ascribe a physical interpretation to the results. To provide a more clear presentation of the experimental results, the proposed theory for collision efficiency will be introduced first in section 6.1. This section will develop the connection between deterministic and probabilistic collision efficiency formulations. It will also present a modification of previous probabilistic collision efficiency statements which accounts for the physical ramifications of polymer adsorption. This describes the unique nature of poly-L-histidine flocculation, and can account for adhesion strength effects on the collision efficiency. Section 6.2. will describe the experimental collision efficiency results and place them in the context of the theoretical results.

6.1. - Collision Efficiency Theory

6.1.1. - Theoretical Collision Efficiency Formulation

The approach taken in this thesis to correlate cell collision efficiencies in polymer flocculation is to use the dimensional analyses of the fluid mechanical theories to formulate non-dimensional numbers obtained from the equations of motion in the presence of interparticle forces. It was shown by Takamura, Goldsmith and Mason (1981) that the trajectory equations developed for ionic coagulation of particles is applicable to polymer flocculation as well accounting for polymer adsorption. This suggests a general form of the collision efficiency based on physical principles will take into account the features of polymer flocculation. The collision efficiency is then posed as a function of dimensionless variables:

$$\alpha_{ij} = f\left[\left(\frac{4\pi\varepsilon_o K \psi_o^2 a_i}{A}\right), \left(\frac{A}{6\pi\eta\dot{\gamma} a_i^3}\right), \left(\frac{a_j}{a_i}\right), C_s \ \ldots\right] \tag{6-1}$$

The first and second groupings will be recognized as C_{RA} and C_A, as introduced in equations (3-11) and (3-12), respectively. As discussed in section 3.5.1.1., the first term in equation (6-1), C_{RA}, describes the relative importance of electrostatic repulsive forces to London-Van der Waals attractive forces. The second term, C_A, represents the relative importance of London-Van der Waals attraction to viscous forces opposing collision. The third term in equation (6-1) is inserted to represent differences in the size of the colliding particles. As demonstrated in section 4.6.2., this should not be a factor for collision kinetics of single animal cells with each other. The term C_S would represent contributions from steric repulsive or attractive forces. The form of such a term for macrocolloidal collisions is not known. Other terms may be added as necessary to account for pertinent physical characteristics of the suspension.

Although equation (6-1) delineates the factors which will influence collision, it does not propose a form for the dependency of the collision efficiency on these factors. It is proposed here that over an appropriate range of magnitude, the dependency of the collision efficiency on the terms C_{RA} and C_A can be represented as a power law functionality:

$$\alpha_{ij} = f\left[\left(\frac{4\pi\,\varepsilon_o K \psi_o^2 a_i}{A}\right)^w \left(\frac{A}{6\pi\eta\dot{\gamma} a_i^3}\right)^x \left(\frac{a_j}{a_i}\right)^y C_s^z \ \ldots\right] \tag{6-2}$$

This proposition for C_{RA} is derived from the results of Delichatsios and Probstein (1975) and Melik and Fogler (1985). Both of these experimental studies showed power law dependency of the collision efficiency on ionic coagulant concentration in the slow coagulation regime. It was shown via equations (3-27) and (3-28) that the coagulant concentration could be related to a change in surface potential, which enters into the numerator of C_{RA}. Since C_{RA} is a repulsive term, the exponent w should be negative.

That is, as surface potential increases, collision efficiency should decrease. In the studies of Delichatsios and Probstein, the exponent w was found to be -1.7. In the studies of Melik and Fogler, the value of w was -3.2 for 0.166 μm latex and -1.9 for 0.255 μm latex. The collision efficiency should be affected by the surface potential of the particles provided that C_{RA} is large enough. The theoretical results of Van de Ven and Mason (1977) (and others, as reviewed in section 3.5.1.1.) indicate that for C_{RA} values less than 25, the suspension may be considered completely destabilized, in the sense that further coagulant addition does not affect the collision efficiency. It was shown in section 3.5.1.1. that for London-Hamaker constant estimates on the order of 10^{-14} erg and a typical cell radius of 8 μm, C_{RA} only falls below 25 for absolute surface potentials less than 2 mV. This means that except for situations where the surface potential is almost completely neutralized by the adsorption of a flocculant, collision efficiency will be affected by the flocculant dose.

The power law formulation has been abused for description of collision efficiency on the parameters in C_A. Researchers have considered the results of Van de Ven and Mason (1977) to have almost universal validity without acknowledging that this correlation has a limited range of application. Notably, it is only valid under conditions of shear dominated collision, Pe > 60, complete destabilization, $C_{RA} < 25$, and viscous force dominated collision, $10^{-1} > C_A > 10^{-5}$. In keeping with the results of Van de Ven and Mason (1977), Feke and Schowalter (1985), and Melik and Fogler (1985), we expect that for $10^{-1} > C_A > 10^{-5}$, the exponent x will be between 0.18 and 0.23. For $C_A < 10^{-5}$, the results of O'Brien (1977) show that the value of x increases with decreasing C_A to a value of unity for $C_A < 10^{-8}$. As stated in section 3.5.1.1., animal cell collisions are shear-dominated for shear rates above 0.06 s^{-1}. The collision efficiency experiments to be discussed below were conducted over a range of 6 to 60 s^{-1}, a range typical of suspension cell culture agitation. Using the above London-Hamaker constant and cell radius, the value of C_A ranges from 1.73×10^{-5} to 1.73×10^{-6} for these shear rates. This is below the range of

Van de Ven and Mason's results but above the $C_A < 10^{-8}$ criterion of O'Brien, so we expect to see a value of x between 0.20 and 1.0 for experiments which vary the parameters in C_A.

In addition to the weak attractive interaction between the cells, the fact that the cells are not monodisperse will also affect collision efficiency. It was shown in section 4.6.2. that a typical average collision size ratio will be 0.84 to 0.87 for the dispersity encountered in a growing animal cell suspension. This might be accounted for by a term involving the average size ratio as shown in equation (6-1). Practically, the dispersity of the cells does not vary widely, and cannot be readily varied. It would be difficult to test the dependency of collision efficiency on such a factor without a model suspension. Effects of suspension dispersity will be accounted for by the value of x in the correlation of collision efficiency with C_A. It has been shown in the theoretical studies of Adler (1981a) and Melik and Fogler (1985) that the value of x increases with decreasing size ratio (note that a_j/a_i is defined to range between zero and one). Melik and Fogler found that for (a_j/a_i) close to unity, x equalled 0.20. When (a_j/a_i) approaches zero, x equalled 0.33.

6.1.2. - Polyelectrolyte Destabilization of Suspensions

One of the weak points of the flocculation literature is the failure to link a physical model of destabilization induced by polymer adsorption with the state of surface coverage. This section will attempt to address this omission in the literature, and show how the collision efficiency formulations of sections 3.5.1.1., 3.5.1.2., and 6.1.1. are related in their description of suspension destabilization.

In polyelectrolyte flocculation of electrostatically stabilized particles, polymer adsorption destabilizes the suspension by decreasing the particle surface potential. As mentioned in section 3.5.1.2., the polyelectrolyte does not generally lie flat on the particle surface on adsorption, but adsorbs with dangling loops and tails extending out from the

surface. The result is that the adsorbed polymer charge does not necessarily correspond in a 1:1 fashion with the charge it is neutralizing. Oppositely charged patches can occur on the particle surface where the polymer is adsorbed. It is proposed here that the surface charge as a function of the polymer coverage can be modelled by the equation:

$$\sigma = \sigma_o(1 - \theta) + \sigma_o z_p \theta \qquad (6\text{-}3)$$

Here, σ_o and σ are the initial surface charge density with no adsorbed polymer and the charge density at a fractal surface coverage θ. The parameter z_p is the "excess" surface charge induced by polymer adsorption onto a site. This is defined as the ratio of the charge density on covered and uncovered surfaces. It will be assumed for the moment that over the range of polymer adsorption of interest, the polymer conformation on the surface is unchanged. That is, $z_p \neq f(\theta)$.

For potentials less than about 25 mV (@ 25 C), the Debye-Hückel approximation (Hiemenz (1977)) relates the surface charge to the surface potential, as shown previously in equation (3-27):

$$\sigma = \frac{\varepsilon}{4\pi} \kappa \psi_o \qquad (6\text{-}4)$$

Here, κ is the Debye layer thickness, and ε is the medium dielectric permittivity. ψ_o is the particle surface potential. Since surface potential is linearly related to the surface charge, equation (6-3) may be converted to:

$$\psi_o = \psi_o^\circ(1 - \theta) + \psi_o^\circ z_p \theta = \psi_o^\circ[1 - (1 - z_p)\theta] \qquad (6\text{-}5)$$

Here, ψ_o° represents the surface potential with no polymer adsorbed. For larger particle surface potentials, the Gouy-Chapman results (Hiemenz (1977)) may be applied to describe the surface potential dependence on the surface charge. For animal cells in culture medium, typical values of ψ_o° are in the range of -20 to -30 mV, so the Debye-Hückel results should apply. When z_p is less than zero (polyelectrolyte adsorption results in a patch with opposite charge sign), the overall particle surface potential will change sign as surface

coverage increases. For the simple case of $z_p = -1$, the particle surface potential reverses symmetrically from no adsorption to complete coverage.

When C_A and other factors are unchanged in a polyelectrolyte flocculation process, the collision efficiency can be reduced to an expression dependent on the fractional surface coverage. Equation (6-5) may be inserted into C_{RA}, which will enter into equation (6-2) for the collision efficiency:

$$\alpha = f\left[(1 - (1 - z_p)\theta)^{2w} \right] \qquad (6\text{-}6)$$

This relation can account for previously observed phenomena in polymer flocculation, specifically the existence of an optimum dose for flocculation, and optimal flocculation over a broad range of surface coverages. Although the values of w and z_p are not known *a priori* without solving the equations of motion and knowing the flocculant adsorption isotherm, expected values may be determined which account for collision efficiency from empirical observations. The right side of equation (6-6), which will be denoted $f(\theta)$, represents the magnitude of the electrostatic forces between colliding particles relative to the forces between untreated particles. This expression goes from unity at zero surface coverage, to a minimum value of zero for $z_p \leq 0$. The value of $[1-f(\theta)]$ is a measure of the reduction in repulsion, or the tendency of the particles to aggregate. At $[1-f(\theta)] = 1$, surface potential is zero, and the electrostatic repulsion has been completely eradicated. As the residual electrostatic forces approach a minimum, the suspension is maximally destabilized, and collision efficiency should approach a maximum.

Figure 6-1 shows $[1-f(\theta)]$ versus θ for $z_p = -1$ and varying w. It will be recalled that experimental data for ionic coagulation (both turbulent shear and Brownian motion induced) show absolute w values in excess of unity, from -1.7 to -3.8. For $w > 0.5$, the electrostatic force reduction curves in Figure 6-1 are concave downward. Comparison with Figures 3-2 and 3-3 shows that these curves correspond qualitatively to the probabilistic

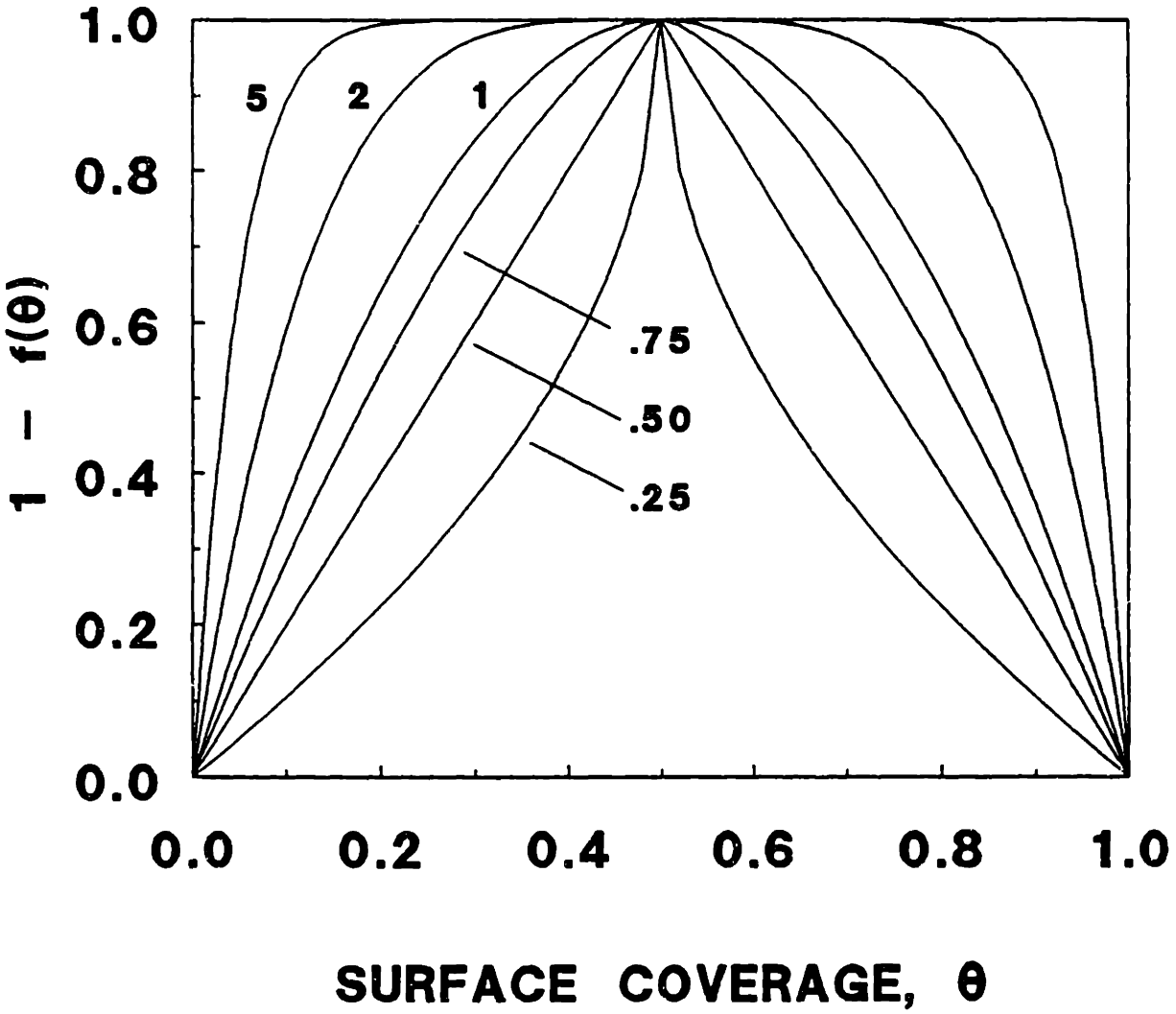

Figure 6-1. [1-$f(\theta)$] versus fractional surface coverage for $z_p = -1$ and varying w. w values are indicated on the figure.

theories with different numbers of interacting sites. The case of $z_p = -1$, $w = 1$ corresponds directly to the LaMer (Smellie and LaMer (1958)) probabilistic development. It is seen that the probabilistic collision efficiency models have stated in a crude way the reduction of the interparticle repulsion due to polymer adsorption. This observation links the probabilistic and deterministic theories together.

In the general case, z_p may take on a value other than negative one. For these situations, the residual electrostatic force behavior is interesting. Polymer adsorption can render the particle charge greater than the initial value, or may never eradicate the particle charge. Figure 6-2 shows $[1-f(\theta)]$ versus θ for various z_p at w equal to one. The residual forces are symmetric with respect to the theta value at particle neutrality, but not symmetric with respect to a particle surface coverage of 1/2, as is implied by previous probabilistic collision efficiency models. As z_p increases, the theta (θ) value at which net repulsion is zero decreases. This points out that it is erroneous to ascribe a zero surface or zeta potential measurement to half-coverage of the particle. To describe the physical process of particle destabilization, the adsorption isotherm must be coupled with zeta potential measurements to describe the charge versus surface coverage. The results of figure 6-2 may explain the experimental results of Hahn and Stumm (1968) shown in figure 3-4. In this figure, it was seen that collision efficiency went through a maximum at a surface coverage less than one half. Adsorption of flocculant to their experimental particles may have resulted in a strong reversal of the particle charge.

Although the exponent w should be greater than unity from previous experimental results, it is unlikely that it will take on extremely large values that the Hogg (1986) and Deason (1987) models imply for small polymer size relative to the particle size. The Hogg and Deason probabilistic models may have been modelled after experimental cases where $z_p < -1$, and the electrostatic force dropped off rapidly to zero at small surface coverage. Although the current development with $z_p < -1$ predicts a rapid drop of collision efficiency

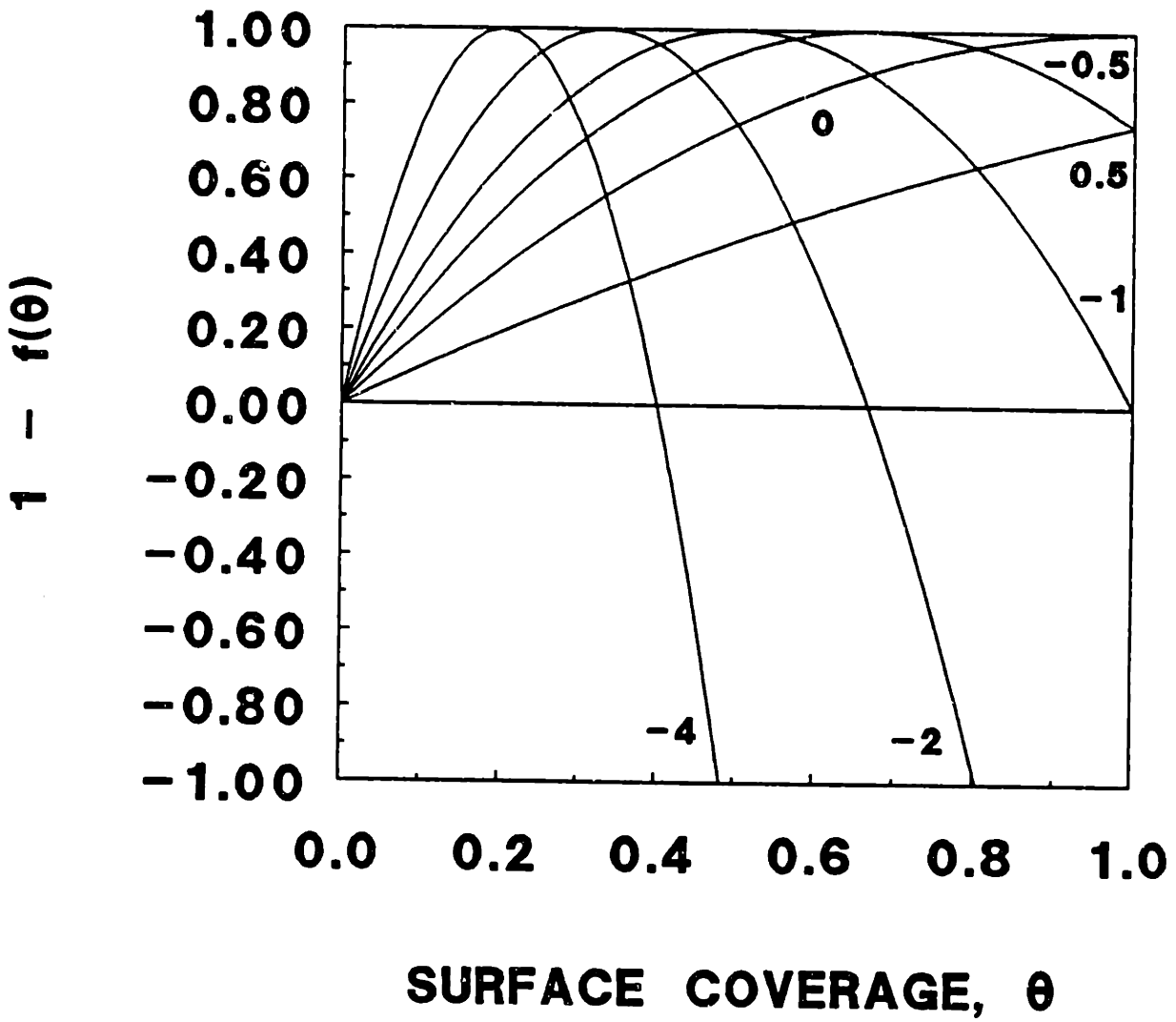

Figure 6-2. [1-$f(\theta)$] versus fractional surface coverage for w = 1 and various z_p. z_p values are indicated on the figure.

with further polymer adsorption, there are two idealizations which do not apply to actual flocculation. First, the Debye-Hückel theory will not describe the relation between ψ_o and σ if particle potentials are large. Particle surface potential is not infinitely variable, but plateaus to a high, limiting value (Hiemenz (1977)). Second, as the particle surface becomes covered with polymer, the assumption that the polymer conformation is unchanged, $z_p \neq f(\theta)$, will not be correct. As the particle surface potential reverses, a net electrostatic repulsion exists between the particle and unadsorbed polymer, even though local interactions may still be attractive and allow adsorption. The effect would be that polymer extension from the particle surface is larger, perhaps allowing polymer chains to sample a greater fraction of a passing particle's surface for net attractive local interactions. Thus, a change in regime may occur whereby local particle surface interactions dominate the flocculation behavior, where at lower coverages the global particle interactions dominate flocculation behavior. From this point of view, only the upward curving branches of the plots in Figure 6-2 are meaningful. These branches are akin to the curves generated by the Deason and Hogg models with large numbers of adsorption or interaction sites. This may explain broad ranges of polymer dose which promote flocculation of particles.

6.1.3. - Probabilistic Collision Efficiency and Adhesion Strength

It was shown in the development above that the results of the probabilistic theories of collision efficiency in the literature can be reconciled with the deterministic theory by accounting for polyelectrolyte modification of cell surface properties. This is considered to be fortuitous, for the reason that the probabilistic developments are predicated on the idea that microscopic interaction between individual adsorption sites will determine collision efficiency rather than the global particle state. A more consistent probabilistic formulation of the collision efficiency would calculate the net interaction between all of the involved site pairs, and only count those collisions between mutually attractive particles as effective. For

example, for the situation shown in Figure 3-1, both the Hogg and Deason models would consider the encounter to produce adhesion since one site pair is in an attractive mode. However, the particle i sites sum to a net charge of -1, and the particle j sites sum to a charge of -3. Thus, if the total interparticle force is considered, there is a net repulsion, and adhesion should not occur. The following development is a probabilistic collision efficiency formulation which is consistent with the physical idea that the collision efficiency is determined by the net interparticle force. The resulting collision efficiency dependency on surface coverage is shown to be different than previous theory, and it will be seen in section 6.2. that this theory is supported by experimental collision efficiencies. The theory may also be viewed as a statement of adhesion strength, and this view is also supported by the experimental data.

Two assumptions are the basis for the proposed theory. The first, as mentioned above, is the idea that the net interparticle force will determine whether a collision is effective in producing an adhesion. The second is that for a given particle, or over a region of a particle, charge dispersity will occur due to the random adsorption of polymer. Like the Hogg and Deason models, the particle surface is viewed as having discrete sites for polymer adsorption. The probability of an individual site being covered is equal to the average particle surface coverage, θ, as before. If we assume that a simple one-to-one correspondence exists between the charge on a covered and an uncovered site ($z_p = -1$), the average probability that two sites on opposing particles will have an attractive interaction is given by the LaMer statement, $2\theta(1-\theta)$. For a finite number of sites interacting, the probability of observing a number m of these n sites in an attractive mode is given by the binomial theorem, equation (3-22) as put forth by Deason (1987):

$$Pr(m,n) = \frac{n!}{m!\,(n-m)!}\,[2\theta(1-\theta)]^{m}\,[1-2\theta(1-\theta)]^{n-m} \qquad (6\text{-}7)$$

This statement may be used to calculate the probability of two surfaces with mutual attraction colliding with each other. For cases where $z_p \neq -1$, the equation expressing $[1 - f(\theta)]$ can be substituted into equation (6-7) rather than the LaMer calculation to give:

$$Pr(m,n) = \frac{n!}{m!\,(n-m)!}\left[1 - (1 - (1-z_p)\theta)^{2w}\right]^m \left[(1 - (1-z_p)\theta)^{2w}\right]^{n-m} \tag{6-8}$$

This refinement is valuable only insofar as z_p and w are known. Again assuming that polymer adsorption results in simple charge reversal ($z_p = -1$), the configurations with net attraction will be all those with $m > n/2$. The collision efficiency may then be expressed as:

$$\alpha = \sum_{m=n/2}^{n} Pr(m,n) \tag{6-9}$$

Like the Hogg and Deason developments, equation (6-9) reduces to the LaMer model in the limit of $m = n = 1$, and $z_p = -1$. For the general case where $z_p \neq -1$, the summation should be taken over $m \geq n/(1 - z_p)$, or the closest integer value. From a physical viewpoint, equations (6-7) and (6-9) may be thought of as expressing polymer adsorption as a smeared, or average charge affecting a set of sites rather than affecting adhesion between individual sites. Adhesion occurs not due to individual bridge formation, but to net attraction between particles. This is true to the observations of Takamura, Goldsmith, and Mason (1981).

The collision efficiency statement of equation (6-9) is, like the Hogg and Deason models, dependent on the choice of n. If total particle charge is of interest, then the assumptions of equation (3-21), the Hogg model, may be an appropriate calculation for n. If only local interactions are being considered, a calculation for n akin to equations (3-24) or (3-25), the Deason model, might be appropriate to determine the number of interacting sites. Since the formulation of collision efficiency proposed above is a net force calculation, the number of sites expected to interact should ideally be calculated based on arguments about the range of the forces involved and the characteristic particle and site size. When the electrical double layer is large relative to the site and particle size, all sites on the

particles can be expected to affect the collision. This corresponds to the Hogg calculation of the number of sites. When the electrical double layer is small relative to the particle size, most of the particle surface charge will be screened by medium ions, and only closely approaching sites will interact. This corresponds roughly to the Deason calculation. For aggregation of animal cells in high ionic strength culture medium, it would be expected that only a small fraction of the sites on the cell surface will interact.

The collision efficiencies predicted by the combination of equations (6-7) and equation (6-9) are shown in Figure 6-3 for varying values of n. The results of the simulation are interesting, in that they do not resemble the LaMer, Hogg, or Deason models for $n > 1$. The curves take a normal distribution shape, and predict that there will be a "lag" in the collision efficiency for very low and very high polymer coverage. In fact, for large values of n and intermediate surface coverage, equation (6-7) can be replaced by the normal distribution function with $\mu = n[2\theta(1 - \theta)]$ and $\sigma = \sqrt{n[2\theta(1-\theta)][1 - 2\theta(1-\theta)]}$. Due to the sparseness of polymer collision efficiency versus surface coverage data in the literature, it is not possible to compare the shapes of these curves to data for polyelectrolyte flocculation. However, it should be possible to discriminate between the conceptually different approaches of this development and the previous literature probabilistic theory from the mere shape of experimental collision efficiency versus surface coverage.

An interesting observation of Figure 6-3 is the collision efficiency curve width versus the value of n. When n is large, the curve narrows so that collision efficiency is lower at very high and low surface coverage than for small n. It is a common experimental observation that flocculation is promoted at lower concentrations and over a broader range for high molecular weight flocculants (Nevo, DeVries and Katchalsky (1955), Walles (1968)). When the flocculant polymer is large, the corresponding n value predicted by (3-21), (3-24), or (3-25) is lower, and the collision efficiency is predicted to be high over a broader range of surface coverage. This is counter to the behavior of the Hogg and Deason

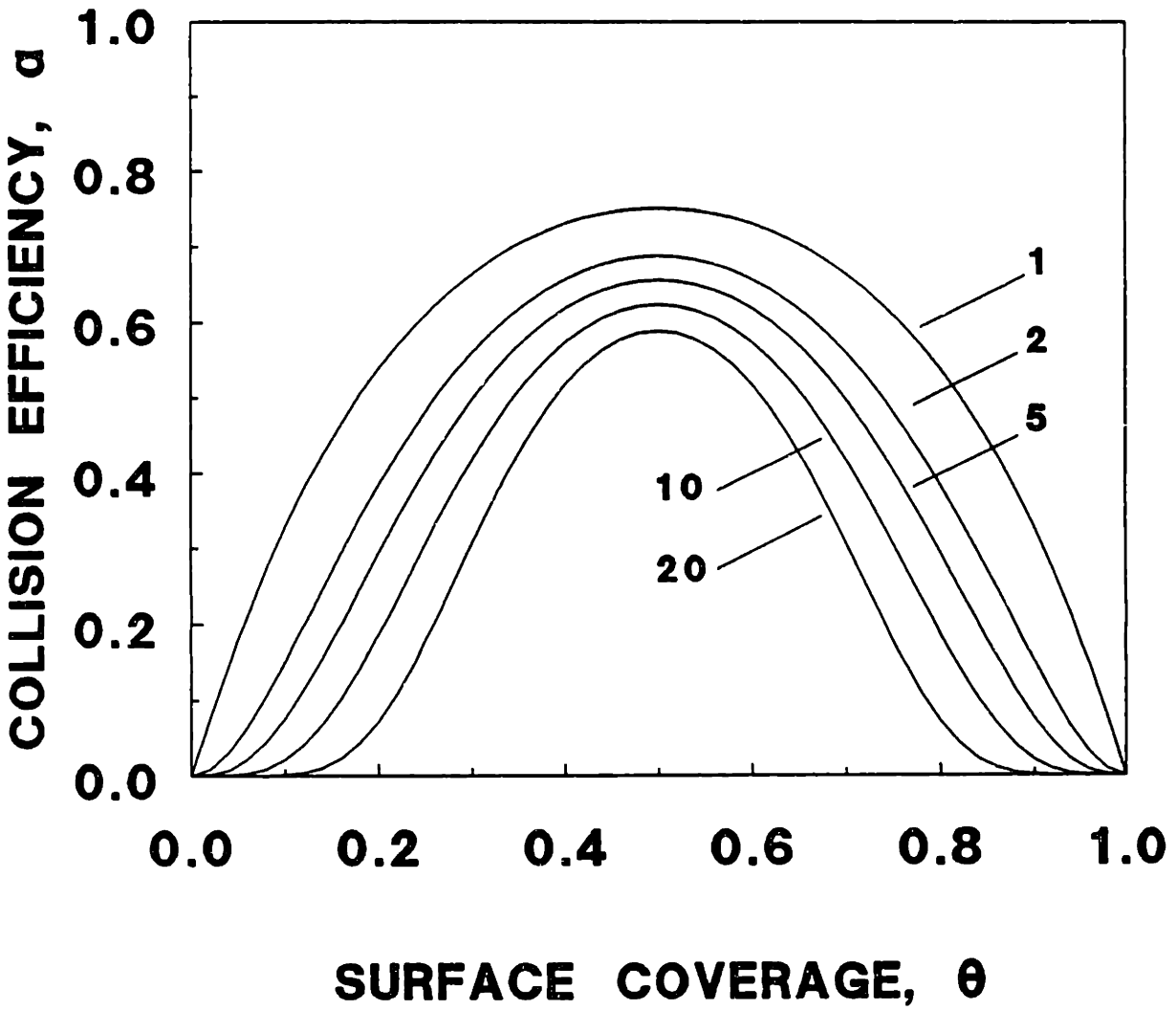

Figure 6-3. Collision efficiency versus fractional surface coverage predicted by equations (6-7) and (6-9) for various n, and m = n/2.

developments, which would predict smaller collision efficiencies for higher polymer molecular weight. In addition, the collision efficiency values are higher for a given surface coverage at lower n, another common observation of flocculation with polyelectrolytes.

In addition to representing the probability of finding particles with net attraction, the collision efficiency predicted by equation (6-9) may also be viewed as a statement of adhesion strength between the particles. The summation can be changed to count the probabilities of finding particles with slightly more or less than half of the sites in an attractive mode. In fact, equation (6-9) can be made equal to the Deason model by summing from m = 1 to n. This discounts only collisions between completely bare and completely covered surfaces encountering each other. The more stringent requirement for adhesion is likely to be more realistic in situations where fluid shear is driving the aggregation and also serving to stress the bonds formed between particles. Figure 6-4 shows the collision efficiency predicted by equations (6-7) and (6-9) varying the lower limit of the summation index from 1 to n for n = 5. By lowering the summation index, *i.e.* - lowering threshold bond strength necessary to initiate aggregation, it can be seen that collision efficiency is significant over a broader range of surface coverage.

From a modelling standpoint, collision efficiency formulations such as the combination of equations (6-7) and (6-9) still do not account for the magnitude of interparticle and hydrodynamic force interactions, and cannot be expected to predict absolute collision efficiency values. Substitution of (6-8) for (6-7) will more closely account for the magnitude of electrostatic forces. Combining this with a factor for hydrodynamic interactions would allow for the dispersion of surface coverage for the suspension, and may model collision efficiency better than a simple formulation such as equation (6-2). The drawback to this approach is that the intended simplicity of the probabilistic formulation is lost. Not only must the values of z_p and w be determined, the

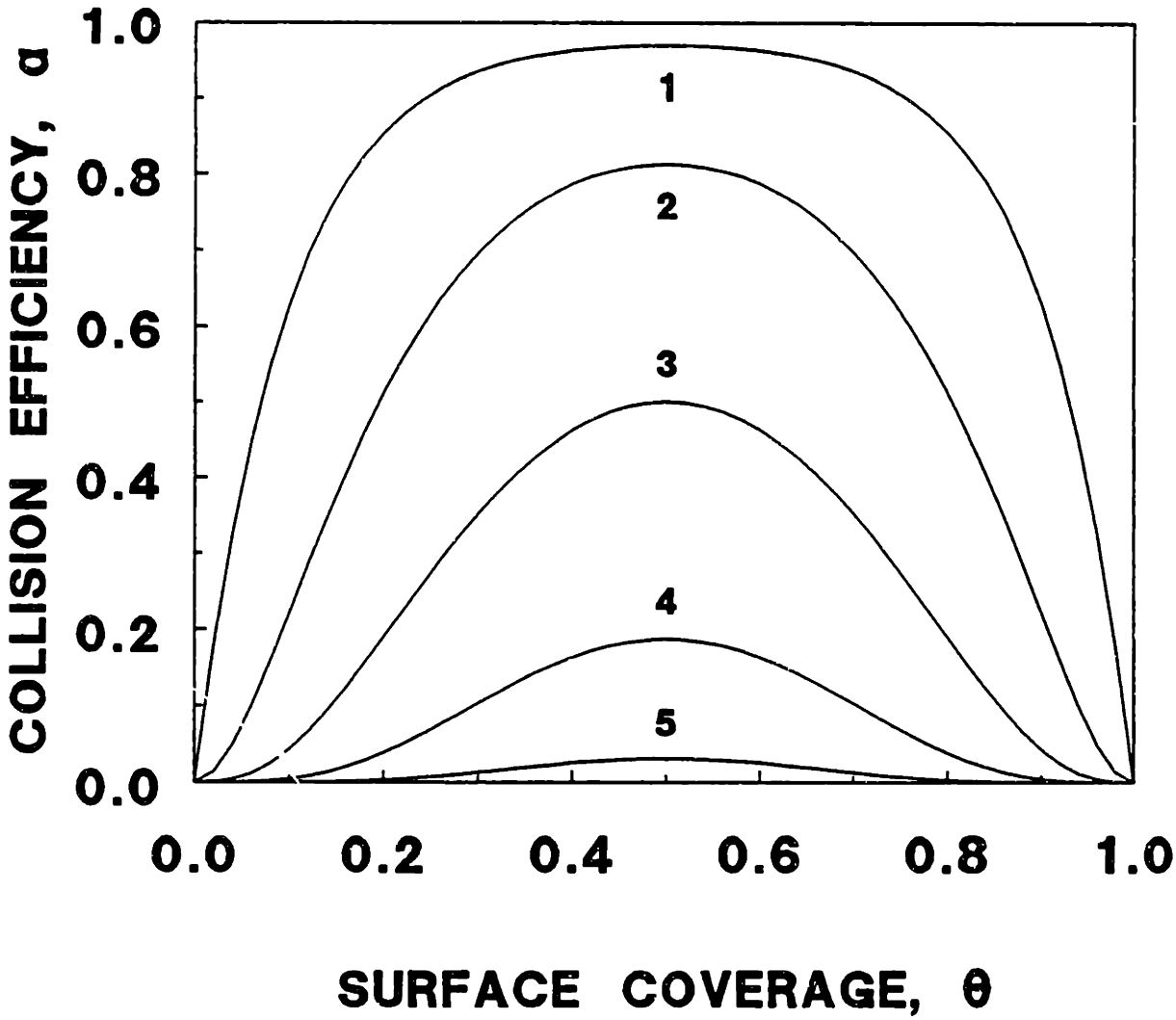

Figure 6-4. Collision efficiency versus fractional surface coverage predicted by equations (6-7) and (6-9) for various m, and n = 5.

values of n and m must also be fit to the experimental data, and predictive capacity is lost in the process.

6.2. - Experimental Suspension Destabilization Results

6.2.1. - Polymer Adsorption and Surface Potential

In order to test the theory presented above, it is necessary to have a measure for the extent of polymer adsorption to the cell, and its effect on the cell surface properties. Unfortunately, poly-L-histidine precipitates completely at pH 7 and physiological ionic strength, so the equilibrium soluble polymer concentration is practically zero. It is thus not practical to determine an adsorption isotherm, since all polymer will eventually deposit onto the cell surface given time. The fractional surface coverage may, however, be estimated assuming that all of the polymer transports to the cell surface given sufficient time. The transport rate of polymer to the cell surface is a first order process in both cell and polymer concentrations:

$$\frac{dP}{dt} = -kCP \qquad (6\text{-}10)$$

Here, P is the polymer concentration, and C is the cell concentration. Given a value of k, this equation may be integrated to find the polymer concentration over time. The k value can potentially be calculated via equation (3-6).

The rate of change of open adsorption site concentration in suspension is equal to the rate of polymer disappearance multiplied by the probability of the polymer depositing on an open site. The open site concentration in the suspension is given by the cell concentration, C, multiplied by the sites per cell, n_i, and the fraction of open sites, $(1 - \theta)$. It is implicitly assumed that the area covered by one polymer molecule defines a site. As above, equation (3-21) might be used to estimate n_i. Combining these statements gives:

$$\frac{d(Cn_i(1-\theta))}{dt} = (1 - \theta)\frac{dP}{dt} = - (1 - \theta)kCP \qquad (6\text{-}11)$$

This equation may be integrated with substitution of (6-10) to yield:

$$\theta = 1 - \exp\left[\frac{P_o}{Cn_i}(\exp(-kCt) - 1)\right] \qquad (6\text{-}12)$$

Here, P_o is the initial polymer concentration. At long times, the inner exponential decays to zero to give the final surface coverage:

$$\theta = 1 - \exp\left[-\frac{P_o}{Cn_i}\right] \qquad (6\text{-}13)$$

Equation (6-13) points out the fact that surface coverage is not simply the ratio of polymer to cell surface area. Rather, the increase in surface coverage decays exponentially with additional polymer due to polymer deposition on previously covered surface. The relationship of the exponential term to the polymer dose is:

$$\frac{P_o}{Cn_i} = \frac{Da_{cell}}{n_i} \qquad (6\text{-}14)$$

Here, D is polymer dose (mass) per total cell surface area, and a_{cell} is the surface area of a single cell. It is still necessary to define n_i to calculate the surface coverage for a given dose, and this is inaccessible except for estimates such as equation (3-21). However, the value of a_{cell}/n_i may be estimated experimentally by correlating the change of a particle surface property with polymer dose.

The most conspicuous particle property which should be affected by polymer adsorption is the particle surface potential. The experimental determination of cell surface potential is shown in Figure 6-5 as a plot of the zeta potential versus the polymer dose. With no polymer present, the cell zeta potential is approximately -18 mV. This value is typical of cultured cells and erythrocytes. Literature studies report values ranging from -10 to -30 mV, depending on the physical environment and manipulations of the cells

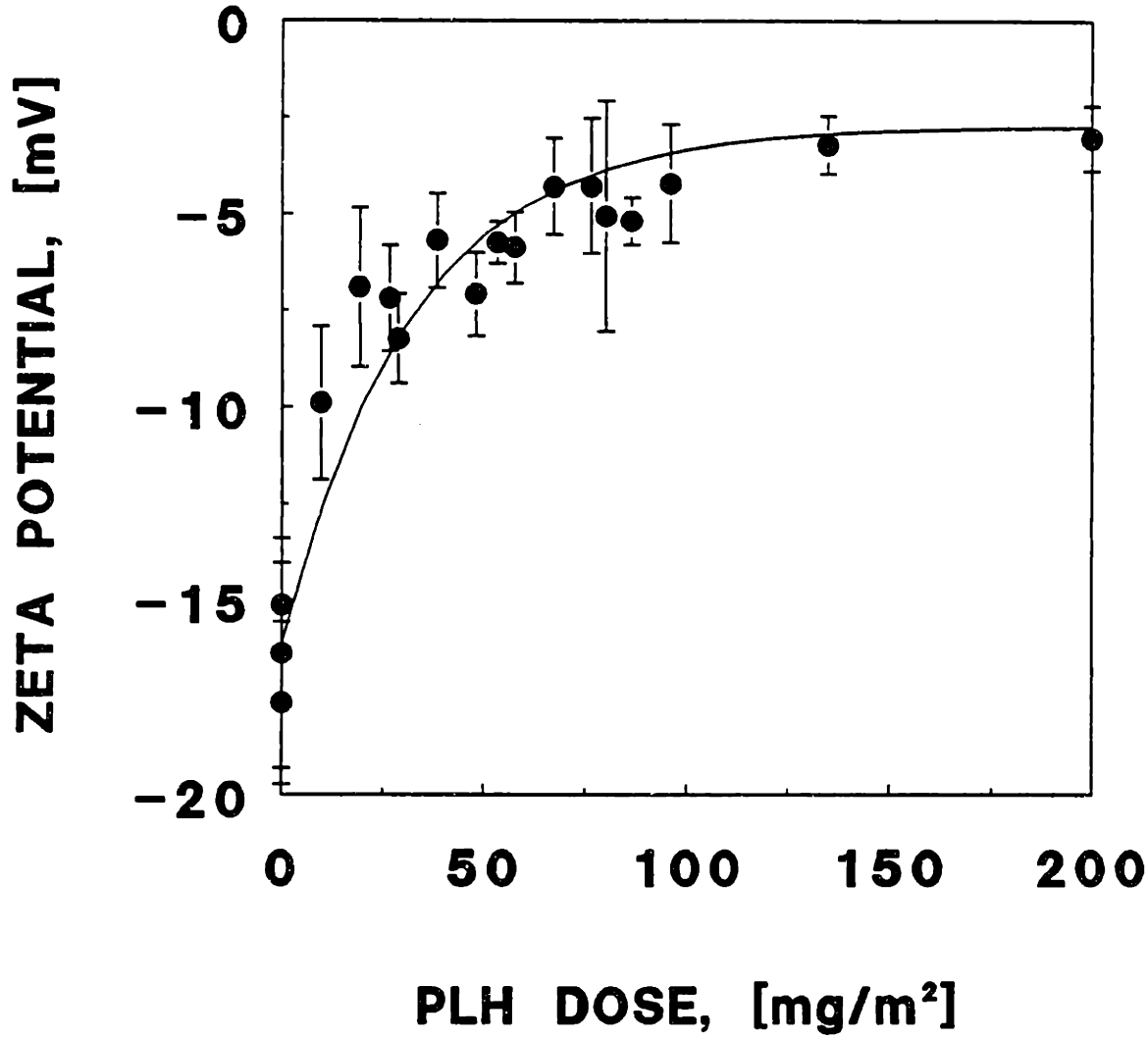

Figure 6-5. Zeta potential of CRL 1606 cells versus poly-L-histidine dose. Solid curve is the best fit regression of the combined equations (6-5) and (6-13) to the data.

(Forrester (1965), Redmann, Jenssen, and Köhler (1974)). As polyhistidine is added, the cell zeta potential increases asymptotically to a maximum of around -4 mV at high polymer concentrations. Light microscope observations of the cells at doses greater than 200 mg/m^2 show that the cells are completely covered with polymer under these conditions. These values will be useful in correlating the collision efficiency to the particle surface potential via equation (6-2); given that the collision efficiency follows the expected power law functionality, a log-log plot of collision efficiency versus the zeta potential squared will give the value of w. It will be noted that under the conditions investigated, the cell zeta potential never drops below the 2 mV necessary to render it negligible by Van de Ven and Mason's criterion. Thus, polymer dose should play a role in suspension destabilization at all concentrations investigated.

The particle zeta potential behavior is very interesting in the case of poly-L-histidine adsorption. At complete surface coverage, the particle charge does not go to zero, much less reverse, as might be expected from other observations of polyelectrolyte interaction with cells (Nevo, DeVries and Katchalsky (1955)). This means that from the modelling standpoint of equation (6-3), z_p is actually greater than zero. That is, complete polymer adsorption does not result in an erasure of the particle surface charge. The constitutive equation (6-5) may be combined with the particle transport model (6-13) to correlate the change in zeta potential versus polymer dosage. Non-linear regression of the zeta potential versus polymer dose to the combined equations yields values of Ψ_o^c = -16.1 mV, z_p = 0.18, and a_{cell}/n_i = 0.031 m^2/mg. Inserting these numbers into equations (6-5) and (6-13) results in the line in Figure 6-5. Although the fit is not perfect, due to the error associated with the zeta potential measurements, it does provide a reasonable description of the surface state versus polymer dose. The value of a_{cell}/n_i may be used to calculate the fractional particle surface coverage versus polymer dose. The calculated theta values may then be used to examine the functionality of the collision efficiency on the surface coverage. This

exercise may be used in conjunction with the theory presented in section 6.1. to evaluate the utility of probabilistic and deterministic correlations.

6.2.2. - Collision Efficiency Versus Polymer Dose

It was shown in the above section that polymer adsorption acts to reduce the cell surface potential to an almost negligible value at high surface coverages. Provided that electrostatic forces are partially responsible for suspension stability, collision efficiency should be dependent on the cell surface potential. Equation (6-2) anticipates a collision efficiency dependency on the dimensionless variable C_{RA}, which describes the magnitude of the electrostatic repulsive force to the London-Van der Waals attractive forces. A log-log plot of the collision efficiency versus the zeta potential squared will determine whether collision efficiency can be correlated by equation (6-2), and elucidate the value of the empirical parameter w. This plot is shown in Figure 6-6. For all but the highest particle surface potentials (lowest surface coverage), a dependency on zeta potential to the -2.4±0.2 power is observed. This is consistent with the observation that w should be less than -1. The experimental correlation gives w = -1.2, which is in reasonable agreement with the results of Delichatsios and Probstein (1975), and Melik and Fogler (1985). At the most negative surface potential, however, the collision efficiency behavior deviates from the power law functionality. This result is disturbing, since the interparticle potential should influence collisions most profoundly in this region. This result is thought to be due to weak interparticle bonds at low surface coverage.

A more extensive investigation of the collision efficiency versus polymer dose at a shear rate of 30 s^{-1} is shown in Figure 6-7. The collision efficiency here is seen to possess a distinctly sigmoidal shape versus the polymer dose, unlike the anticipation of either equation (6-2), or the conventional probabilistic collision efficiencies shown in Figures 3-2 and 3-3. It appears that a threshold polymer dose is necessary to instigate flocculation.

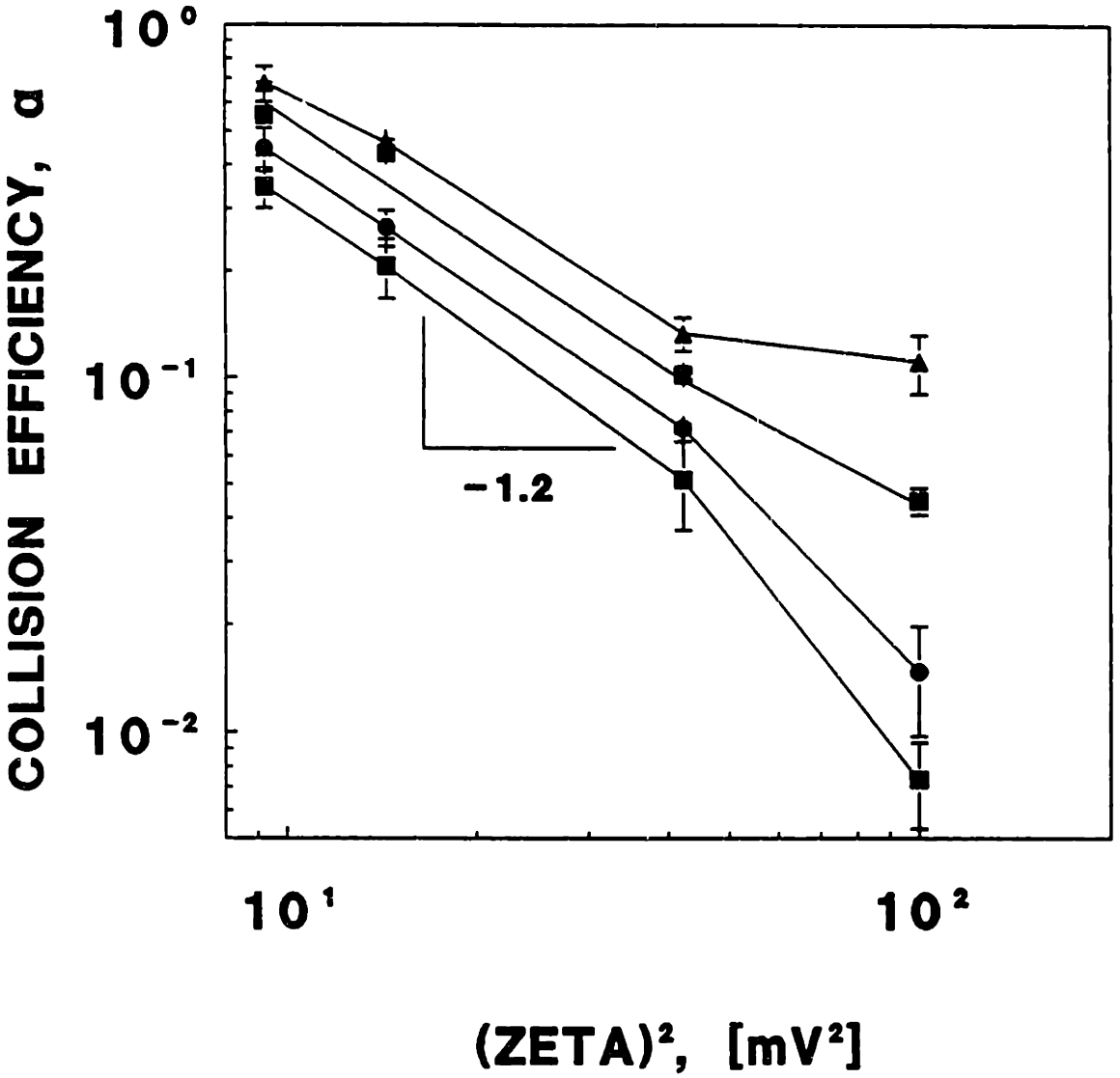

Figure 6-6. Experimental collision efficiency of CRL 1606 cells versus zeta potential squared at various shear rates. ■ - 6 s^{-1}, ◆ - 12 s^{-1}, ● - 30 s^{-1}, ▲ - 60 s^{-1}.

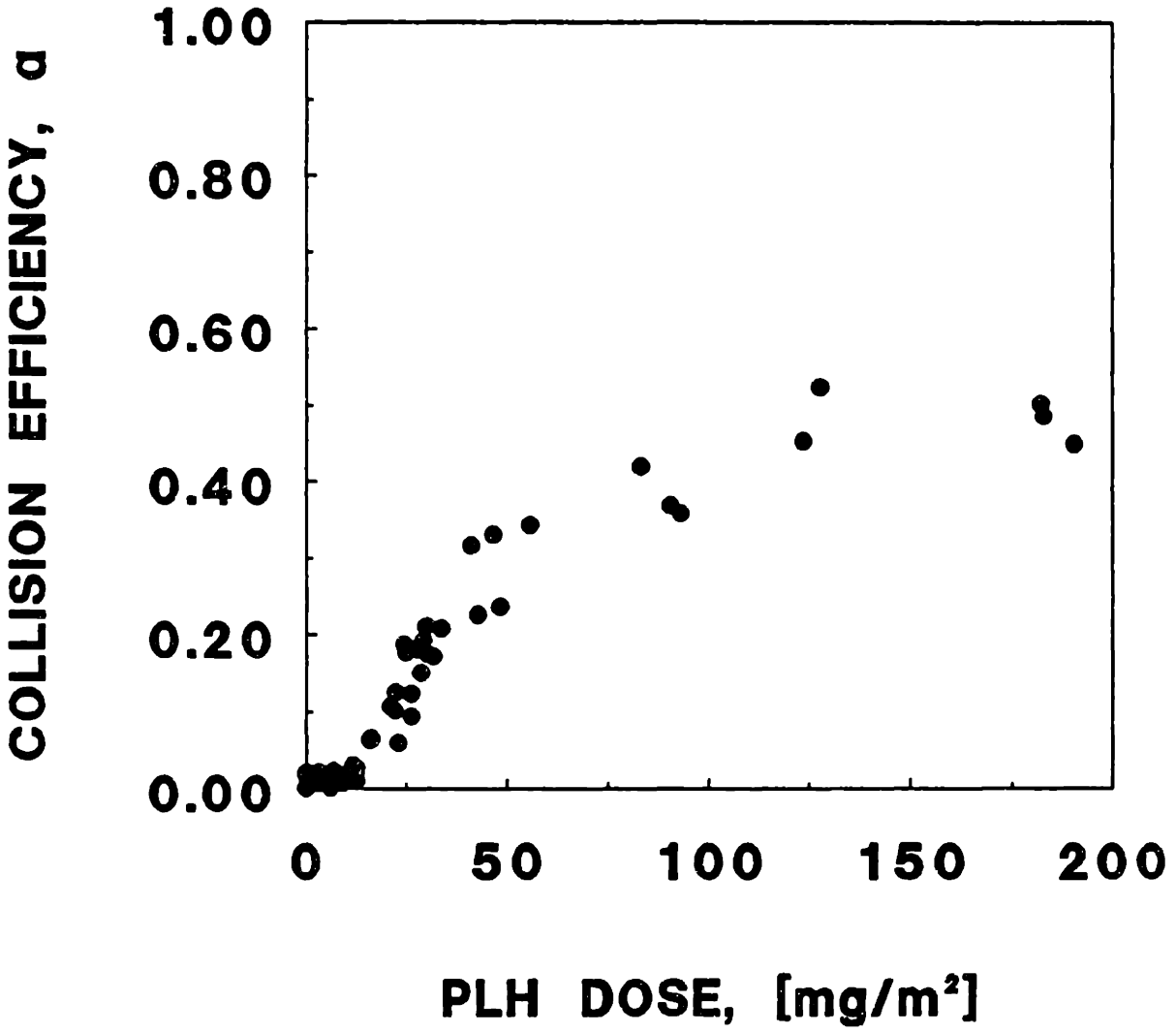

Figure 6-7. Experimental collision efficiency of CRL 1606 cells versus poly-L-histidine dose at 30 s^{-1} shear rate.

This is more clearly seen when the polymer doses are converted to surface coverage values via the value of a_{cell}/n_i regressed from the surface zeta potential versus polymer dose. It will be noted that the collision efficiencies in Figures 6-6 and 6-7 do not go to unity under the conditions investigated; this indicates that hydrodynamic forces are significant, and prevent attainment of unit collision efficiency even at completely destabilizing conditions. The collision efficiencies obtained in Figure 6-7 may additionally be normalized to a nominal maximum value of 0.533 in order to compare the cell collision behavior with the probabilistic theories discussed above (which are expected to predict collision efficiencies between zero and unity). A plot of the normalized collision efficiency versus the calculated surface coverage is shown in Figure 6-8. It can be seen from this curve that the sigmoidal shape of the collision efficiency curve is even more pronounced when the polymer dose is converted to fractional surface coverage. This is because the decaying exponential dependency in equation (6-13) expands the low polymer dose region into significant changes in cell surface coverage, where higher polymer doses are squeezed into a small region of surface coverage. It is evident from the sigmoidal shape that the collision efficiency does not remotely resemble the LaMer, Hogg, or Deason models of collision efficiency. The dashed line in the figure represents $[1 - f(\theta)]$ using the value of $w = -1.2$ found above for the high polymer dose (low zeta potential) data. This curve represents the prediction of equation (6-2). It can be seen that where the curve approaches the data at high surface coverage, it does a poor job of predicting the collision efficiency over the whole range of surface coverage.

With the data at hand, it is possible to evaluate the predictions of the proposed probabilistic collision efficiency/adhesion strength theory. We possess a value of z_p from the zeta potential measurements, and a value of w from the high surface coverage data. The predictions of equations (6-8) and (6-9) can now be evaluated at different values of m and n to gain insight as to whether this theory accurately describes collision efficiency. It will be

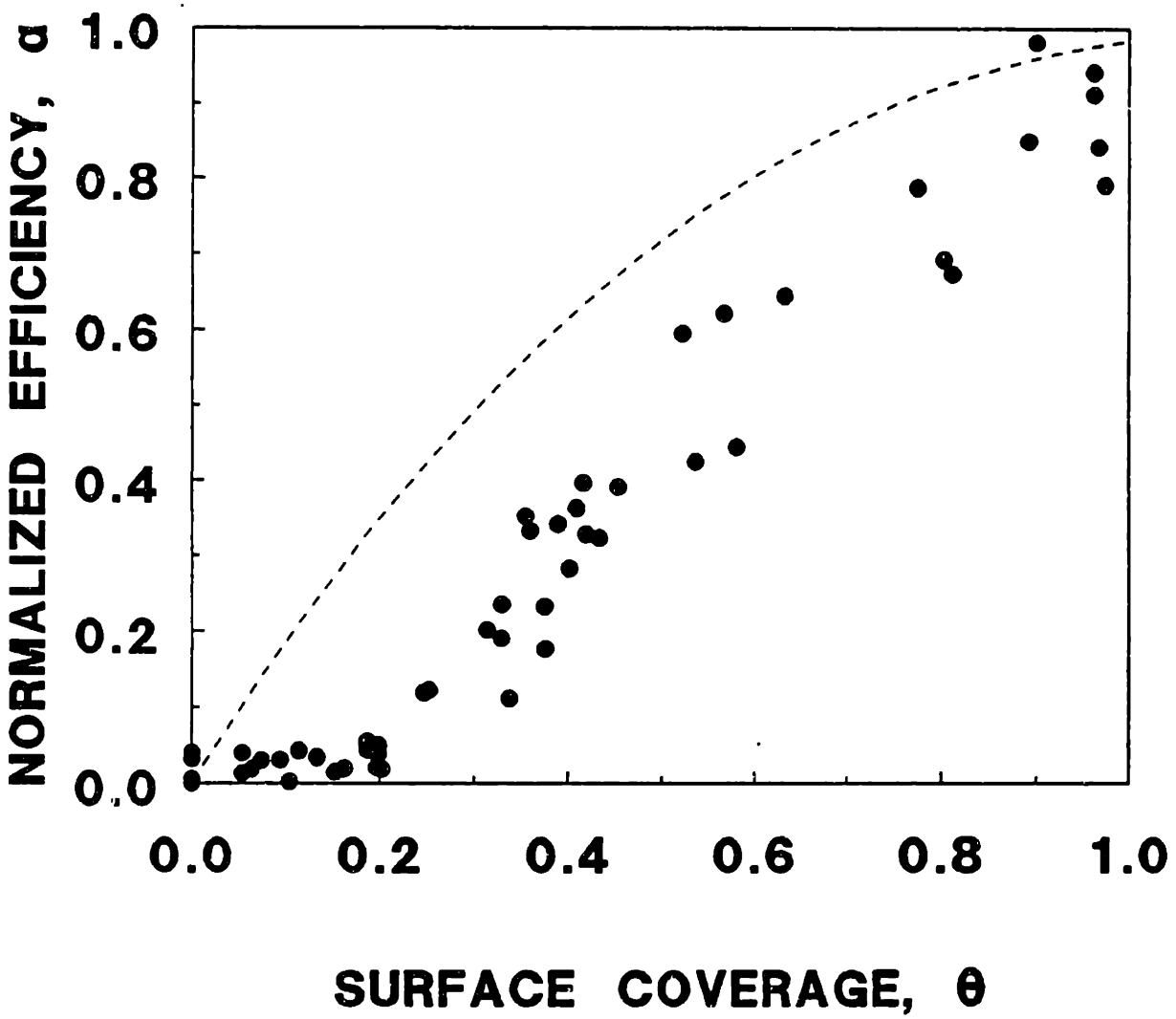

Figure 6-8. Normalized experimental collision efficiency of CRL 1606 cells from Figure 6-7 versus the fractional surface coverage of the cells calculated from Figure 6-5.

recognized here that the experimental value of z_p for the CRL 1606-polyhistidine system is positive, which means that according to physical reasoning, the summation of equation (6-9) should be taken from m = n/(1-0.18) = 1.22n. Obviously, the value of m cannot exceed n. What this signifies is that the best data fit should be for m ≈ n, requiring a very strong interparticle bond to establish adhesion. The normalized collision efficiency data is re-plotted in Figure 6-9 versus the theory of equations (6-8) and (6-9) for various values of n, and m = n. It can be seen that low values of n give the best fit to the data, which is consistent with the proposition that few sites should interact. Calculation of the residual error over all m and n values between 1 and 20 shows that the best data fit occurs for m = n = 3. Figure 6-10 shows a three-dimensional plot of the residual error versus values of m and n. For m < n, the residual is significantly larger than for m ≈ n, indicating that our expectation of m = n for the summation is most consistent with the data. The experimental values of m and n are thus consistent with the physical ideas proposed in section 6.1.3. For a large particle and site size relative to the Debye layer, it was postulated that the number of interacting sites should be small, since most of the particle surface charge will be screened. This is the case in animal cell culture medium, and the value of n reflects this situation.

As mentioned above, the value of a_{cell}/n_i can potentially be used to back out a value for the total sites per particle. However, this number only gives the polymer mass per cell at saturation, equal to 6.5 pg/cell. A conversion factor equal to the mass of polymer per site is needed to calculate the number of sites, and this is not readily available. For this reason, it is most convenient to define the number of sites by a calculation such as equation (3-21) and knowledge of the cell and polymer precipitate characteristic size. The precipitate size evolution over time was determined by dynamic light scattering, as described in section 4.5.3. The precipitate size versus time is shown for three poly-L-histidine concentrations in Figure 6-11. The precipitate Stokes' diameter is on the order of 1.5 μm, although this

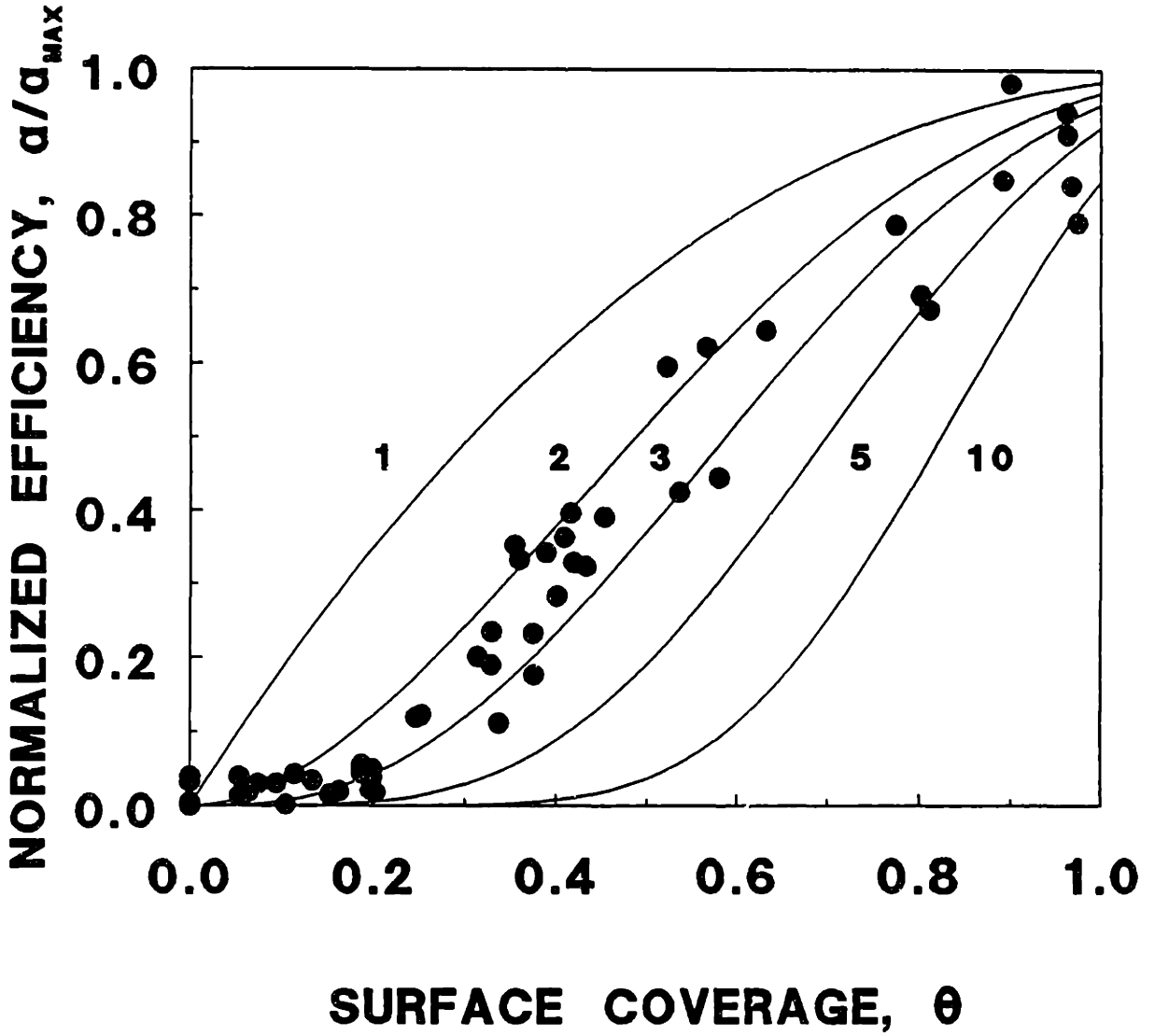

Figure 6-9. Normalized experimental collision efficiency of CRL 1606 cells from Figure 6-7 versus the calculated fractional surface coverage. The solid curves are the theoretical collision efficiencies predicted by equations (6-8) and (6-9) versus fractional surface coverage. The values of n_i are shown in the figure.

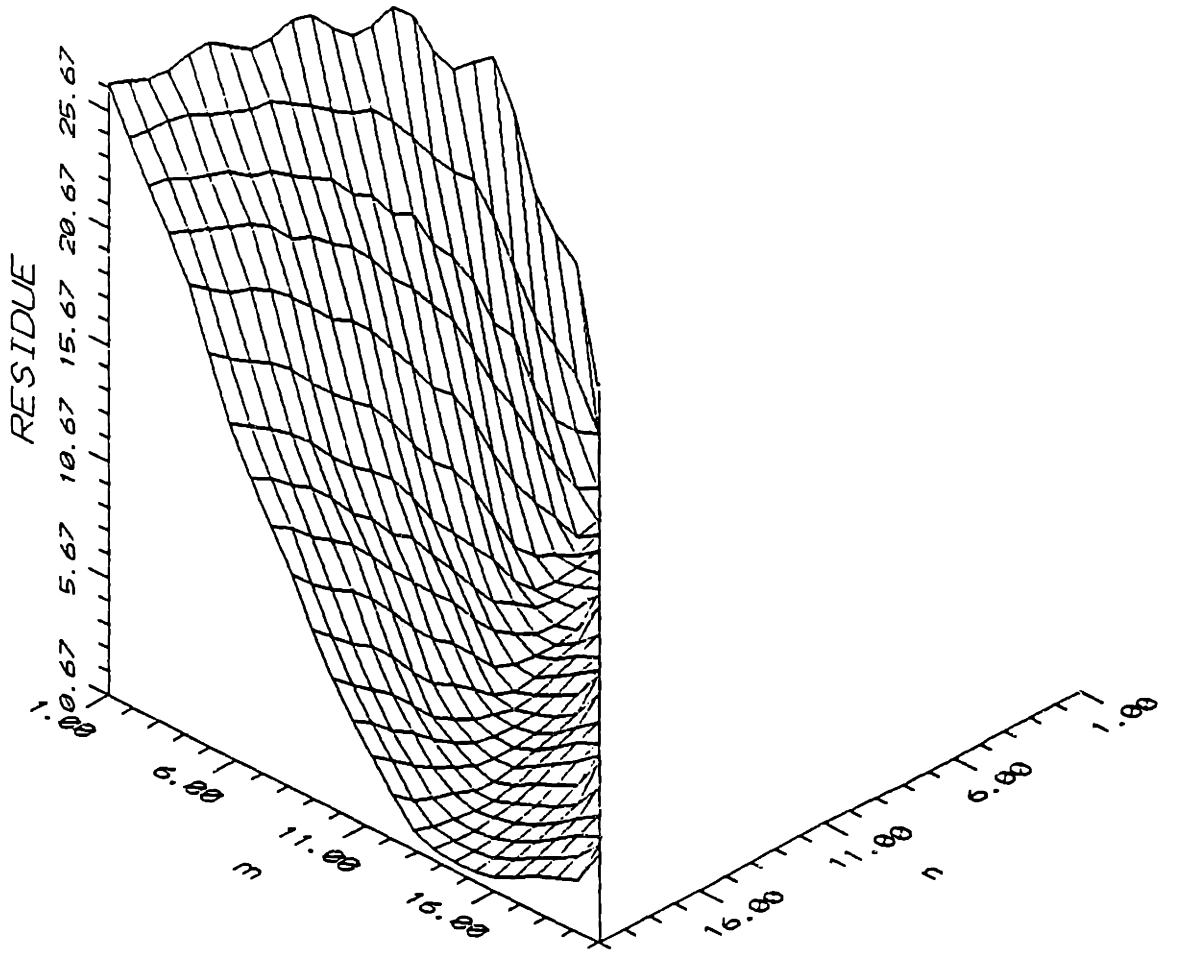

Figure 6-10. Residual error of estimation for the data and theoretical predictions of Figure 6-9 versus the values of m and n.

varies slightly with concentration. Using this value in equation (3-21) along with a characteristic cell radius of 8 μm, the total sites per cell is on the order of 115! This number is much greater than the number of interacting sites from the collision efficiency experiments, and confirms the contention that only a small fraction of the surface is involved in the collision process.

The low value of n from the collision efficiency experiments points out the reason why the probabilistic statement of adsorption heterogeneity models collision efficiency at low surface coverage more accurately than a strictly deterministic formulation such as equation (6-2). As the number of sites increases to infinity, the probability that the surface coverage will equal θ goes to unity. For small numbers of sites, there is a significant probability that the surface will be at a non-θ condition. It is thus necessary to account for the probability of non-θ coverage. For polyhistidine flocculation, at low surface coverage there is a significant likelihood that not all of the sites will be covered with polymer. From interparticle force arguments it was shown that these collisions will not lead to adhesion. At high surface coverage, the probability of finding a surface configuration with complete coverage is maximal. Thus, the deterministic model matches the collision efficiency at high surface coverage better than at low surface coverage.

It remains to be stated what the final proposed form is for the collision efficiency functionality on the destabilization conditions. Although the probabilistic collision efficiency function was shown to fit the normalized collision efficiency data, this still does not describe the absolute values of the collision efficiency. A constant of proportionality describing the collision efficiency under maximum destabilization is still necessary. However, modelling collision efficiency by equation (6-2) will require a constant of proportionality as well, so this is of small concern. It will be noted that all collision efficiency statements proposed to date require unknown London-Hamaker and retardation constants to obtain absolute collision efficiencies. The other parameters in the variable C_{RA}

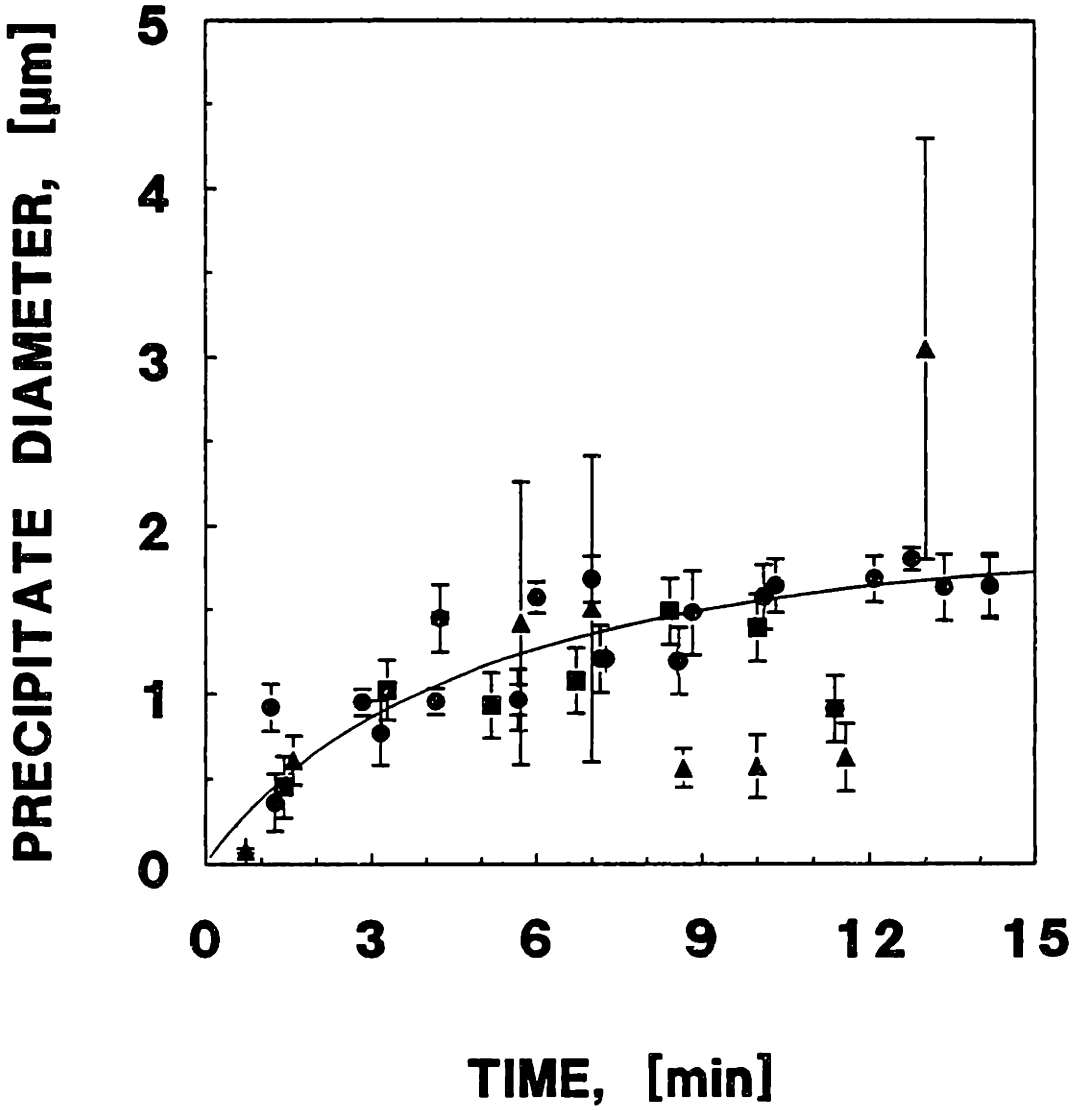

Figure 6-11. Poly-L-histidine precipitate hydrodynamic diameter as determined by QELS versus time of precipitation in 0.15 M NaCl, pH 7. ● - 20 mg/L, ■ - 10 mg/L, ▲ - 3.3 mg/L.

are independent (excepting perhaps A) of polymer dosage, and may be separated out of the collision efficiency statement. Incorporating the heterogeneity of the polymer adsorption into the surface potential term leads to the final model:

$$\alpha_{ij} = k\left(\frac{4\pi\varepsilon_o K(\psi_o^o)^2 a_i}{A}\right)^w \left(\frac{A}{6\pi\eta\dot{\gamma} a_i^3}\right)^x \sum_{m=\frac{n}{1-z_p}}^{n} \frac{n!}{m!(n-m)!}[1-(1-(1-z_p)\theta)^{-2w}]^m [1-(1-z_p)\theta)^{-2w}]^{n-m} \quad (6\text{-}15)$$

Under the experimental conditions of this investigation, $z_p = -0.18$, $w = -1.2$, and $m = n = 3$.

6.2.3. - Collision Efficiency Versus Fluid Shear Rate

Having assessed the suspension stability versus the polymer dose, it was desirable to quantify the effects of hydrodynamic forces on the particle collision efficiency. Investigating the cell collision efficiency at constant polymer dose (surface coverage), allows the assessment of hydrodynamic effects on collision behavior. Experimentally, we wish to determine collision efficiencies versus the parameters in C_A, to elucidate the value of the exponent x in equation (6-15). Although the Hamaker constant of the system is not readily changed (or measured), and cell size varies only over a small range ($6.0 < a < 8.5$ μm), the fluid shear rate and medium viscosity may be varied. The most easily varied parameter is the shear rate; in addition to the polymer dose, this is the other major independent, controllable variable in the flocculation process which can be used to vary the speed of aggregation. Theory for ionic coagulation predicts that the exponent x on the term C_A should be between 0.18 and 0.33. This translates to a -0.18 to -0.33 dependency on the shear rate. The theoretical result is applicable when London-Van der Waals forces are small compared to the viscous forces ($10^{-5} < C_A < 10^{-1}$), and electrostatic repulsion is low ($C_{RA} < 25$). Using shear rates between 6 and 60 s^{-1}, it was shown above that $1.7 \times 10^{-7} <$

$C_A < 1.7x10^{-6}$. This is below the range for which the theoretical correlations were derived, and points out that hydrodynamic forces will dominate the particle collisions. In addition, it was shown in section 6.2.1. that C_{RA} is always greater than 25 for the flocculation system being investigated. It will therefore be of considerable interest to observe the actual dependency of the collision efficiency in this regime uncovered by theoretical correlations.

Figure 6-12 shows the collision efficiency versus shear rate at four different polymer doses representing low and high surface coverages. The collision efficiency follows a power law functionality for all polymer doses over the range of shear rates investigated. For all but the lowest polymer dose, the slopes of the plots are comparable. For moderate to high doses, the slope increases slowly with decreasing dose, going from -0.28±.05 at 215 mg/m^2 to -0.41±.04 at 40 mg/m^2. The mean slope of the experimental data is -0.32 ± .06, which is close to theoretical predictions. As noted in section 6.1.1., we expect that the collision efficiency will be higher than 0.23 for non-monosized suspensions with C_A values less than 10^{-5}. The experimental values are encouraging since we are not within the theoretical correlations' applicable range, nor are we confident that the same collision mechanisms are operative. Steric forces and polymer conformation, and cell surface roughness, surface heterogeneity and size polydispersity may all play a role in divergence from ionic coagulation theory.

Although the collision efficiency shows only a mild shear dependency for high doses, this dependency changes slowly as dose is decreased. At 13 mg/m^2, the slope changes radically to -1.2. ± 0.1, signifying a shift in flocculation regimes. This dependency is similar to that found by Koh, Andrews and Uhlherr (1987), who observed a shear rate dependency of -1.3 for scheelite suspensions destabilized by oleic acid. This dependency was arrived at by fitting particle size distributions to a population balance equation, however. The strong dependency on shear observed in the current work at low polymer dosage may reflect the growing importance of electrostatic forces, or may signify

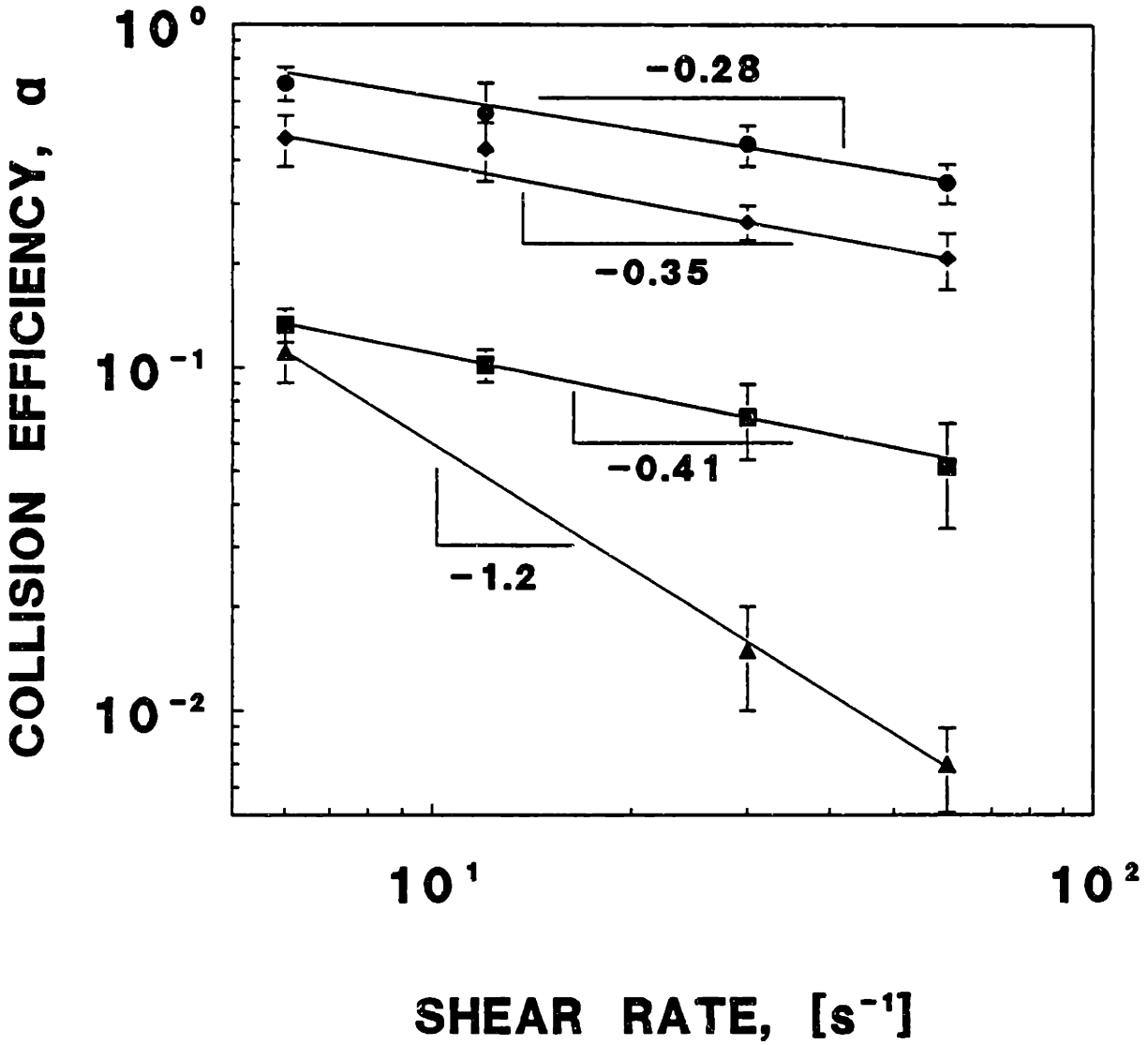

Figure 6-12. Collision efficiency of CRL 1606 cells versus shear rate at various polymer doses. ▲ - 12 mg/m^2, ■ - 40 mg/m^2, ◆ - 133 mg/m^2, ● - 215 mg/m^2.

weak bonding and breakage. Qualitative observations at low polyhistidine doses show that the maximum floc sizes seen for these doses are very small, rarely comprising more than 100 cells even for high cell concentrations and long flocculation times. This is considered evidence of weak bonding and low floc strength at these doses. This result is consistent with the experimental collision efficiency results versus polymer dose shown in section 6.2.2. At low polymer dose (surface coverage), most of the bonds formed are weak, and cannot withstand the fluid force tending to separate the particles. It is interesting that where most cationic polyelectrolytes are toxic to animal cells, poly-L-histidine is relatively benign. In light of the collision efficiency behavior at lower polymer dose, the absence of toxicity may be due to weak polymer association with the cell surface.

The strong dependency of the collision efficiency on shear rate at low polymer dose has important practical ramifications for flocculation process operation. The low polymer dose region is preferable for maintenance of culture viability, as shown by Figure 5-11. However, at low polymer doses the collision efficiency is low, so the flocculation will proceed slowly. Without access to experimental collision efficiencies, and relying on the Van de Ven and Mason correlation, one would expect that increasing the process shear rate would increase the speed of aggregation by the factor $\dot{\gamma}^{0.82}$. In reality, the collision efficiency dependency on shear rate is stronger than the collision frequency dependency, such that the overall flocculation velocity dependency on the fluid shear rate is $\dot{\gamma}^{-0.2}$. Increasing the mixing intensity would then actually decrease the rate of aggregation. This points out the importance of determining individual parameters in the aggregation kernel function.

It will be recognized that this dependency can only be considered valid for the conditions investigated; decreasing the shear rate infinitely will not lead to increasing flocculation velocity. At some low shear rate value, the fluid shear stress tending to

separate the cells will become less than the characteristic bond strength, and will not affect collision efficiency. Under these conditions the collision efficiency would be expected to revert back to the weak dependency found at higher polymer doses.

6.2.4. - Collision Efficiency Versus Fluid Viscosity

The experiments presented in the above section suggest that the collision efficiency dependency on hydrodynamic conditions follows the theory proposed for ionic coagulation of particles. Given the closeness of the experimental results versus shear rate to the theoretical dependency, my committee demanded to know whether the phenomenon was fortuitous or not. In the parameter C_A, the medium viscosity appears with the shear rate in the viscous hydrodynamic force terms. Collision efficiency should thus show a similar dependence on viscosity as on shear rate. In the literature reviewed in section 3.5.2., it will be noted that only the experimental study of Mifflin and Schowalter (1988) has dealt with viscosity effects on collision. Unfortunately, it is not possible to extract collision efficiency dependency on viscosity from their experiments, which were conducted in semi-dilute, viscoelastic polymer solutions. The experiments conducted here with animal cells thus represent the first reported results of viscosity effects on collision efficiency.

Since animal cells are being studied, medium viscosity cannot be changed with low molecular weight solutes due to the necessity to maintain medium isotonicity relative to the cells. A large range of viscosity was anticipated to be necessary since a weak viscosity dependency should result based on the theory and shear rate data. To test the effects of viscosity on collision efficiency, 500,000 MW dextran was employed since it gives a large range of viscosity at concentrations which negligibly change the medium osmotic strength. At the shear rates and polymer concentrations used in this investigation, 500,000 MW dextran exhibits Newtonian behavior as assessed by measurements in the Couette viscometer used in the collision efficiency studies. In addition to being a Newtonian fluid,

dextran should be inert with respect to the cell surface. This is demonstrated by the lack of flocculation promotion by dextran discussed in section 5.1.4.

Figure 6-13 shows the collision efficiency versus medium viscosity at 30 s^{-1} shear rate, and 200 mg PLH/m^2. This data shows a dependency on the viscosity to the -0.98 ± 0.15 power, radically different from the previous shear rate data. The dependency may be explained by either modification of surface forces, or steric interference with collision. Fluid stress effects are not a factor, since the maximum shear stress tending to separate touching spheres in a shear field is given by Goren (1971) as:

$$|F_{max}| = 19.23\eta\dot{\gamma}a_i^2 \qquad (6\text{-}16)$$

From this relation, it is seen that the maximum fluid force pulling the cells apart has the same dependency on the shear rate as on the viscosity. Additional electrophoresis experiments showed that although the dextran affected cell electrophoretic mobility, it had no effect on the cell zeta potential. Since the interparticle electrostatic forces are unaffected, this suggests that a steric factor inhibiting adhesion may be present. The dextran used has a fairly high molecular weight, and its hydrodynamic radius in solution is approximately 21 nm (Garg and Stivala (1978)). At the highest viscosities used, polymer concentration is well into the semi-dilute range, where the polymer chains will entangle and overlap each other. Steric interference with particle collision and adherence can arise from configurational entropy decrease and unmixing of dextran molecules confined between the cell surfaces, as well as the inability of the polymer to diffuse from between the particles during approach.

The possibility of steric hindrance was investigated by changing the molecular weight of the polymer and holding viscosity constant. Figure 6-14 shows collision efficiency at a constant viscosity of 4.9 cP, 30 s^{-1} shear rate, and 200 mg PLH/m^2 for dextran molecular weights between 9,000 and 500,000. There is a marked effect of molecular weight, and inherently dextran concentration, even though viscosity is constant.

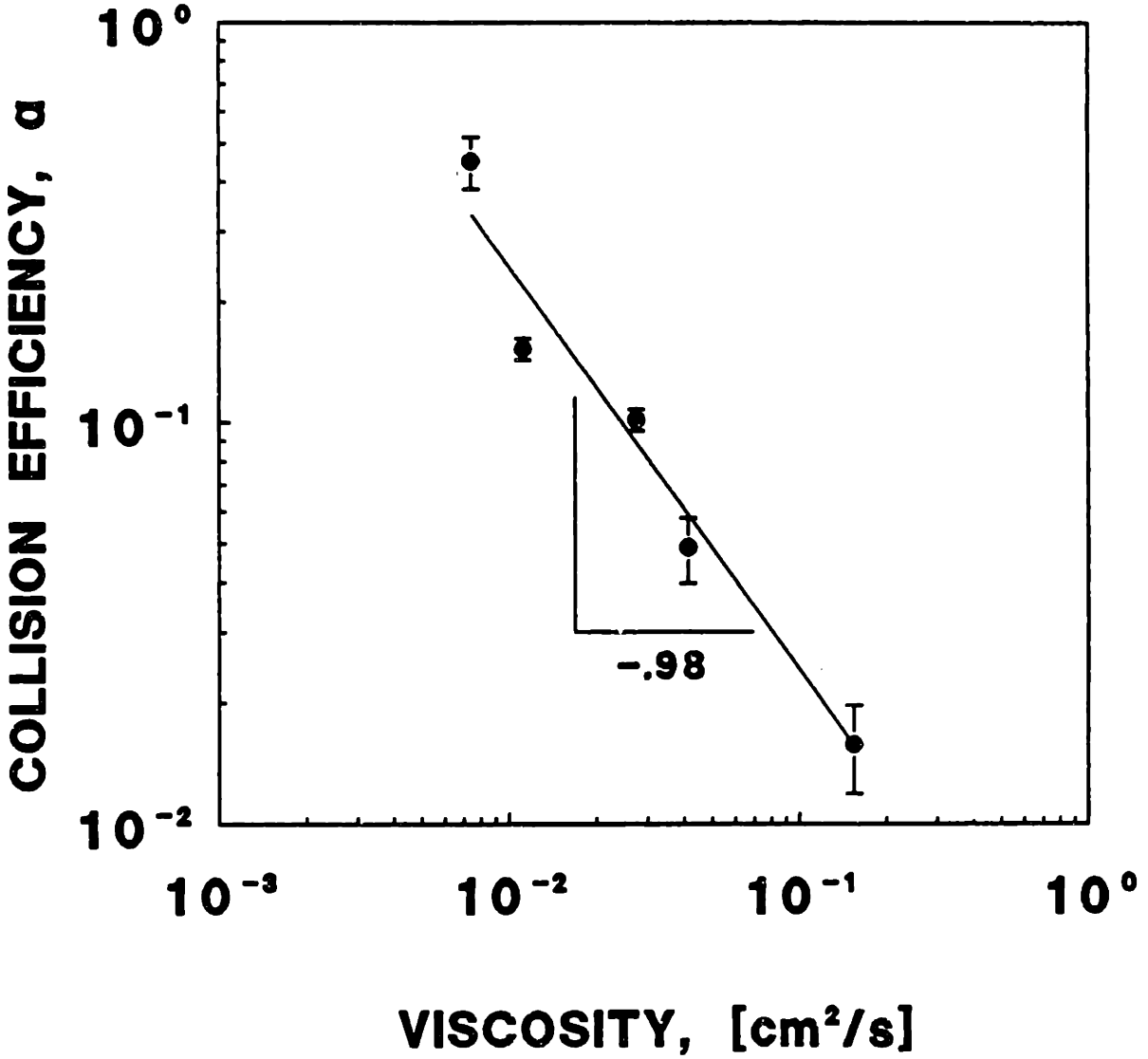

Figure 6-13. Collision efficiency of CRL 1606 cells versus viscosity using 500,000 MW dextran as viscosity enhancer at 215 mg PLH/m^2, shear rate = 30 s^{-1}.

As molecular weight is lowered, greater concentrations are necessary to obtain the same bulk viscosity. This is due to the decreased size of the molecules, and concomitantly lesser degree of entanglement between chains. If the effect of dextran addition is a chemical effect, it would be expected to decrease collision efficiency in proportion to its concentration, that is, at lower molecular weights. This is exactly opposite the trend seen in Figure 6-14. If the effect of dextran addition is a steric hindrance, it should positively correlate with molecular size. This is exactly the trend shown in Figure 6-14, and it indicates that the strong collision efficiency dependency found in Figure 6-13 is due to a combination of viscosity effects and steric hindrance to collision. As dextran molecular weight is decreased, the collision efficiency asymptotically approaches a constant value. It is anticipated that in the limit of small molecular weight, the steric inhibition of collision will disappear, and the collision efficiency will follow the same dependency on viscosity as on shear rate. At a viscosity of 4.9 cP, the expected collision efficiency can be calculated from the shear rate experiments at the same polymer dose and shear rate, and adjusted by the -0.28 power law. This expectation is shown as the dashed line in Figure 6-14. It is seen that as polymer molecular weight decreases below 10,000, the steric inhibition to collision disappears and the collision efficiency plateaus to the expected value at this viscosity. This further demonstrates the validity of a deterministic correlation of collision efficiency versus hydrodynamic factors.

Although theories of steric stabilization of suspensions are fairly well developed for particles flocculating by Brownian motion (Napper (1983)), theories for the corresponding shear aggregation case are nonexistent. Assuming that the effect of C_A may be factored out of the dependency on viscosity in Figure 6-13, we might find collision efficiency to correlate to a factor describing steric interactions, C_S, introduced in section 6.1.1. This factor raised to the exponent y would ostensibly involve the medium viscosity or a related variable to the -0.66 power.

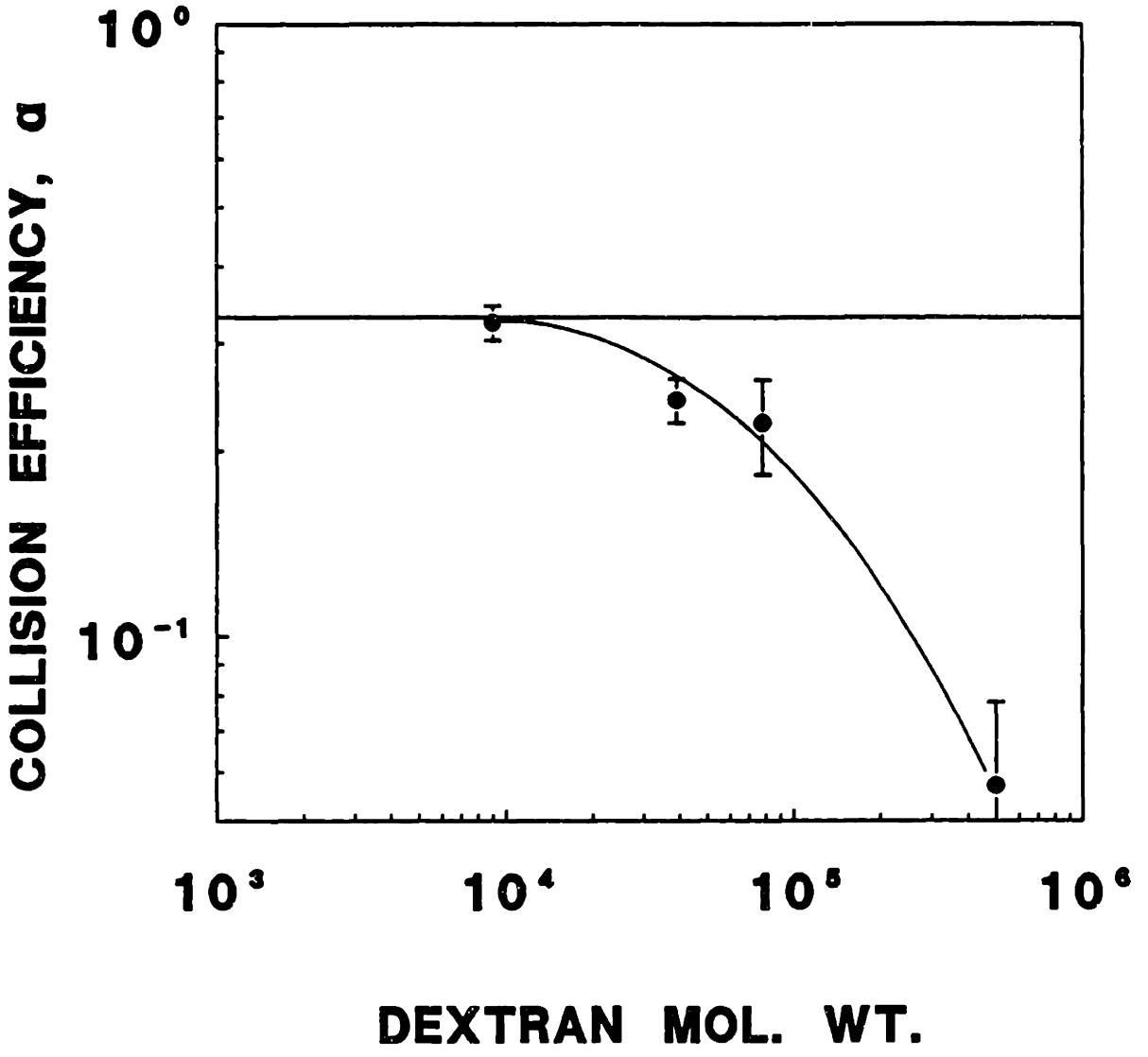

Figure 6-14. Collision efficiency of CRL 1606 cells versus dextran molecular weight at η = 4.9 cP, 200 mg PLH/m^2, shear rate = 30 s^{-1}.

The procedure for calculating the steric interaction effect in the simplest case is straightforward and would be similar to the development of the ionic coagulation theory for electrostatic and London-Van der Waals force influences on collision. From thermodynamic arguments, the free energy of interaction is calculated as a function of the particle separation distance. The derivative of the free energy with respect to the particle separation distance can be equated to the force promoting or opposing collision. These force calculations for cell adhesion have been developed by Bongrand and Bell (1984), and Grieg and Jones (1976). The interparticle force versus radial distance would then be incorporated into the F_R term in equation (3-10a), and the equations of motion solved as before.

This approach would probably serve well to describe the effects of adsorbed macromolecules, *e.g.* cell surface polysaccharides, but may not describe the effects of soluble macromolecules on collision due to the finite encounter times between particles. A theory for steric stabilization in the orthokinetic regime would require consideration of the characteristic time for polymer transport from the gap between the cells versus the relative time for particle encounter. An order of magnitude estimate can be made to show that polymer diffusion from an intercell gap may control collision. The results of Manley and Mason (1952) show the maximum lifetime of a passing, non-adhering doublet:

$$\tau_{max} = \frac{2\pi}{\dot{\gamma}} \tag{6-17}$$

The characteristic diffusion time for a macromolecule escaping from an intercell gap will be equal to a characteristic diffusion path length divided by the molecular diffusivity:

$$\tau_{diff} = \frac{L^2}{\mathcal{D}} \tag{6-18}$$

Here L is the characteristic diffusion path length, which will scale as the particle radius, and $\mathcal{D}$ is the diffusion coefficient. The ratio of the two characteristic times is an indication of

the importance of steric inhibition of collision due to the inability of dextran to diffuse from between the cells during the collision:

$$\beta_{steric} = \frac{a_i^2 \dot{\gamma}}{2\pi \mathcal{D}} \qquad (6\text{-}19)$$

When β_{steric} is large, hindrance is significant. The results of Callaghan and Pinder (1983) may be used to describe the dextran diffusion coefficient. Their study showed that over a range from 10,000 < MW < 400,000, dextran diffusivity follows $\mathcal{D} = 1.14 \times 10^{-4}\ MW^{-.51}$. Substituting this relation along with a = 8 μm and $\dot{\gamma} = 30\ s^{-1}$ allows calculation of β_{steric} versus dextran molecular weight for the experimental conditions used. Figure 6-15 shows the derived relation. Although this can only be considered an order of magnitude estimate, the plot shows that β_{steric} drops to near unity around a polymer molecular weight of 10^4. For the larger molecular weight dextrans, β_{steric} is larger than one, and indicates that the dextran was incapable of quick response to being squeezed between the cells. This calculation provides encouragement for the conclusion above that increasing viscosity with high molecular weight polymer provides steric hindrance to collision in addition to viscous resistance.

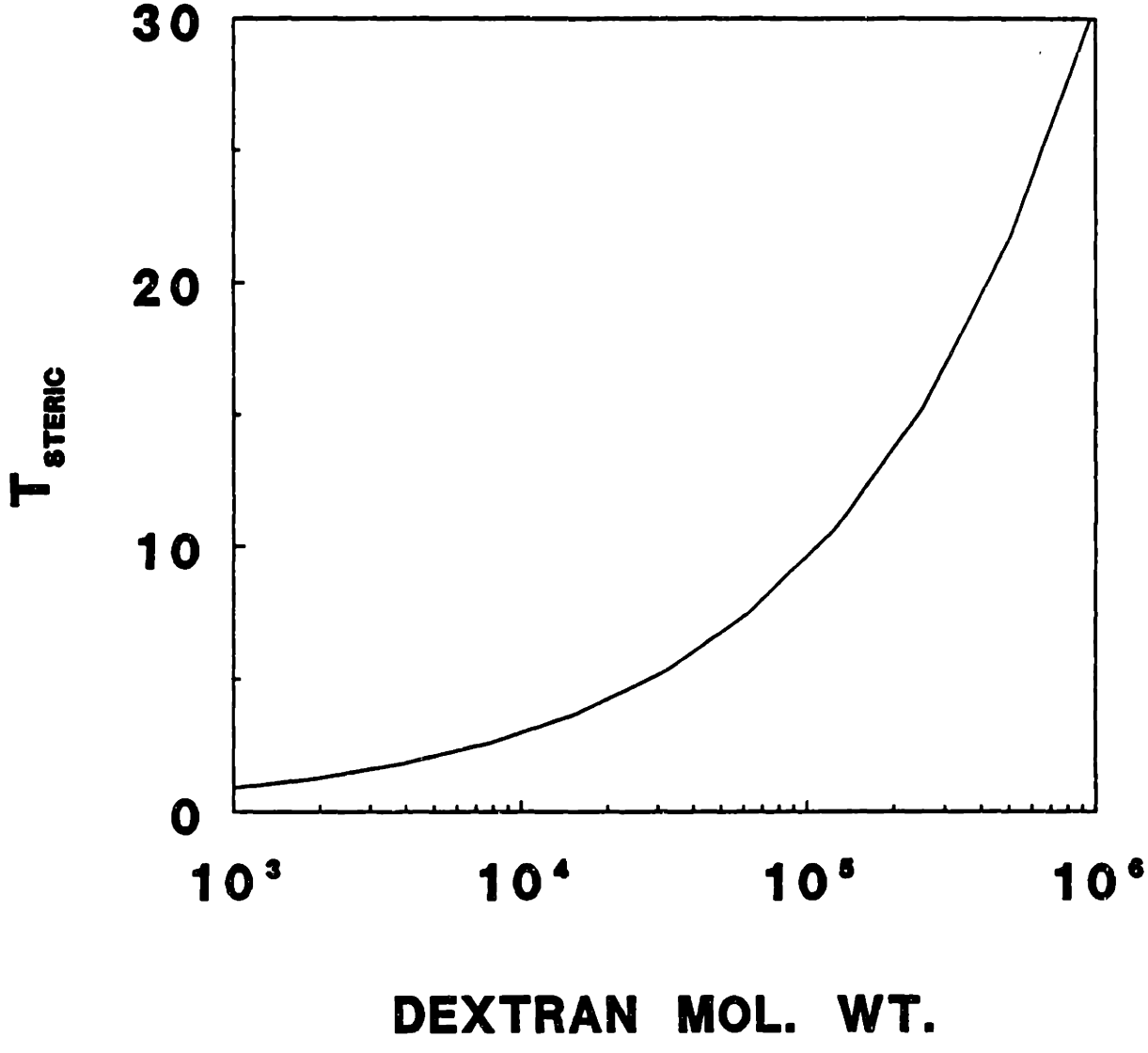

Figure 6-15. Characteristic time ratio, T_{steric}, versus dextran molecular weight for an 8 μm radius particle.

7. - FLOC STRUCTURE RESULTS

There were two goals to the investigation of floc structure. The first goal was to investigate the dependency of the floc porosity versus size on flocculation conditions, and to compare these results with literature theory and experiment. The second goal was to develop a relation which describes the floc friction coefficient dependency on the fractal dimension. Such a relation could then be used to describe floc sedimentary properties, and to reassess literature correlations of floc porosity versus size which have used floc sedimentary velocity to determine porosity. In order to provide an easy comparison of literature results with current experiments, the theory for fractal floc friction coefficients will be presented in section 7.1.1. A literature reevaluation will be presented in section 7.1.2., and the experimental results will be presented in section 7.2.

7.1. - Fractal Floc Transport Properties

7.1.1. - Fractal Cluster Friction Coefficient Theory

As shown in section 3.6.3.2., the dependency of the friction coefficient on floc size and porosity is not simple. In the limit of small degrees of aggregation, $i \approx O(1)$, the particles in the cluster experience free-stream drag. In the limit, as i approaches infinity, most of the particles will screen each other from the fluid flow. When the particles are tightly packed, the cluster friction behavior versus scale will approximate that of a solid sphere. When the particles are strung together loosely, the particles may experience free-stream drag. At intermediate degrees of aggregation and packing density, the behavior of the cluster is complex, and has not been described for fractal structures. In this section, a simple model will be developed for fractal flocs in creeping flow. This theory states that the friction coefficient should scale by a power law function with a fractal coefficient which is dependent on the cluster fractal dimension.

In the free draining limit, each particle in the floc experiences the free stream fluid velocity and hence possesses its single cell friction coefficient. The aggregate friction coefficient, $f(i)$, is the sum of the individual coefficients, as expressed by equation (3-45):

$$f(i) = i\zeta = 6\pi\eta a_1 i \tag{7-1}$$

Equation (7-1) shows that for a free-draining floc, the friction coefficient dependency on the cluster size i is unity. As pointed out in section 3.6.3.2., the floc will be free-draining only when it is very loosely structured, $D < 3$, or when the floc is small.

If the floc is non-draining, the friction coefficient should be the same as for a solid Stokes' sphere of the same radius, $f(i) = 6\pi\eta a_i$. Substituting the fractal relation, equation (3-29), for a_i gives equation (3-46):

$$f(i) = 6\pi\eta\left(\frac{i}{k}\right)^{1/D} \tag{7-2}$$

In a non-draining floc, then, the dependency on i is the inverse of the fractal dimension. This will be a good approximation only as D approaches three, or as the floc size approaches infinity. When these conditions are met, the friction coefficient should scale with $i^{1/3}$.

The dependency for $1 < D < 3$ and finite cluster size should be somewhere in between, and it is this relationship that we seek. A general relation is proposed for the creeping flow regime:

$$f(i) = 6\pi\eta k_f i^{D_f} \tag{7-3}$$

Here, k_f is a constant of order a_1. D_f is a constant dependent on the fractal dimension. This formulation is essentially the same relation as equation (3-47), with $D_f = \sigma$. When D approaches three, D_f should approach 1/3. When D approaches one, D_f should approach one. In order to use this formulation of the friction coefficient, the value of D_f must be known for $1 < D < 3$.

Chen, Deutch and Meakin (1984) calculated the translational friction coefficient of computer generated fractal aggregates for a single case of aggregate structure with D equal to 2.52 and cluster sizes $10 < i < 600$. Using Kirkwood-Riseman theory to calculate the hydrodynamic interactions between the particles, the friction coefficients of the aggregates followed the form of (7-3) with a coefficient $D_f = 0.479 \pm 0.01$. For a non-draining aggregate the exponent would be expected to be $1/2.52 = 0.397$. Clearly, the flocs do not possess solid sphere friction coefficients even at this high value of D. For flocs of lower dimensionality, the difference between D_f and 1/D should become significant. It is unfortunate for generalization to other fractal dimensions that these authors investigated only one fractal dimension.

Since there are no simulations for the frictional dependency at other fractal dimensions to guide us, a universal relation is proposed as follows. There are three collocation points for the value of D_f. These are D_f equals 1, 0.479, and 3 at D equals 1, 2.52, and 3. In addition, as the floc becomes increasingly dense, D_f should approach 1/D smoothly:

$$\frac{dD_f}{dD} = \frac{d(1/D)}{dD} = -\frac{1}{9} \qquad @ \qquad D = 3 \tag{7-4}$$

As the floc approaches D equal to one, D_f should approach one asymptotically as well:

$$\frac{dD_f}{dD} = 0 \qquad @ \qquad D = 1 \tag{7-5}$$

These conditions may be used to approximate the functionality of D_f on D. Since there is no exact form for this functionality, it is most easily posed as an infinite polynomial series:

$$D_f = \sum_i c_i D^i \cong \frac{c_{-1}}{D} + c_o + c_1 D + c_2 D^2 + c_3 D^3 \tag{7-6}$$

On the far right hand side of this equation, the series has been truncated to five terms; this

truncation allows solution for the coefficients which will satisfy the boundary conditions exactly. From the five boundary conditions above, matrix algebra was used to solve for the five coefficients c_i:

$$D_f = \frac{0.41}{D} - .677 + 2.31D - 1.23D^2 + .184D^3 \qquad (7\text{-}7)$$

This function of D is plotted in Figure 7-1. Along with this is plotted the sole calculated value of D_f and the relation 1/D. The polynomial quickly diverges from the 1/D relation at values less than three, indicating that for fractal dimensions that are close to two, as we might expect from the computer simulations reviewed in section 3.6.1., the friction factor dependency on the cluster size is significantly stronger than the hard sphere value. It will be recognized that where this development may prove to be a very valuable tool for "intermediate" floc sizes, it probably will not apply to either very small, or very large clusters. In order to test the limits of the relation, simulations using Kirkwood-Riseman theory, like those of Chen, Deutch and Meakin, would need to be performed on very large clusters, and for different fractal dimensions. These would provide other rigorous values of D_f to test the polynomial approximation and its range of applicability.

7.1.2. - Fractal Cluster Sedimentary Properties

As mentioned in section 3.6.2.2., many empirical correlations of floc porosity rely on sedimentation velocity versus size correlations. The assumptions underlying these correlations will be examined in this section, and related to the fractal theory above.

To calculate the terminal velocity of a floc, equation (7-3) is multiplied by the velocity of the floc to calculate the total drag force. This is balanced with the buoyant force on the floc, equation (3-35) multiplied by the floc volume and gravitational acceleration. The resulting relation for the terminal velocity versus floc size is:

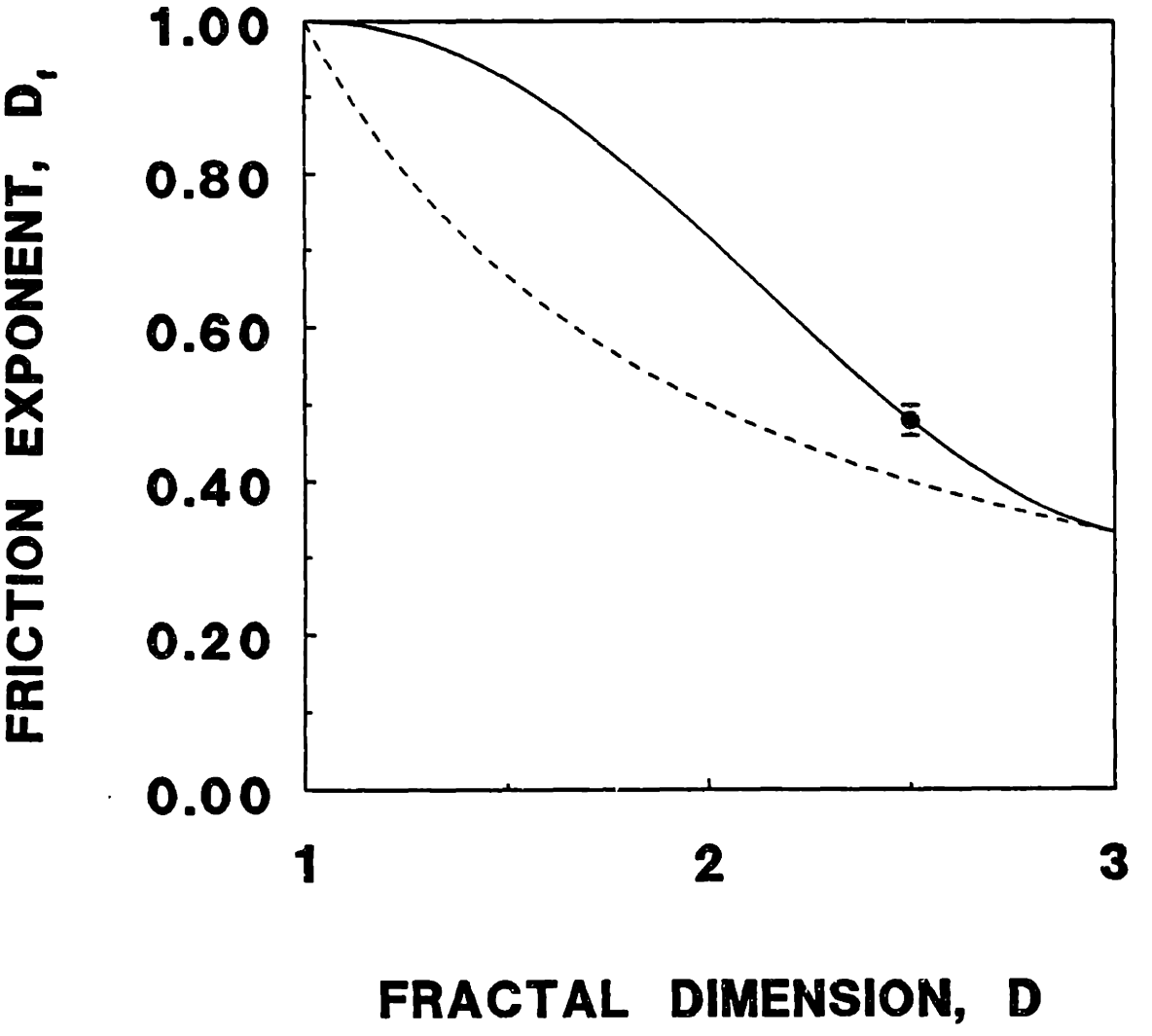

Figure 7-1. Friction exponent, D_f, calculated by equation (7-7) versus the fractal dimension, D.

$$U_{term,1} = \frac{\frac{4}{3}\pi a_1^3 ((a_1^3 k) a_1^{D-3})(\rho_{coll} - \rho_{liq})g}{6\pi\eta k_f (k a_1^D)^{D_f}} = \left(\frac{2a_1^2 (\rho_{coll} - \rho_{liq})g}{9\eta}\right) k^{1-D_f} a_1^{D(1-D_f)} \tag{7-8}$$

On the far right hand side of equation (7-8),the value of k_f has been set equal to a_1 to emphasize the connection between this form and the settling velocity of the primary particles composing the floc. Although equation (3-47) proposed by Chen, Deutch and Meakin uses $k_f = a_1$ exactly, this is not necessarily correct. It can be seen from this equation that the floc sedimentary velocity is not a straightforward dependency on the floc fractal dimension. In particular, the friction coefficient is not given by the 1/D relation. This latter assumption has been used without critical evaluation by Sundheim (1987) for prediction of sedimentation of aerosol clusters. Equation (7-8) may be used to predict sedimentary velocity enhancement when the values of D and D_f are known.

In previous empirical correlations of floc density based on sedimentary velocity, the observed floc porosity has been calculated by the relation:

$$(1 - \varepsilon_1)_{obs} = \frac{U_{term,obs} f(a_1)}{\frac{4}{3}\pi a_1^3 g(\rho_{coll} - \rho_{liq})} \tag{7-9}$$

The friction coefficient $f(a_i)$ has traditionally been taken to be a hard sphere value such as given by Concha and Almendra (1979). For illustration, the Stokes-Einstein relation may be substituted at low Re, and equation (7-9) becomes:

$$(1 - \varepsilon_1)_{obs} = \frac{9\eta U_{term,obs}}{2a_1^2 g(\rho_{coll} - \rho_{liq})} \tag{7-10}$$

This is the general form that has been used to correlate floc porosities from experimental size versus settling velocity data. In reality, the terminal velocity U_{term} is represented by equation (7-8); substituting this relation into (7-10) yields the value which is truly correlated in a size-sedimentary velocity determination of cluster porosity:

$$(1 - \varepsilon_i)_{obs} = (a_i^2 k^{1 - D_f}) a_i^{D(1 - D_f) - 2} = k' a_i^{-\lambda} \qquad (7\text{-}11)$$

On the far right hand side of this equation, λ is the exponent which is determined by the correlation, and it is seen to be a function of the fractal dimension of the floc and its corresponding value of D_f. This dependency of the observed floc porosity on a_i is compared to the true porosity dependency, $\lambda = D-3$, given by equation (3-31). We see that the frictional dependency on floc structure causes the exponents to be unequal. When D_f is set equal to 1/D, the non-draining value, equation (7-11) predicts the correct porosity dependency, $\lambda = D-3$. It is thus seen that except for situations where the cluster is in the non-draining limit, a size-sedimentary velocity correlation will not give the true porosity dependency on floc size. Figure 7-2 shows a plot of the observed variable, $[D(1 - D_f) - 2]$ versus the true variable, [D - 3] for a fractal floc, using equation (7-7) to describe D_f versus D. This figure clearly illustrates that except at high values of D where the friction coefficient dependency approaches the non-draining value, the estimate of floc porosity dependence on the floc size will be significantly different from the true dependency. This plot illustrates the utility of fractal theory in correctly assessing suspension properties.

It is instructive to recalculate the literature data reviewed in section 3.6.2.2. and compare the fractal dimensions obtained using equation (7-11) to those which would be calculated from the data using equation (3-32). These values are found in Table 7-1. The first column represents the measured correlational dependency on the floc size. The second column is the fractal dimension that would be calculated from this value using equation (3-32), the hard sphere relation. The third column represents the value of the fractal dimension deduced from the above friction coefficient arguments using equations (7-7) and (7-11).

It is readily seen that the values in the two right-most columns are significantly different. Where some values in the second column are outside the range of theoretical

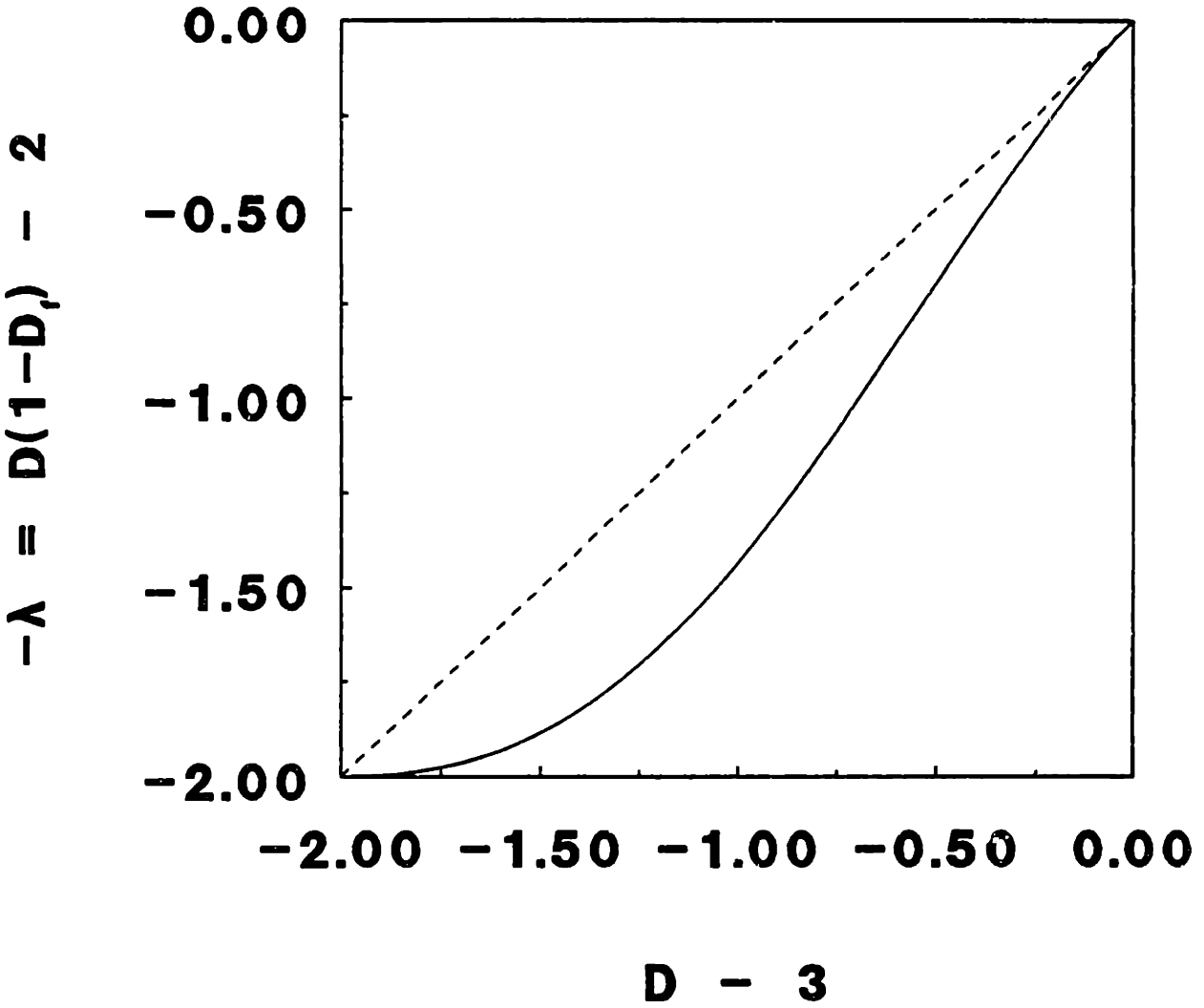

Figure 7-2. Correlated exponent, $-\lambda$, for sedimentary velocity correlations of porosity versus floc size versus the actual porosity dependency, (D - 3).

Table 7-1
Fractal Dimensions Calculated from Literature Floc Porosity Correlations

Floc Substance	Ref.	-λ	D calc.	D act.
Kaolin:Al	Tambo & Watanabe (1979a)	1.03-1.41	1.59-1.97	2.02-2.29
Kaolin:Fe	"	1.08	1.92	2.26
Kaolin:Mg	"	1.09	1.91	2.25
Color:Al	"	1.23-1.33	1.67-1.77	2.08-2.15
Color:Fe	"	1.31-1.42	1.58-1.69	2.01-2.10
Color:Mg	"	1.52	1.48	1.93
Activated Sludge	"	1.7	1.3	1.76
Bulking Sludge	"	2.0	1.0	1.0
Kaolin:Polymer	Glasgow & Hsu (1984)	0.59-1.17	1.83-2.41	2.19-2.56
Quartz:Polymer	Klimpel & Hogg (1986)	0.88-1.56	1.44-2.12	1.89-2.38
Activated Sludge	Li & Ganczarczyk (1987)	1.55	1.45	1.99

values shown in Table 3-4, the values in the right hand column of Table 7-1 fall well into the range of fractal dimensions in Table 3-4 found for computer generated fractal clusters which have undergone rearrangement. This is consistent with the idea that the flocs from these experimental studies have experienced fluid shear in their formation. In general, the fractal dimensions calculated by assuming the friction coefficient developed above are more consistent with the theoretical values than the fractal dimensions calculated by assuming solid sphere friction coefficients. This difference in perceived and actual values of floc density has important ramifications for mathematical treatment of flocculation and sedimentation processes. In addition to the effects on the sedimentary properties, mass balances based on perceived density values and size distributions will be in error if the wrong density dependence is used. For microbial floc processes, nutrient transport to the microorganisms in the floc will differ from estimates, affecting predictions of process performance (Logan and Hunt (1988), Tsiveriotis and Stephanopoulos (1988)).

Although the theoretical development of section 7.1.1. pertains strictly only to flocs in creeping flow, literature correlations do not seem to exhibit changes in correlation regime even with floc Reynolds numbers greater than unity. In the intermediate draining case, the increase in friction does not necessarily arise from floc permeability, or flow through the floc, as proposed by Klimpel, Dirican and Hogg (1986), and by Sonntag and Russel

(1986a). As stated by Chen, Deutch, and Meakin (1984) and Meakin and Deutch (1988), a large part of the increased friction comes from the surface irregularity of a fractal structure, and the dangling branches of the floc. For the D = 2.52 computer generated fractals studied by these researchers, the radius of gyration was significantly greater than the nominal hydrodynamic radius. It is notable that these authors came to this conclusion regarding a tight floc structure with D = 2.52. For flocs with lower dimensionality, this observation should be even more relevant.

In actual practice, flocs are usually held together by polymers or insoluble coagulants which may interfere with the idealized view of a fractal structure. Although the arrangement of the primary particles may be fractal, polymer presence may serve to render the floc a smooth, solid, non-draining sphere. The actual value of the fractal dimension is probably somewhere between the value which we estimate from equation (7-11), and the value which would be estimated from the hard sphere drag assumption. The values of D_{calc} and D_{act} in Table 7-1 thus represent outer bounds on the actual fractal dimensions.

7.2. - Experimental Structure Results

In order to complete the aggregation kernel for flocculating animal cells, it was desired to measure the correlation of floc size versus the number of cells in the floc, for the conditions of aggregation investigated in Chapter 6. It was specifically desired to know whether the flocs could be described as fractals, and whether the fractal dimension changed with aggregation conditions.

The experiments performed to determine the fractal dimension of animal cell flocs used a light microscopic technique; the floc was sized along a long axis, and the dimension perpendicular to this axis at the bisecting point was measured. The geometric mean of the two was recorded as the floc characteristic dimension. The advantage of this technique is that it avoids the errors associated with sedimentation velocity correlations, as discussed

above. The disadvantage is that it only measures a two-dimensional projection of the floc rather than an average of three dimensions. If the flocs generated deviate significantly from spherical, the technique will overestimate the floc size for the number of cells, and thus underestimate the fractal dimension. In addition, the measurement requires focussing through several focal planes to count the cells in the floc. For large flocs, some of the cells may be obscured, which will lower the number counted and also lower the fractal dimension recorded.

A plot of i versus a_i is shown for a typical determination in Figure 7-3. The floc mass versus size relation can be seen to be a linear correlation on the log-log plot, indicating that the flocs exhibit the power law functionality expected of a fractal structure. The ratio of the long and perpendicular dimensions measured, an indication of the sphericity of the flocs, was calculated to be typically 0.7±0.15. This indicates that the grossly asymmetric, string-like flocs found for shear aggregation by Ali and Zollars (1987) are not present in our aggregation experiments. As mentioned in section 4.7., the data is truncated at flocs comprising less than 10 cells to avoid small scale errors in the calculated fractal dimension. On the large scale, these correlations must be considered good only for the range of floc sizes investigated, since computer generated fractals have been found to converge to a constant fractal dimension only on scales greater than thousands of particles (Meakin (1988a)). In addition to the question of convergence, larger flocs may experience different flocculation mechanisms and possess different fractal dimensionalities.

7.2.1. - Fractal Dimension Versus Polymer Dose

The polymer dose was shown in section 6.2.2. to affect collision efficiency through its reduction of interparticle repulsive forces. However, this effect was shown to be analogous to an effect on the bond strength via the probabilistic collision efficiency formulations in section 6.1.3. Since the polymer dosage is able to affect bond strength on

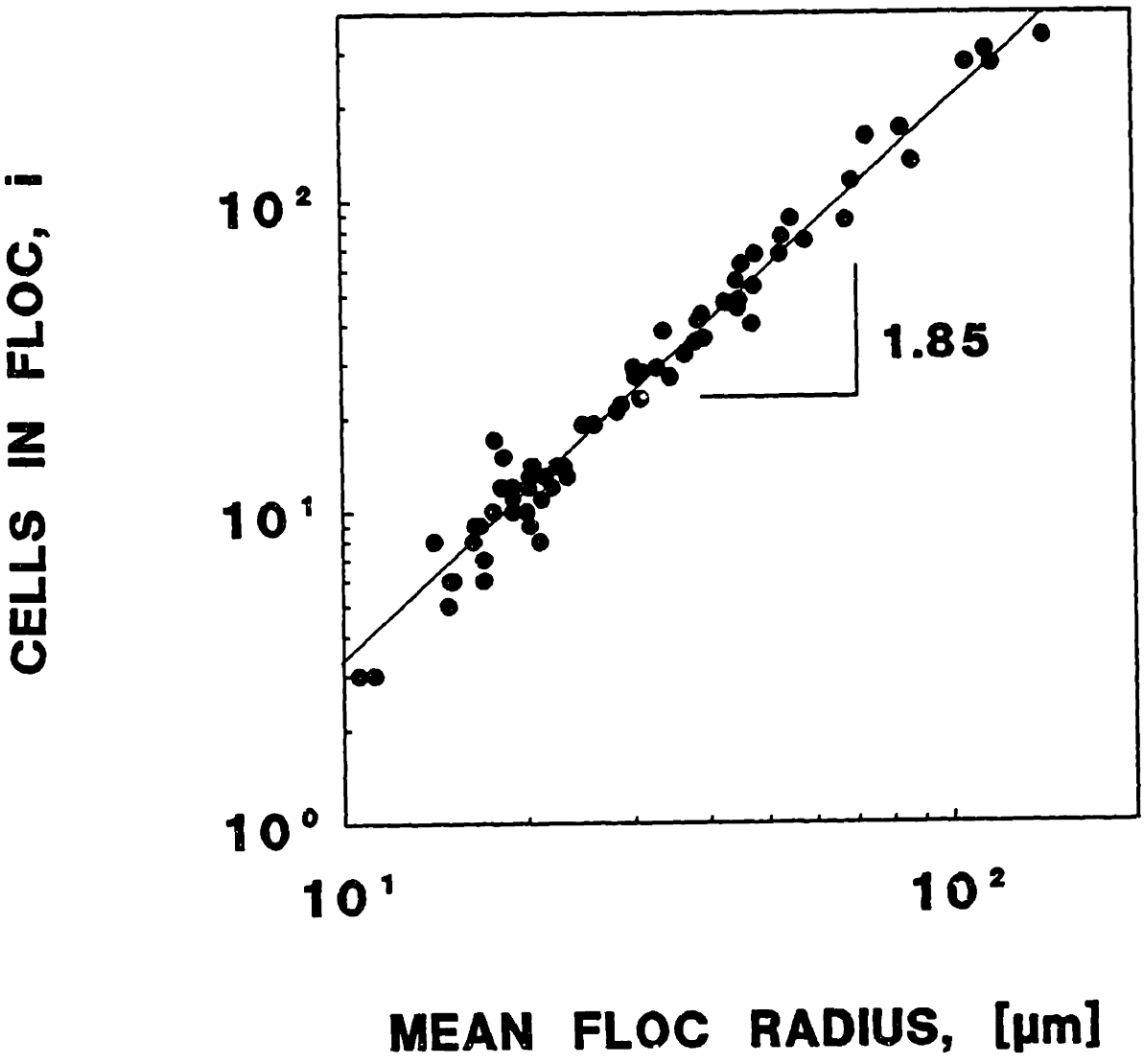

Figure 7-3. Number of cells in CRL 1606 flocs versus the geometric mean radius of the floc, for 50 mg/m^2 poly-L-histidine flocculant dose and 30 s^{-1} shear rate.

the scale of single particle collisions, it is reasonable to expect that it will affect the overall strength of a floc on the large scale. It is expected that a weak floc will be more susceptible to rearrangement than a strong floc, and will possess a higher fractal dimension. This was shown in the work of Tambo and Watanabe (1979a) for Kaolin flocculated by alum. As alum dose decreases in Table 3-5, the fractal dimension calculated from their correlations of floc porosity increases.

The effect of the polymer dosage on the floc structure was investigated over the range from 25 to 100 mg PLH/m^2, and is shown in Figure 7-4 for shear rates between 5 and 50 s^{-1}. These experiments were conducted in a turbulent cell culture spinner vessel at impeller Reynolds numbers between 500 and 2500. The general trend shows that as the polymer dose decreases, the fractal dimension increases. This trend is expected from the collision efficiency results. It is significant that the largest increases in fractal dimension come at the low flocculant doses where bond strength was shown to be significantly affected in section 6.1.3.

The results can be explained by two alternative, somewhat equivalent views. The first view is that fluid forces rearrange the flocs at low polymer dose. Weak interparticle bonding at the low doses would create "floppy", rearrangeable flocs relative to higher doses. The flocs are compacted until enough intercellular contacts are made to stabilize the structure against further compaction. The second view is that in shear aggregation, a law of "survival of the fittest" is operative. This view is consistent with the probabilistic calculations of section 6.1.3., which states that flocs will form with a random distribution of bond strengths. However, in a fluid shear environment, only those flocs which are strong and have many inter-cell contacts survive to be observed. This last view is supported by the general observation that at low doses the average and maximum floc sizes are much lower than for high polymer doses.

The range of fractal dimensions found here is within the range of theoretical values

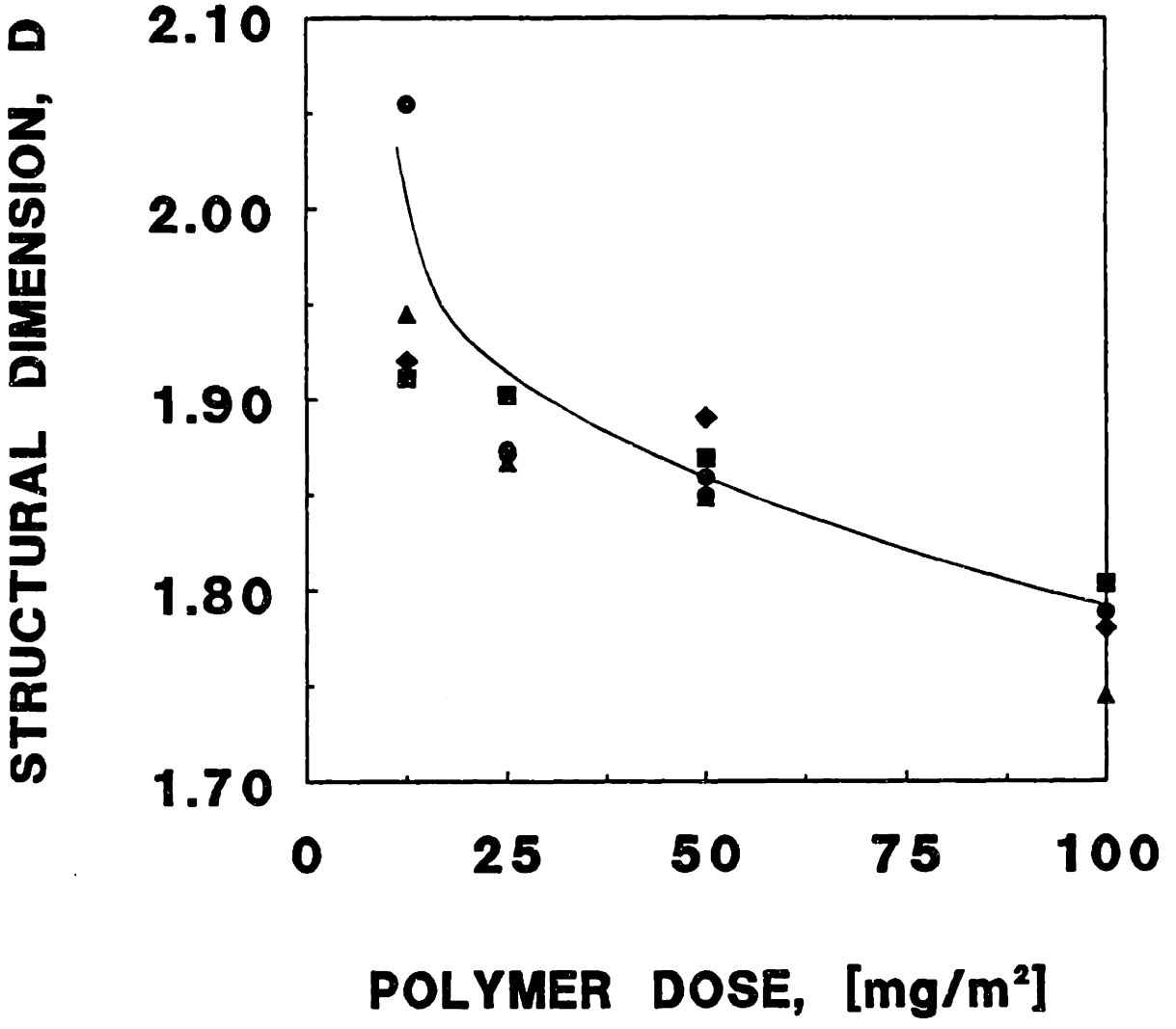

Figure 7-4. Fractal dimension for CRL 1606 flocs versus polymer dose at various shear rates. ● - 53 s^{-1}, ▲ - 32 s^{-1}, ◆ - 12 s^{-1}, ■ - 5.3 s^{-1}.

calculated in Tables 3-4. However, the theoretical values for rearranged flocs are slightly higher than the fractal dimensions found in the above experiments. This may be due to the measurement technique used in this investigation. As mentioned above, the microscopic determination will tend to give lower fractal dimensions than actual if errors are present.

7.2.2. - Floc Structure Versus Hydrodynamic Conditions

Although the results of the polymer dose experiments show that the polymer dose is influential in determining the fractal dimension of the flocs produced, the results in Figure 7-4 do not show a strong effect of the fluid shear rate on the fractal dimension. This is consistent with the results of Tambo and Watanabe (1979a) in Table 3-5, who found over a limited range of agitation intensity that shear rate had no effect on the fractal dimension. The results of Klimpel and Hogg (1986) in Table 3-6 show that the fractal dimension decreases with increasing shear rate, counter to intuition. Due to the apparent weak effects shown in the polymer dose experiments, and the inconclusiveness of the literature, it was of interest to determine the fractal dimension over a larger range of agitation intensity for the CRL 1606/polyhistidine system.

The effect of the hydrodynamic environment was investigated at a single polymer dose of 50 mg PLH/m^2 in both Couette flow and in turbulent flow. These results are presented in Figure 7-5 versus the average shear rate in the agitation vessel. Impeller Reynolds numbers in the spinner vessel ranged from 500 to 12,000. There is a mild trend of increasing fractal dimension with increasing fluid shear for both sets of data. This is consistent with the polymer dose observations; larger fluid forces tend to either compact flocs or destroy weak flocs. Again, at the highest shear rates, the floc sizes were decidedly smaller on average, lending credence to the idea that weak floc destruction, rather than rearrangement is the mechanism for obtaining higher fractal dimensions. It seems that the distribution of floc strength and the relative magnitude of the fluid shear stress will

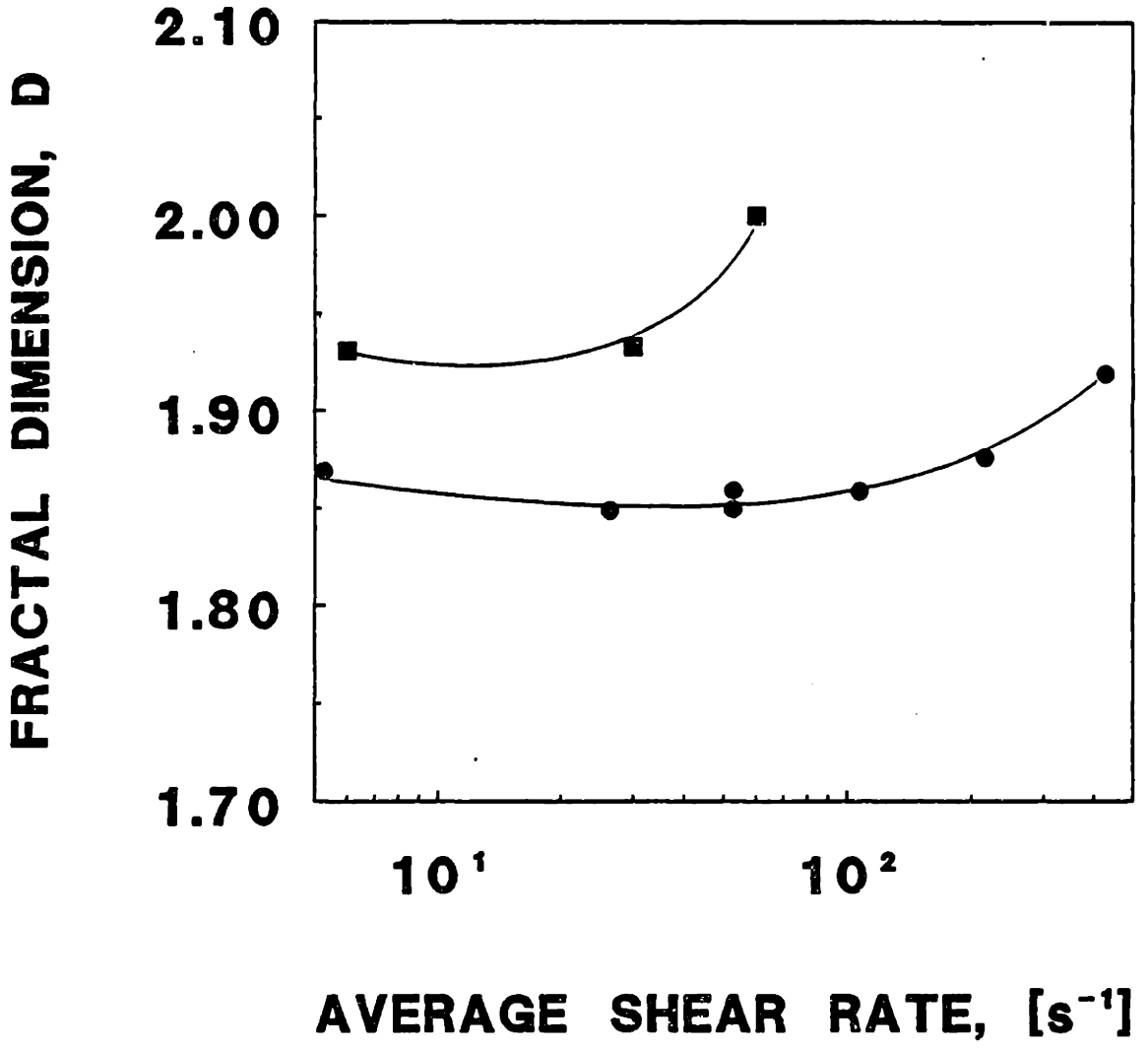

Figure 7-5. Fractal dimension for CRL 1606 flocs versus average fluid shear rate at 50 mg PLH/m^2. ■ - Couette flow, ● - spinner vessel.

determine the fractal dimension.

It is not readily apparent why the fractal dimensions obtained in the Couette flow device differ from those found in the spinner vessel. There are two possible explanations for this result. The first explanation is that the dimensions of the flocs relative to the Couette viscometer influenced aggregate structure. The viscometer gap width is 1250 μm, compared with maximum measured floc dimensions of 370 μm. This raises the possibility of wall interactions which may have compacted the flocs. The second explanation is that particle trajectories differ in the two vessels. Table 3-4 shows that computer generated clusters with ballistic trajectories produce more compact flocs than diffusive trajectories. The Couette flow trajectories are roughly ballistic (excepting the influences of hydrodynamics and interparticle forces), since the flow is purely a shear field. In the spinner, turbulent combination of flocs may occur in a pseudo-diffusive fashion, especially for flocs which are on or above the Kolmogorov scale. Assuming isotropic turbulent energy dissipation and the existence of the Kolmogorov viscous subrange, the Kolmogorov eddy length ranged between 430 and 140 μm for the shear rates investigated, which means that for maximum floc sizes of 370 μm, the number of flocs on the eddy length scale increases with increasing shear rate. If particle trajectories influence the floc formation, the increasing number of flocs produced by diffusive combination can account for the slowly increasing value of the fractal dimension versus shear rate. Again it must be emphasized that although trends in the fractal dimension behavior can be interpreted in terms of the theoretical values, it is not possible to deduce the mechanisms of floc formation from the absolute value of the fractal dimension measured.

8. - SEDIMENTARY ENHANCEMENT BY FLOCCULATION

The goal of characterizing flocculation kinetics and floc structure in the experimental and theoretical work performed in this thesis has been to investigate those variables which affect the aggregative terms in the population balance equation. These variables are largely unreported for large, biological particles undergoing shear flocculation via polymer adsorption. Where previous literature investigations have fit parameter values for inorganic suspensions from population distributions, the parameters have not been investigated independently. The two parameters which affect the aggregation terms in the population balance equation are the collision efficiency and the floc size versus particle number relationship. These variables were reported in chapters 6 and 7 over a range of process conditions in which are likely to be found in animal cell flocculation. The development in section 8.1. shows how these variables interact in a simplistic solution to the population balance equation.

The results of a population aggregation simulation can be further used along with the floc sedimentary properties developed in section 7.1.2. to predict the sedimentary enhancement of the suspension versus process variables and time. The sedimentary enhancement will be demonstrated in section 8.2. for the experimental data obtained with the animal cell flocculation system studied here.

Lastly, to optimize a flocculation process for animal cells, the major concerns will be the viability of the cells and the speed with which the flocculation and sedimentation can be conducted. Using the sedimentary enhancement development of section 8.2. and the toxicity data presented in chapter 5, it is possible to define optimum conditions for aggregation of animal cells within the range of variables studied, and point out areas for further study. This will be shown in section 8.3.

8.1. - Flocculation Kinetics

To calculate the evolution of particle size versus process variables and time requires solution of the population balance equation for a distributed spectrum of cluster sizes, as shown in equations (3-1a) and (3-1b). In lieu of such a rigorous exercise, the effects of changing process variables may be assessed semi-quantitatively by solving the rate of change of suspension properties for a monodisperse suspension. For this problem, the rate of change of particle concentration versus time is formulated via equation (3-7) as:

$$\frac{dN}{dt} = -\frac{4}{3}\dot{\gamma}\alpha(2a)^3 N^2 \qquad (8\text{-}1)$$

Here, N is the total particle concentration, and a is the particle, or cluster size for the monodisperse suspension. The effect of non-unit collision efficiency is seen to be a straightforward retardation of the rate of aggregation. The effects of non-coalescent floc structure are considered below.

In previous calculations of shear aggregation rates, the Swift and Friedlander (1964) approximation of constant particle volume fraction has traditionally been substituted to remove the size dependent term in equation (8-1). This involves substituting the relation:

$$\Phi = \frac{4}{3}\pi a^3 N \qquad (8\text{-}2)$$

This reduces the dependency of the particle collision rate to first order in the particle concentration, which is not strictly correct. This is because the effective volume fraction occupied by the particles in suspension, Φ, changes when the suspension is not coalescent.

The Swift and Friedlander simplification is a statement of volume conservation. In lieu of this approximation, a conservation relation is needed, that is, the equation for floc excluded volume versus mass. This has been posed for fractal clusters in the form:

$$\frac{N_o}{N} = i = k a_i^D. \qquad (8\text{-}3)$$

To use this statement, the value of k is required. Unfortunately, an order of magnitude estimate is all that is available for the general case of $D \neq 3$. Here, $k \approx O(a_1^{-D})$, and a constant of proportionality is needed. For the case of D = 3, in the limit $i >> 1$, floc porosity is constant, consistent with equation (8-2). The relation for the absolute floc size versus the cells in the floc and the (constant) porosity is:

$$\frac{4}{3}\pi a_1^3 = \frac{\frac{4}{3}\pi a_o^3 i}{\phi} \tag{8-4}$$

Here, ϕ is the intrafloc volume fraction occupied by the particles, rather than the suspension volume fraction, Φ. Comparing equations (8-3) and (8-4), we obtain for D = 3:

$$k = \frac{\phi}{a_1^3} \tag{8-5}$$

Since ϕ is not constant versus floc size for other dimensionalities, obtaining a similar result for these cases has not been possible. A general form for k may be assumed:

$$k = \frac{\phi}{a_1^D} \tag{8-6}$$

Here, ϕ is the proportionality constant we seek, and it is assumed to be less than unity. This equation satisfies the exact result for the limiting case of D = 3, and is consistent for lesser values of D. Substituting (8-6) into (8-3) and then into (8-1) yields the final rate equation:

$$\frac{dN}{dt} = -\frac{32}{3}\dot{\gamma}\alpha a_o^3 \left(\frac{N_o}{\phi}\right)^{3/D} N^{2-3/D} \tag{8-7}$$

Integrating this equation with the initial condition $N = N_o$ at t = 0, and rearranging results in a final relation for the evolution of the particle concentration versus time:

$$\frac{N}{N_o} = \left[1 - \frac{32}{3}\left(\frac{3-D}{D} \right) \frac{\dot{\gamma}\,\alpha\, a_o^3 N_o}{\phi^{3/D}} t \right]^{\frac{D}{3-D}} \tag{8-8}$$

Non-dimensionalization of the flocculation time allows comparison across different theoretical and experimental cases of flocculation. The time for flocculation may be non-dimensionalized by a characteristic flocculation time, τ:

$$\tau = \frac{3D\phi^{3/D}}{32(3-D)\alpha\dot{\gamma}a_1^3 N_o} \tag{8-9}$$

The non-dimensional time for flocculation is then given by $\Theta = t/\tau$. Inserting this dimensionless time into equation (8-8) yields:

$$\frac{N}{N_o} = [1 - \Theta]^{\frac{D}{3-D}} \tag{8-10}$$

When D = 3, the Swift and Friedlander approximation is correct, and equation (8-7) does not solve to equation (8-8) since dN/dt becomes linear in N. For this case, equation (8-7) solves to an exponential form:

$$\frac{N}{N_o} = \exp\left(- \frac{32\alpha\dot{\gamma}a_1^3 N}{3\phi} t \right) \tag{8-11}$$

A characteristic time may again be defined by:

$$\tau_3 = \frac{3\phi}{32\alpha\dot{\gamma}a_1^3 N} \tag{8-12}$$

and equation (8-11) simplifies to:

$$\frac{N}{N_o} = \exp(-\Theta) \tag{8-13}$$

Flocculation velocity is enhanced by increases in α and $\dot{\gamma}$, and decreased by increases in D. Increasing the shear rate for a given polymer dose increases flocculation speed by increasing the frequency of collision. However, it also decreases the collision

efficiency, and increases the fractal dimension. These two effects will decrease the flocculation speed. The balance of these competing factors determine whether flocculation speed is enhanced overall. The ramifications of non-idealities in aggregation may be examined by comparing the reduction in the particle number versus that for "ideal" aggregation with D = 3 and $\alpha = 1$. The effect of fractal dimensions less than three on the normalized particle concentration as a function of reduced time is shown in Figure 8-1. For D values much less than three, flocculation proceeds more rapidly than the exponential decay of ideal aggregation. This is due to the expansion of the hydrodynamic volume (excluded volume) occupied by the particles. The effects of polymer dose and fluid shear on the flocculation speed may also be compared by the characteristic time constant given by equation (8-9). The inverse of the time constant is a measure of the collision frequency under the given destabilization and floc structure conditions. When divided by the inverse of the "ideal" time constant given by equation (6-11) with $\alpha = 1$, the result is a dimensionless measure of flocculation acceleration over ideal conditions of aggregation.

Flocculation acceleration for the polyhistidine/CRL 1606 experimental system may be calculated using the collision efficiency data shown in Figure 6-7, and the fractal dimension data shown in Figure 7-4. A plot of τ_3/τ is shown in Figure 8-2 for the experimental data versus the polymer dose for the shear rates investigated. The graph shows that increasing the fluid shear increases flocculation speed except for the lowest polymer dose. This is a consequence of the overall aggregation rate dependency on shear rate to roughly the 0.7 power. Since the fractal dimension is only weakly dependent on shear rate at constant polymer dose, the aggregation rate is dominated by the collision efficiency effects. In Figure 8-2, at the lowest polyhistidine dose, the opposite trend is observed; aggregation acceleration decreases with increasing shear rate. This is due to the extreme sensitivity of the collision efficiency to the shear rate at this dose. An interesting observation is that despite the non-linear collision efficiency dependence on polymer dose,

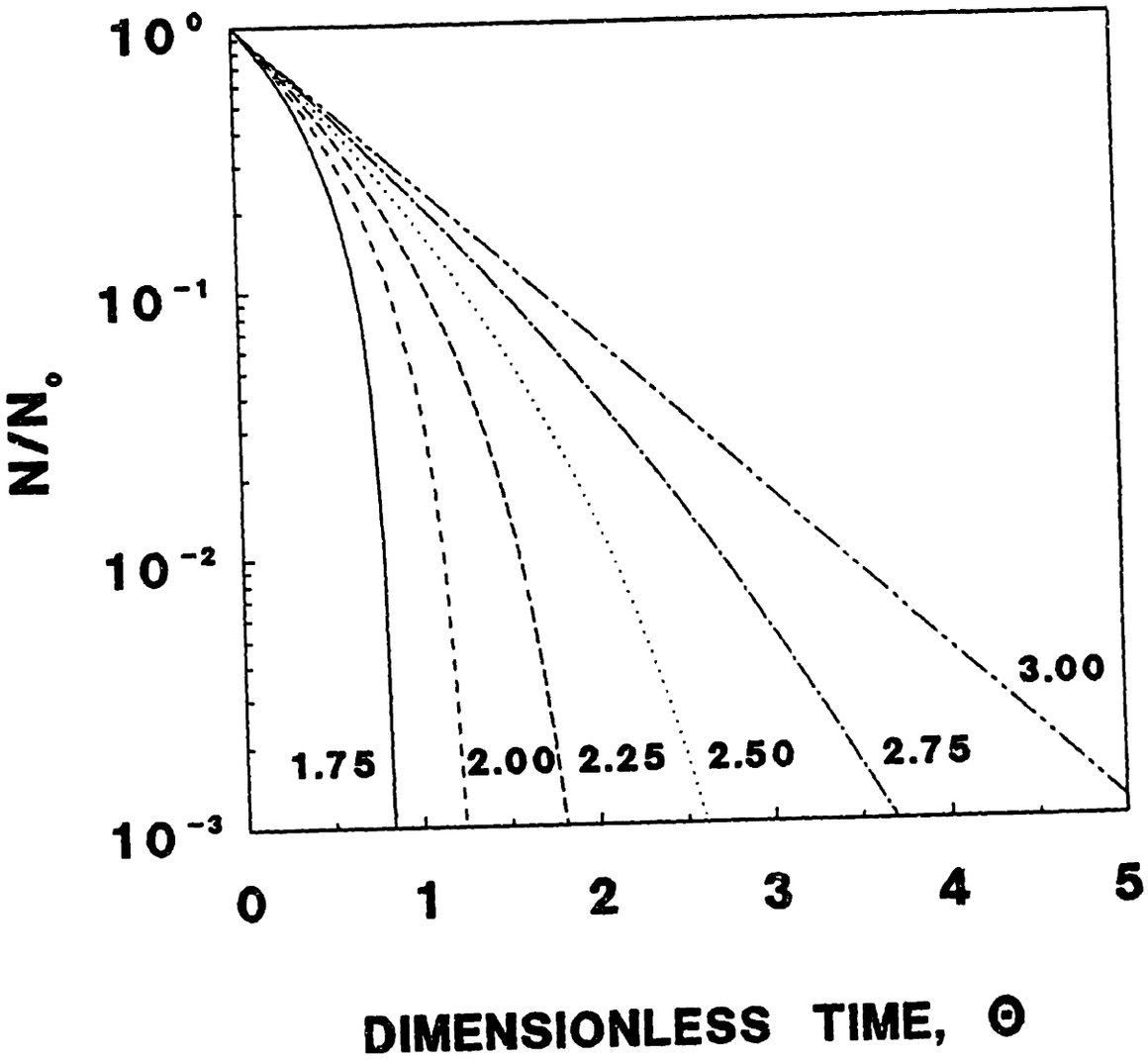

Figure 8-1. Normalized particle concentration versus dimensionless time for various fractal dimensions, with $\alpha = 1$, $\dot{\gamma} = 1\ s^{-1}$.

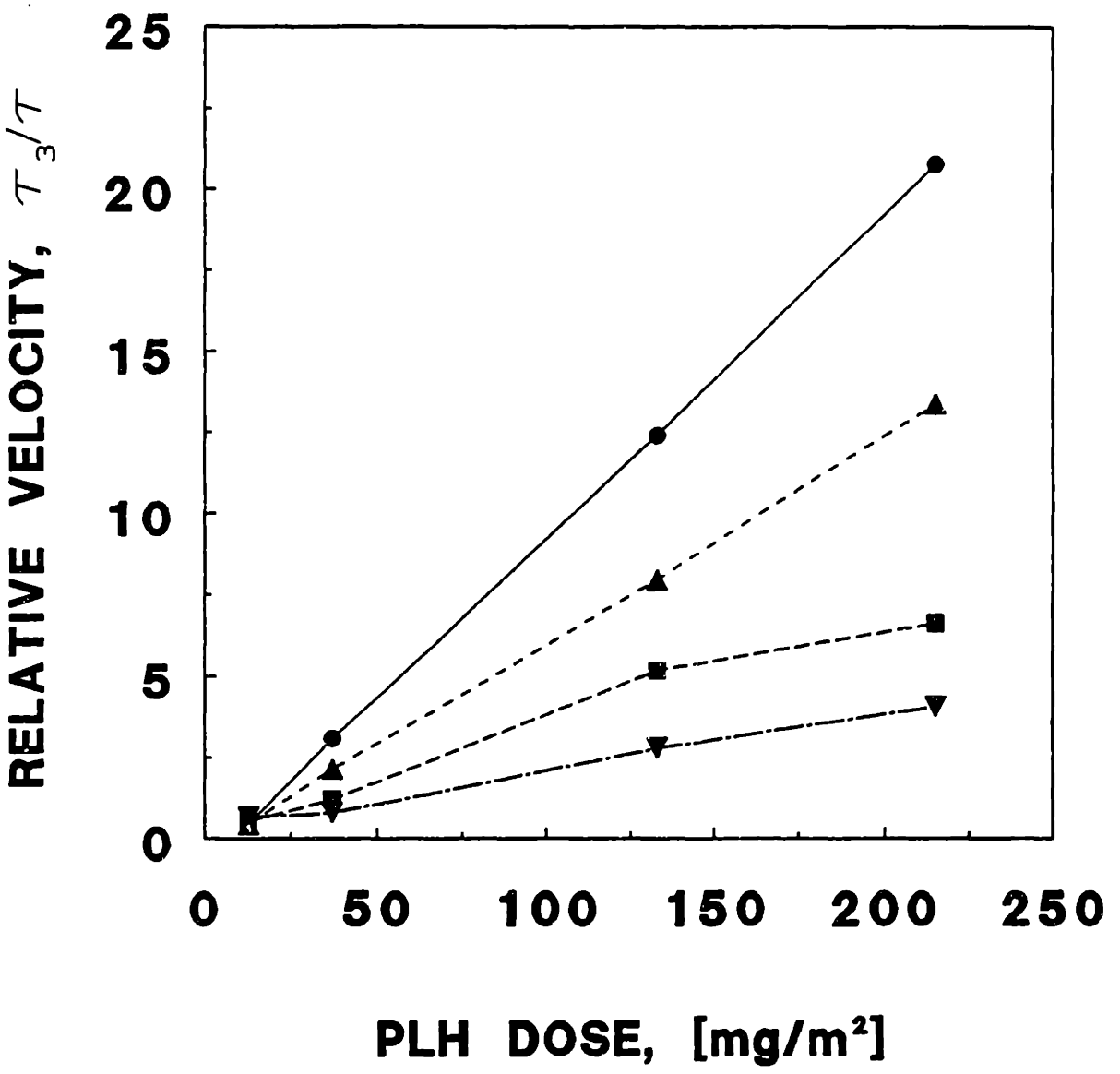

Figure 8-2. Experimental normalized flocculation rate constants versus poly-L-histidine dose at various shear rates. ▼ - 6 s^{-1}, ■ - 12 s^{-1}, ▲ 30 s^{-1}, ● - 60 s^{-1}.

due to the changes in fractal dimension at low dose the overall flocculation acceleration is roughly linear with polymer dose.

8.2. - Floc Sedimentary Properties

In addition to affecting flocculation kinetics, floc structure effects will change the floc sedimentary properties. As outlined in sections 3.6.3.2. and 7.1.2., the fractal dimension will affect the floc effective density and the friction coefficient. As developed in section 7.1.2., the relation for sedimentary velocity of an i sized floc is given by equation (7-8):

$$U_{term,i} = \frac{\frac{4}{3}\pi a_i^3 ((a_1^3 k) a_i^{D-3})(\rho_{cell} - \rho_{liq})g}{6\pi\eta k_f (k a_i^D)^{D_f}} = \left(\frac{2a_1^2 (\rho_{cell} - \rho_{liq})g}{9\eta}\right) k^{1-D_f} a_i^{D(1-D_f)} \tag{8-14}$$

Here, D_f is the fractal exponent on the floc size in the constitutive relation for floc friction coefficient (equation (7-3)), and k_f is a constant of proportionality, $O(a_1)$. k_f has been set equal to a_1 in the far right hand equality. The term in brackets on the far right hand side is the sedimentary velocity of an individual particle; this term may be brought to the left side of the equation to calculate the sedimentary velocity enhancement for a given floc size. The floc radius may also be replaced with the correlation given by equation (8-3), to give an expression in terms of i (or N_o/N), rather than the floc radius. Equation (8-14) may then be converted to the simple relation:

$$\frac{U}{U_o} = \left(\frac{N}{N_o}\right)^{D_f - 1} \tag{8-15}$$

To use this relation, a connection between D and D_f is needed. A polynomial approximation to the function D_f was proposed in section 7.1.1. as:

$$D_f = \frac{0.41}{D} - .677 + 2.31D - 1.23D^2 + .184D^3 \qquad (8\text{-}16)$$

The flocculation velocity enhancement given by (8-15) and (8-16) aggregation state and fractal dimension is shown in Figure 8-3. The difference in the sedimentary velocity enhancement is small for low degrees of particle aggregation, but is substantial for large flocs. The difference in sedimentary velocity between fractal dimensions of 1.75 and 2 is significant, so the range of fractal dimension which has been observed experimentally will affect sedimentary properties at high degrees of aggregation. Equations (8-15) and (8-16) may be combined with equation (8-10) or (8-13) to give the enhancement of sedimentary velocity explicitly versus time. Figure 8-4 shows the theoretical enhancement of sedimentary velocity versus dimensionless time for various fractal dimensions and $\alpha = 1$. The dimensionless time here has been re-scaled to the value of τ_3 with $\alpha = 1$ and $\dot{\gamma} = 1$ to place the flocculation times on a comparable, but dimensionless scale. This plot is interesting, as it shows that depending on the process time constraints, there will be several fractal dimensions which give the same sedimentary enhancement. It also shows that whereas at low flocculation times the best process is one which produces the highest fractal dimension for the flocs, at long times, the acceleration in the flocculation kinetics outweighs the retardation of sedimentary velocity to produce faster settling flocs more quickly.

For a real system with varying fractal dimensions and collision efficiencies, the behavior shown in the above graph may never materialize. Theoretical enhancement of sedimentary velocity versus dimensionless time (again re-scaled as in figure 8-4) is shown in Figures 8-5 through 8-8 for the experimental data obtained at the various PLH doses. Figures 8-6, 8-7, and 8-8 show that the increase in the collision frequency and the lowered cluster friction coefficient (from the increased fractal dimension) outweigh the decrease in the collision efficiency and cross-section presented by the more compact flocs at higher

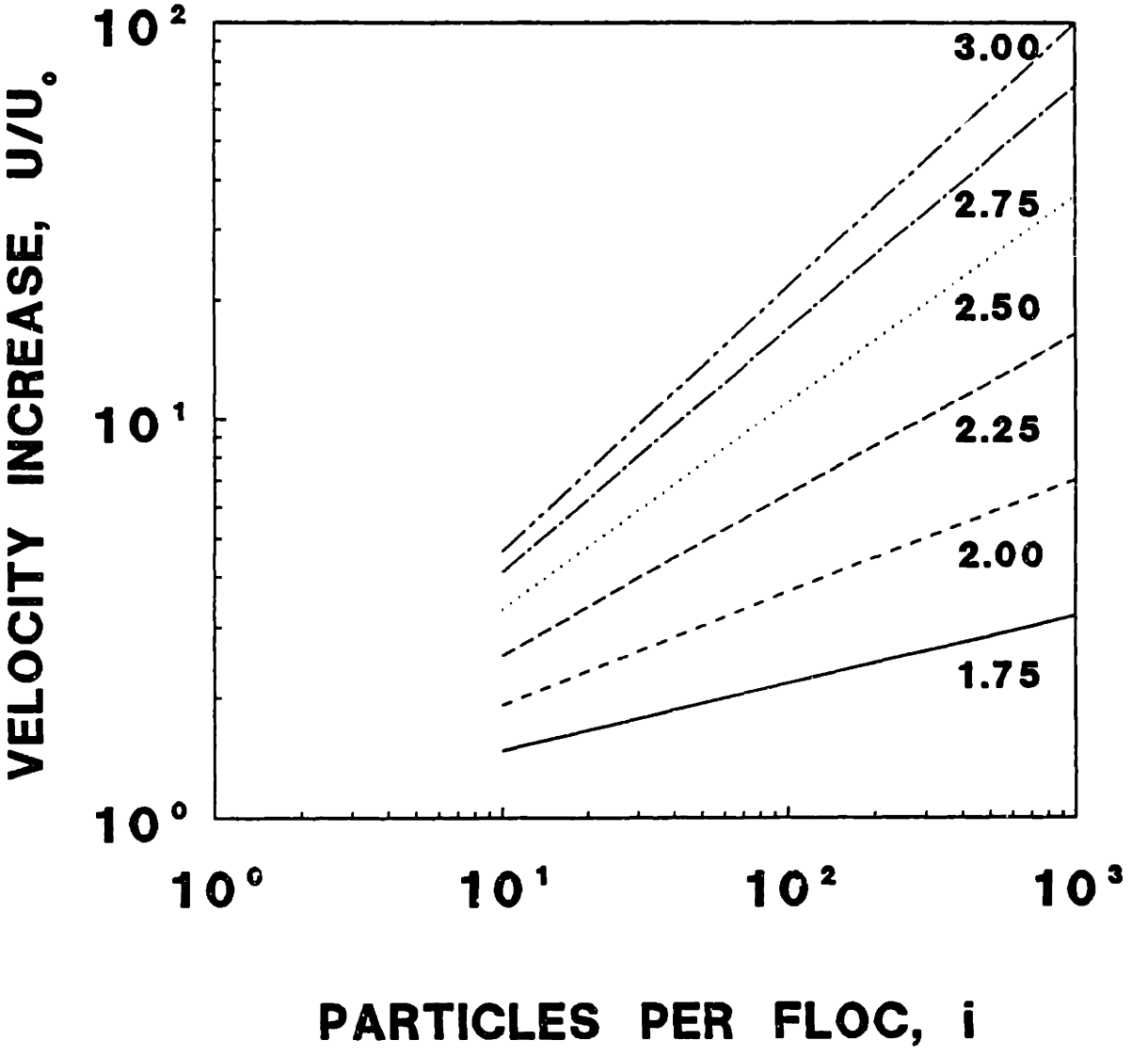

Figure 8-3. Sedimentary velocity enhancement versus the degree of flocculation for various fractal dimensions. The fractal dimensions are shown on the figure.

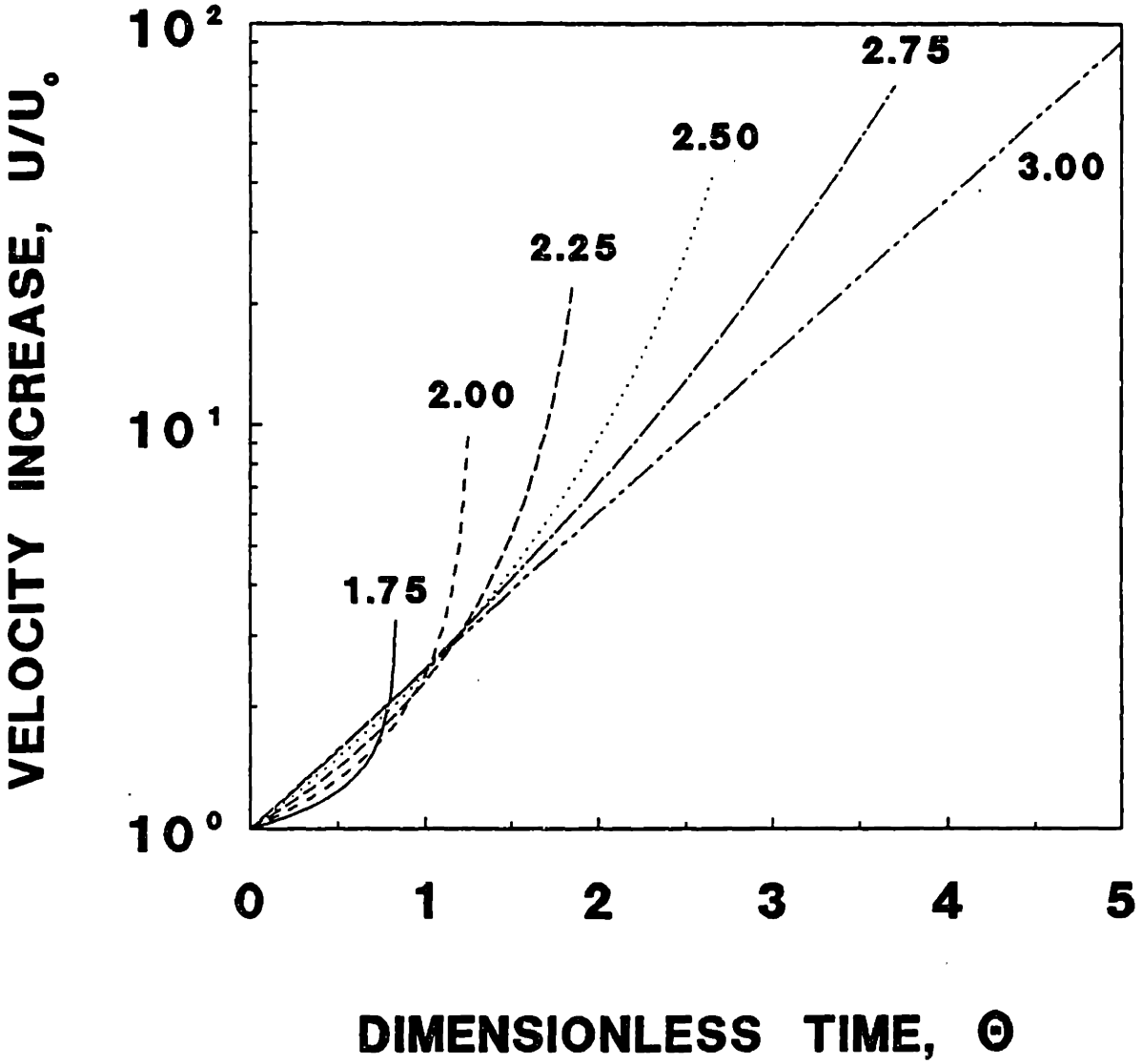

Figure 8-4. Sedimentary velocity enhancement versus dimensionless time for various fractal dimensions, with $\alpha = 1$, $\dot{\gamma} = 1\ s^{-1}$. The fractal dimensions are shown on the figure.

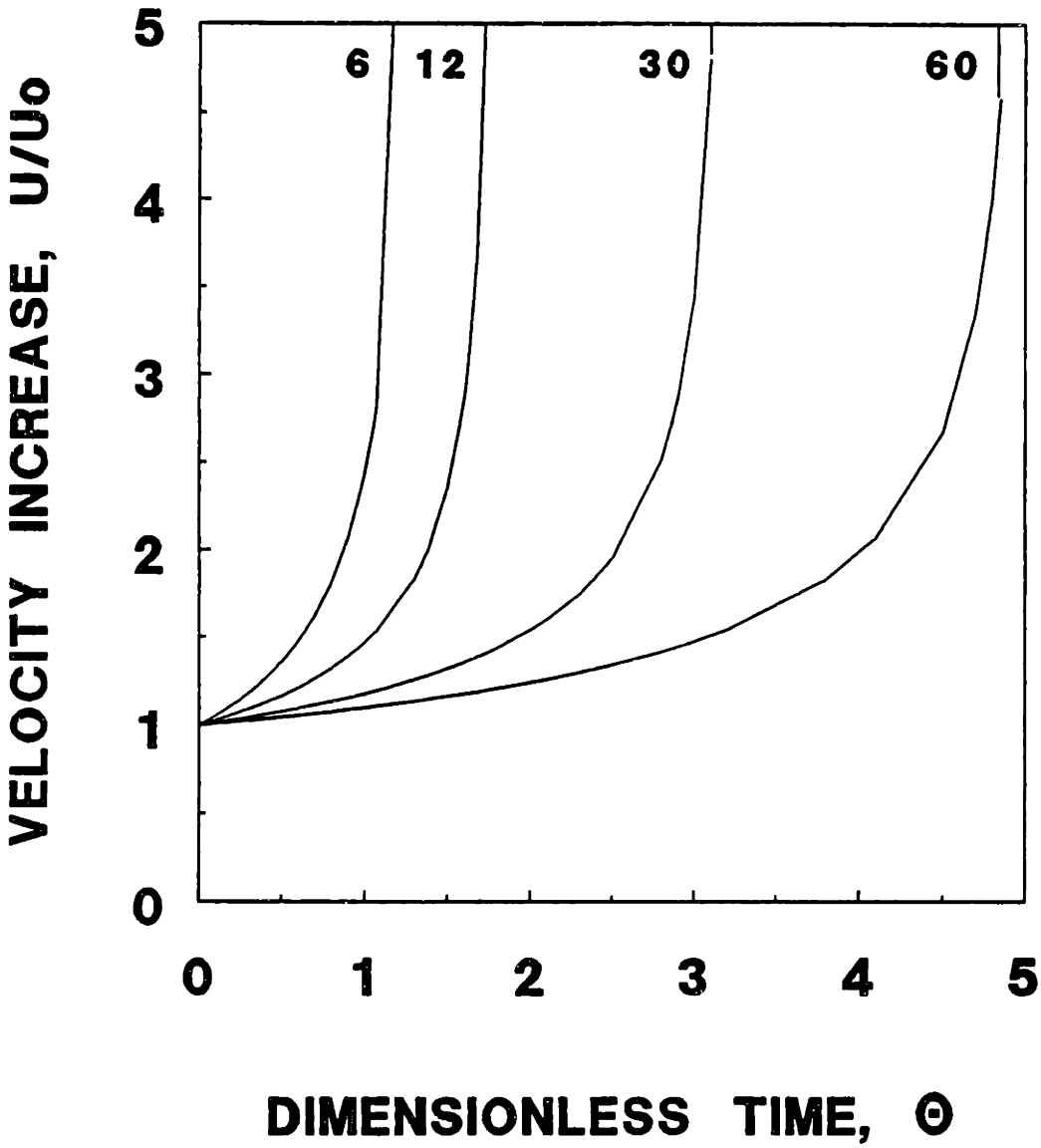

Figure 8-5. Sedimentary velocity enhancement versus dimensionless time predicted by equations (8-10), (8-15) and (8-16) for a polymer dose of 12 mg PLH/m^2, using the experimental data from chapters 6 and 7. The values of fluid shear rate are shown on the figure.

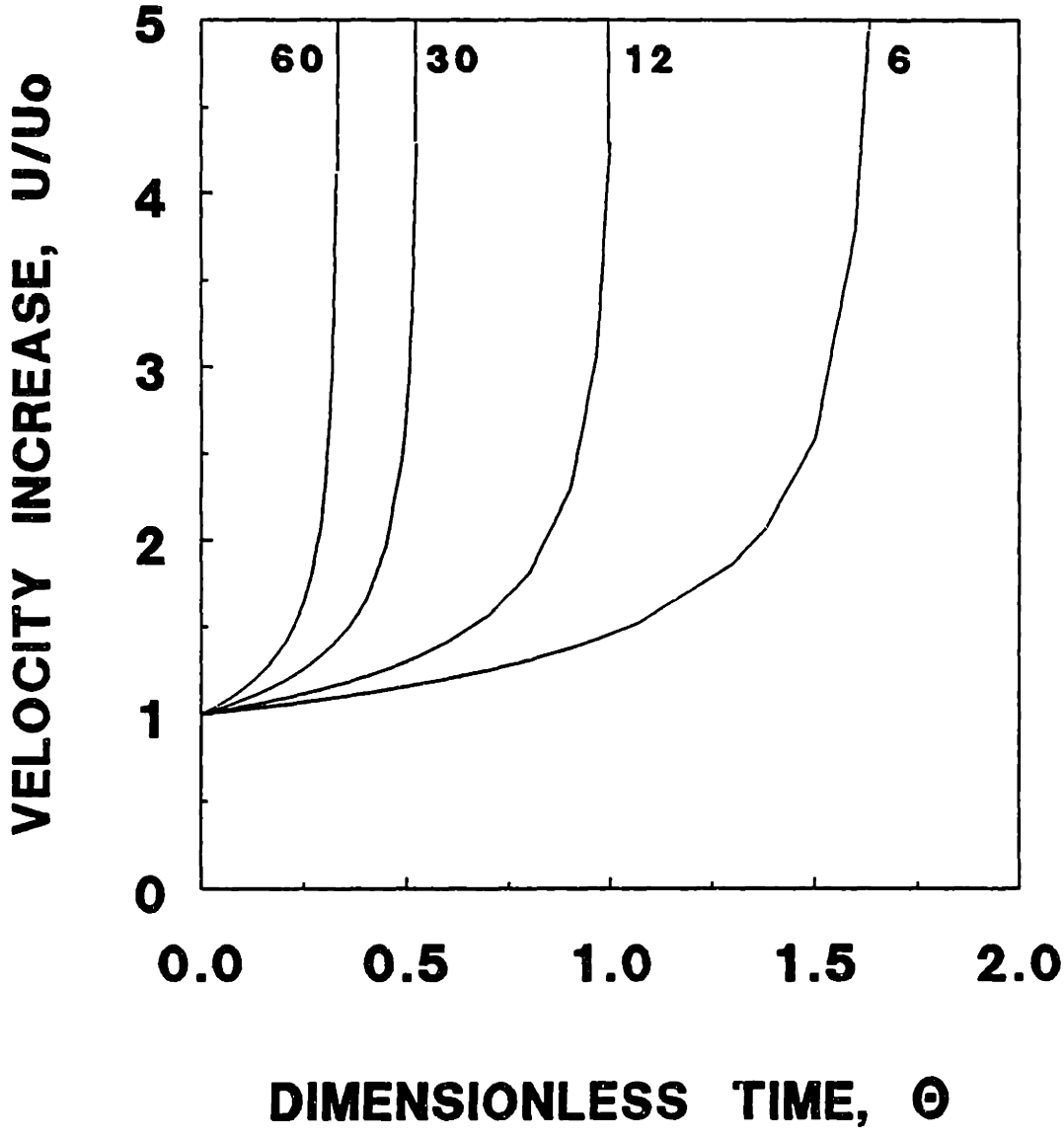

Figure 8-6. Sedimentary velocity enhancement versus dimensionless time predicted by equations (8-10), (8-15) and (8-16) for a polymer dose of 40 mg PLH/m^2, using the experimental data from chapters 6 and 7. The values of fluid shear rate are shown on the figure.

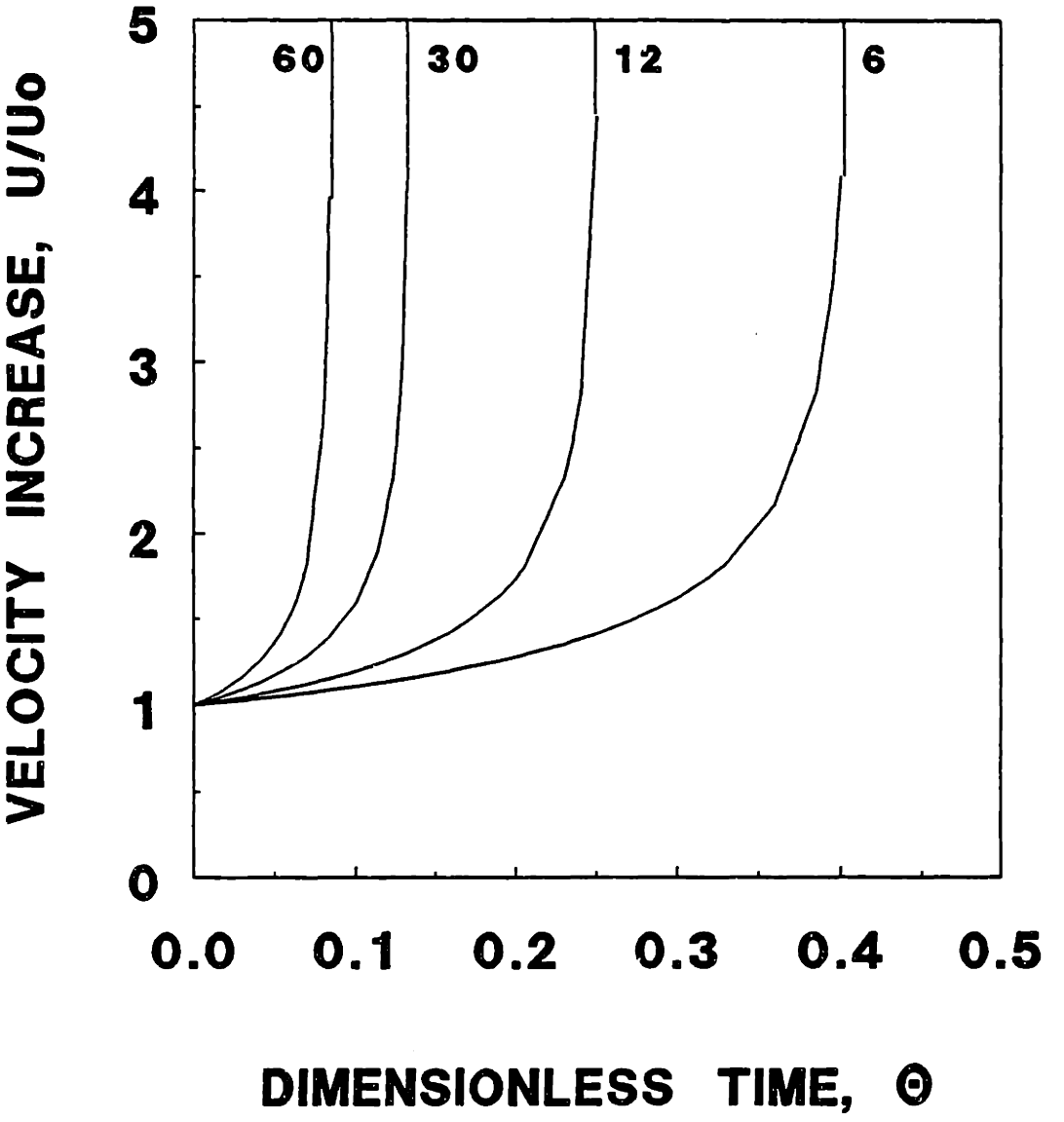

Figure 8-7. Sedimentary velocity enhancement versus dimensionless time predicted by equations (8-10), (8-15) and (8-16) for a polymer dose of 133 mg PLH/m^2, using the experimental data from chapters 6 and 7. The values of fluid shear rate are shown on the figure.

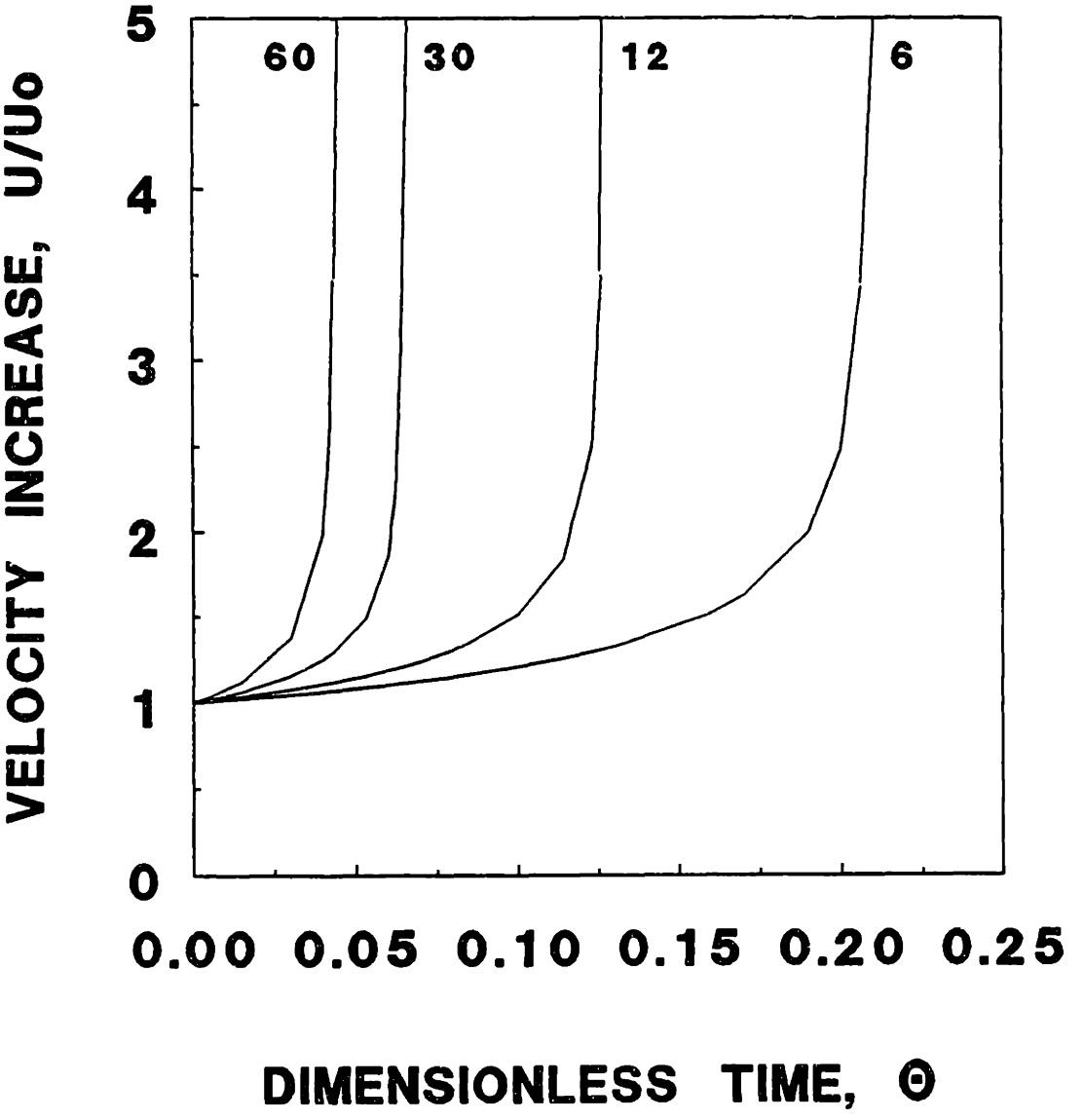

Figure 8-8. Sedimentary velocity enhancement versus dimensionless time predicted by equations (8-10), (8-15) and (8-16) for a polymer dose of 215 mg PLH/m^2, using the experimental data from chapters 6 and 7. The values of fluid shear rate are shown on the figure.

shear rates. Thus, increasing the process shear rate will enhance the sedimentary velocity more quickly. Figure 8-5 shows the opposite trend however. At this low polymer dose, decreasing the fluid shear rate increases sedimentary velocity more quickly due to the strong collision efficiency dependency on shear. The fact that the different fractal dimensions obtained do not heavily influence the results again illustrates that for the range of fractal dimensions found, the system performance will be collision efficiency and frequency dominated.

8.3. - Flocculation Process Optimization

The above sections have simplistically outlined the effects of non-idealities on the flocculation and sedimentation behavior of a system. It is of interest to apply these results to animal cell flocculation with the data at hand in order to analyze the ramifications of process parameters on flocculation, sedimentation, and culture performance.

Briefly recapping the experimental results with CRL 1606 and poly-L-histidine, collision efficiency decreases with shear rate by the -0.35±.05 power for moderate to high polymer doses. At the lowest doses, collision efficiency dependency on shear rate is to the -1.2 power. The fractal dimension of the flocs was found to vary from 1.76 to 2.05 under the conditions studied. The fractal dimension increased with decreasing polymer dose, showing greatest sensitivity at low polymer dosage. The effect of the shear rate on the fractal dimension is mild for shear rates between 6 and 60 s^{-1}. The effect of polymer dose on cell viability was shown to be a decaying function of polymer dose, which plateaus out at around 60% viability at high polymer doses. The effect of hydrodynamic conditions on cell death was not investigated.

The sedimentary enhancement versus aggregation state, fractal dimension and dimensionless flocculation time was shown in Figures 8-5 through 8-8 for the experimental data presented in chapters 6 and 7. The overall conclusion for the flocculation kinetics and

floc structure studies is that increasing the hydrodynamic intensity in the flocculation process is beneficial for enhancing the rate of clarification of the resulting suspension. The same applies for increasing the flocculant dose. The exception to this rule is at very low polymer doses, where floc breakage or rearrangement may be significant, altering the collision frequencies and the fractal dimensions from the high polymer coverage cases. Predictions of the flocculation velocity and sedimentation enhancement are reversed at these low doses due to the overriding effect of the collision efficiency.

The combination of factors influencing sedimentary enhancement is always decreasing with polymer dose over the range of doses and shear rates investigated. That is, a low shear rate with a low polymer dose produces flocs with a high fractal dimension and little loss in effective collision frequency over a moderate polymer dose. This still does not increase sedimentation velocity faster than a moderate dose of polymer at the same shear rate, which produces a lower fractal dimension and only slightly higher effective collision frequency. This is seen by a plot of sedimentary velocity enhancement versus time for a constant shear rate of 6 s^{-1} and varying polymer dose in Figure 8-9. Although it might be hoped that the low polymer case would give better aggregation than higher doses to minimize polymer usage and toxicity to the cells, this is unfortunately not the case for the experimental data at hand. It is highly likely, however, that the hydrodynamic and polymer dose conditions under which flocs are generated will affect the subsequent viability of the cells. Although Figure 8-9 shows that higher polymer doses produce large floc faster, these flocs will also be less viable than the low polymer, low shear flocs.

The viability of the flocs must be factored into process optimization to determine the polymer dosage and fluid conditions which produce acceptably viable flocs in the shortest flocculation time. A viability versus flocculation time curve may be generated for a given sedimentary velocity enhancement, and process time and viability constraints will determine the process operating conditions. There are three variables of interest in process

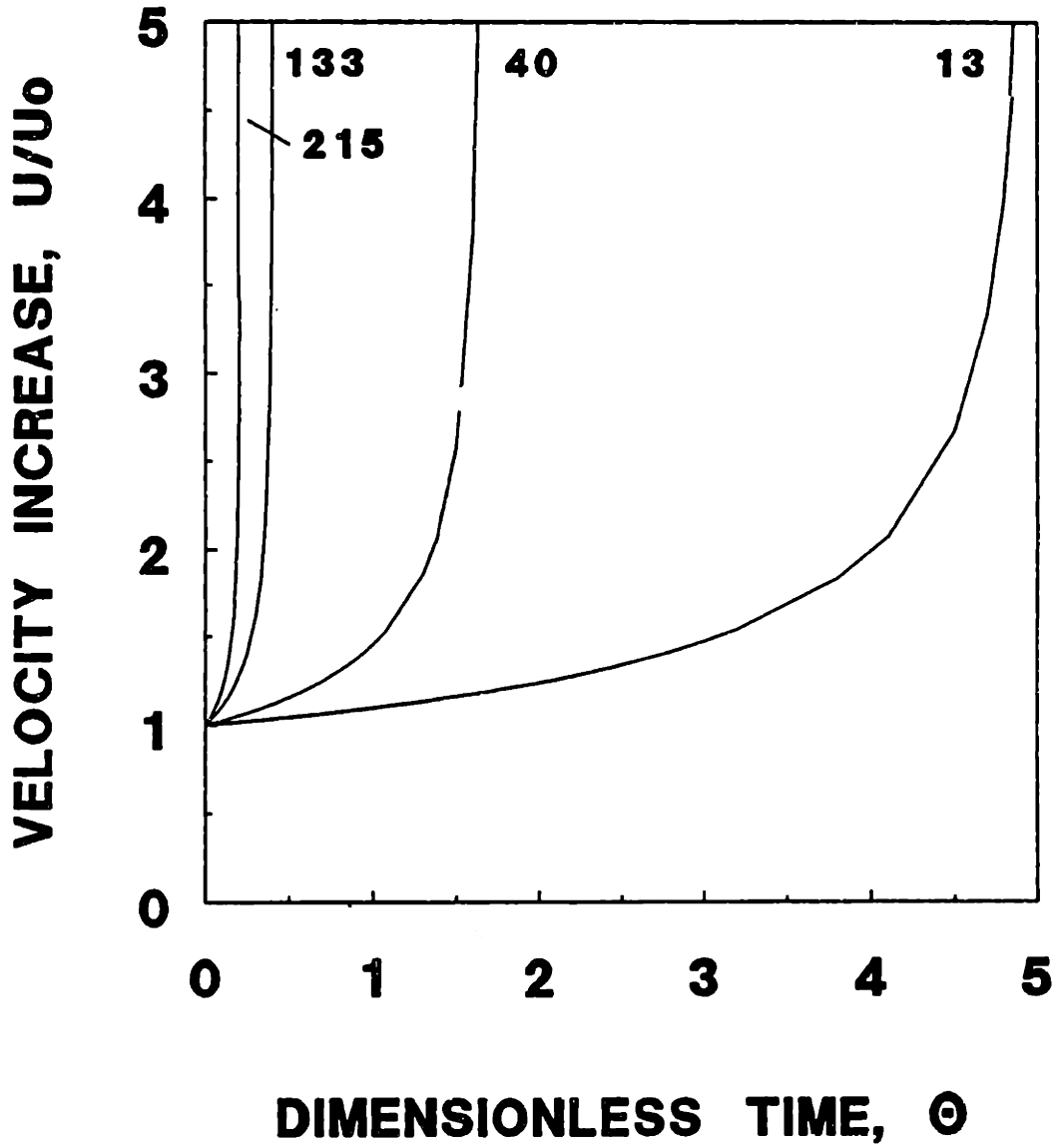

Figure 8-9. Sedimentary velocity enhancement versus dimensionless time predicted by equations (8-10), (8-15) and (8-16) for a shear rate of 6 s^{-1}, using the experimental data from chapters 6 and 7. The values of polymer dose in mg/m^2 are shown on the figure.

optimization: the flocculation time, the cell viability, and the sedimentary enhancement. Fixing two of these will determine the third, along with the process operation conditions necessary to achieve the operating state. Since sedimenter operation is usually fixed by the equipment and throughput, this will usually be one of the two constrained variables. The cell viability may then be plotted versus the necessary flocculation time for various operating conditions.

Assuming cell death to be solely a function of flocculant dose, the viability versus flocculation time curves for the experimental data are shown in Figure 8-10 for the constraint of 100-fold sedimentary velocity enhancement. For other sedimentary enhancement constraints, the figure will be similar, but will have different absolute values of the characteristic flocculation time. The optimum process conditions can be seen to change depending on the constraints that are placed on the system. If flocculation time is constrained, for example at 0.5 dimensionless time units, the highest shear rate will produce the 100-fold increase in sedimentary velocity with the highest viability. This is because the polymer dose can be decreased for the higher shear rate. If the process time requirements are not as stringent, for example greater than 2.5 dimensionless time units, it can be seen that the lowest shear rate will produce the highest viability.

It is much more likely that cell viability will be the second constrained variable in the flocculation process, since the object of recycle is to return as many live cells to the bioreactor as possible. If the process is constrained to operate above 75% viability, it can be seen that the process conditions which will give the shortest flocculation time will be at the highest shear rate. If the process is constrained to operate at high viability, however, greater than 85%, the polymer dose necessary to achieve this viability places the flocculation process in the region where collision efficiency is strongly shear dependent. This is responsible for the cross-over of the constant shear rate curves. For an 85% viability constraint, the lowest shear rate produces the desired floc velocity in the shortest

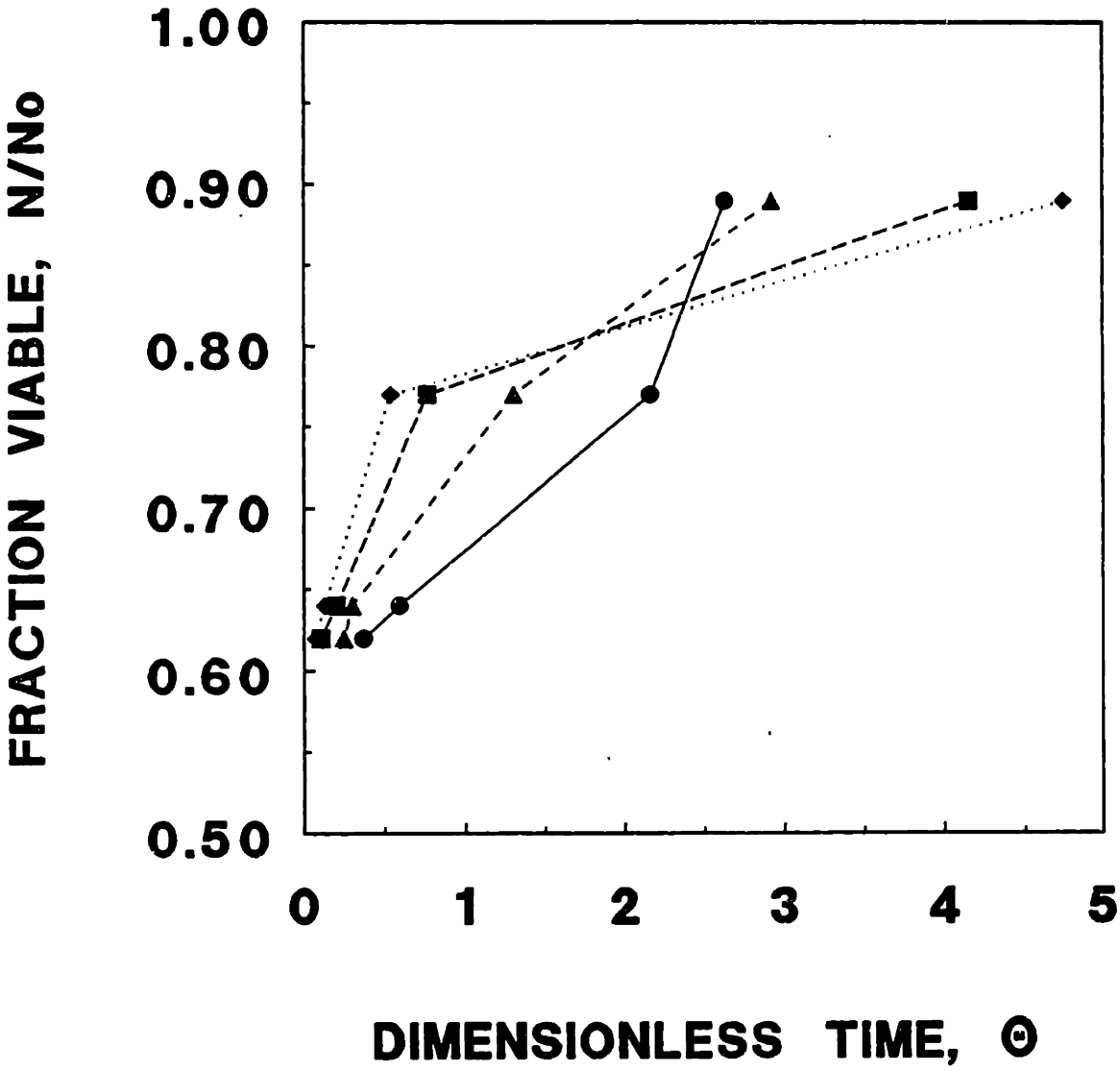

Figure 8-10. Fractional viability of CRL 1606 cells versus dimensionless flocculation time for various fluid shear rates from the experimental data of chapters 5, 6 and 7. ● - 6 s^{-1}, ▲ - 12 s^{-1}, ■ - 30 s^{-1}, ◆ - 60 s^{-1}.

time. This has been shown previously in figure 8-5. The behavior becomes interesting for the cross-over region around 80% viability. It is seen that for this value of cell viability, a moderate shear rate of 12 s^{-1} may produce the desired floc the fastest. However, more data must be obtained in this low polymer dosage region to make accurate observations on process optimization. It can be seen that in the high cell viability region in which animal cell flocculation processes would be constrained to operate, process optimization is not straightforward due to the interactions of the collision frequency, collision efficiency, and floc structure. With the current data, it appears that for high cell viability operation, the quickest process is one at low shear. Effects which have not been considered here are cell viability, maximum floc size and floc strength as functions of the hydrodynamic conditions of flocculation. These will enter into a true optimization procedure as well. For example, flocs may be so weak at the polymer level necessary to achieve 90% viability that a floc which has a 500-fold increase in sedimentary velocity cannot exist under the flocculation shear conditions necessary to generate them within a given time constraint. The current analysis is unfortunately limited to the data at hand. It illustrates, however, the utility of determining individual parameters in flocculation in order to formulate the process optimization. To completely describe and optimize the flocculation process, it will be necessary to have all of the functionalities available to solve an accurate population balance equation. This is an interesting subject for future work in the field.

9. - CONCLUSIONS

9.1. - Flocculant Characterization Conclusions

The above experiments have shown the development and characterization of a flocculant of several types of animal cells in suspension culture. It was found that where commercial flocculants were either incapable of aggregating cells or were toxic, a peptide homopolymer of L-histidine (PLH) was able to aggregate several cell lines and leave the majority viable for recycle. The cells that were not rendered nonviable by the flocculation were alive and unaffected by the polymer. It was shown that repeated harvesting of the cells was possible using PLH flocculation, and it is concluded that the goal of identifying and characterizing a system for the flocculation and recycle of animal cells had been achieved.

It is not possible to state conclusively at this point what drives PLH flocculation of cells, or what allows it to mediate flocculation without the toxicity exhibited by other compounds. The flocculation promoting activity of the polymer is most likely due to neutralization of cell surface charge by the weak base groups on the polymer. It has been inferred by several studies (Capo *et al.* (1981), Deman and Bruyneel (1974)) that electrostatic repulsion is a mechanism by which cell suspensions are stabilized. However, it is likely that stability of the initial suspension is not only due to electrostatic repulsion, but also to steric repulsion from cell surface glycoproteins. Thus, flocculation by poly-L-histidine may result from at least three possibilities. The first is the obvious neutralization of electrostatic forces. This will influence suspension stability, but in 0.15 M ionic strength medium, the Debye layer thickness is on the order of 1 nm. The particle surface potential is also not large to begin with, as will be shown in section 6.2.1. This lends further credibility to a steric factor inhibiting adhesion. Steric repulsion may originate when the configurational states of surface polysacccharides are constrained on close approach of the cells. If the particles are sterically stabilized, PLH may destabilize the

suspension in two ways. Adsorption of PLH precipitates will coat the cell surfaces and mask the polysaccharide interaction. At this point, PLH-PLH and PLH-cell contacts may occur with no steric factor to interfere. The second way in which PLH adsorption might act is if the PLH precipitates are not solid-like at their surfaces, but also have "dangling" chains. Since the high ionic strength milieu provides poor solvent conditions for PLH (as witnessed by the low solubility), the free energy of the dangling chains is reduced upon contact with other dangling chains (or cell surface polysaccharides) on another particle. The net result here is a steric attraction caused by reduction of PLH free energy on association with itself or bare cell surface. The relative magnitudes and operative ranges of steric and Van der Waals interactions need to be known in order to test this idea. In addition to these strictly physical explanations, there is also the possibility of molecular recognition of nonionized histidine. This is not likely, since histidine present in the medium at comparable concentrations (30 mg/L) should compete with polyhistidine for adsorption.

It appears that the combination of low ionization and having the flocculant in the solid phase is responsible for the lowered toxicity of polyhistidine relative to the strong polycations tested. This is consistent with the evidence of Hartmann and Galla (1978), which showed that strong polycation adsorption caused liposome membrane deformation and crystallization. Such adsorption may be responsible for cell death. Wang and Huang (1984) also found that poly-L-histidine promotes fusion of liposomes at low pH, where the above experiments have demonstrated PLH toxicity. However, these researchers also found that polyhistidine was much less effective at promoting liposome fusion at neutral pH, where the above experiments demonstrate attenuated toxicity. This suggests that the lowered ionization weakens the polymer-membrane association, and allows viable aggregation of cells.

Wang and Huang do not mention PLH precipitation in their experiments at neutral pH; however, it is evident from the differences in the toxicity of soluble and insoluble forms of poly-L-lysine and DEAE dextran that the solid state is preferable for interaction with the cell surface. However, Bentonite and chitosan, both solid phase substances in cell culture medium, were both toxic to CRL 1606. It appears that it is necessary but not sufficient for the flocculant to be in the solid state. A reduction in the adhesive force as well as a favorable adhesion geometry may also be necessary. That is, the degree of toxicity may be dependent on the shape and local structure of the particulate flocculant. As with hypotheses for adsorption driving force, the microscopic geometry of the flocculant binding is not available through the above experiments. Polyhistidine shows ordered conformation (Oshima and Kumanotani (1986)) at alkaline pH in precipitate gels and in solid form, whereas it is a random coil at low pH. This may lead to unique properties which reduce toxicity. This is consistent with the behavior of polylysine as well; where polylysine is a random coil in aqueous solution at neutral pH, polylysine adsorbed to culture dishes may present an essentially planar surface (as do microcarriers with DEAE dextran groups). Bentonite and other colloidal clays may present "sharp" plate edges with cationic charge which are able to deform the membrane and cause cell death.

It is not difficult to think of additional experiments which may elucidate the forces and geometry of association between the cell membrane and flocculant compounds. Many of these could be fairly straightforward experiments using idealized models of the cell membrane and novel polymers or solid phases for interaction. Without an extensive program aimed at elucidating and minimizing the factors responsible for toxicity, however, further study and screening of flocculant compounds will be fruitless. Since it was not the goal of this thesis to understand cell-flocculant interactions on a microscopic basis, these experiments have not been performed.

9.2. - Collision Efficiency Conclusions

The theory developed in section 6.1. is a unification of existing ionic coagulation and polymer flocculation collision efficiency literature. It points out common themes of both sets of theory, and provides the basis for more rigorous treatments of polymer flocculation collision efficiency. In the theoretical development, the focus was on the contributions of the electrostatic force to the particle collision efficiency, since this is the major factor which changes upon polyelectrolyte adsorption to particles. The dimensional analysis proposed in equation (6-2) and modified in equation (6-15) can take into account the factors of particle size ratio, Van der Waals force influences, and steric repulsion or attraction from adsorbed or soluble species. Although the current theory is no substitute for correctly posing the equations of motion with appropriate interaction terms, due to the difficulty of solution of these equations, it is a convenient method for setting expectations of particle collision efficiency under various conditions.

In section 6.2., the collision efficiencies of individual animal cells were determined versus the major independent variables of flocculation: the shear rate, medium viscosity, and polymer dosage. The collision efficiency behavior exhibited the classical, expected power law functionality with respect to the two dimensionless groups C_{RA} and C_A at moderate to high polymer doses. The dependency on C_{RA} was similar to experiments on ionic coagulation of latex and other sols. The dependency on C_A was similar to theoretical developments of collision efficiency for ionic coagulation. Since we are aggregating animal cells, investigations have necessarily been conducted under narrow physiochemical constraints. Although it was not possible (or desirable in this case) to test variables over a large range, these experiments indicate that the dimensional analysis of interparticle forces and hydrodynamic interactions is valid in determining particle collision efficiencies under

destabilizing conditions. It appears that no exhaustive experimental treatment of the subject has been conducted with polymers as flocculant.

At low poly-L-histidine dose, the dependency of the collision efficiency deviated from the strictly deterministic power law functionality proposed by equation (6-2). This was attributed to weak interparticle bonding which lowers collision efficiency, and makes the collision efficiency more sensitive to the fluid shear rate at these doses. It was shown that the phenomenon at constant shear rate could be modelled by accounting for the heterogeneity of polymer adsorption onto the cells. This necessitates a probabilistic statement of the polymer effects on the cell surface, which will be discussed below. The deterministic model of collision efficiency was combined with a constitutive equation for surface potential modification by polymer adsorption. Insertion of this relation into the collision efficiency correlation statement allowed comparison with probabilistic literature developments of collision efficiency.

Previous probabilistic theory accounts for polymer adsorption effects as modifications of local interaction forces, or surface "stickiness". The formulation proposed in section 6.1.1. describes the effect of polymer adsorption not as a stickiness *per se*, but as a modification of the net electrostatic force controlling particle collision. It is interesting that the probabilistic models reviewed in section 3.5.1.2. show the same behavior versus surface coverage as the deterministic theory. This is despite the fact that probabilistic models do not consider the magnitude of the electrostatic force between particles at different surface coverages. It was shown above that with appropriate parameter values, equation (6-6) captures the essential features of the probabilistic predictions, and is directly analogous to probabilistic formulations of collision efficiency for certain parameter values. This observation suggests that the probabilistic calculations fortuitously incorporate interparticle force by virtue of the form of calculation.

While equation (6-2) is able to describe the relative contributions of forces governing collision, it is not able to describe the random process of polymer adsorption over the range of average surface coverage as probabilistic theory can. In the development of section 6.1.2., probabilistic theory was presented to calculate the collision efficiency of particles based on the net force interaction between a number of polymer adsorption sites and their average coverage state. This theory is a modification of previous literature theory; in order to have an effective collision, the sum of the interactions of the sites must be net attractive rather than having any single attractive interaction promoting adhesion. The proposed description of collision efficiency accounts for several effects in polymer flocculation. As with previous theory for polyelectrolyte flocculation, the current theory predicts a maximum in the collision efficiency versus surface coverage, although the theories produce qualitatively different curves. In addition to a maximum versus polymer dose, the theory correctly predicts trends of collision efficiency versus molecular weight, unlike previous theory. Increased collision efficiency with higher polymer molecular weight has traditionally been viewed as a result of greater polymer extension into solution. However, this phenomenon is accounted for by the current model in a different way. For a given interaction surface area, there are fewer polymer adsorption sites for a larger polymer, producing a lower n value than a small molecular weight polymer. The current theory shows in Figure 6-3 that for small n, the range of surface coverages over which flocculation is promoted is greater.

The relevance of any theory lies in the ability to test it versus experimental data, and discriminate between it and other models. Where the previous literature theory, shown in Figures 3-2 and 3-3 gives a characteristic concave downward shape, the current collision efficiency theory (shown in Figure 6-3) is usually a bell curve shape, which sets it apart from previous literature theory. It is proposed that the shape of this curve could be used to distinguish the validity of the current formulation over previous theory. Unfortunately,

there is no literature which can be used to test this proposal other than the experiments presented above for a rather unique system of precipitating flocculant and animal cell particles. The experiments performed here show that collision efficiency follows the distinct curvature that sets the theory of section 6.1.2. apart from literature collision efficiency. The experimental results obtained with this system show that the probabilistic theory proposed here predicts normalized collision efficiencies well over the spectrum of polymer doses, and is an improvement over the averaged surface coverage formulation of equation (6-2). This led directly to the modification of equation (6-2) to equation (6-15). The probabilistic modification may be thought of as a description of average interparticle bond strength, as it calculates the fraction of configurations which produce "strong" attractive bonds. This view is bolstered by evidence of collision efficiency susceptibility to hydrodynamic forces.

In summary, the experimental collision efficiency of polyhistidine flocculated animal cells has been shown to follow the predictions of lyophobic colloid stability theory reviewed in chapter 3 and modified in section 6.1. This is an encouraging result, which in retrospect is not surprising for this system. The factors for animal cell collision which would render biophysical theory predictions invalid are not present in the current situation. The large size of the polymer precipitates will mask the presence of surface macromolecules and surface asperities which would alter collision. Although other modes of action cannot be precluded, as discussed in section 5.3., it appears from the correlation of collision efficiency with surface potential that polyhistidine acts by reducing the surface potential of the cells.

9.3. - Floc Structure Conclusions

In section 7.1.1., logical argument was presented for the use of fractal geometric and physical theory to assess suspension properties. It was proposed that in the

intermediate region between small and infinitely large flocs, the friction coefficient of a fractal cluster should follow a power law relation with a fractal exponent dependent on the fractal dimension of the cluster. From this development, relations for the floc sedimentary properties versus the floc structure, or fractal dimension, were presented. Figure 7-2 shows that for a truly fractal structure, the floc porosity calculated from settling velocity-size correlations will be in error if the experimenters are using hard sphere friction factors or drag coefficients in their calculation of the data. Analysis of the literature data in Table 7-1 shows that substantially different fractal dimensions are calculated depending on the friction coefficient assumptions made. The fractal dimensions calculated using the current friction theory are in better agreement with the theoretical literature, this work, and other independent measurements of the fractal dimension. Although the proposed form of the friction coefficient is not a rigorous development in the fluid mechanical sense, in lieu of making elaborate calculations it provides the researcher with some expectation for the frictional dependency of the structure being studied.

To make truly rigorous calculations, one of two approaches can be taken. The first is to perform calculations as Chen, Deutch, and Meakin have done using simulations which generate aggregates with different fractal dimensions. This would give the dependency of the friction coefficient on the fractal dimension. Unfortunately, the current computer models have only generated a small number of D values, so this approach will not produce enough values of D_f to generalize to the entire spectrum. It would, however, allow a more refined estimation of D_f, and would allow testing of the size limits of equation (7-3). The second method would be to ensemble average particle densities over radial position for computer generated flocs, and use this particle, or "segment" distribution to solve Brinkman's equation for a porous sphere with radially variable permeability. For this purpose, fractal theory predicts the form of the radial particle distribution in the floc to be $c(\bar{r}) = kr^{D-3}$, so this approach may be more easily generalized to fractal dimensions other

than the computer generated ones. The difficulty of this method is that a constitutive equation is required to link the porosity distribution with the permeability distribution.

The animal cell aggregates studied experimentally here showed the expected fractal behavior for randomly generated aggregates. The fractal dimension behavior versus polymer dose is consistent with the collision efficiency data in that low polymer doses produce substantially weaker flocs than moderate to large doses. This observation may be explained by either floc rearrangement or destruction. Somewhat surprisingly, the average fluid shear rate does not have as strong an effect on the fractal dimension as the polymer dose. Although the weak dependency observed may be ascribed to increasing mechanical stress on the flocs, it may also be reconciled by a gradual change in the trajectories of the colliding flocs from ballistic to pseudo-diffusive at higher levels of turbulence. Unfortunately, sedimentation experiments have not been conducted to assess whether the flocs investigated in this study exhibit the increase in frictional properties predicted by the theory proposed in section 7.1.1. More sophisticated experimental and theoretical treatments should rectify the limitations of the present work and allow truly correct assessment of the flocculation literature.

In fact, although many flocs are observed to follow trends consistent with fractal theory, the existence of long-range power law correlations of floc behavior is poor evidence for the existence of fractal structure. Although fractal geometric arguments may be accurate for inorganic flocs, the presence of growing microorganisms in biological flocs will modify the short and medium range correlations of particle density in these flocs. In keeping with current thought on floc creation (François and Van Haute (1985)), a large floc may be thought of as consisting of small floccules, which are comprised of primary particles (cells). Floccules are structures which are small enough such that they are not readily affected by fluid stress. A floc composed of floccules, however, is a dynamically changing structure due to the addition and subtraction of floccules by fluid forces. Thus,

10. - RECOMMENDATIONS FOR FURTHER RESEARCH

The results of chapters five, six, seven and eight point out several areas concerning animal cell flocculation, and flocculation in general, which merit further research. The most pertinent continuations of the current research are discussed briefly in the sections below.

10.1. - Animal Cell Flocculant Optimization

Although it was shown in chapter 5 that animal cells may be flocculated by poly-L-histidine and recycled to a bioreactor, the flocculation was not optimized to produce a scheme with minimal toxicity. Such optimization would make flocculation and sedimentation as attractive as current methods of centrifugation and microfiltration. There are two areas of immediate research which could be pursued in order to conduct such an optimization. The first is to understand the nature of the cell-flocculant interaction. The second is to explore pragmatic methods of reducing flocculant toxicity. The first area of research would be aimed at understanding the mechanism(s) by which polycation adsorption is toxic to the cells. This would focus on determining which aspect of membrane structure or function which is disrupted by the adsorption. Determination and quantification of the toxicity mechanism would make possible a rational search for (or synthesis of) flocculants for animal cell culture. Since the adsorption of flocculants used in this study is a generic chemical interaction rather than a specific biochemical one, however, a study is not likely to yield a specific cellular function which is disrupted by polycation adsorption. A more fruitful course of study would then be to determine the requirements for nontoxic association with the cell membrane. The current research, combined with results of past aggregation/agglutination studies and adherent cell culture studies suggest that there are two requirements for cell adhesion/attachment to a surface or structure. These

are a favorable geometric interaction, and a favorable chemical interaction. Several practical directions might be taken to minimize flocculant toxicity.

The first requirement for nontoxic adhesion is a favorable geometric interaction. It has been suggested by the results in this thesis that a solid or semi-solid flocculant will be advantageous to conduct flocculation. The effects of flocculant geometry could be assessed by using chemically similar flocculants, *e.g.* - cationic latex spheres with identical surface charge density (or surface potential), but with different radii. It would be expected from the chapter 5 results that as latex size decreases, toxicity would increase from more radical deformation of the membrane. It has been shown in studies of anchorage-dependent cells that below a certain minimum diameter, spherical and cylindrical supports will not promote cell growth (Perry (1987)). Polystyrene latexes are easily generated in a range of sizes from less than 100 nm to micron-sized, and may be easily derivatized to give known surface properties. Geometries other than spherical might also be explored, for example, cylindrical or flat plate. The latter might be generated by surface treating minerals which are plate-like crystals, *e.g.* - mica.

The second requirement for nontoxic adhesion is a favorable chemical interaction. The effects of the chemical interaction may be investigated by investigating solid flocculants of known and constant geometry, but varying surface properties. Using latexes of constant (and perhaps "optimum") size, it would be possible to study the effects of flocculant surface potential on the cytotoxicity, as well as other variables. For example, it is possible to generate latexes coated with surfactants or macromolecules. Such particles would allow study of flocculation via steric attraction, or via specific chemical interactions, for example, antibody-antigen interaction.

One interesting experiment would be to examine the effect of poly-L-histidine geometry and chemical nature on toxicity. For example, an anionic latex could be coated with PLH at acid pH where the polymer is soluble and highly protonated to produce a PLH

coating. This latex could then be used as a model PLH precipitate to determine independently the effects of PLH protonation and geometry.

10.2. - Flocculation Kinetics

A major theme of this thesis is that for an accurate description of flocculation, the individual processes should be quantified separately and synthesized into a simulation, rather than measuring an overall index of flocculation and fitting parameters to a simulation. This is due to the complex nature of the flocculation process, and the interaction of process variables. Although there are many subjects which need clarification in the flocculation literature, there are three areas of immediate interest. These are the theoretical collision efficiencies of particles incorporating forces other than electrostatic and Van der Waals, the collision efficiency of clusters with each other, and determination of floc populations.

The first subject, theoretical collision efficiency solutions, is of interest for the description of particle collision in the presence of macromolecules. This situation is increasingly relevant due to recent interest in steric stabilization and flocculation of colloids. It is probably also directly relevant to the stability of animal cell suspensions. As described in section 9.2., a theoretical approach would solve the equations of motion with the incorporation of steric forces. The force expressions would be derived via thermodynamic analysis of the interaction energy versus particle separation distance (see Grieg and Jones (1976), Napper (1983), Bongrand and Bell (1984)). The derivative of the interaction energy with respect to the separation distance gives the interaction force. This force can be incorporated into the equations of motion, which are then solved numerically or via perturbation techniques as previously done.

The second subject, determination of floc collision efficiencies, is of interest due to the predictions of equations (3-35) and (3-36) for floc collisions. Both of these relations were envisioned for flocs of constant porosity (permeability). These equations reason that

as the floc grows larger, the relative permeability, $1/\xi$ (see section 3.6.3.1.), goes to zero and hydrodynamic forces overwhelm the ability of the clusters to approach each other. For fractal clusters, this is not likely to be the case, as permeability increases with floc size. The ramifications of a fractal permeability distribution for floc collision were discussed in section 3.6.3.1. The experimental determination of floc collision efficiency is missing from the literature, however. This would necessitate observation of individual floc encounters, via a technique similar to that used by Goldsmith and Mason (1975), Takamura, Goldsmith and Mason (1981), and Goldsmith *et al.* (1981). To collect the necessary data would require observation of a large number of collisions. This in turn would require automation of data collection and processing. A video imaging and digitization system could be arranged to collect the necessary data with appropriate computer programming for its analysis.

The last subject is the experimental and theoretical determination of floc populations. Having obtained individual parameters for the collision rate kernel function, it is desirable to know whether a strictly aggregative population balance can describe animal cell floc formation. If a theoretical population balance solution is not capable of describing experimental floc populations, it will signal under what conditions floc breakage and rearrangement must be considered. At a minimum, such a description will improve the description of floc properties over the monodisperse development of chapter 8.

10.3. - Floc Structure and Properties

The virgin scientific territory of this thesis is the structural investigation of flocculated cells and description of structure effects on the physical properties of the cluster. There are two areas which merit study for the purpose of describing flocculation and sedimentation. These are the determination of orthokinetically produced floc structure by

improved methods, and characterization of the floc friction coefficient versus structure for both orthokinetically and perikinetically aggregated suspensions.

In the method described in section 4.7., a two-dimensional representation of the animal cell floc is obtained. A three-dimensional representation would be preferred for accurate assessment of floc characteristics. An alternative method of determining the floc structure is desirable. It is not easy to visualize methods which assess the floc structure independent of structurally dependent physical properties. The most promising method of obtaining accurate structure correlations would be a light-scattering technique. These methods potentially allow *in situ* , non-destructive structural determination on individual flocs. As pointed out in section 3.6.2.2., however, these measurements have not been applied to primary particles as large as animal cells. This is largely because the relationships between the scattering and absorption characteristics of the particle are complex for particle sizes on or above the wavelength of the scattered light. In essence, Maxwell's equations must be solved for an arbitrary geometry, size and refractive index of the scattering particle. With the advent of small, powerful computers, the application of light scattering to animal cell flocs would allow application of techniques established for smaller particles. Ideally, a "flow flocometer" could be envisioned, akin to the flow cytometers used today for studies of individual cells. Such a device would make measurements of scattered light intensity at multiple angles on individual flocs as they traverse a laser light source. In addition, total light scattering/absorption would be measured. The scattering measurements would allow calculation of the scattering center density correlation. The total absorbed/scattered light measurement would give a measure of the individual floc size (projected area). From observation of a number of flocs, the structure correlation could be deduced handily.

Perhaps more interesting than the determination of absolute floc structure is the determination of floc structure and size effects on the floc transport properties. To conduct

this study, a simple size-sedimentary velocity determination could be employed like the studies of section 3.6.2.2. It would be extremely interesting to examine the experimentally determined fractal dimensions from such a method, and compare them to independently obtained fractal dimensions. This would give information on the friction coefficient of the flocs, and would test the validity of the arguments presented in chapter 7.

In addition to conducting studies on "real" flocculating systems, a brute force method might be employed to determine floc frictional properties. Flocs of known fractal dimension could be generated using an on-lattice Monte-Carlo computer technique. The particle positions could be easily replicated in actual models from the computer information. These macroscopic model flocs could then be suspended in a fluid of known density and viscosity, and allowed to sediment at low Reynolds number. From the terminal velocity, the floc friction coefficient versus the size and fractal dimension of the floc could be unequivocally established for a number of clusters, albeit at some labor cost.

Independent of an experimental program, the theoretical calculations of floc frictional properties using Kirkwood-Riseman models should be conducted on flocs with varying fractal dimensions. This was discussed in section 9.3. Extension of the Chen, Deutch and Meakin (1984) study to other floc structures and sizes would allow great progress to be made in the description of floc properties. Such an extensive study is the computer equivalent of the experimental brute force method described above. To conduct such a study, one would generate clusters via the Monte-Carlo technique, but at random stages of aggregation, the clusters would be "frozen", and the Kirkwood-Riseman procedure performed to determinc the friction coefficient. As the clusters grow to large size, however, the number of calculations per floc rises by i^2 by the Oseen method. Thus, for large flocs, a great amount of computer time is necessary to evaluate the frictional properties for a large enough cluster ensemble to average the results meaningfully. Advanced algorithms and parallel processing computers may alleviate this stumbling block.

REFERENCES

Adema, E. (1987) M.I.T. Department of Applied Biological Sciences, Cambridge, MA. Personal communication, April 1, 1987.

Adler, P.M. (1981a)"Heterocoagulation in Shear Flow" J. Colloid & Interface Sci., 83, 106.

Adler, P.M. (1981b)"Interaction of unequal spheres. I. Hydrodynamic interaction. Colloidal forces"J. Colloid Interface Sci., 84, 461.

Adler, P.M. (1981c)"Interaction of unequal spheres. II. Conducting spheres"J. Colloid Interface Sci., 84, 475.

Adler, P.M. (1981d)"Interaction of unequal spheres. III. Experimental"J. Colloid Interface Sci., 84, 489.

Adler, P.M. (1981e)"Streamlines in and around porous particles" J. Colloid Interface Sci., 81, 531.

Alberts, B., D. Bray, J. Lewis, M. Raff, K. Roberts, J. D. Watson (1983) "Molecular biology of the cell" Garland Pub. Co., New York, p. 285.

Ali, S.I., & R.L. Zollars (1987)"Changes in coagulum configuration resulting from shear-induced coagulation" J. Colloid Interface Sci., 117, 425.

Aunins, J.G., J.M. Goldstein, M.S. Croughan, & D.I.C. Wang (1986)"Engineering developments in homogeneous culture of animal cells: Oxygenation of reactors and scaleup" Biotech. Bioeng. Symp., 17, 699.

Aunins, J.G., B.A. Woodson, T.K. Hale & D.I.C. Wang (1990)"Effects of paddle impeller geometry on power input and mass transfer to small-scale animal cell culture vessels" Biotech. Bioeng., 34, in press.

Avgerinos, G. (1988) Collaborative Research, Lexington, MA. Personal communication, Sept. 26, 1988.

Axelos, M.A.V., D. Tchoubar & R. Jullien (1986)"X-ray scattering functions of fractal structures: comparison between simulations and experiments" J. de Physique, 47, 1843.

Ballard, P.L. & G.M. Tomkins (1970)"Glucocorticoid-induced alteration of the surface membrane of cultured hepatoma cells" J. Cell Biol., 47, 222.

Bartok, W., & S.G. Mason (1957)"Particle motion in sheared suspensions. V. Rigid rods and collision doublets of spheres" J. Colloid Sci., 12, 243.

Ben Ohoud, M., F. Obrecht, L. Gatineau, P. Levitz, & H. Van Damme (1988)"Surface area, mass fractal dimension, and apparent density of powders" J. Colloid Interface Sci., 124, 156.

Biesinger, K.E., & G.N. Stokes (1986)"Effects of synthetic polyelectrolytes on selected aquatic organisms" J. Water Poll. Ctrl. Fed., 58, 207.

Birkner, F.B. & J.J. Morgan (1968)"Polymer flocculation kinetics of dilute colloidal suspensions" J. Am. Water Wks. Assoc., 60, 175.

Bongrand, P. and G.I. Bell (1984)"Cell-cell adhesion: Parameters and possible mechanisms" in "Cell surface dynamics: Concepts and models" A.S. Perelson, C. DeLisi, F.W. Wiegel, Eds., Marcel Dekker, New York, pp. 459-493.

Boycott, A.E. (1920)"Sedimentation of blood corpuscles" Nature, 104, 2621.

Brinkman, H.C. (1947)"A calculation of the viscous force exerted by a flowing fluid on a dense swarm of particles" Appl. Sci. Res., A1, 27.

Brossmer, R., & Th. Pfleiderer (1966)"Zum mechanisms der thrombozytenaggregation I" Naturwissenschaften, 53, 464.

Brown, D.E. & F.R. Abdul Salam (1984)"A new filter for cell separation" Biotech. Lett., 6, 401.

Bungay, H.R. (1979)"Shallow-depth sedimentation of yeast cells" Biotech. Bioeng., 21, 1081.

Bungay, H.R. & M. Millspaugh (1984)"Cross-flow lamellar settlers for microbial cells" Biotech. Bioeng., 26, 640.

Burger, W.C. & M.A. Stahmann (1952)"The agglutination and growth inhibition of bacteria by lysine polypeptides" Arch. Biochem. Biophys., 39, 27.

Callaghan, P.T. & D.N. Pinder (1983)"A pulsed field gradient NMR study of self-diffusion in a polydisperse polymer system: Dextran in water" Macromolecules, 16, 968.

Calleja, G.B. (1974)"On the nature of forces involved in the sex-directed flocculation of a fission yeast" Can. J. Microbiol., 20, 797.

Calleja, G.B. (1984) "Microbial aggregation", CRC Press, Boca Raton, FL.

Camp, T.R., & P.C. Stein (1943)"Velocity gradients and internal work in fluid motion" J. Boston Soc. Civil Eng., 30, 219.

Capo, C. F. Garrouste, A.M. Benoliel, P. Bongrand, & R. Depieds (1981) "Non-specific binding by macrophages: Evaluation of the influence of medium-range electrostatic repulsion and short-range hydrophobic interaction" Immun. Comm., 10, 35.

Chen, Z.-Y., J.M. Deutch, & P. Meakin (1984)"Translational friction coefficient of diffusion limited aggregates"J. Chem. Phys.,80, 2982.

Concha, F. & E.R. Almendra (1979)"Settling velocities of particulate systems, 1. Settling velocities of individual spherical particles"Int. J. Mineral Proc., 5, 349.

Coulaloglou, C.A. & L.L. Tavlarides (1977)"Description of interaction processes in agitated liquid-liquid dispersions"Chem. Eng. Sci., 32, 1289.

Curtis, A.S.G. (1967) "The cell surface: Its molecular role in development", Academic Press, London.

Curtis, A.S.G. (1969)"The measurement of cell adhesiveness by an absolute method" J. Embryol. Exp. Morph., 26, 295.

Curtis, A.S.G. & L.M. Hocking (1970)"Collision efficiency of equal spherical particles in a shear flow. Influence of London-Van der Waals forces" Trans. Faraday Soc., 66, 1381.

D'Souza, S.F., J.S. Melo, A. Deshpande, & G.B. Nadkarni (1986) "Immobilization of yeast cells by adhesion to glass surface using polyethylenimine" Biotech. Letters, 8, 643.

Darnell, J.E., H. Lodish, D. Baltimore (1986) "Molecular cell biology", Scientific American Books, New York, p. 1045.

Davidson, M.G. (1988)"The effects of molecular configuration on the hindered transport of macromolecules in microporous membranes" Ph.D. dissertation, Department of Chemical Engineering, Massachusetts Institute of Technology, Cambridge, MA, February, 1988.

Davis, R.H. & T.P. Hunt (1986)"Modeling and measurement of yeast flocculation" Biotech. Progress, 2, 91.

De Vries, A., Y. Stein, O. Stein, J. Feldman, J. Gurevich & E. Katchalski (1954) Proc. 4th Int. Congr. Intl. Soc. Hematol., VII-8, 385.

Deason, D.M. (1987)"Statistical model for bridging efficiency in polymeric flocculation" in "Flocculation in biotechnology and separation systems", Y.A. Attia, Ed., Elsevier, Amsterdam, p. 21.

Debye, P. & A.M. Bueche (1948)"Intrinsic viscosity, diffusion, and sedimentation rate of polymers in solution" J. Chem. Phys., 16, 573.

Delichatsios, M. & R.F. Probstein (1976)"Coagulation in turbulent flow: Theory and experiment"J. Colloid Interface Sci., 51, 3.

Deman, J.J. & E.A. Bruyneel (1974)"Evidence for long-range electrostatic repulsion between HeLa cells" Exp. Cell Res., 89, 206.

Dixon, J.K., & M.W. Zielyk (1969)"Control of the bacterial content of water with synthetic polymeric flocculants" Env. Sci. Tech., 3, 551.

Donaldson, T.L., E.F. Boonstra, & J.M. Hammond (1980)"Denaturation of proteins at a gas-liquid interface" J. Colloid Interface Sci., 74, 441.

Duband, J.-L. & J.P. Thiery (1984)"Adhesive molecules and their role during the ontogeny of the peripheral nervous system" in "Cellular and molecular control of direct cell interactions" H.-J. Marthy, Ed., Plenum Press, New York, pp. 85-118.

Elvin, P. & C.W. Evans (1983)"Cell adhesiveness and the cell cycle: Correlation in synchronized Balb/c 3T3 cells"Biol. Cell, 48, 1.

Elvin, P. & C.W. Evans (1984)"Cell adhesion and experimental metastasis: A study using the B16 malignant melanoma model system" Eur. J. Cancer Clin. Oncol., 20, 107.

Feke, D.L. & W.R. Schowalter (1983)"The effect of Brownian diffusion on shear-induced coagulation of colloidal dispersions" J. Fluid Mech., 133, 17.

Feke, D.L. & W.R. Schowalter (1985)"The influence of Brownian diffusion on binary flow-induced collision rates in colloidal dispersions" J. Colloid Interface Sci., 106, 203.

Forrester, J.A. (1965)"Microelectrophoresis of normal and polyoma virus transformed hamster kidney fibroblasts" in "Cell Electrophoresis", E.J. Ambrose, Ed. Little, Brown & Co., Boston, pp. 115-124.

François, R.J., & A.A. Van Haute (1985)"Structure of Hydroxide Flocs" Water Res., 19, 1249.

Gad, A.E. (1983)"Cationic polypeptide-induced fusion of acidic liposomes" Biochim. Biophys. Acta, 728, 377.

Garg, S.K., & S.S. Stivala (1978)"Assessment of branching in polymers from small-angle X-ray scattering (SAXS)"J. Polymer Sci.:Polymer Phys., 16, 1419.

Gasner, L.L. & D.I.C. Wang (1970) "Microbial cell recovery enhancement through flocculation" Biotech. & Bioeng., 12, 873.

Gasner, L.L. (1971) "Microbial cell recovery enhancement through flocculation" Ph. D. Thesis, Department of Nutrition & Food Science, Massachusetts Institute of Technology, Cambridge, MA, February 1971.

Glacken, M.W. (1987)"Development of mathematical descriptions of mammalian cell culture kinetics for the optimization of fed-batch bioreactors" Sc.D. Dissertation, Department of Applied Biological Sciences, Massachusetts Institute of Technology, Cambridge, MA, April 1987.

Glasgow, L.A., & J.-P. Hsu (1984)"Floc characteristics in water and wastewater treatment" Particulate Sci. Tech., 2, 285.

Goldsmith, H.L., O. Lichtarge, M. Tessier-Lavigne, & S. Spain (1981)"Some model experiments in hemodynamics: VI. Two-body collisions between blood cells" Biorheology, 18, 531.

Goldsmith, H.L., & S.G. Mason (1975)"Some model experiments in hemodynamics. V. Microrheological techniques" Biorheology, 12, 181.

Goren, S.L. (1971)"The hydrodynamic forces on touching spheres along the line of centers exerted by a shear field" J. Colloid Interface Sci., 36, 94.

Gregory, J. (1982)"Particle interactions in flowing suspensions" Adv. Colloid Interface Sci., 17, 149.

Grieg, R.G. & M.N. Jones (1976) "The possible role of steric forces in cellular cohesion" J. Theo. Biol., 63, 405.

Grieg, R.G., M.N. Jones & S.R. Ayad (1976) "The electrophoretic properties and aggregation of mouse lymphoma cells, Chinese-Hamster fibroblasts, and a somatic-cell hybrid" Biochem. J., 160, 325.

Grinnell, F., M. Milam, & P. Srere (1973)"Attachment of normal and transformed hamster kidney cells to substrata varying in chemical composition" Biochem. Med., 7, 87.

Gutcho, S. (1977)"Waste treatment with polyelectrolytes and other flocculants" Noyes Data Corp.: Park Ridge, NJ, pp. 38 - 80.

Hahn, H.H., & W. Stumm (1968)"Kinetics of coagulation with hydrolyzed Al (III). The rate-determining step" J. Colloid Interface Sci., 28, 134.

Harris, R.H., & R. Mitchell (1973)"The role of polymers in microbial aggregation" Ann. Rev. Microbiol., 27, 27.

Hartmann, W., H.-J. Galla (1978)"Binding of polylysine to charged bilayer membranes. Molecular organization of a lipid•peptide complex" Biochim. Biophys. Acta, 509, 474.

Henry, J.D. (1972)"Cross flow filtration" in "Recent Developments in Separation Science, vol. II", N.N. Li, Ed., CRC Press, Boca Raton, FL, p. 205.

Hermanowicz, S.W., & J.J. Ganczarczyk (1983)"Some fluidization characteristics of biological beds" Water Res., 10, 71.

Hiemenz, P.C. (1977) "Principles of Colloid and Surface Chemistry" Marcel Dekker, NY, pp. 364-373, 435-441.

Higashitani, K., R. Ogawa, G. Hosokawa & Y. Matsuno (1982a)"Kinetic theory of shear coagulation for particles in a viscous fluid"J. Chem. Eng. Japan, 15, 299.

Hodge, H.M. & S. N. Metcalfe, Jr. (1958)"Flocculation of bacteria by hydrophilic colloids" J. Bacteriol., 75, 258.

Hogg, R. (1984)"Collision efficiency factors for polymer flocculation" J. Colloid & Interface Sci., 102, 232.

Horikoshi, T., A. Nakajima, & T. Sakaguchi (1981)"Studies on the accumulation of heavy metal elements in biological systems. XIX. Accumulation of uranium by microorganisms" Eur. J. Appl. Microbiol. Biotechnol., 12, 90.

Humphreys, T., T. Humphreys, & J. Sano (1977) "Organization of sponge polysaccharides and aggregation factor" J. Supramol. Struct., 7, 339.

Hurd, A.J. & W.L. Flower (1988)"*In situ* growth and structure of fractal silica aggregates in a flame"J. Colloid Interface Sci., 122, 178.

Israelachvili, J.N. (1985) "Intermolecular and Surface Forces" Academic Press, New York, p. 139.

Jan, K.-M., S. Usami & S. Chien (1982)"The disaggregation effect of dextran 40 on red cell aggregation in macromolecular suspensions" Biorheology, 19, 543.

Jensen, J.W., R.M. Debusk, & A.G. Debusk (1984)"Induction of cellular efflux by a galactosamine polymer from *Neurospora crassa*" J. Gen. Microbiol., 130, 557.

Jones, M.N. (1976) "Hydrogen bonding in cellular cohesion" FEBS Letters, 62, 21.

Jones, M.N., & R. Perry (1979)"The kinetics of cellular aggregation induced by turbulent flow" J. Theo. Biol., 81, 75.

Jones, M.N., & R. Perry (1980)"The application of particle size analysis to the aggregation of Chinese Hamster Cells by Concanavalin A" Exp. Cell Res., 128, 41.

Jullien, R., R. Botet, & P.M. Mors (1987)"Computer simulations of cluster-cluster aggregation" Faraday Discuss. Chem. Soc., 83, 125.

Karkare, S.B., P.G. Phillips, D.H. Burke, & R.C. Dean (1985)"Continuous production of monoclonal antibodies by chemostatic and immobilized hybridoma culture" in "Large-Scale Mammalian Cell Culture", Academic Press, NY, pp. 127-149.

Katchalski, E., L. Bichowski-Slomnitzki & B.E. Volcani (1953)"The action of some water-soluble poly-α-amino acids on bacteria" Biochemistry, 55, 671.

Katchalski, E., & M. Sela (1958)"Synthesis and chemical properties of poly-α-amino acids" Adv. Protein Chem., 13, 243.

Katchalsky, A. (1964)"Polyelectrolytes and their biological interactions" Biophys. J., 4, 9.

Katchalsky, A., D. Danon, A. Nevo, A. De Vries (1959)"Interactions of basic polyelectrolytes with the red blood cell. II. Agglutination of red blood cells by polymeric bases." Biochim. Biophys. Acta, 33, 120.

Kenney, A.C. (1985)"A process for separating animal cells from a liquid culture" European Patent 0 160 520.

Kenney, A.C. (1986)"Separating animal cells from a liquid culture" U.S. Patent 4,589,987.

Kilejian, A. (1976)"Does a histidine-rich protein from *Plasmodium lophurae* have a function in merozoite penetration?" J. Protozool., 23, 272.

Kim, S.G., & J.R. Brock (1987)"Growth of ferromagnetic particles from cation reduction by borohydride ions" J. Colloid Interface Sci., 116, 431.

Kirkwood, J.G., & J. Riseman (1948)"The intrinsic viscosities and diffusion coefficients of flexible macromolecules in solution" J. Chem. Phys., 16, 565.

Klimpel, R.C., C. Dirican, & R. Hogg (1986)"Measurement of agglomerate density in flocculated fine particle suspensions" Particulate Sci. Tech., 4, 45.

Klimpel, R.C. & R. Hogg (1986)"Effects of flocculation conditions on agglomerate structure" J. Colloid Interface Sci., 113, 121.

Knorr, D. & R.A. Teutonico (1986)"Chitosan Immobilization and Permeabilization of *Amaranthus tricolor* Cells" J. Agric. Food Chem., 34, 96.

Knox, R.J., F.J. Nordt, G.V.F. Seaman, & D.E. Brooks (1977)"Rheology of erythrocyte suspensions: Dextran-mediated aggregation of deformable and nondeformable erythrocytes" Biorheology, 14, 75.

Koh, P.T.L., J.R.G. Andrews & P.H.T. Uhlherr (1987) "Modelling shear-flocculation by population balances" Chem. Eng. Sci., 42, 353.

Kroner, K.H. & V. Nissinen (1988)"Dynamic filtration of microbial suspensions using an axially rotating filter"J. Membrane Sci., 36, 85.

Kuboi, R., I. Komasawa, & T. Otake (1972a)"Behavior of dispersed particles in turbulent flow"J. Chem. Eng. Japan, 5, 349.

Kuboi, R., I. Komasawa, & T. Otake (1972b)"Collision and coalescence of dispersed drops in turbulent liquid flow"J. Chem. Eng. Japan, 5, 423.

Lagvankar, A.L. & R.S. Gemmell (1968)"A size-density relationship for flocs" J. Am. Water Works Assoc., 9, 1040.

Larsen, B. & K. Olsen (1968)"Inhibitory effect of polycations on the transplantability of mouse leukaemia reversed by heparin" Eur. J. Cancer, 4, 157.

Levich, V. (1962)"Physicochemical hydrodynamics" Prentice-Hall, Englewood Cliffs, NJ, pp. 207-230.

Levine, D.W., D.I.C. Wang, & W.G. Thilly (1979)"Optimization of growth surface parameters in microcarrier cell culture" Biotech. Bioeng., 21, 821.

Levine, S. & W.I. Friesen (1987)"Flocculation of colloid particles by water-soluble polymers" in "Flocculation in biotechnology and separation systems", Y.A. Attia, Ed., Elsevier, Amsterdam, p. 3.

Li, D.-H. & J.J. Ganczarczyk (1987)"Stroboscopic determination of settling velocity, size and porosity of activated sludge flocs"Water Res., 21, 257.

Li, D.-H. & J.J. Ganczarczyk (1988)"Flow through activated sludge flocs"Water Res., 22, 789.

Lim, F. & R.D. Moss (1981)"Microencapsulation of living cells and tissues"J. Pharm. Sci., 70, 351.

Linnemans, W.A.M., P.H. Wiersema, F. Spies, & P.F. Elbers (1976a)"A kinetic model for cell agglutination" Exp. Cell Res., 101, 184.

Linnemans, W.A.M., F. Spies, Th.M.de Ruyter de Wildt, & P.F. Elbers (1976b) "Kinetics of cell agglutination: A quantitative assay of concanavalin A mediated agglutination of *Acanthamoeba castellani*" Exp. Cell Res., 101, 191.

Logan, B.E. & J.R. Hunt (1988)"Bioflocculation as a microbial response to substrate limitations"Biotech. Bioeng., 31, 91.

Logtenberg, E.H.P., & H.N. Stein (1985)"Coagulation in a shear field generated by stirring in a cylindrical vessel" J. Colloid Interface Sci., 104, 258.

Lu, C.F., & L.A. Spielman (1985)"Kinetics of floc breakage and aggregation in agitated liquid suspensions" J. Colloid Interface Sci., 103, 95.

Lydersen, B.K., G.G. Pugh, M.S. Paris, B.P. Sharma, & L.A. Noll (1985)"Ceramic matrix for large scale animal cell culture" Bio/Technology, January, 1985, 63.

Mamelak, M., S.L. Wissig, R. Bogoroch, I.S. Edelman (1969)"Physiological and morphological effects of poly-L-lysine on the toad bladder" J. Membrane Biol., 1, 144.

Mandelbrot, B.B. (1982)"The fractal geometry of nature",W.H. Freeman & Co., NY.

Manley, R.St.J., & S.G. Mason (1952)"Particle motions in sheared suspensions. II. Collisions of uniform spheres" J. Colloid Sci., 7, 354.

Maroudas, N. (1975)"Adhesion and spreading of cells on charged surfaces" J. Theo. Biol., 49, 417.

Marshall, K.C. (1985)"Mechanisms of bacterial adhesion at water-solid interfaces" in "Bacterial adhesion: mechanisms and physiological significance" D.C. Savage, M. Fletcher, Eds. Plenum Press, NY, pp. 133 - 161.

Mason, S.G. (1977)"Orthokinetic phenomena in disperse systems"J. Colloid Interface Sci., 58, 275.

McCord, R.W., E.W. Blakeney, Jr., W.L. Mattice (1977)"Conformational changes induced in ionized poly(L-arginine) and poly(L-histidine) by sodium dodecyl sulfate" Biopolymers, 16, 1319.

McGarry, M. (1970) "Algal flocculation with aluminum sulfate and polyelectrolytes" J. Water Poll. Ctrl. Fed., 42, r191.

McKeehan, W.L., & R.G. Ham (1976)"Stimulation of clonal growth of normal fibroblasts with substrata coated with basic polymers" J. Cell Biol., 71, 727.

Meakin, P. (1984)"Particle-cluster aggregation with fractal particle trajectories and on fractal substrates" in "Kinetics of aggregation and gelation", F. Family, D.P. Landau, Eds., Elsevier, Amsterdam, pp. 91-99.

Meakin, P. (1988a)"Fractal aggregates" Adv. in Colloid Interface Sci., 28, 249.

Meakin, P. (1988b)"A multifractal description of the hydrodynamic force distribution for reaction-limited aggregates" J. Chem. Phys., 88, 2042.

Meakin, P., Z.-Y. Chen, & P. Evesque (1987)"Aggregation of anisotropic particles"J. Chem. Phys., 87, 630.

Meakin, P. & J.M. Deutch (1987)"Properties of the fractal measure describing the hydrodynamic force distributions for fractal aggregates moving in a quiescent fluid"J. Chem. Phys., 86, 4648.

Meakin, P. & Z.B. Djordjevic (1986)"Cluster-cluster aggregation in two-monomer system" J. Phys., A19, 2137.

Melik, D.H., & H.S. Fogler (1984)"Gravity-induced flocculation" J. Colloid Interface Sci., 101, 72.

Melik, D.H., & H.S. Fogler (1985)"Prediction and measurement of initial flocculation rates in quiescent media" J. Colloid Interface Sci., 108, 503.

Mifflin, R.T. & W.R. Schowalter (1988)"Flocculation of colloids suspended in a viscoelastic fluid undergoing shear"AIChE J., 34, 1839.

Mijnlieff, P.F., & F.W. Wiegel (1978)"Intrinsic viscosity and friction coefficient of polymer molecules in solution: Porous sphere model" J. Polymer Sci.: Polymer Phys., 16, 245.

Mill, P.J. (1964) "The nature of the interactions between flocculent cells in the flocculation of *Saccharomyces cerevisiae*" J. Gen. Microbiol., 35, 61.

Mors, P.M., R. Botet, & R. Jullien (1987)"Cluster-cluster aggregation with dipolar interactions"J. Phys., A20, L975.

Moudgil, B.M., B.D. Shah, & H.S. Soto (1987)"Collision efficiency factors in polymer flocculation of fine particles" J. Colloid Interface Sci., 119, 466.

Moudgil, B.M., & T.V. Vasudevan (1989)"Role of active sites in selective flocculation" J. Colloid Interface Sci., 127, 239.

Nagata, S. (1975)"Mixing: Principles and Applications" J. Wiley & Sons, NY, pp. 24-32.

Napper, D.H. (1983)"Polymeric stabilization of colloids", Academic Press, New York.

Nevo, A., A. DeVries & A. Katchalsky (1955)"Interaction of basic polyelectrolytes with the red blood cell. I. Combination of polylysine with single cells" Biochim. Biophys. Acta, 17, 536.

Nilsson, K., S. Birnbaum, S. Flygare, L.Linse, U. Schröder, U. Jeppeson, P.O. Larsson, K. Mosbach and P. Brodelius (1983)"A general method for the immobilization of cells with preserved viability" Eur. J. Appl. Microbiol. Biotechnol., 17, 319.

Northrop, J.H. & P.H. DeKruif (1922) "The stability of bacterial suspensions. II. The agglutination of the bacillus of Rabbit Septicemia and of Bacillus Typhosus by electrolytes" J. Gen. Phys.,4, 639.

O' Brien, R.W. (1977)"Properties of suspensions of interacting particles" Ph. D. Dissertation, Cambridge University, Cambridge, England.

Okada, T.S., M. Takeishi, K. Yasuda, & M.J. Ueda (1974) "The role of divalent cations in cell adhesion" Adv. in Biophys., 6, 157.

Oshima, R., & J. Kumanotani (1986)"Spherulites of poly(L-histidine hydrochloride)" Macromolecules, 19, 938.

Patchornik, A., A. Berger, & E. Katchalski (1957)"Poly-L-histidine" J. Am. Chem. Soc., 79, 5227.

Parseghian, V.A. and D. Gingell (1972)"Some features of physical forces between biological cell membranes" J. Adhesion, 4, 283.

Pay, T.W.F., A. Boge, F.J.R.R. Menard, and P.J. Radlett (1985)"Production of Rabies vaccine by an industrial scale BHK 21 suspension cell culture process" Dev. Biol. Std., 60, 171.

Perry, R., & M.N. Jones (1978)"The aggregation of Chinese Hamster cells: Aggregate size distributions and temperature dependence" Exp. Cell. Res., 112, 167.

Perry, S. (1987)"Packed fiber bed reactor design for animal cell culture" M.S. Dissertation, Department of Chemical Engineering, Massachusetts Institute of Technology, Cambridge, MA, September, 1987.

Pierschbacher, M.D. & E. Ruoslahti (1984a)"Cell attachment activity of fibronectin can be duplicated by small fragments of the molecule"Nature, 309, 30.

Pierschbacher, M.D. & E. Ruoslahti (1984b)"Variants of the cell recognition site of fibronectin that retain attachment-promoting activity"PNAS, 81, 5985.

Piret, J.M., C.L. Cooney (1987) "Characterization of immobilized cell reactor" paper presented at ACS National Meeting, New Orleans, LA, Sep. 1-5, 1987.

Radlett, P.J., T.W.F. Pay, & A.J.M. Garland (1985)"The use of BHK suspension cells for the commercial production of Foot and Mouth Disease vaccines over a twenty year period" Dev. Biol. Std., 60, 163.

Ramkrishna, D. (1981)"Analysis of population balance-IV. The precise connection between Monte Carlo simulation and population balances" Chem. Eng. Sci., 36, 1203.

Ray, D.T., & R. Hogg (1987)"Agglomerate breakage in polymer-flocculated suspensions" J. Colloid Interface Sci., 116, 256.

Redmann, K., H.-L. Jenssen, & H.-J. Köhler (1974)"Experimental and functional changes in transmembrane potential and zeta potential of single cultured cells" Exp. Cell Res., 87, 281.

Reerink, H., & J. Th. G. Overbeek (1954)"The rate of coagulation as a measure of the stability of silver iodide sols" Discuss. Faraday Soc., 18, 74.

Rietema, I. (1964)"Segregation in liquid-liquid dispersions"Adv. Chem. Eng., 5, 237.

Roos, E. (1984)"Cellular adhesion, invasion and metastasis" Biochem. Biophys. Acta, 738, 263.

Roseman, S. (1984)"Complex carbohydrates and intercellular adhesion", in "Biology and chemistry of eucaryotic cell surfaces", Miami Winter Symposia v.7, E.Y.C. Lee, E.E. Smith, eds., pp. 317 - 354.

Rubin, A.J. & G.P. Hanna (1968) "Coagulation of the bacterium *Escherichia coli* by aluminum nitrate" Env. Sci. & Tech., 2, 359.

Rushton, J.H., E.W. Costich, & J.H. Everett (1950)"Power characteristics of mixing impellers. Part II" Chem. Eng. Prog., 46, 467.

Ryser, H.J.-P. (1967)"A membrane effect of basic polymers dependent on molecular size" Nature, 215, 934.

Saffman, P.G. & J.S. Turner (1956)"On the collision of droplets in turbulent clouds" J. Fluid Mech., 1, 16.

Sampson, K.J. & D. Ramkrishna (1985)"Particle size correlations and the effects of limited mixing on agglomerating particulate systems" J. Colloid Interface Sci., 104, 269.

Sanders, F.K. & J.D. Smith (1970)"Effect of collagen and acid polysaccharides on the growth of BHK/21 cells in semi-solid media" Nature (London), 227, 513.

Schaefer, D.W., J.E. Martin, P. Wiltzius, & D.S. Cannell (1984)"Fractal geometry of colloidal aggregates" Phys. Rev. Lett., 52, 2371.

Schönherr, O., H. Roelofs & J. Lepoutre (1979)"Continuous flow centrifugation of cell cultures under aseptic conditions" Dev. Biol. Std., 46, 97.

Sirica, A.E., & R.J. Woodman (1971)"Selective aggregation of L1210 leukemia cells by the polycation chitosan" J. Nat. Canc. Inst., 47, 377.

Smellie, R.H. & V.K. LaMer (1958)"Flocculation, subsidence and filtration of phosphate Slimes. VI. A quantitative theory of filtration of flocculated suspensions" J. Colloid Sci., 13, 589.

Sonntag, R.C. & W.B. Russel (1986a)"Structure and breakup of flocs subjected to fluid stresses I. Shear experiments"J. Colloid Interface Sci., 113, 399.

Sonntag, R.C. & W.B. Russel (1986b)"Structure and breakup of flocs subjected to fluid stresses II. Theory"J. Colloid Interface Sci., 113, 378.

Stephanopoulos, G., K.-Y. San, & B.H. Davison (1985)"A novel bioreactor-cell precipitator combination for high-cell density, high-flow fermentations" Biotech. Progress, 1, 250.

Strandberg, G.W., S.E. Shumate II, & J.R. Parrott, Jr. (1981)"Microbial cells as

biosorbents for heavy metals: Accumulation of uranium by *Saccharomyces cerevisiae* and *Pseudomonas aeruginosa*" Appl. & Env. Microbiol.,41, 237.

Stuart, J.T. (1958)"On the non-linear mechanics of hydrodynamic stability"J. Fluid Mech., 4, 1.

Sutherland, D.N. (1966)"Comments on Vold's simulation of floc formation" J. Colloid Interface Sci., 22, 300.

Swift, D.L., & S.K. Friedlander (1964)"The coagulation of hydrosols by Brownian motion and laminar shear flow" J. Colloid Sci., 19, 621.

Takamura, K., H.L. Goldsmith, & S.G. Mason (1981)"The microrheology of colloidal dispersions. XIII. Trajectories of orthokinetic pair collisions of latex spheres in a cationic polyelectrolyte" J. Colloid Interface Sci., 82, 190.

Takeichi, M., & T.S. Okada (1972)"Roles of magnesium and calcium ions in cell-to-substrate adhesion" Exp. Cell Res., 74, 51.

Tambo, N. & Y. Watanabe (1967)"A study on aluminum floc density 1." J. Japan Water Wks. Assoc., 379, 2. (Japanese)

Tambo, N. & Y. Watanabe (1979a)"Physical characteristics of flocs-I. The floc density function and aluminum floc" Water Res., 13, 409.

Tambo, N. & Y. Watanabe (1979b)"Physical aspect of flocculation process-I. Fundamental treatise" Water Res., 13, 429.

Tanford, C. (1962) "Physical chemistry of macromolecules" J. Wiley & Sons, New York, pp. 509-512, 548-552.

Tang, P., D.E. Colflesh, & B. Chu (1988)"Temperature effect on fractal structure of silica aggregates" J. Colloid Interface Sci., 126, 304.

Tenney, M.W., W.F. Echelberger, Jr., R.G. Schuessler & J.L. Pavoni (1969) "Algal flocculation with synthetic organic polyelectrolytes" Appl. Microbiol., 18, 965.

Tenney, M.W. & W. Stumm (1965) "Chemical flocculation of microorganisms in biological waste treatment" J. Water Poll. Ctrl. Fed., 37, 1370.

Teot, A.S. & S.L. Daniels (1969) "Flocculation of negatively charged colloids by inorganic cations and anionic polyelectrolytes" Env. Sci. & Technol., 3, 825.

Tolbert, W.R., M.M. Hitt, J. Feder (1980)"Cell aggregate suspension culture for large-scale production of biomolecules" In Vitro, 16, 486.

Tsezos, M., & B. Volesky (1981)"Biosorption of Uranium and Thorium" Biotech. Bioeng., 23, 583.

Tsiveriotis, K. & G. Stephanopoulos (1988)"Convective nutrient transfer in porous particles with immobilized cells" Paper presented at AIChE Annual Meeting, Washington, D.C., Nov. 27-Dec. 2, 1988.

Urushihara, H., M. Takeichi, A. Hakura & T.S. Okada (1976)"Different cation requirements for aggregation of BHK cells and their transformed derivatives" J. Cell Sci., 22, 685.

Van de Ven, T.G.M. (1981)"Effects of polymer bridging on selective shear flocculation" J. Colloid Interface Sci., 81, 290.

Van de Ven, T.G.M., and S.G. Mason (1976)"The microrheology of colloidal dispersions. IV. Pairs of interacting spheres in shear flow" J. Colloid Interface Sci., 57, 505.

Van de Ven, T.G.M., and S.G. Mason (1977)"The microrheology of colloidal dispersions. VII. Orthokinetic doublet formation of spheres" Colloid Polymer Sci., 255, 468.

Van Diemen, A.J.G., & H.N. Stein (1983)"Coagulation of aqueous dispersions of quartz in a shear field" J. Colloid Interface Sci., 96, 150.

Van Haecht, J.L., M. Bolipombo, & P.G. Rouxhet (1985) "Immobilization of *Saccharomyces cerevisiae* by adhesion: Treatment of the cells by Al ions" Biotech. Bioeng., 27, 217.

Vold, M.J. (1963)"Computer simulation of floc formation in a colloidal suspension" J. Colloid Sci., 18, 684.

Von Smoluchowski, M. (1917)"Versuch einer mathematischen theorie der koagulationskinetik kolloide losungen" Zeitschr. Phys. Chem., 92, 129.

Walles, W.E. (1968)"Role of flocculant molecular weight in the coagulation of suspensions" J. Colloid Interface Sci., 27, 797.

Wang, C.-Y., & L. Huang (1984)"Polyhistidine mediates an acid-dependent fusion of negatively charged liposomes" Biochemistry, 23, 4409.

Warren, L., J.P. Fuhrer, & C.A. Buck (1972)"Surface glycoproteins of normal and transformed cells: A difference determined by sialic acid and a growth-dependent sialyl transferase" PNAS, 69, 1838.

Weeks, M.G., P.A. Munro & P.L. Spedding (1983) "New concepts for rapid yeast settling. I. Flocculation with an inert powder" Biotech. Bioeng., 25, 687.

Weitz, D.A. & M. Oliveria (1984)"Fractal structures formed by kinetic aggregation of aqueous gold colloids"Phys. Rev. Lett., 52, 1433.

Weitz, D.A., J.S. Huang, M.Y. Lin & J. Sung (1985)"Limits of the fractal dimension for irreversible kinetic aggregation of gold colloids"Phys. Rev. Lett., 54, 1416.

Whiteley, J.M. & J.H. Galivan (1982)"Interaction of methotrexate(polylysine) with rat liver tumor cells" in "Biological activities of polymers", ACS Symp. Ser., 186, pp. 255 - 268.

Wiegel, F.W. & P.F. Mijnlieff (1977)"Intrinsic viscosity and friction coefficient of permeable macromolecules in solution" Physica, 89A, 385.

Weitz, D.A. & M. Oliviera (1984)"Fractal structures formed by kinetic aggregation of aqueous gold colloids" Phys. Rev. Lett., 52, 1433.

Weitz, D.A., J.S. Huang, M.Y. Lin, & J. Sung (1985)"Limits of the fractal dimension for irreversible kinetic aggregation of gold colloids" Phys. Rev. Lett., 54, 1416.

Wigsten, A.L., & R.A. Stratton (1984)"Polymer adsorption and particle flocculation in turbulent flow" in "Polymer adsorption and dispersion stability", ACS Symp. Ser., 240, E.D. Goddard, B. Vincent, eds. pp. 429-444.

Witten, T.A., & L.M. Sander (1981)"Diffusion-limited aggregation, a kinetic critical phenomena" Phys. Rev. Lett., 47, 1400.

Wong, K., B. Cabane, & R. Duplessix (1988)"Interparticle distances in flocs" J. Colloid Interface Sci., 123, 466.

Wu, Y.C. (1978) "Chemical flocculability of sludge microorganisms in response to growth conditions" Biotech. Bioeng., 20, 677.

Zeichner, G.R. & W.R. Schowalter (1977)"Use of trajectory analysis to study stability of colloidal dispersions in flow fields"AIChE J., 23, 243.

Zeichner, G.R., & W.R. Schowalter (1979)"Effects of hydrodynamic and colloidal forces on the coagulation of dispersions" J. Colloid Interface Sci., 71, 237.

Zimm, B.H. (1980)"Chain molecule hydrodynamics by the Monte Carlo method and the validity of the Kirkwood-Riseman approximation" Macromolecules, 13, 592.

Zoletto, R. (1985)"A multiplate settling vessel to increase the separation speed of cells from growth medium" Dev. Biol. Std., 60, 313.

Zydney, A.L. and C.K. Colton (1986)"A concentration polarization model for the filtrate flux in cross-flow microfiltration of particulate suspensions" Chem. Eng. Comm., 47, 1.